STUDIES OF THE HEAT EXCHANGE PROCESS ASSOCIATED WITH THE NUCLEATE BOILING OF A LIQUID.

by

Suresh Chandra GARG.,
B.Sc.(Hons.) Chemistry; B.Sc.(Hons.) Eng.

A thesis presented for the degree of

Doctor of Philosophy

of the

University of Edinburgh.

October 1963.

Acknowledgement.

This research was carried out in the Sanderson Engineering Laboratories of the University of Edinburgh and the author is indebted to Professor R.N. Arnold for the facilities placed at his disposal. The author offers his most sincere thanks to Dr. T.D. Patten for the guidance given during the period October 1959 - September 1963. The assistance given by other members of the staff of the University of Edinburgh, directly or indirectly, is gratefully acknowledged.

This research was made possible by financial support from the Central Electricity Generating Board.

TABLE OF CONTENTS

OLD COLLEGE,
SOUTH BRIDGE,
EDINBURGH.

A film was submitted to supplement the contents of the thesis. The single copy of the film is lodged with the first copy of the thesis in the University Library.

Gong (S.C.)

Appendices.

NOMENCLATURE.

SYMBOL		UNITS
A_o	area of outer surface of heating tube	ft^2
A_i	Area of inner surface of heating tube.	ft^2
C_D	Drag coefficient.	
D	Maximum diameter of the bubble.	ft
H	Heat generation rate per unit volume.	B.t.u./ft^3.hr.
L	Latent heat of evaporation.	B.t.u./lb.
Q	Total amount of heat per hour.	B.t.u./hr.
T	Temperature.	^oF.

Suffices: b = bulk liquid in the test tank; i = stabilizing fluid at inlet to the test section; ℓ = transient temperature of liquid near the heating tube at any time; m = mean liquid temperature near the heating tube; o = stabilizing fluid at outlet from the test section; s = saturation; T = inner surface of heating tube; w = outer surface of heating tube.

ΔT	Average Tw - Ts.	deg.F.
ΔT_{fb}	Arithmetic mean temperature difference between stabilizing fluid and bulk liquid.	deg.F.
ΔT_{wb}	Temperature difference between heater outer wall and bulk liquid, Tw - Tb.	deg.F.
ΔT_{Tf}	Arithmetic mean temperature difference between inner tube wall and stabilizing fluid.	deg.F.
ΔT_{sf}	Temperature change in the stabilizing fluid bulk within the heated length of the test section.	deg.F.
ΔT_{TW}	Temperature drop across the tube wall.	deg.F

U	Overall heat transfer coefficient	B.t.u./ft.^{2}hr.$^\circ$F.
V	Velocity.	ft/hr.
b	Thickness of the superheated layer	ft.
c_L	Specific thermal capacity of liquid	B.t.u./lb.$^\circ$F.
c_{sf}	Specific thermal capacity of stabilizing fluid.	B.t.u./lb.$^\circ$F.
c_{tc}	Specific thermal capacity of the thermocouple wire.	B.t.u./lb.$^\circ$F.
d	Diameter of the thermocouple wire.	ft.
d_i	Diameter of heater tube at inner surface	ft.
d_o	Diameter of heater tube at outer surface	ft.
f	Frequency of bubble formation at a nucleation site	hr.$^{-1}$
g	Acceleration due to gravity	ft/hr.^{2}
g_o	Conversion factor	
h	Heat transfer coefficient.	B.t.u./ft.^{2}hr.$^\circ$F.
	suffices: nc = natural convection; fc = forced convection.	
k	Thermal conductivity of test liquid.	B.t.u./ft.hr.$^\circ$F.
	suffices: sf = stabilizing fluid; T = Tube material.	
ℓ	Total length of heater tube	ft.
m	Flowrate of stabilizing fluid	lb/hr.
N	Number of nucleation sites per unit area.	ft.$^{-2}$
p	Pressure.	lbs/ft^2
$p_{cr.}$	Critical pressure	lbs/ft^2
q_v	Heat flux	B.t.u./ft.^{2}hr.
$q_{vcr.}$	Critical heat flux	B.t.u./ft.^{2}hr.
r_i	Radius of tube at inner surface	ft.
r_o	Radius of tube at outer surface	ft.

t	Time	hr.
v	Volume	$ft.^3$
α	Thermal diffusivity of liquid	$ft^2/hr.$
β	Temperature coefficient of volumetric expansion.	$^oF.^{-1}$
μ	Absolute viscosity.	lb./hr.ft.
σ	Surface Tension.	lb./ft.
ρ	Density.	$lb./ft.^3$
	Suffices: ℓ = liquid; v = vapour; tc = Thermocouple	
τ	Response time of the 0.002 inch diameter thermocouple.	sec.
ϕ	Angle of contact between liquid and vapour.	degrees.
$\lambda_1, \lambda_2, \lambda_3 \cdots$	Constants.	
Re	Reynolds number.	
Pr	Prandtl number.	
St	Stanton number.	

CHAPTER 1.

INTRODUCTION.

The process known as boiling may be employed for the production of vapour, as in the steam generator, or as a means of rejecting heat from a surface, as in the case of nuclear reactors and rocket motors. In either case, this process can be a most effective method of heat transfer. Boiling usually occurs at a solid-liquid interface and this investigation is confined to boiling from a solid surface.

This work was undertaken to investigate the process of heat transfer by pool boiling of saturated water. A horizontally - mounted stainless-steel tube, 0.125 inch outer diameter, was used as the heating surface in this investigation. Therefore, the literature referred to in this thesis is generally connected with pool boiling of water from horizontal flat or cylindrical metal surfaces.

The characteristics of boiling heat transfer are most simply represented on a logarithmic plot of heat flux q against the temperature difference between heated surface and saturation temperature of the bulk liquid $T_w - T_s$, as illustrated in Figure 1.

AB is the natural convection region. Equations have been derived which permit the prediction of heat transfer rate in this region, e.g. heat transfer rate by natural convection on the outer surface of a horizontal tube is given by McAdam [1][1],

$$\frac{h_{nc} \cdot d_o}{k_m} = 0.53 \left[\frac{d_o^3 \rho_m^2 \cdot g \cdot \beta_m \cdot \Delta T_{wb}}{\mu_m^2} \cdot \left(\frac{c_p \cdot \mu}{k} \right)_m \right]^{1/4} \qquad (1)$$

[1] Number in parentheses refer to the list of references at the end of the thesis.

where h_{nc} = Heat transfer coefficient in natural convection.

k = Thermal conductivity of liquid.

d_o = Outer diameter of the heating tube.

ρ = Density of liquid.

β = Temperature coefficient of volumetric expansion.

c_p = Specific thermal capacity of the liquid.

μ = Absolute viscosity of liquid.

ΔT_{wb} = Temperature difference between heater wall and liquid $(T_w - T_b)$ and subscript g denotes that the property values of fluid corresponds to arithmetic mean temperature between tube surface temperature and bulk fluid temperature.

Nucleate boiling starts at B when the heater wall temperature is a few degrees higher than the saturation temperature. For initiation of a bubble at atmospheric pressure, this temperature difference amounts to less than $10^{\circ}F$ at suitable surface conditions. A thin layer of superheated liquid is formed on the heating surface. Bubbles nucleate at the heating surface and grow in the superheated layer. With increase in wall temperature, the frequency of bubble formation at a particular nucleation site increases and the number of such active sites increases. Heat transfer rate increases sharply along BC.

Various mechanisms have been suggested to account for the sharp increase in heat transfer rate. Gunther and Kreith [2] postulated, "Some form of random micro-convection excited by bubble activity in the normally laminar sublayer." Forster and Grief [3] have suggested a "pumping" of the liquid by bubble action through the boundary layer. Chang and Snyder [4] have attributed this increase in heat transfer rate to increase of effective thermal

conductivity due to agitation effects of the bubble.

Various mechanisms suggested to explain high heat transfer rates in boiling depend primarily upon the maximum diameter of a bubble. It is, therefore, necessary to derive an expression for predicting maximum diameter of a bubble.

For saturated pool boiling of water, various existing correlations for predicting bubble diameter at departure are summarised in chapter 5.1. None of these correlations were found satisfactory when applied to conditions at subatmospheric pressures.

An equation based on energy considerations is derived in chapter 5.1. which predicts departure diameter of a bubble in saturated pool boiling of water at subatmospheric pressures. Comparison of available experimental data in the subatmospheric region with analytical prediction is satisfactory. A second correlation, which depends upon the reduced pressure ($P/P_{cr.}$) is derived which predicts bubble departure diameter for saturated pool boiling of water over the pressure range between 1.0 psia and 3,200 psia. The comparison with available data is satisfactory.

The relationship between heat transfer rate and temperature difference (Tw-Ts) in the nucleate boiling region can be ~~expressed~~ as,

$$q \propto (\Delta T)^x$$

expressed

for moderate boiling only. However, at large heat fluxes near the critical region, the heat flux reaches a maximum. Various values of x have been suggested including a value of 2 by Rohsenow [5] and a value of 3 by Levy [6]. The value of x obtained in this investigation at subatmospheric pressures lies between 4 and 6.

As point C is approached, the slope of the heat transfer curve decreases and finally, at point C, a further increase in wall temperature is accompanied by a decrease in heat flux.

Many empirical correlations have been suggested in literature for predicting critical heat flux at point C. The existing correlations are summarised in chapter 5.2. The theoretical approach to the problem of predicting critical heat flux has met with little success.

Using a logical approach to the problem of heat transfer under critical conditions, supported by photographic evidence, an equation for predicting critical heat flux in saturated pool boiling is arrived at. Comparison of available experimental data over the entire pressure range, from 1.0 psia up to critical pressure, with predicted values is satisfactory.

CD is the transition boiling region. In this region, an increase in the heater surface temperature results in a decrease in heat flux, until point D is reached. In this investigation, examination beyond point C has not been carried out.

At D, there is a thin continuous vapour film surrounding the heating surface. DE is the film boiling region.

The most effective regime, from a heat transfer standpoint, is nucleate boiling region BC in Fig.1. The temperature difference between heater surface and saturation for critical conditions $(T_w-T_s)_{cr}$ is low, Bernath [7] At atmospheric pressure, this critical temperature difference is less than 75^0F for heat transfer rate of 5.2×10^5 B.t.u. per square feet per hour. To transfer heat at this rate in the film boiling region, a temperature difference in excess of $1,000^0F$ would probably be necessary.

If the heat input to the heating surface is constant, as in the case of electric and nuclear heating, then near point C there is a tendency for excursion from nucleate boiling into the film boiling region DE. This excursion may ultimately result in a complete burnout of the heating surface.

Therefore, a better understanding of the phenomenon of boiling is essential for a most effective use of the nucleate boiling regime in heat transfer problems.

There is a lack of [redacted] experimental data in heat transfer in the subatmospheric region. Also, there has been no work done previously on the nature of temperature transients in the superheated layer associated with the bubble growth and departure. It was felt that an investigation into the nature of temperature transients may help in obtaining a better understanding of the mechanism of heat transfer in boiling at relatively low heat fluxes.

Three reasons for choosing subatmospheric pressure range for this investigation were:

1) Departure diameter of bubbles is large,

2) Heater surface temperature T_w is large for low heat fluxes. This may provide large temperature transients and, hence, a large measurable signal.

3) Temperatures are low and, hence, heat losses are low.

The principal objectives of this investigation were as follows:-

1) Determination of critical heat flux in saturated pool boiling of water under stabilised conditions.

2) Investigation of the temperature gradient in the superheated layer near the heating surface and the thickness of the superheated layer.

3) Investigation of temperature transients in the superheated layer associated with bubble growth and departure.

4) Analytical prediction of bubble diameter at departure and critical heat flux in nucleate pool boiling of saturated liquids.

While the order of presentation of this thesis is indicated fully in the list of contents, it is felt that some explanation for the chosen order should also be included. The phenomenon of boiling is complex and this work was aimed at uncovering only a few of the mysteries of boiling heat transfer. The approach to this was primarily experimental and therefore this aspect has been dealt with first. Chapters 2, 3 and 4 respectively deal with description of the apparatus used in this investigation, the experimental procedure, and analysis of the information thus obtained. In chapter 5, after reviewing existing theories and expressions, an effort is made to predict departure diameter of a bubble and critical heat flux in saturated pool boiling of water. Chapter 6 summarises the results obtained in this investigation.

Despite the accent on the experimental nature of this work, it has not been possible to summarise all the impressions and experience which has been gained of the nucleate boiling heat transfer process - after hours of experimentation and hundreds of hours of examination of photographs and other experimental records.

CHAPTER 2.

DESCRIPTION OF APPARATUS

2.1 TEST SECTION.

2.1.1 Form of heating element.

If the problem of surface geometry is assessed as a problem of arranging a source of bubbles suitable for visual examination, a choice has to be made from three basic forms of heat source:-

1) point source (non-dimensional),

2) line source (one-dimensional),

3) flat surface (two-dimensional).

A flat surface was found unsuitable for two main reasons. Firstly, from the point of view of high speed photography, it would have been impossible to measure the distance of the bubble wall from the thermocouple junction with horizontal camera alignment. The possibility of vertical camera alignment was discarded because disturbances on the water surface would have screened the heating surface. Secondly, it would have been extremely difficult to work in the region of critical heat flux due to danger of burnout.

A point source geometry possessed a marginal advantage for an investigation such as this. The probability of recording a bubble on the high speed film, during brief exposure period of 0.8 second, would have been higher. However, the disadvantages outweighed the advantages. Some of the disadvantages were:

1) From an experimental point of view, feasible heating systems for a point source are either electric heating or the use

of a LASER. LASER energy sources were only under development at the beginning of this work and were not available commercially. At low pressures, the bubbles are large and the bubble growth period is of the order of 20 - 30 milliseconds, Patten [8]. With electric heating, blanketing of the point source by the vapour bubble for this duration would most probably result in an excursion into the film boiling region even at low heat fluxes.

2) The temperature fluctuations of the heating surface, due to complete blanketing by the bubble, will be large.

3) The value of voltage and current will be very small and measurement of these quantities will be inaccurate.

4) With a point source, it is difficult to determine heat flux.

No suitable system could be devised which would overcome above difficulties.

Something approximating to a line source was the final choice. Thin wires provide good line sources and for work in the sub-atmospheric region (when the bubble departure diameter is large) thick wires or small tubes may be used. Tubes were preferred because, as will be explained later, it is possible to experiment in the region of critical heat flux using a stabilizing system. The stabilizing system prevents an excursion into the film boiling region by removing excess heat from the heating surface.

Another decision to be made simultaneously with the form of heating surface is the origin of heat energy. It was decided to use electric heating in preference to steam heating for the following reasons:-

1) the heat energy input is uniform over the surface area,

2) the control of heat flux is relatively simple and high heat fluxes can be obtained,

3) measurement of thermal energy input to the heating surface is easy and accurate.

The tube was mounted horizontally to ensure constant heat transfer coefficient along the length of the tube and to prevent bubbles from one section of the tube interfering with the other.

2.1.2. Dimensions of the heating tube.

To be consistent with a line source, the diameter of the tube was to be as small as possible. A lower limit for diameter was imposed by the magnitude of the pressure drop over the test length, for the stabilizing fluid flowing through the tube.

The magnitude of the current required to produce heat fluxes of the order of 5.0×10^5 B.t.u. per hour per square feet sets a limit to the maximum possible thickness of the tube wall. Minimum wall thickness was limited by two factors:-

1) problems of handling of the tube and of brazing it to the busbars,

2) effect of tube wall thickness on critical heat flux.

A polished stainless steel tube was chosen to prevent corrosion of the tube surface and to keep water free from contamination during boiling. No microscopic check was made on the surface conditions of the tube because it is known that critical heat flux is independent of surface conditions of the heating surface, Berenson [9] and Bernard [10]. Also, none of the existing correlations for predicting critical heat flux in saturated pool

boiling contain terms involving surface conditions of the heating element.

The final specifications for the test section were:-

Length of the test section	= 6 inches,
Outside diameter of the test section	= 0.125 inch.
Wall thickness	= 0.005 inch.
l/d_o	= 48

Figures 2 and 3, reproduced from Ivey [11], show the effect of the heater diameter and tube wall thickness on critical heat flux. It is clear from figure 2 that the diameter of 0.125 inch. corresponds both to large diameter tubes and flat surfaces at atmospheric pressure.

From experimental points plotted in Figure 3, it is clear that the value of critical heat flux for heater thickness of 0.005 inch. is only 10 - 15% less than the corresponding value for very thick tubes. This difference is smaller than the scatter of experimental results for thickness of the order of 0.005 inch. In the case of the experimental arrangement adopted here, however, the use of a stabilizing system is assumed to nullify any effect of heater wall thickness on the critical heat flux. The use of a stabilizing fluid provides a source and sink of heat should the heater surface temperature fall or rise above the mean stabilizing fluid temperature. Large temperature fluctuations of the heater surface near maximum heat flux are, thus, damped significantly.

The natural frequency of vibration of the selected tube at

first harmonics was estimated at 6.1×10^3 cycles per second.

2.1.3. Electric current conductors.

The conductors were fabricated from $\frac{3}{4}$ inch. diameter brass rod to give a negligible voltage drop at the estimated maximum current of 150 Amperes. The conductors were Nickel-plated to prevent contamination of water. The stainless steel boiling tube was brazed to these conductors using silver solder, Figure 4.

2.1.4. Test tank.

It was felt that success in the application of high speed photography was dependent upon maximum transmission of light to the heating surface and, therefore, a completely transparent tank was specified. Glass and perspex were both considered and perspex was finally chosen because of the ease with which it can be machined. Also, in the subatmospheric region, the maximum saturation temperature of water was 212°F. which was slightly less than the upper temperature limit for perspex. A thickness of 0.625 inch was fixed on the basis of the deflection at the centre of the largest side which was approximately 11 inches x 12 inches.

The final dimensions for the test tank were:-

length - 11.0 inches,

breadth - 7.0 inches,

height - 12.0 inches.

The factors which determined tank length and breadth were:-

1) dimensions to be much larger than the maximum bubble diameter so that tank size has no effect on the maximum bubble

diameter and growth rate.

2) water level to fall not more than $\frac{1}{4}$ inch in duration of one test of about 10 minutes.

The edges of the perspex sides were joined using perspex cement and the assembly was cured under an ultra-violet lamp. The front plate of the tank was bolted to the tank with a silicone rubber gasket, 0.139 inch. diameter, to provide a leak proof joint. This plate could be removed to allow access to the interior of the tank, whenever necessary. During the commissioning tests, this tank started leaking at the cemented joints. It was clear that, under lowest pressure, sufficient deflection occurred at the cemented joints to cause cracking. It was therefore necessary to redesign the tank.

The following design proved satisfactory:

A brass frame was made from one inch square bars brazed at the corners. All outside faces of the frame were machined and grooved suitably to retain a 0.139 inch. diameter silicone rubber gasket, Figure 5. The perspex sides were screwed to the brass frame, the seal being formed by the rubber gasket on all sides.

Access to the interior of the tank was achieved by removing the front plate. All electrical connections were made through the top plate.

2.2. VACUUM SYSTEM.

The pressure range selected for this investigation was from 1.0 psia to 14.7 psia. The reasons for choosing this range were primarily experimental, namely:-

1) the temperature difference between wall and saturation for initiation are large and a large measurable temperature transient can be expected. At 1.0 psia, initiation temperature difference for boiling on stainless steel tube is about 35°F.

2) bubbles are large at low pressures. The bubble diameter of the order of 1.6 inches is obtained at a pressure of 1.0 psia.

3) temperatures are low and hence heat losses are low.

In addition, the range of property value covered is:

2.4 fold variation in viscosity.

2.5 fold variation in Prandtl number.

1.2 fold variation in surface tension.

12.5 fold variation in vapour density.

The following arrangement provided a very steady vacuum control in the above pressure range. Figure 6. shows the vacuum system.

A vacuum pump type ISC 30, manufactured by Edwards High Vacuum Ltd. with displacement of about 1.10 cubic feet per minute, was used to produce a vacuum in the tank. A water-cooled condenser between the tank and the pump ensures that most of the water vapour is removed before the air-vapour mixture reaches the pump.

The vapour was extracted from the tank through a 2 inches bore connection. All connecting pipes from the tank to the vacuum pump were glass and of the standard sizes supplied by Q.V.F. LTD. The condensate collecting vessel was of 5 litre capacity and fitted with a drain-cock.

To regulate and maintain low pressures in the tank, a Cartesian Manostat was first fitted. During operation fluctuations in pressure of the order of ± 0.1 pounds per square inch occurred. This was considered unacceptable for low pressure work and, therefore, the Manostat was replaced by an Edwards air admittance valve type R.S.1. just upstream of the vacuum pump. In addition, a needle valve type W.S.1. was connected to the test tank. These two valves provided excellent control over the vacuum in the tank which was measured by a mercury manometer. Atmospheric pressure was measured to within ± 0.002 inch. of mercury using a Fortin barometer.

2.3 POWER CIRCUIT

2.3.1 Power supply.

It was decided to use direct current to heat the test section for two main reasons:-

1) to avoid any influence of 50 cycles per second current and voltage ripple on bubble growth rate.

2) to avoid A.C. pick-up by 0.002 inch. diameter thermocouple situated near the heating surface. An A.C. pick-up by the thermocouples would have spoiled any recording of temperature transients in the superheated layer near the heating surface during bubble growth.

For an assumed value of the critical heat flux in nucleate pool boiling of 5×10^5 B.t.u. per hour per square feet

at atmospheric pressure, the power requirement was about 150 Amps. at 15 Volts. It was decided to use a 20 volts, 400 Amps. D.C. motor-generator unit. Continuous current control was available over the entire range.

The general arrangement is shown in Figure 7.

A trial run was made to estimate the amount of A.C. in the D.C. Supply from the generator. This was done on the basis of A.C. picked up by 0.002 inch. diameter thermocouples placed near the heating tube. The pick-up was of the order of 0.5 milivolt. ($\equiv 22^{\circ}F$) for 6 volts across the heating tube. This was considered high compared with the maximum transient temperature of the order of $30^{\circ}F$.

It was, therefore, necessary to smooth the D.C. supply using condensers. The best combination, after trial and error, was found to be 6,000 μF capacitance across the field and 6,000 μF across the output from the generator, as shown. The negative lead from the generator was earthed to give acceptable conditions. The pick-up was reduced to about $\pm$ 0.04 milivolt. ($< \pm 2^{\circ}F$.) with this arrangement, the frequency of pick-up being 600 C/s modified by 50 C/s A.C. supply.

2.3.2. Measurement of heat flux.

A standard resistance of 0.00025 ohm was connected in series with the output from the generator. The voltage drop across the resistance provided the value of current flowing in

the circuit. Two stainless steel clips were fixed rigidly on to the test section at a measured distance between them. The clips had sharp edges so that the distance between the clips could be measured accurately using a travelling microscope. Leads from the clips were connected through a 400/1 voltage ratio box to a potentiometer circuit to determine the voltage.

The values of voltage, current, together with the dimensions of the tube and distance between stainless steel clips provided the heat flux values.

2.4. STABILIZING CIRCUIT

2.4.1 Process of stabilisation.

The use of stabilising fluid for determining heat transfer coefficients in nucleate boiling in the region of critical heat flux was first suggested by Poletavkin & others [12].

The boiling curve for water at 1 - atmospheric pressure was first published by Nukiyama [13] and has since been confirmed by many research workers, at various pressures. Figure 1. shows the form of this curve which generally applies for many different liquids and many different experimental arrangements. Heat flux q is plotted against the temperature difference between heating surface and saturation temperature Tw-Ts on a log-log scale.

Over most of the boiling range, at any fixed value of heat flux, there may be three different wall temperatures. These three wall temperatures correspond to the three boiling regimes,

viz. nucleate boiling, transition boiling and film boiling. In the vicinity of point C, there is a tendency for an excursion into the film boiling regime resulting in eventual "burnout" of the heating surface. Investigation of nucleate boiling at critical heat flux is made difficult by the possibility of instability. It is essential, if reproducable experiments are to be made, to provide some method to prevent the change of operating conditions from C to E. Such an excursion into the film boiling region is prevented by the use of a stabilizing fluid.

Consider a constant heat flux line xx in Figure 1. In nucleate boiling, the heat flux q_F corresponds to tube wall temperature T_{WF} at point F. The tube inner surface temperature is T_{TF}. Under steady state conditions, with stabilizing fluid flowing through the tube, if inlet stabilizing fluid temperature T_i is equal to T_{TF} then the outlet stabilizing fluid temperature T_o is also equal to T_{TF}. No heat transfer takes place between the stabilizing fluid and the tube. All the electric heat input to the tube is dissipated by boiling on the outer surface of the tube.

If, due to instability, the operating point jumps from F to H, both tube outer and inner surface temperatures acquire a new value, say T_{WH} and T_{TH} respectively. Some heat energy proportional to $T_{TH} - T_{TF}$ will then be transferred to the stabilizing fluid. As a direct result, the operating point on the curve will come down along HD.

In principle, tube failure can be avoided if the stabilizing fluid can remove heat input equivalent to $(q_F - q_D) \times A_o$.

For atmospheric pressure, and an assumed value of $(q_c - q_D)$ of 4.7×10^5 B.t.u. per hour per square feet, the required heat capacity of stabilizing fluid, for tube diameter of 0.125 inch, is 7660 B.t.u. per hour.

2.4.2 Choice of stabilizing fluid.

Calculations were carried out for water and two other commercial heat transfer liquids, viz. Shell Voluta 45 and Mobiltherm 600, to decide upon the best stabilizing fluid suitable for this investigation.

It was clear from calculations, appendix I, that for the required stabilizing capacity, the pressure drop across the heating section was least for water, viz. less than 1.0 psi for water compared with 67 psi for Mobiltherm 600 and 94 psi for Shell Voluta 45.

This experimental investigation was restricted primarily to subatmospheric pressures. Under these conditions, wall temperatures are low ($300^{\circ}F$ at atmospheric pressure). Using water as the stabilizing fluid, the pressure in the stabilizing tank need not therefore exceed 120 psig.

Because there are no decomposition products, as may occur with the other liquids, it was decided to use water as the stabilizing fluid.

2.4.3 Stabilizing system.

To reduce costs, a mild steel tank was designed for use as a

stabilizing fluid tank. To reduce corrosion to a minimum, the tank was coated on the inside with Araldite type 18. The internal dimensions of the tank were 12 inches diameter x 18 inches high. Standard spiral electric heating elements enclosed in pyrex glass tubes were installed inside the tank for heating the stabilizing fluid. Two such 1,000 watts.heaters, connected in parallel, were supported from the top of the stabilizing fluid tank. A temperature controller was installed and connected to the heaters through a variac. The variac in conjunction with temperature controller provided control over stabilizing fluid temperature to within $\pm$ 0.1^{o}F. over a period of ten minutes. The mild steel tank was insulated with one inch thick glass wool insulation.

To avoid boiling in the stabilizing system with test section inner wall temperatures of up to 300^{o}F, it was necessary to raise the pressure, and hence the saturation temperature, in the stabilizing system. A nitrogen supply, a pressure gauge, a safety valve and control valves were installed to obtain and maintain any desired pressure in the stabilizing system up to 120 psig.

A circulating pump type KR1-B, manufactured by Sigmund pump Ltd. specially modified to withstand temperatures up to 300^{o}F and pressures up to 130 psig, was installed finally after unsuccessful attempts to modify a type 10 Stuart Turner pump. A Fischer and Porter flowrator was included in the circuit to measure flowrates between 1.0 Igph and 15.0 Igph. A by-pass valve enabled adjustments of the flowrate through the test section. The general arrangement is shown in figure 8.

SWG34, insulated, nickel-aluminium/nickel-chromium alloy thermocouples were used to measure the temperature of the stabilising fluid at inlet to and outlet from the test section. The thermocouple assembly is as shown in Figure 4.

Each thermocouple was located in and kept in position by a set of two ceramic holders. The ceramic holders were separated by a stainless steel rod.

The position of thermocouples was 1½ inch upstream of the entry and 1½ inch downstream of the exit of the actual test section. An air gap in the approach tubes was provided to prevent local boiling of the liquid in the test tank.

2.4.4 Tube outer surface wall temperature.

Among various methods of measuring tube wall temperature two commonly used are:-

1) measuring the electrical resistance of the heating element.

2) using a thermocouple welded to the surface of the heating element.

There are difficulties in measuring tube surface temperature using either of the above two methods. Since the surface temperature fluctuates due to the bubble growth and departure, the current drawn by the heating element fluctuates for the same applied voltage. Also, temperature coefficient for stainless steel is very small. Method one was, therefore, considered inaccurate. Method two was discarded on following grounds:-

1) difficulties of welding a thermocouple to the tube surface.

2) necessity of calibration for D.C. voltage pick-up.

3) welding to the tube surface will change the surface conditions at the point and, hence, temperature measured will not be an average surface temperature.

4) the thermocouple junction could only be welded at one point. The rest of the surface area of the junction will come in contact with liquid and vapour. This will introduce error.

5) presence of thermocouple will influence nucleation conditions locally at the thermocouple.

In the present investigation, the above difficulties were overcome by measuring stabilizing fluid temperature. The tube wall temperature was derived from stabilizing fluid temperature, as in Appendix II.

Since the stabilizing fluid temperature at inlet and outlet was not measured at exactly the beginning and end of the test section, but at a distance of $1\frac{1}{4}$ inch, an error is introduced. The error is mainly due to heat lost from the stabilizing fluid by conduction and convection in the approach tubes and conductors. The extent of these losses is of the order of 315 B.t.u. per hour per degree F temperature difference between the stabilizing fluid and the bulk in the test tank. The extent of these losses was determined as in appendix III and correction applied to all results. At critical heat flux in nucleate boiling at 1.0 psia, this correction amounted to about 10%.

To apply correction, a temperature difference between inlet and outlet of stabilizing fluid, equivalent to losses, was maintained during actual experiments.

In determining losses, (appendix III), it was assumed that

the losses at entry and at exit are equal. The tube inside wall temperature was, therefore, obtained as the arithmetic mean of stabilizing fluid temperature at inlet and outlet,

$$T_T = \frac{T_i + T_o}{2}$$

Outside wall temperature (Tw) was determined from tube inside wall temperature (T_T) as in appendix II.

The sensitivity of the stabilizing system was determined as shown in appendix IV.

2.5 MANUFACTURE AND MOUNTING OF 0.002 INCH DIAMETER THERMOCOUPLES.

2.5.1 Manufacture.

T_1 & T_2 base metal (nickel-aluminium/nickel-chromium), uninsulated, thermocouple wires of 0.002 inch diameter were used in this project for recording temperature transients in the superheated layer and for measuring the temperature gradient in the superheated layer. An electric discharge welder, Figure 9, produced a butt-welded joint between the two wires.

By a system of trial and error, the working values of voltage and capacitance, for welding of 0.002 inch diameter wires, was found to be,

voltage = 47 volts on the output side,

capacitance = 16 μF.

The arrangement used for holding and aligning the wires is shown in figure 10.

A two feet length of each wire was taken. The ends of the wire were cut with a sharp razor blade to obtain a cut perpendicular to the axis of the wire. A $\frac{1}{4}$ inch length of each wire projected outwards from the instrument clips. A butt-welded joint was obtained with the axis of both wires lying in the same straight line. A very small pressure was maintained between the butt-ends before passing the discharge. Absence of vibrations was necessary for alignment.

A low resolving (x 50), binocular type, microscope was used for alignment of the wires and examination of the junction. A thermocouple was only accepted if it satisfied the following conditions:

a) junction must be cylindrical in shape and of diameter not greater or less than 0.002 inch, as seen through the microscope. Any appreciable amount of discontinuity at the junction disqualified the thermocouple.

b) The junction must stand 3 - 4 mild jerks. About one razor cut in 15 produced a cut perpendicular to the axis of the wire. Only one discharge in 20 produced an acceptable thermocouple.

Each thermocouple was first calibrated at ice point and boiling point of water to test if the junction gives a steady output. The thermocouples were next calibrated at intervals of $30^{\circ}F$. between $100^{\circ}F$ and $300^{\circ}F$. Only those thermocouples with deviations not exceeding $\pm 3\mu V$ ($\equiv 0.13^{\circ}F$) up to $300^{\circ}F$, were accepted. The calibration value was $44.2^{\circ}F$. per milivolt of thermocouple output.

2.5.2 Mounting.

A yoke-shaped stainless steel carrier was manufactured for rigid thermocouple mounting. Two different yoke types were tried. The first one is shown in Figure 11a. The stainless steel carrier had a groove $\frac{1}{8}$ inch wide and $\frac{1}{8}$ inch deep to retain a small spring. The carrier also had a small perspex piece at either end, joined to it by Araldite type 18. The perspex pieces were grooved with a spacing of 0.006 inch between each V-shaped groove. Grooves on both legs were in a line perpendicular to the vertical axis of the stainless steel carrier.

The thermocouples were fixed and tightened in a special jig, (Figure 12), so that the junctions of all the thermocouples were in line with the vertical axis of the carrier. A small amount of Araldite No. 18 was applied on each end of the yoke and the assembly left to dry for 48 hours and then cured at 80°C. for 2 hours. Six thermocouples were mounted with 0.006 inch spacings between them to cover the whole superheated layer of an assumed thickness of about 0.03 inch.

A spring was fitted in the yoke groove after curing to keep the thermocouples wires taut. The distance between adjacent thermocouple junctions was measured accurately using a Vickers projection microscope. With a magnification of 138.7 $\pm$ 0.6%, distances were measured to an accuracy of better than 1×10^{-4} inch. Figure 13 shows photograph of the thermocouple junctions.

While working at pressures of 7.0 and 14.7 psia, sagging was observed in the thermocouples. It was felt that this might

be due to softening of perspex. It was, therefore, decided to adopt another yoke type carrier as shown in Figure 11b.

The second carrier had no groove for spring and no perspex pieces. Both legs of the carrier were thoroughly cleaned and dried. A small amount of cold cure Araldite was applied to each leg and allowed to set and cure. Excess Araldite was milled out. The Araldite was then levelled and finally grooved with a spacing of 0.008 inch between the V-shaped grooves.

Thermocouples were fixed and tightened as before. A small amount of Araldite was applied and the assembly was cured for 72 hours at room temperature. The distance between the thermo-:couples was measured to an accuracy of 2×10^{-4} inch. using a high power microscope. The cold cure Araldite held the thermocouples firmly in position for pressures up to atmospheric without sagging.

Response time of the 0.002 inch diameter thermocouple was estimated to be about 0.276 millisecond, appendix V.

2.6 TANK ASSEMBLY.

The current carrying conductors were bolted to the top plate of the tank through silicone rubber gasket 'o' rings, care was taken to ensure that the 0.125 inch diameter hole in each conductor was in the same straight line. The gaskets were squeezed against the conductor and perspex plate to provide a leak-proof joint.

A stainless steel tube specimen was selected with care to ensure that there were no kinks, discontinuity or bends on the tube as observed with the naked eye. The tube surface was then

observed under a microscope with a magnification of about x 50. A few small cavities were observed on the surface while the rest of the tube surface was generally smooth but no special selection process was carried out.

The stainless steel tube was inserted between the conductors and then silver soldered. The test length of the section between the conductors was 6 inches. The perspex plate was kept in water to ensure that the heat conducted along the brass conductors did not soften the perspex plate during soldering.

The tube surface was polished with "Brasso" to remove the oxide layer formed on the tube surface during soldering. The surface was then cleaned several times with carbon tetrachloride to remove Brasso, and traces of dirt, oil and grease. The tube was further cleaned with acetone and finally washed with hot, distilled and de-ionized water.

The top plate of the tank was then screwed to the nickel-plated brass frame, the seal being formed by 0.139 inch diameter silicone rubber gasket. The left and right hand side perspex plates were similarly screwed to the frame. The stainless steel approach tubes (to carry stabilising fluid) were inserted and screwed to the conductor using a washer and a thin P.T.F.E. ribbon to provide a leak-proof joint. Silicone rubber 'o' rings were used to provide leak-proof seals between the approach tubes and the perspex sides. The bottom, back and front perspex plates were screwed to the tank and the tank was tested to ensure that it was leak-proof.

Stainless steel voltage taps were fixed on the heating tube.

The distance between clips was measured to an accuracy of ± 0.005 inch. using a travelling microscope.

Glass-enclosed spiral resistance heaters for the bulk liquid were then fixed in the tank and electrically connected. A calibrated thermocouple No. 34, manufactured from nickel-aluminium/nickel-chromium alloy wires, was located in line with the heating tube and at a horizontal distance of 2 inches away from it, to measure the mean bulk temperature of the test liquid. The thermocouples measuring the stabilizing fluid temperature were also fixed in position as shown in Figure 4.

After the tank assembly, it was thoroughly cleaned with tissue paper dipped in acetone and finally with distilled and de-ionized water. The tank was placed in position and connected to the vacuum, stabilizing and power circuits. All thermocouple circuits were completed and checked.

2.7. CHOICE OF TRANSIENT RECORDING SYSTEM.

2.7.1. Requirements of the system.

From Patten [8], Figure 4, bubble radial growth rate in the initial stages of growth was taken as 10 feet per second. Assuming the thickness of the superheated layer to be of the order of 0.03 inch, the maximum frequency of temperature transient was estimated to be 2,000 cycles per second, for a bubble growing on the heating surface immediately below the thermocouple junction. The maximum possible transient amplitude was estimated at 40°F. corresponding to temperature difference between tube wall and bulk liquid for moderate boiling at 1.0 psia.

To check the amplitude and frequency of temperature transient associated with bubble growth, a prototype tank was used. This tank was that used in previous work referred to in [8]. A Ni-chrome wire, 0.018 inch. diameter, was fixed between two current-carrying conductors approximately 6 inches apart. Power was obtained from a 12 Volts D.C. accumulator. A nickel-aluminium/nickel-chromium alloy, 0.002 inch diameter, uninsulated thermocouple was mounted on an adjustable perspex support which was moved in such a way that the thermocouple junction was brought in contact with the wire by manipulation from outside. A vertical movement of the support was also possible and this helped in accurate alignment of the junction near the centre of the wire.

The thermocouple was connected to a Nagard type 103 oscilloscope with internal D.C. amplifier type 103/3 of continuous gain up to 100,000, and also to a Kelvin-Hughes paper recorder type MK5 through a recorder D.C. amplifier. The bulk water in the tank was heated by glass-enclosed spiral heaters situated inside the tank. Vacuum in the tank was produced and maintained by a vacuum pump and Cartesian Manostat.

Under boiling conditions, the 0.002 inch. diameter thermocouple was brought close to the wire surface and the transients were observed on the oscilloscope. When the transient amplitude appeared to be a maximum the recorder was run at the maximum paper speed of 4 inches per second. The response on the recording paper was flat for frequencies up to 100 cycles per second only. This limit of recorder frequency prevented

an adequate recording of fast transients.

A rough check was made on the oscilloscope by comparing the transients against a standard 2 KC/s signal displayed on the second oscilloscope channel. The maximum frequency did not exceed 2 KC/s on visual examination of the oscilloscope screen.

Another attempt was made to record these transients using a drum camera. The transients and a standard 2 KC/s signal was displayed on the scope and a recording was made using Southern Instruments Oscilloscope drum camera type M731 at a speed of 700 inches per second. The circumference of the drum of 20 inches restricted the actual exposure to 30 miliseconds. The small number of high frequency transients made it necessary to try yet another method of photographing the oscilloscope screen.

A single shot Shackman 35 mm. oscilloscope camera was tried and proved successful as a check and much less expensive. Prints of successfully exposed frames were made and analysis of prints confirmed the calculations that the maximum transient frequency was of the order of 2 KC/s. Temperatures as high as 25°F. were recorded in transients for moderate boiling, Figure 14.

This experience showed that neither of these methods was really suitable and the final choice rested on the Ultra-violet recorder type 1185, manufactured by Honeywell Control Ltd. Maximum paper speed on the recorder was 120 inches per second. A possible resolution of 0.010 inch provided a maximum accuracy for time measurement of just under 0.1. m.sec. This is less than the interval between successive frames in high speed film records

at 6,000 frames per second.

In selecting a set of suitable galvanometers, it was noted that galvanometers with high natural frequency had low sensitivity. The maximum transient frequency of 2 KC/s required at least a natural frequency of 3 KC/s for the galvanometer to get response flat to within ± 5% up to 2 KC/s. BBA 3,000 with natural frequency of 3 KC/s were, therefore, found suitable for this investigation. Sensitivity of the type BBA 3,000 galvanometer was 1.22 volts ± 25% per inch deflection depending upon the position of galvanometer in the magnetic block. Minimum sensitivity was, therefore, 1.53 volts per inch deflection on the recording paper.

A D.C. pre-amplifier was required to raise the input level of the thermocouple signal to a value which could give a measurable deflection on the recorder. The maximum transient amplitude was 1 mil/ivolt (equivalent to 44°F.), therefore an amplification of x 2000 was required. The D.C. decade amplifier type AA900, manufactured by Solartron Electronic Group Ltd., was selected. The gain on this amplifier can be selected between x 20 and x 2000 with continuous variation. The use of this D.C. Amplifier increased the minimum sensitivity of thermocouple circuit of 1.53 volts per inch to 1.31 inches per mil/ivolt of thermocouple output.

During actual calibration of the thermocouple-pre-amplifier - UV-recorder combination, the minimum deflection was 1.6 inches per mil/ivolt thermocouple output. For a resolution of 0.010 inch,

the possible accuracy of 0.3°F. of temperature difference was obtained on the recording paper.

Maximum permissible short duration current output from the D.C. amplifier AA900 was 35 milli-amperes. The galvanometer resistance was 100 ohms. This set a limit of 3.5 volts across the galvanometer and at x 2000 amplification, an upper limit of 1.8 millivolts on the thermocouple output.

2.7.2 The cold junction.

To ensure that the upper limit of 1.8 millivolt of thermacouple output mentioned above was not exceeded, the cold junction was necessarily at a steady temperature much higher than 32°F. to reduce the D.C. level to the UV-recorder. It was decided to limit the D.C. component of the signal to less than 0.5 millivolt. The cold junction was, therefore, maintained at about 20°F. below the bulk liquid temperature in the test tank. To avoid confusion, this junction will be termed as "the controlled junction".

A 9 inches diameter x 12 inches high insulated glass tank was used as the controlled junction tank. A steady temperature was maintained with the help of a circulation pump and a glass enclosed spiral heater. A variac was connected across this heater to provide fine control.

The temperature of the controlled junction tank was measured by a thermocouple.

The cold junction ends of the thermocouples measuring bulk temperature in the test tank, stabilizing fluid inlet and

outlet temperatures, and all 0.002 inch diameter thermocouples measuring transients near the tube surface were enclosed in paraffin-filled glass tubes which were supported in the controlled junction tank.

During experiments in which heat transfer coefficients were determined, the controlled junction tank was not heated.

2.8 PHOTOGRAPHIC TECHNIQUE.

2.8.1 The Camera.

For high speed photography, a Fastax camera was used. The maximum film speed obtainable with this camera is 8,000 FPS. Film capacity of the camera is 100 feet x 16 mm.

Since bubble nucleation was random both in time and space, therefore, the choice of both of area of field of view and rate of boiling had to be a compromise. Too small a field of view or too low a rate of boiling resulted in wastage of film stock and experimental time if a bubble failed to develop during the brief (0.8 second) recording period. Too high a rate of boiling had also to be avoided since relating the temperature transients to a specific bubble would have been impossible.

For pressures 1.0 and 3.0 psia, the actual field of view recorded was 3 inches wide. Two stainless steel needles 0.763 inch apart located in the tank beneath the test length and within the field of view acted as fiducial marks. For pressures 7.0 and 14.7 psia, the field of view was reduced to one inch and the needles were 0.706 inch apart.

2.8.2 Lighting.

The lighting system consisted of four 750 watts, 115 Volts reflector lamps. Two lamps, with diffused light, lighted the front of the tank and two lamps were placed behind the tank to provide edge lighting; care was taken to prevent flare in the camera lens. A black velvet cloth was placed behind the tank to increase contrast. The lights were set up, both front and back, about one foot from the tank surface and at an angle of 45° to the camera axis.

To filter infra-red radiation from the light source, perspex filter tanks $\frac{1}{2}$ inch. deep and fille d with 10% copper sulphate solution were placed between the lamps and the tank. This arrangement reduced the intensity of heat from light sources at the tank face to less than 5% of un-attenuated value.

Brightness values at perspex surface were:-

Front 1×10^4 ft. - candles.

Back 6×10^4 ft. - candles.

For photographic purposes using Ilford HPS film stock, an aperture of f5.6 was required with standard 16 mm. aperture slit, for film speed of 6,000 fps. Figures 15, 16 and 17 are general stereoscopic views of the set up. Figure 15 shows Dexion tripod, front lighting and infra-red filters. Figure 16 shows close-up of test tank and front lighting arrangement. Figure 17 shows an oblique view of the relationship between camera and oscilloscope. Cardboard tube connecting oscilloscope and camera was made in two units sliding inside each other to facilitate removal of film.

A close-up of the test tank is shown in Figure 18 in which can be identified current-carrying conductors, stabilising fluid carrying tubes, test section, voltage measuring clips, the thermocouple bridge and the fiducial marks.

The easiest way to examine these pictures in three dimensions is to use a standard stereoscopic viewer. Hold the viewer close to the eye and move the picture backward and forward to obtain focus. When in focus it may be helpful to rotate the picture slightly to obtain fusion. Alternatively, a piece of cardboard held between the eyes, such that one eye can see only one picture, can provide a three dimensional view with no magnification. The distance between the pictures and eye should be adjusted by trial and error.

2.8.3 Synchronization of recording unit.

Two systems were tried for synchronization, the second of which proved more reliable.

In the first system, the available channel of the Fastax camera was used for marking 1 KC/s time base on the edge of the film. The operation of the camera circuit also operated a double pole solenoid which fed a synchronizing marker to the UV- recorder and to a Cossar double beam oscilloscope. The UV-recorder also had a time base of 100 C/s throughout the reading period at a paper speed of 120 inches per second.

The high speed multichannel UV-recorder received signals from three thermocouples while one, fed in parallel the second

channel of the oscilloscope. The display on both oscilloscope channels was imaged on the optical channel of the Fastax camera as shown in Figure 17. Thus, both film and recording paper were marked both with a time base throughout the recording period and a synchronising event signal common to both. The purpose of oscilloscope and double recorded thermocouple recording was to ease the problem of correlating the film and paper record together on analysis.

However, due to excessive load taken by the camera and lights at the moment of switching on, this system proved erratic and unreliable and it was decided to modify the camera circuit.

The final system included a spark timer unit which provided two time marking channels on the camera, one on either edge of the film. Figure 19 shows the final synchronising circuit. It was thus no longer necessary to use an oscilloscope.

The "Goose" control which initiated both camera and lights, was switched on manually an instant after the UV-recorder was switched on. The operation of camera circuit also operated relays A and B. Relay B provided a 1 KC/s timing marker throughout the film on one edge and relay A provided a synchronising mark on the other edge, 0.4 second after switching on the camera. Relay A, Figure 20, also provided the synchronising mark to the recorder.

The total recording time was approximately one second for the film and about 1.5 second for the UV-recorder which was switched offmanually at the end of the film run.

CHAPTER 3.

OPERATING PROCEDURE

3.1 Preparation of tank and heating surface.

At the beginning of each series of tests, the test tank, glass enclosed heaters and the stainless steel heating tube were thoroughly cleaned with acetone to remove traces of dirt, oil etc. Final washing is done by distilled and deionized water. The overall duration of a test series was never more than 8 hours.

3.2 Preparation of water.

Ordinary tap water was singly distilled in a pyrex still. It was then deionized in an ion-exchange deionizer. The purity of this deionized water was tested by measuring the electrical resistivity which was found to be greater than 1×10^7 ohms-cm. Water with resistivity less than or equal to 1×10^7 ohms-cm. was never used in these experiments.

Distilled water was stored in polythene bottles and, at the beginning of each series of tests, this water was freshly deionized to ensure minimum electrical conductivity and, hence, maximum purity.

3.3 Pre-test procedure.

The selection of working pressures within the range 1.0 psia to 14.7 psia in this investigation was based upon the vapour

density of water. The vapour density of water for the selected pressures was in a geometric progression with a common ratio of approximately 2. The selected pressures were 1.0, 3.0, 7.0 and 14.7 psia.

The test tank was filled with freshly distilled and deionized water to a level of 4 inches above the heating tube. This water was next heated by bulk water heaters to a temperature 4 - 5°F. above the saturation temperature corresponding to half the test pressure. The pressure in the test tank was then reduced gradually to half the test pressure, thus causing bulk boiling. Water was then boiled on the heating tube surface for about half an hour under saturated conditions to minimize the quantity of gas absorbed on the heating tube surface and contained in the bulk liquid. After this pre-treatment, vacuum in the test tank was broken completely. This was done so that the bulk temperature could be raised to the saturation temperature for the test pressure quickly by increasing the voltage across the glass enclosed heaters.

3.4 Determination of heat losses in conductors and tubes.

As explained in chapter 2.4.4, the location of thermocouples 1.25 inch distant from the entrance to and exit from the test section introduces an error in heat flux measurements, if the inlet and outlet stabilizing fluid temperatures, T_i and T_o are maintained equal during experiments.

A simple test was devised to estimate the extent of these losses in conductors and tubes, the main source of error, during

experiments in boiling.

With atmospheric pressure in the test tank, stabilizing fluid was passed through the test section at a steady measured flowrate. The temperature of the stabilizing fluid was maintained at a higher temperature than the bulk in the test tank, for different values of bulk temperature in the test tank. Under steady state, values of stabilizing fluid flowrate, Ti, To and Tb were measured.

The extent of losses and necessary correction to be applied during experiments was determined as in Appendix III.

3.5 Determination of nucleate boiling heat transfer rate and critical heat flux.

It was decided to determine heat transfer rates with the temperature difference between tube inner wall and saturation increasing or decreasing in steps of approximately $5^{\circ}F$. A predetermined value of stabilizing fluid temperature for the test pressure was first chosen and the temperature controller and variac were set to provide this value. A fully charged 2 volt accumulator was connected to the potentiometer at least 4 hours prior to the beginning of a test.

The stabilizing fluid pump, D.C. Generator and the vacuum pump were switched on for at least 30 minutes before the start of the test. The output current from the D.C. Generator was less than 20 Amperes. The voltage on the stabilizing fluid heaters was adjusted by the variac to maintain the required steady state temperature of the stabilizing fluid at inlet to the test

section. The flowrate of the stabilizing fluid was adjusted using the by-pass valve.

The water in the test tank was heated up to saturation temperature for the test pressure. The pressure in the test tank was reduced to the required test value with the help of an air leak valve and finally adjusted with the help of the needle valve. Power input to the heating tube was gradually increased to obtain a temperature difference in the stabilizing fluid between inlet and outlet equivalent to losses in conductors and tubes, Figure 21. To be able to apply the correction from Figure 21, the mass flow rate of stabilizing fluid was maintained constant for the whole duration of each experiment.

When steady state conditions were reached, the following quantities were measured in the given order:

Inlet and outlet temperature of the stabilizing fluid, bulk temperature of water in the test tank, controlled junction temperature, voltage drop across the voltage taps, voltage drop across the standard resistance, cold junction temperature, vacuum in the test tank, pressure in the stabilizing fluid tank, stabilizing fluid flowrate and barometric pressure.

The height of water level above the tube surface was recorded both at the beginning and at the end of the test whereas room temperatures was measured at the end of the test.

After the completion of one test, the temperature controller and variac were adjusted to correspond to a new value of stabilizing fluid temperature. Power output from the generator was reduced to about 20 Amperes and vacuum in the test tank was

partially broken. This was done to prevent unnecessary evaporation of water from the tank during the period which the stabilizing fluid will take to attain a new value.

Heat transfer rates were determined from initiation of nucleate boiling up to critical heat flux for pressures of about 1.0, 3.0, 7.0 and 14.7 psia. The critical heat flux at point C, Figure 1, was identified by negligible increase of heat flux for further increase of stabilizing fluid temperature. High speed films of boiling at critical heat flux were taken at 6,000 frames per second, using the Fastax camera for pressures of approximately 1.0, 3.0, 7.0 and 14.7 psia.

3.6 Temperature gradient in the superheated layer.

A nickel-aluminium/nickel-chromium alloy thermocouple, 0.002 inch. diameter butt-welded, was mounted on a yoke shaped stainless steel carrier as described in chapter 2.5.2. The thermocouple was connected to the potentiometer and the distance of the thermocouple junction above the tube was adjusted. The carrier was raised or lowered, as necessary, in steps of 1.25×10^{-3} inch. in such a way that the thermocouple junction always remained on the vertical centre line of the tube. The micrometer arrangement is shown in Figure 22.

Steady state conditions were reached as in chapter 3.5, for initiation conditions, point B on Figure 1. The initiation temperature was obtained from the experiments described in chapter 3.5.

The thermocouple junction was taken a distance of 0.1 inch

above the tube and first reading was taken. The distance of the thermocouple junction from the tube was measured by a travelling microscope. It was necessary to damp the galvanometer since the drift due to convection currents was large. The thermocouple junction was lowered towards the tube in steps of 0.005 inch and the temperature in the layer was measured by the potentiometer. Shorter steps of 0.0025 inch were taken nearer the tube surface.

The nearest position of 0.002 inch. diameter thermocouple junction was 0.001 inch at which distance the junction touched the heating tube surface. The thermocouple junction-heating tube contact was determined optically by a telescope/microscope of magnification x 50. Since the outside surface of the junction was slightly oxidized, it was difficult to ascertain electrical contact.

The temperature gradient in the superheated layer was measured at or slightly below the initiation temperature for pressures of about 1.0, 3.0, 7.0 and 14.7 psia.

3.7 Recording of temperature transients.

The yoke carrying one 0.002 inch diameter thermocouple described in chapter 3.6 was removed and replaced by the stainless steel yoke carrying six thermocouples. This was fixed in position inside the tank and adjusted to ensure that the junctions were in line with the centre line of the heating tube. The end of these 0.002 inch. diameter thermocouples were soldered to extension wires of the same material, 34 SWG, which connected with the controlled junction tank via the top plate

of the test tank. The thermocouple output leads were connected to the D.C. Amplifers and UV-recorder.

The D.C. Amplifiers and UV-recorder were switched on at the same time as the stabilising fluid pump and vacuum pump, i.e. 30 minutes before the start of the actual test. Steady state conditions were attained for moderate boiling and the same quantities were measured as in chapter 3.5.

The amplification on the D.C. Amplifiers was increased to x 2000. The thermocouple carrier was lowered until the thermocouple output from the three (or two) chosen thermocouples displayed large temperature transients on the screen of the Ultra-Violet recorder. A minimum of 0.006 inch. distance was maintained between the top of the tube and the centre of the nearest thermocouple junction.

Glass enclosed heaters in the test tank and controlled junction tank were disconnected an instant before the actual transient recording. This was necessary to reduce the A.C. signal picked up by the 0.002 inch. diameter thermocouples to a minimum. The recording on film and UV-sensitive paper was completed in about one second, at the end of which the UV-recorder was switched off manually.

The generator and the stabilising fluid pump were switched off to stop boiling and convection currents in the water near the tube surface. The distance between the thermocouple nearest to the heating tube and the top of the heating tube was measured by determining the vertical displacement necessary for the thermocouple to contact the heating tube. The accuracy of

measurement was $\pm 6.2 \times 10^{-4}$ inch. The contact between the junction and the tube was ascertained optically using the telescope/microscope placed at the back of the test tank.

At the end of the test run, the vacuum in the tank was completely broken by admitting air through the air admittance valve. The height of the water level above the heating tube and the room temperature were recorded.

CHAPTER 4.

RESULTS AND DISCUSSION OF RESULTS.

4.1 Heat transfer rate and critical heat flux.

4.1.1 Heat transfer rates.

Heat transfer rates were determined for nucleate pool boiling of water under saturation conditions for pressures of approximately 1.0, 3.0, 7.0 and 14.7 psia, from the natural convection region, AB on figure 1, up to and including the critical heat flux. As has been explained in Chapter 2, the use of a stabilizing system permits determination of critical heat flux without danger of burnout. The experimental results are presented in table 1 to table 12 and in figures 23 to 27 which are log - log plot of heat flux v temperature difference between tube outer wall and saturation. Three different series of tests were carried out for each of the four pressures. In the first series, the temperature difference between wall and saturation ($T_w - T_s$) was increased in steps of approximately $5^{\circ}F$. The second series was carried out for decreasing wall temperatures starting at the critical heat flux. The third series was a repetition of the first series. By comparing the results of the three series for any one pressure, it is observed that the results are consistent and reproducible within limits of $\pm$ 2%.

The experimental results for the three series at an average pressure of 1.03 psia are plotted in figure 23. The experimental results of Braunlich [14] at 1.3 psia, Cryder and Finalborgo [15] at 0.6 psia and 2.16 psia, Van Stralen [16] at

1.93 psia and Patten [8] at 0.935 psia are also plotted in figure 23 for comparison.

The experimental results for the three series at an average pressure of 2.97 psia are plotted in figure 24. The experimental results of Braunlich [14] at 2.25 psia, Cryder and Finalborgo [15] at 2.16 and 4.3 psia, and Van Stralen [16] at 1.93 psia and 3.87 psia are also plotted in figure 24 for comparison.

The experimental results for the three series at an average pressure of 7.01 psia are plotted in figure 25. The experimental results of Braunlich [14] at 6.0 psia and 8.13 psia, Cryder and Finalborgo [15] at 8.8 psia, Nishikawa and Urakawa [17] at 6.03 and 9.96 psia, and Van Stralen [16] at 8.13 psia are also plotted for comparison in the same figure.

The experimental results of the three series at an average pressure of 14.7 psia are plotted in figure 26. The experimental results of Braunlich [14], Cryder and Finalborgo [15], Van Stralen [16] and Nishikawa and Urakawa [17] are also plotted, for a pressure of 14.7 psia in each case, in figure 26 for comparison.

The experimental values of heat flux obtained in this investigation at pressures of approximately 1.0, 3.0, 7.0 and 14.7 psia are plotted in figure 27 against temperature difference between tube outer wall and saturation. For a fixed temperature difference (Tw-Ts), the heat transfer rate increases with increase in pressure. This observation is in agreement with the work of other authors, Braunlich [14], Cryder and Finalborgo [15], Van Stralen [16], Nishikawa and

Urakawa [17], Bonilla and Perry [18] and Cichelli and Bonilla [19].

In figure 23, the experimental results of Patten [8] for a pressure of 0.935 psia fall slightly on the right of the experimental values obtained in this work at a pressure of 1.03 psia and, therefore, conform to the general pattern. The stainless steel tube used in this investigation was polished and, therefore, the surface of the tube had fewer nucleation sites. Large temperature differences (Tw-Ts) for moderate boiling are to be expected for such a heating surface, Kurihara and Myers [20]. The experimental points are, therefore, on the right of those obtained by Cryder and Finalborgo. The same observation is made from figures 24, 25 and 26.

From established boiling up to about 80% critical heat flux, the heat transfer rate q may be related to the temperature difference Tw-Ts by an empirical relationship of the type,

$$q \propto (Tw-Ts)^{x}$$

where x is a constant.

The values of x for 1.0, 3.0, 7.0 and 14.7 psia are 5.9, 5.4, 5.5 and 4.6 respectively. These values of x may be compared with values at higher pressures obtained by other authors. Rohsenow [5] has suggested a value of ~~2~~ 3 ? and Levy [6] a value of 3. Higher values of x at sub-atmospheric pressures were expected since the ratio of heating tube diameter to maximum bubble diameter was low. Effect of each bubble on heat flux will be large for large bubble diameters.

Bonilla and Perry [18] have proposed a relationship which correlates the temperature difference (Tw-Ts) to pressure,

for a constant heat flux. The relationship is,

$$(\Delta T)_p = (\Delta T)_1 \; p^{-\frac{1}{4}} \qquad (2)$$

where

$(\Delta T)_1$ = (Tw-Ts) at atmospheric pressure and a specified heat flux in boiling.

and $(\Delta T)_p$ = (Tw-Ts) at a pressure of p in atmospheres for the same heat flux.

For a constant heat flux, the ratio $\frac{(\Delta T)_p}{(\Delta T)_1}$ for pressures of 1.0, 3.0 and 7.0 psia, from equation (2), is 1.95, 1.5 and 1.2 respectively. The corresponding experimental values from figure 27 are 1.6, 1.4 and 1.34. Equation (2) fits the experimental data of Addoms, from [1], at higher pressures up to 2500 psia satisfactorily. It may be that the ratio of temperature differences may also be dependent on nucleation characteristics of the heating surface or liquid properties which become significant only at low temperatures and pressures.

The experimental values of critical heat flux in saturated pool boiling of water in the range 1.0 psia and 14.7 psia are plotted in figure 28. Other experimental values available in literature, in this pressure range, are those of Patten [8] for boiling on a wire of 0.018 inch diameter, Braunlich [14], Van Stralen [16] for a wire of 0.02 inch diameter, and Lienhard and Schrock [21] for a wire of 0.02 inch diameter. The values of critical heat flux for water from these references are also plotted in figure 28 for comparison. The lower values

of critical heat flux obtained by other authors is expected. It is shown in chapter 5 that for boiling on wires or small diameter tubes, at a pressure where the maximum bubble diameter is larger than 4 times the heater surface diameter, the critical heat flux depends upon the diameter of the heating tube or wire and may be assumed as,

$$q_{cr} \propto do^{0.156} \qquad (3)$$

From equation (3), the ratio of critical heat fluxes for a tube of 0.125 inch diameter and a wire of 0.02 inch diameter, when the bubbles surround the heating surface completely at low pressures, is 1.36, i.e. an increase of 36%, in the value of critical heat flux, over the values for wires of 0.02 inch diameter can be expected in this investigation. The results from literature are modified using equation (3) to correspond to a tube of 0.125 inch diameter and plotted in figure 29. Comparison is satisfactory. A maximum deviation of $\pm$ 24% is obtained between the results of Patten, Lienhard and Schrock and the values obtained in this investigation.

Reference may be made to the curve due to Bernath [7] at atmospheric pressure, figure 2. From this curve, for a heater diameter of 0.03 inch or less,

$$q_{cr} \propto do^{\frac{1}{2}}$$

which does not agree with equation (3). According to Bernath's curve, for heater diameters of more than 0.03 inch, the effect of diameter on critical heat flux reduces gradually until a diameter of about 0.06 inch, after which the critical heat flux is independent

of heater diameter. As shown in chapter 5, the heater size of 0.03 inch corresponds to a maximum bubble diameter of 0.12 inch, for no effect of heater diameter on critical heat flux. At atmospheric pressure, the maximum bubble diameter obtained in this work is between 0.10 inch and 0.19 inch.

For reasons stated in chapter 5, provided that the bubble departure diameter is small compared to heater diameter, the heater size should have no effect on the critical heat flux, at higher pressures.

From experimental results in figure 28, it is noted that the critical heat flux increases with increase in pressure. Also, the critical temperature difference (Tw-Ts) cr. decreases with increase in pressure, figure 27. The value of critical temperature difference at 1.0 psia is about 80-84°F. compared with a value of 60°F. at 14.7 psia.

4.1.2 Accuracy of measurement.

4.1.2.1 Heat flux (q)

Voltage measurement.

The error in voltage measurement due to voltage fluctuations from the power supply, and due to limits of accuracy of the potentiometer, was less than ± 0.15%.

Current measurement.

Error due to change in current drawn by the heating tube because of fluctuations of voltage across the heating tube and average temperature of the tube, was less than ±1% in the worst case of boiling near maximum heat flux. This was

determined by measuring the minimum and maximum values of voltage drop across the standard resistance over a period of one minute during the test.

Surface area of tube.

The diameter of the stainless steel tube, 0.125 inch, was assumed constant over the test length. The maximum variation was less than ± 0.0001 inch along the length of the tube. Error due to edge thickness of voltage taps and measuring error in distance between voltage taps was less than ± 0.3%.

Error in measurement of heat losses in conductors and tubes.

Accuracy of the natural convection equation is ± 30%. Maximum possible error in determination of heat losses due to the use of natural convection equation was less than ± 25%, since the heat energy dissipated by losses in tubes and conductors was larger than the heat dissipated by natural convection, appendix III.

For the worst case, in the pressure range from 1.0 psia to 14.7 psia, at 1.0 psia (largest (T_w-T_s) cr. for smallest $q_{cr.}$) these losses amount to 10% of the critical heat flux values. Therefore, maximum error in heat flux measurement due to error in estimation of losses = ± 2.5%.

If e_v, e_i, e_a and e_e denote the percentage errors in voltage, current, surface area of heating tube and estimation of heat losses measurements, then error in heat flux measurement (e_q) is obtained by, Wilson [22],

$$e_q = \sqrt{e_v^2 + e_i^2 + e_\omega^2 + e_t^2}$$

from which, a value of maximum percentage error in heat flux measurements is calculated as ± 2.7%.

4.1.2.2 Outer tube wall temperature (Tw).

Error in tube inner wall temperature due to error in temperature measurement of the stabilizing fluid = ± 0.12°F. (Appendix IV).

Maximum possible error in thermocouple calibration = ± 0.35°F.

Maximum possible error in intermediate junction temperature = ± 0.05°F.

Maximum possible error in cold junction temperature = ± 0.05°F.

Therefore, maximum possible error in average wall temperature (Tw) = ± 0.57°F.

4.1.2.3 Bulk temperature measurement (Tb).

Maximum possible error in calibration = ± 0.35°F.

Maximum possible error in measurement = ± 0.1°F.

Maximum possible error in intermediate junction temperature = ± 0.05°F.

Maximum possible error in cold junction temperature = ± 0.05°F.

Therefore, maximum possible error in bulk temperature measurement (Tb) = ± 0.55°F.

4.1.3 Analysis of high speed film records at critical heat flux.

One film of 100 feet length was taken at a maximum speed of 6000 fps, at critical heat flux in saturated pool boiling, for each of the four pressures, 1.0, 3.0, 7.0 and 14.7 psia.

The total surface area of the tube available for boiling was 2.36 square inches. 1.59 square inches of this surface area was recorded on the high speed films at critical heat flux. Since the heating surface was cylindrical, only half of this 1.59 square inches was actually visible in the films. Grids were set up on the projected area to correspond to equal areas of the tube surface. The total number of grids was 462 over the actual area of the tube of 0.795 square inch, visible on the films. Films taken at 1.0 and 3.0 psia were analysed frame by frame for percentage of heater surface area in contact with liquid.

The value of critical heat flux for the film at 1.0 psia is 2.6×10^5 B.t.u. per square feet per hour at a temperature difference (Tw-Ts) of $84.8^{\circ}F$. The percentage of surface area in contact with liquid for this pressure is plotted in figure 30. The time average percentage area of heating tube surface in contact with water is $16.4 \pm 1.6\%$. The maximum value of percentage area of heating surface in contact with liquid was 52% and the minimum value was 0% which did not last for more than 4 milliseconds, figure 30.

The critical heat flux value for the film at 3.0 psia is 3.06×10^5 B.t.u. per square foot per hour at a temperature

difference of 82.1°F. The percentage of surface area in contact with liquid is plotted in figure 31. The time average percentage area of heating tube - water contact is 7.1 ± 0.7%, the maximum value was 22% and the minimum was 0% which did not last for more than 9 milliseconds.

Figures 32, 33, 34 and 35, which are reproduced from the high speed films taken under critical conditions at 1.0, 3.0, 7.0 and 14.7 psia respectively, show clearly that liquid - solid contact exists under critical conditions. A short length of the film from each of the above four films is included as a supplement to this thesis. From a visual examination of the films taken at all four pressures, it is clear that some liquid-solid contact always existed under critical conditions in saturated pool boiling in these tests, ignoring a short spell of 4 milliseconds out of 680 milliseconds at 1.0 psia and another of 9 milliseconds duration out of 510 milliseconds at 3.0 psia when there was no liquid - solid contact. If a larger heating tube area were considered, these short durations will also show some liquid - solid contact.

These short durations of zero liquid - solid contact, which exist due to a small size of the heating surface used in experiments, could account for departure from stable conditions in a non-stabilized heating surface.

It is also noted that bubbles are spherical in early stages of their growth and that bubble departure equivalent diameter reaches a value very nearly equal to the bubble departure diameter at low heat fluxes. Actual measurements of maximum

bubble diameter at critical heat flux are made and discussed later in this chapter. This observation is contrary to the suggestion by Zuber [23] that a change in diameter by as much as ten times may occur between boiling at critical heat flux and boiling at low heat fluxes.

It is observed from these films that the behaviour of bubbles is chaotic both in time and space. After initiation of a bubble and for a fraction of its total growth period, a bubble is spherical. For most part of the growth period afterwards, the bubble is distorted to an unrecognizable shape and is surrounded by other bubbles. Bubbles touch and coalesce with other bubbles either originating from the same site or from the neighbouring site. Not all bubbles grow to the same maximum size under these conditions. Some bubbles touch and coalesce with other bubbles in early stages of their growth and do not develop to the same maximum size.

It is also noted that the removal of the vapour bubbles from the surface is limited due to the limiting velocity of the vapour phase away from the heating tube. In other words, if bubbles could be removed faster from the heating surface, there will be more area available for heat transfer between solid and liquid and higher heat fluxes will result. This evidence suggests that the critical heat flux is limited by the average vapour velocity away from the heating surface. The average vapour velocity will depend upon the buoyancy forces and drag forces on the bubble.

A further increase in surface temperature of the heater will reduce the minimum necessary duration of liquid - solid

contact for nucleation and, hence, more blanketing of the heating surface takes place. The heat transfer rate accordingly begins to fall.

Therefore, a maximum limit to the critical heat flux is set due to hydrodynamic forces only, i.e. burnout is believed to be primarily a hydrodynamic phenomenon. The possibility of a thermodynamic instability is discarded on grounds that various authors [8,10,24] have observed that critical heat flux is independent of (Tw-Ts) cr.

Approximate maximum bubble diameters were measured under critical conditions, just before coalescence, by the method of counting squares on the projected image of the bubble. From this area was then deduced the diameter of an equivalent circle, this diameter being taken as the maximum bubble diameter at departure. These bubble diameters are compared in table 13 with maximum bubble diameters obtained at low heat fluxes in this investigation. From comparison, it is noted that the bubble departure diameter vary little between boiling at low heat fluxes and critical heat flux. The diameter of a fully developed bubble at critical heat flux was never less than 60% the diameter at low heat fluxes. This is not unexpected since, as assumed in chapter 5, the departure diameter only depends upon the energy available in the superheated layer. Figures 36, 37, 38 and 39 show one such developed bubble under critical conditions at pressures of 1.0, 3.0, 7.0 and 14.7 psia respectively.

Measurement of liquid - solid contact area under critical conditions was not carried out for pressures of 7.0

and 14.7 psia. Since the maximum bubble diameters for these higher pressures were small, and the bubbles did not envelop the heating surface completely, those bubbles which formed on the underside of the horizontally mounted tube were found to "climb" up along the tube periphery and then to leave the surface. For small maximum bubble diameters, the average frequency of bubble formation and total number of bubbles per unit area were large. Under these conditions, it was too difficult to determine the projected liquid - solid contact area.

4.2 Temperature gradient in the superheated layer above the heated cylindrical surface.

Figures 40, 41, 42, 43 and 44 show the temperature gradient in the superheated layer measured above the horizontal heated tube. The thickness of the superheated layer, assuming steady state conduction only, is given by a broken line on each of these figures. Figures 40, 41 and 42 show the temperature gradient in the superheated layer in the natural convection region, AB on figure 1. Figures 43 and 44 show the temperature gradient in the superheated layer at initiation.

These figures show that the thickness of the superheated layer on top of the horizontal tube is three to five times the thickness given by the conduction equation for steady state conditions. This is not unexpected because of the convection currents above the heated surface.

Jakob [26] has presented temperature distribution for a similar geometry. Photographs show the temperature

distribution around a hot horizontal cylinder in air, using Schlieren and Interferometric technique. From figure 27.12 of the above reference, it is observed that the thermal layer thickness at the sides and bottom of the cylinder is much less than the top of the cylinder. This is due to convection currents set up in hot air above the cylinder.

Figure 27.5 of the above reference shows that the heat flux at the side and bottom of the cylinder is higher than the top of the cylinder. Since the thickness of the layer is larger at the top, the heat transfer rate will be smaller.

If the average thickness of the superheated layer around the tube is considered, the thickness will, obviously, be less than shown by measurements for the top of the tube, in figures 40, 41 and 42.

In the established boiling region, however, these convection currents are very insignificant since the superheated layer is constantly broken by the bubbles growing and departing from the heating tube. The time average thickness of the superheated layer at any position around the circumference of the heating tube may be assumed to be constant if measured under boiling conditions. In other words, heat transfer rate may be assumed to be constant around the periphery of the tube.

Figures 43 and 44 show the temperature gradient in the superheated layer at initiation, point B on figure 1. It is observed that the thickness of the superheated layer is twice that given by conduction equation, compared to three to five times in figures 40, 41 and 42. This is not unexpected

because as explained above, natural convection currents are significantly less in boiling.

Examination of the experimental points in figures 40 to 44 suggest that a linear temperature gradient may be assumed to represent the temperature gradient in the superheated layer.

Consider a semi-infinite slab of thickness b_1, fabricated from material of thermal conductivity k. If the temperature at its two faces is maintained at Tw and Tb, then the amount of heat transferred across the slab is given by,

$$q_v = \frac{k\,(Tw-Tb)}{b_1} \qquad (4)$$

In boiling of liquids, the superheated layer is being constantly agitated by bubbles growing and departing from the heating surface. Due to this constant agitation of the superheated layer, heat transfer rate in convection will be higher than in pure conduction. For the same value of k, Tw-Tb and b_1, the value of heat flux q_v will be higher in convection than in conduction. Alternatively, if the heat fluxes in convection and conduction are considered to be the same, then the thickness of the superheated layer will be larger in convection due to agitation effects. Therefore, for convection when steady state has reached after the departure of a bubble,

$$b = \frac{k\,(Tw-Tb)}{q_v}\,\lambda_1 \qquad (5)$$

where λ_1 = constant.

and b = thickness of superheated layer in convection.

Comparison of the experimental points and conduction equation in figures 43 and 44 give a value of λ_{eq} equal to 2.0 $\pm$ 0.05. In other words, it may be assumed that, in boiling, the thickness of the superheated layer at bubble initiation is equal to twice the equivalent thickness in case of pure conduction.

4.3 Analysis of bubble growth rate and maximum bubble diameter data at low heat fluxes.

Twenty films, each one hundred feet long, were analysed for growth rate and departure diameter of bubbles. These films were produced at 6,000 fps. Frame by frame analysis was made on a LYTEX IV-16 analysing projector, figure 45. The overall magnification on the projector screen was 1.99 times the original dimensions for films taken at pressures 1.0 and 3.0 psia. The error in measuring diameters at these two pressures was never more than $\pm$ 0.02 inch. Bubbles which were spherical during growth were measured over the whole growth period. Bubbles which either joined other bubbles in early stages of their growth or were distorted for some other reason were ignored during bubble dimeter measurements. The bubble diameter for any one bubble was measured from initiation up to its maximum size at departure. These diameters were measured in two planes perpendicular to each other and the arithmetic mean was assumed to be the characteristic diameter of the bubble at any instant of time. Further, the bubble was assumed spherical and the volume

of the bubble was calculated from this diameter. The volume of the tube covered by the bubble was subtracted from this volume to arrive at the true volume of the vapour in the vapour bubble. Regression lines, assuming $v = \lambda_2 t^{x_1}$, were obtained for these corrected volumes separately for each bubble using a Ferranti SIRIUS computer. Also, the diameter of an equivalent sphere was calculated from the corrected volume.

The overall magnification on the projector screen of the analysing projector was 4.27 times the original dimensions for films taken at pressures of 7.0 and 14.7 psia. The error in measuring diameters at these pressures was never more than $\pm$ 0.01 inch. Since bubbles at 7.0 and 14.7 psia did not envelop the tube, correction for tube volume was not applied at these two pressures. Regression lines for bubble volumes at 7.0 and 14.7 psia were also obtained for each individual bubble using the SIRIUS programme.

The pressure range covered in this analysis is 0.95 to 14.7 psia. Bubble diameters, volumes and regression lines for bubble volumes are plotted against time in figures 46 to 72.

Bubble diameters v time for 16 bubbles are plotted to a linear scale in figures 46 and 47 for pressures ranging between 0.95 and 1.06 psia. The corrected volumes for these bubbles are plotted on a log - log field in figures 48, 49 and 50, and regression lines for volumes are plotted in figure 51. The exponent of t for regression lines in figure 51 for approximately 1.0 psia varies between 1.91 and 3.45 with an arithmetic average of 2.25. If the diameter of the bubble

at any time is written as a function of time in the form,

$$D = \lambda_2 t^{x_2} \qquad (6)$$

then the arithmetic average values of λ_2 and x_2, for 1.0 psia, are 2.24 and 0.75 respectively. D and t are measured in feet and seconds respectively.

Bubble diameter v time for 17 bubbles are plotted to a linear scale in figures 52, 53 and 54 for pressures between 3.03 and 3.08 psia. The corrected bubble volumes for these bubbles are plotted on a log - log field in figures 55, 56 and 57, and regression lines for volumes are plotted in figure 58. The exponent of t for regression lines plotted in figure 58 for approximately 3.0 psia varies between 0.925 and 2.225 with an arithmetic average of 1.415. From equation (6), the arithmetic average values of λ_2 and x_2 are 0.51 and 0.47 respectively.

Bubble diameter v time for 18 bubbles at a pressure of 7.0 psia are plotted to a linear scale in figures 59, 60 and 61. Bubble volumes for these bubbles are plotted on a log - log field in figures 62, 63 and 64, and regression lines for volumes are plotted in figure 65. The exponent of t for regression lines plotted in figure 65 for 7.0 psia varies between 1.075 and 1.576 with an arithmetic average of 1.33. From equation (6), the arithmetic average values of λ_2 and x_2 are 0.30 and 0.44 respectively.

Bubble diameter v time for 18 bubbles at pressures of 14.23 and 14.8 psia are plotted to a linear scale in figures 66, 67 and 68. Bubble volume for these bubbles are plotted on a log - log field in figures 69, 70 and 71, and

regression lines for volumes are plotted in figure 72. The exponent of t for regression lines in figure 72 for pressures of 14.23 and 14.8 psia varies between 0.527 and 1.607 with an arithmetic average of 0.975. From equation (6), the arithmetic average values of λ_2 and x_2 are 0.041 and 0.325 respectively.

The maximum, minimum and average values of x_2 and average values of $\lambda 2$ for various pressures are tabulated in table 14 for easy comparison.

The growth rate of bubbles for saturated boiling at atmospheric pressure were also obtained by Zmola [27]. The exponent of t varied between 0.25 and 0.44 compared to the values obtained in this work between 0.176 and 0.53.

Such large variations in growth rate of a bubble among various bubbles at the same pressure confirm the non-steady nature of the conditions existing in the superheated layer when a bubble nucleates. This factor of uncertainty precludes the formulation of an exact physical model. Analytical expressions for bubble growth rates cannot, therefore, account for such wide variations.

The average value of x_2 in equation (6) is found to decrease with an increase in pressure, in these experiments. For low pressures, and high initiation temperatures, the total amount of energy of the superheated layer per unit area is larger than higher pressures. The required high initiation temperatures and high vapour specific volume may, perhaps, explain large growth rates in boiling at low pressures.

The distance of centre of gravity of the bubble from the top of the heating tube is plotted in figures 73, 74, 75 and

76. Time reference for all bubbles at a pressure of 1.06 psia, plotted in figures 73, 74 and 75, is taken at the time of bubble nucleation. When the bubble has completed its growth and is about to leave the heating tube, the position of its C.G. is plotted v time to a linear scale. In figure 76, time reference is taken when the bubble is about to leave the heating tube, at 3.08 psia. This was done because it was not possible to ascertain the exact time of initiation of the bubble. In figure 77, for a pressure of 7.0 psia, the distance of top of the bubble from top of the heating tube is plotted. This was considered necessary since, as explained earlier, the bubbles were found to "climb" along the tube periphery while departing.

From all the eleven bubbles plotted in five figures, the slope of the distance of C.G. of the bubble with time is linear, just before the bubble leaves the heating tube. In other words, the bubble reaches a constant velocity before it leaves the heating tube. This bubble departure velocity will depend upon the buoyancy and drag forces on the vapour bubble. To check this, the buoyancy force was equated to the drag on the vapour bubble and the drag coefficient was determined for bubbles at each of the three pressures, viz. 1.0, 3.0 and 7.0 psia. These experimental values of drag coefficients were compared with the drag coefficients for freely rising vapour bubbles, given by Cole [42]. For 1.0 psia, the drag coefficient agrees with the experimental value for the bubble sphericity of 0.89. Similarly, the value of C_D for 3.0 and 7.0 psia corresponds to sphericities of 0.90 and 0.96

respectively given by Cole [42] . These values show agreement with theory.

4.4 Temperature transients in the liquid near the heating tube.

The temperature transients in the liquid near the heating tube associated with bubble growth and departure v time are plotted to a linear scale in figures 78 to 90. The distance of the bubble wall from thermocouple junction is also plotted in each case and is shown by heavy lines.

The transient recording thermocouple picked up a certain amount of D.C. from the D.C. field in water during experiments in boiling. This could not be avoided without increasing the A.C. pick up to a high level. The extent of D.C. pick up varied from experiment to experiment depending upon the electrical conductivity of water in that experiment and the voltage across the busbars. However, during the filming and recording period of about one second during a test, it was assumed that the electrical conductivity of water and the voltage across the busbars remained constant.

In an effort to determine the change in D.C. field pick up when a bubble covered the thermocouples, a nickel-aluminium wire, 0.002 in diameter, was mounted instead of the thermocouples and connected to the recorder through the D.C. amplifier. Water which had been used in previous tests, and remained in the test tank for more than three weeks, was used for this test. Under similar boiling conditions as the tests for temperature transient recordings, change in D.C. field pick up of less than 0.12 inch vertical displacement on the recording paper took place

at 1.00 psia when a bubble enveloped the thermocouple bridge completely. This was equivalent to less than 3.0°F.

Very pure water was used in actual experiments and, therefore, D.C. pick up and change in D.C. pick up should be even smaller. However, this change in the amount of D.C. pick up did not effect the results since temperature measurements on the recording paper were discontinued after the bubble surrounded the thermocouple junction. Temperature transients of direct interest only occurred when the junctions were covered in liquid, and, therefore, measurements of transients does not include an error due to change in D.C. field pick up.

The datum on transient records was fixed at saturation temperature for that pressure. The position of the signal on the recording paper to correspond with saturation temperature was decided as follows:

The synchronizing marker on the high speed film and recording paper synchronized one particular frame to a fixed position on the recording paper. A 1KC/s time marker on the film and a 100 C/s time marker across the recording paper throughout the recording period made it easy to relate any particular frame on the film to the corresponding position on the recording paper.

During bubble growth, the bubble wall covered the thermocouple junctions when the bubble was growing in the vicinity of the junction. The frame in which the bubble wall has completely covered the thermocouple junctions was taken as the frame corresponding to saturation temperature on the recording paper. The corresponding position of the temperature signal

on the recording paper was then determined by synchronizing marker. This temperature signal was assumed to correspond to saturation temperature and, hence, the datum.

The error, therefore, in temperature position in transient measurement was chiefly due to calibration of thermocouple - amplifier - recorder combination, besides the error in ascertaining the exact position of saturation temperature datum on the recording paper.

The maximum possible error was calculated as follows:

Maximum possible error due to A.C. pick up = ± 0.03 inch.

Maximum possible error in calibration of the thermocouple - amplifier - recorder combination = ± 0.02 inch in 1.5 inches.

Measuring accuracy of signal on paper record = ± 0.02 inch.

∴ Overall accuracy = ± 0.07 inch

= ± 1.75°F.

Error in synchronization of time.

Error in synchronization of time = ± 0.01 inch.

Measuring error in time base = ± 0.01 "

∴ Overall error in time = ± 0.02 "

= ± 0.16 millisecond.

Figure 78 shows the temperature variations associated with a bubble initiating at a distance of 1.02 inch from the thermocouple junction, zero millisecond corresponding to initiation as time reference. The thermocouple nearest to the tube, at 0.019 inch, records a maximum temperature of 39°F. at 18 milliseconds after the initiation of the bubble, when the

bubble wall is 0.3 inch away from the thermocouple junction. Maximum possible transient is equal to 46.5°F. corresponding to Tw-Tb. A second maximum is recorded when the bubble wall is very close to the thermocouple junction. All the three thermocouples recorded rather similar temperature transients but are separated on the time base. The thermocouple farthest away from the top of the tube recorded the temperature maximum after the other two thermocouples.

Since there was no other bubble on the 3 inch length of the tube photographed in the test, it is safe to assume that the temperature transient was caused by the bubble 07B1 only. The recording of a peak temperature long before the bubble wall reaches the thermocouple suggests that at the initiation and early growth of a bubble, a disturbance is transmitted throughout the liquid. This [redacted] disturbs the superheated layer and consequently hot liquid is pushed away from the heating surface in the form of a temperature "fin" travelling along the heating tube.

When the pressure pulse reaches the superheated layer just below the thermocouples, the layer travels away from the heating tube at a finite velocity and will take a certain finite time to travel from one thermocouple to the next. Therefore, the temperature transients will be separated on the time base.

In figure 78, at any temperature, the separation of transients recorded by the thermocouples at 0.019 inch and 0.043 inch above the heating tube is 5 to 6 milliseconds, to record the same temperature. If the temperature gradient in

the layer, the thickness of the layer and the velocity of the layer perpendicular to the heating tube are assumed constant during the time the layer travels from one thermocouple to the next, then the vertical velocity of the superheated layer is between 4.0 and 5.0 inches per second. This velocity will depend upon the velocity of the pressure pulse travelling radially in all directions.

At 17 milliseconds from the datum, the temperatures recorded by thermocouples 1, 2 and 3 are 36.4, 18.7 and 0.4°F. at distances of 0.019, 0.031 and 0.043 inch from the tube surface respectively. The recorded temperature difference between thermocouples 1 and 2 is 17.7°F. and between thermocouples 2 and 3 is 18.3°F, both for the same distance of 0.012 inch between them. Allowing for errors in measurements, the temperature gradient in the superheated layer is approximately linear.

If the pressure pulse is assumed to initiate at the same time as a bubble, then time taken by the pulse to travel a distance of 1.02 inch is equal to 10 milliseconds. i.e. a pulse velocity of 8.5 FPS along the tube. Radial growth velocity of the bubble 07B1 when first visible is about 6.6 FPS. Actual growth velocity at initiation will be higher than 6.6 FPS, and perhaps may be of the order of 8 - 9 FPS.

At an average pressure of 1.0 psia, the growth rate of the bubbles in the visible region, after initiation, for 9 different bubbles, growing at distances between 0.14 inch and 1.7 inch from the thermocouple junction, was compared with the

pressure pulse velocity. The temperature transients associated with the bubbles so measured are plotted in figures 78 to 85 and the growth rates at initiation and pressure pulse velocities for these bubbles are presented in table 15. By comparison between the pressure pulse velocity and bubble growth rate at initiation, it is found that the two values are of the same order.

The growth rate at initiation was also measured at 3.0 psia for six bubbles and compared with the pressure pulse velocity in table 15. The comparison is similar to results at 1.0 psia. The temperature transients for three typical bubbles at 3.0 psia are plotted v time to a linear scale in figures 86, 87 and 88.

The recording of second maxima on figure 78 is due to bubble wall pushing the superheated liquid from the heating surface over the thermocouple junctions. The presence of second maxima is also shown in figures 80, 81 and 86.

Temperature transients in the superheated layer after the bubble has left the heating surface are recorded in figures 89 and 90.

The departing bubble produces eddy currents in the liquid resulting in an upward "lift" of the superheated layer. Turbulence in the superheated layer after the departure of a bubble, figure 90, is of low frequency compared to the turbulence created in the superheated layer by the growing bubble. The temperature records show that the overall effect of turbulence is greater after bubble has left than the growth phase.

As shown earlier, the layer has a finite vertical velocity due to the disturbance created by the growing bubble. If the spacing in adjacent thermocouples were increased, the effect on temperature transients records will be two fold. Firstly, the separation of transients on the time base will be large as recorded by various thermocouples and, secondly, the peak temperatures recorded in these transients will differ greatly for various thermocouples.

To determine the temperature variation in the liquid around a growing bubble, the thermocouple bridge carrying one thermocouple was positioned at 0.208 inch above the tube. These experiments were limited to pressures of 1.0 and 3.0 psia since at higher pressures the thermocouple pick up due to A.C. and D.C. field in water was large.

During the film run lasting for about 0.8 second, it was noted that, at 1.0 psia, only two nucleation sites were active near the thermocouple junction, at ΔT_{wb} of $55^{\circ}F$. which produced bubbles with their wall touching the thermocouple junctions at some stage during their growth. One of these sites produced bubbles which touched the thermocouple junction when the bubble diameter was 0.61 inch and the other, when the bubble diameter was 1.48 inches. With temperature difference between tube wall and bulk, ΔT_{wb}, equal to $55^{\circ}F$. maximum temperature in the liquid around the bubble was $3.7^{\circ}F$. above bulk at 0.61 inch bubble diameter. The thickness of the superheated layer was of the order of 0.05 inch under these conditions. For bubbles from the second active site touching

the thermocouples at a diameter of 1.48 inch, the maximum temperature recorded was 1.8°F. above bulk and the thickness of the superheated layer was of the order of 0.08 inch.

There was only one active site which was favourably situated in relation to the thermocouple junction at 3.0 psia. The bubble wall, unfortunately, touched the thermocouple only after the bubble has developed to a diameter of 0.9 inch. This value is very near the maximum bubble size of 1.05 inch at this pressure. For ΔT_{wb} equal to 42.7°F, maximum temperature in the superheated layer around the bubble was measured for five different bubbles. Two bubbles gave maximum temperatures of about 1.0°F. above the bulk fluid, while the other three bubbles gave values of 1.8, 3.5 and 5.3°F. above bulk temperature. The thickness of the layer around the bubble was estimated at about 0.08 inch under these conditions.

Assuming that these temperature gradients in the superheated layer near the bubble wall are the same around the bubble, the model of bubble growth assumed by Bankoff and Mikesell [31] is nearer the true model than the model of Griffith [30], chapter 5.

This method of recording temperature transients using one or more thermocouples could be used to indicate the existance of bubbles when heating surface is not visible or high speed camera not available. This method is largely useful when discrete bubbles are present, e.g. at initiation of nucleate boiling regime in the case of water at low pressures. Confirmation of velocity of propogation of disturbance would

also permit location of nucleus to be deduced without the use of high speed film records.

4.5 Mechanism of heat transfer in boiling.

In chapter 5.1, based on energy balance, it is shown that the latent heat of the bubble may account for all the energy available in the superheated layer over an area covered by the maximum diameter of the bubble. Based on above observations, the following mechanism is proposed for heat transfer in the nucleate boiling region for pool boiling of saturated liquids. The mechanism applies to all forms of heating surfaces.

With saturated liquids, at nucleation, a bubble is formed which produces a disturbance or pressure pulse travelling radially in all directions. The velocity of the pressure pulse is approximately equal to the radial growth velocity of the bubble at initiation. The pressure pulse creates a disturbance in the superheated layer which pushes some of the superheated layer, near the heating tube, into the bulk liquid. The amplitude of the disturbance decreases as the distance from its source increases.

The bubble at departure has absorbed all the superheat energy available in the superheated layer over the surface area covered by the maximum diameter of the bubble, as assumed in chapter 5.1. Outside the heater surface area occupied by the maximum diameter of the bubble, the magnitude of disturbance in the superheated layer is maximum just outside the bubble wall. The slope of heat flux v temperature difference curve

rises steeply. An increase in the number of bubbles per unit area has an additive effect on heat transfer, at first.

With further increase of temperature of the heating surface, a point is reached when the areas of influence of bubbles interfere with each other. The net result will be that the proportional increase in heat transfer due to each bubble decreases with an increase in the number of bubbles. This suggestion is in approximate agreement with the observations of Gaertner and Westwater [28] who proposed the relationship,

$$q = 1400\ n^{0.47} \qquad (7)$$

where n = Number of nucleation sites per unit area.

According to equation (7), the amount of heat energy transfer attributed to each site becomes less as the population of active sites increases.

The increase in bubble population also reduces the average liquid - solid contact area and consequently an increase in heating surface temperature will not increase heat transfer rates as fast as in earlier stages. The slope of q v ΔT decreases. At further increases of superheat, most of the heat transferred from solid to liquid will be used for the generation of bubbles.

Thus, the rate of bubble generation per unit area will determine the heat flux for high heat fluxes. The frequency of bubble generation from each site and the number of sites per unit area, both, have limits. These limits mark the conditions of peak heat flux in boiling. The frequency

of bubble generation from a nucleation site is limited by the maximum possible velocity of vapour depending upon the buoyancy and drag forces, as mentioned in chapter 4.1. The number of sites per unit area is limited by the maximum possible number of bubbles per unit area.

The peak heat flux may, therefore, be evaluated from the latent heat transport. The latent heat transported by the bubbles does not depend on the temperature difference, ΔT, but depends entirely upon the size of the bubble, number of bubbles per unit area, frequency of bubbles and the properties of vapour at saturation temperature. Based on these assumptions, an empirical correlation for predicting critical heat flux in saturated pool boiling is derived in chapter 5.2.

CHAPTER 5.

THEORETICAL ANALYSIS

Jacob [26] proposed that increase in heat transfer rate in nucleate boiling was due to the agitation, by detaching bubbles, of the liquid near the wall. Gunther and Kreith [2] explained this increase by, "some form of random micro-convection excited by bubble activity in the normally laminar sublayer". Forster and Greif [3] have proposed a vapour-liquid exchange mechanism by which a bubble pushed hot liquid away from the heated surface.

Deissler [41] and Rohsenow and Griffith [43] assumed that, at critical heat flux, all the heat transferred can be accounted for as latent heat of the bubbles.

The only visible difference between heat transfer by natural convection and by boiling is the presence of bubbles in the latter. Therefore, the sudden increase in heat transfer rate when bubbles appear on the heating surface must be due to the presence of bubbles only. No matter which mechanism of heat transfer in boiling is accepted to account for high heat transfer rates, the bubble growth rate and maximum bubble size must play an important part in it. It was, therefore, felt necessary to derive a suitable relationship which may predict the maximum bubble diameter in pool boiling.

5.1 Prediction of departure diameter of bubbles for nucleate pool boiling of water.

5.1.1 Previous Work.

Fritz [29] proposed an empirical relationship to predict

maximum bubble diameter which was obtained from static mechanical equilibrium of a bubble attached to a flat surface, and expressed in the form,

$$D = \lambda_3 \cdot \phi \left[\frac{\sigma}{g(\rho_\ell - \rho_v)} \right]^{1/2} \qquad (8)$$

where

D = Maximum diameter of the bubble.

σ = Surface tension.

ρ = Density. (ℓ = liquid, v = vapour).

and ϕ = Angle of contact.

Griffith [30] considered heat transfer rate to be the determining factor in bubble departure diameter. He formulated a mathematical model of bubble growth on a flat heated surface. The following assumptions were made concerning the asymptotic stages of bubble growth:-

a) The growth of the bubble is primarily dependent on the heat transfer from the liquid to the bubble wall.

b) The fluid flow field around the bubble is laminar.

c) Latent heat of vapour is large compared to superheat enthalpy.

d) Bubble growth rate takes place at constant internal pressure.

The growth is a result of evaporation at the bubble wall and the heat to produce vaporization is conducted from the super-heated liquid.

e) The bubble is hemispherical during growth.

From assumption (b), the equation expressing the heat transfer is the general conduction equation,

$$\nabla^2 T = \frac{\rho_l c_l}{k_l}\left[\frac{\partial T}{\partial t} + \bar{V}\cdot\nabla T\right] \qquad (9)$$

Rate of evaporation and rate of growth of bubble were related to obtain an expression for the velocity of the bubble wall. The expression for velocity, the conduction equation and boundary conditions specify the mathematical problem. The results are expressed in terms of dimensionless parameters of radius, time and velocity. The final solution require substitution of an empirical constant. The author suggested that this relationship only holds good for moderate pressures since the assumptions are not valid at low and high pressures. The results fit data for bubble growth rates at atmospheric pressure.

Bankoff and Mikesell [31] assumed a model of bubble growth rate in which the bubble originates entirely within the superheated liquid into the bulk. Irrotatinal radial flow describes the motion of the fluid surrounding the bubble. Equilibrium between the vapour phase in the bubble and liquid bubble wall is assumed. Starting with the conduction equation (9) and several boundary conditions, Lagrangian coordinates are introduced to facilitate the solution of the equations. Solutions were found for two temperature distributions, a linear and an exponential distribution. It was also assumed that liquid remained at a constant temperature everywhere except in a thin layer surrounding the bubble. Thus the volume of fluid experiencing the temperature gradient is small compared to the volume of the bubble. The volume of the bubble boundary layer parameter was obtained empirically from actual bubble growth rate data. Bubble growth rates for saturated boiling

were predicted successfully at atmospheric pressure, but not for subcooled boiling.

Zuber [32, 33] considered the Taylor instability of a liquid - vapour interface in nucleate pool boiling under critical conditions. The liquid - vapour interface was treated as a wave which can be stable or unstable according to whether the wavelength is shorter or longer than the critical value. This critical wavelength is given by,

$$\text{Wavelength} = 2\pi \left[\frac{\sigma}{g(\rho_\ell - \rho_v)}\right]^{\frac{1}{2}} \tag{10}$$

Vapour "slugs" are approximated by spheres of radius equal to a quarter of the wavelength, and under critical conditions, the limits for diameter of bubbles are given by,

$$\pi \left[\frac{\sigma}{g(\rho_\ell - \rho_v)}\right]^{\frac{1}{2}} \leq D \leq \pi \left[\frac{3\sigma}{g(\rho_\ell - \rho_v)}\right]^{\frac{1}{2}} \tag{11}$$

Staniszewski [34] proposed the following relationship between bubble diameter and bubble growth rate, based on experimental observations. He observed that bubbles with higher growth rate, at the same pressure, grew to a larger maximum diameter, viz.

$$D = 0.0071 \left[\frac{2\sigma}{g(\rho_\ell - \rho_v)}\right]^{\frac{1}{2}} \left[1 + 0.435 \frac{dD}{dt}\right] \tag{12}$$

Nishikawa and Urakawa [17] proposed a relationship for bubble departure diameter as a function of system pressure only,

$$D = 0.672 \; p^{-0.575}. \tag{13}$$

where diameter and pressure are measured in inch and pounds per square inch respectively. This relationship successfully correlated the experimental value of departure diameter of bubbles, obtained by the authors, for boiling on a ~~small diameter wire~~ flat plate between pressures of 6.0 and 14.7 psia.

Chang [35] derived a relationship very similar to that of Zuber, viz,

$$D = \sqrt{\frac{2C_s}{C_B}}\left[\frac{2\sigma}{g(\rho_l-\rho_v)}\right]^{\frac{1}{2}} \qquad (14)$$

where Cs and C_B are coefficients of surface tension and buoyancy forces respectively, and are constants.

Semeria [36] correlated experimental data for pressures between 2.0 and 20.0 atmospheres absolute using a relationship similar in form to that of Nishikawa and Urakawa. For boiling on a wire of diameter 0.0315 inch, he obtained

$$D = 0.242\ p^{-\frac{1}{2}} \qquad (15)$$

where D is in inches and p in psia.

Semaria [55] later correlated experimental data for pressures between 150 psia and 2000 psia using a similar relationship of the type, equation (15). The exponent of p, however, was -1.53 instead of -0.5, and the value of the numerical constant was 37.6 instead of 0.242.

Correlating equations (8), (11) and (14) differ from each other only by the value of the constant. For an angle of contact of 45^0, equation (8) is tabulated in table 13 for comparison with experimental data. A change in maximum bubble diameter by only 7% is predicted, from these three equations, between pressures of 1.0

and 14.7 psia. Equation (8) is plotted in figure 91 for comparison with experimental data. According to these results, therefore, these equations do not account for major features which determine maximum bubble diameter.

Solutions in the form of dimensionless integro-differential equations given by Griffith [30] and Bankoff and Mikesell [31] require empirical constants before a solution can be obtained. Equation (12) was proposed to account for different values of maximum bubble diameter, obtained in Staniszewski's experiments at 14.7, 28 and 40 psia, at the same pressure. This equation, however, does not predict the effect of pressure on maximum diameter of the bubble any better than equations (10), (11) and (14).

Equations (13) and (15) indicate a simpler type of correlation which might be used in predicting bubble diameter at break-off, since pressure of the system takes into account the property value changes for liquid and vapour, under saturation conditions. However, as shown in figure 91, equations (13) and (15), themselves, did not fit the experimental values presented here.

5.1.2 Prediction of bubble departure diameter.

For pool boiling under saturated conditions, the latent heat energy of the vapour bubble at departure cannot exceed the total superheat energy available in the superheated layer, since there is no other source of energy near the heating surface, if the amount of heat conducted from the heating surface to vapour is assumed to be negligible. This assumption is justified since the thermal conductivity of water vapour is less than 4% the thermal conductivity of liquid water. The temperature difference Tw-Ts is

low and, hence, the radiation effects are also negligible.

The following assumptions are made which are considered reasonable:

1) Heat conducted or radiated into the bubble from the heating surface is negligible.

2) Total latent heat energy of the bubble at departure is equal to the thermal energy, above saturation temperature, of the volume of superheated liquid displaced by the bubble.

With these two assumptions and the results obtained in chapter 4.2, the maximum diameter of the vapour bubble is predicted for two surface forms.

5.1.2.1 Flat heating surface.

From equation (5), the thickness of the superheated layer is assumed to be,

$$b = \frac{k\,(Tw-Tb)}{q} \cdot \lambda_1$$

where λ_1 is an empirical constant deduced from experiments.

Also, from chapter 4.2, the temperature gradient in the superheated layer is approximately linear. Thermal energy of the superheated liquid above the datum of saturation temperature is, therefore,

$$Q_{\text{liquid}} = \frac{\pi}{4} \cdot D_f^2 \cdot \frac{k \cdot \Delta T}{q} \cdot \lambda_1 \cdot \rho_l \cdot c_l \cdot \frac{\Delta T}{2} \qquad (16)$$

where D_f = Maximum bubble diameter from a flat surface.

Assuming the bubble to be perfectly spherical, the latent heat energy of the bubble is given by,

$$Q_{\text{bubble}} = \frac{\pi}{6} \cdot D_f^3 \cdot L \cdot \rho_v \qquad (17)$$

From equations (16) and (17),

$$D_f = \frac{3}{4}\left(\frac{\rho_l}{\rho_v}\right)\left(\frac{C_l}{q.L}\right) k.(\Delta T)^2.\lambda_1 \qquad (18)$$

The value of λ_1 obtained from experiments on cylindrical surface, chapter 4.2, is 2. Assuming that the value of λ_1 for flat surfaces and cylindrical surfaces to be the same,

$$\text{then, } D_f = \frac{3}{2}\left(\frac{\rho_l}{\rho_v}\right)\left(\frac{C_l}{qL}\right) k.(\Delta T)^2 \qquad (19)$$

5.1.2.2 Cylindrical tube or wire.

If the bubble surrounds the tube completely, the thermal energy of the liquid displaced is given by,

$$Q \text{ liquid} = \pi d_o . D_T . \frac{k.\Delta T}{q} . \rho_l . C_l . \frac{\Delta T}{2} . \lambda_1 \qquad (20)$$

if it is assumed that the thickness of the superheated layer is small compared to the diameter of the heating tube or wire, where

d_o = Outer diameter of the heating tube or wire.

and D_T = Maximum diameter of the bubble from tube or wire.

For a spherical bubble, latent heat energy is given by equation (17). From equations (17) and (20),

$$\therefore D_T^2 = 3 d_o \left(\frac{C_l}{qL}\right)\left(\frac{\rho_l}{\rho_v}\right) k.(\Delta T)^2.\lambda_1 \qquad (21)$$

Using, as previously, a value of 2 for λ_1 chapter 4.2,

$$D_T^2 = 6 d_o \left(\frac{\rho_l}{\rho_v}\right)\left(\frac{C_l}{q.L}\right) k.(\Delta T)^2 \qquad (22)$$

5.1.2.3 Comparison of predicted results with experiment.

Equations (19) and (22) are compared with experimental values

of bubble diameter obtained in this work and from Patten [25] in table 13. Column 4 of table 13 presents experimental values of bubble diameter obtained from a wire of 0.018 inch diameter [25], and from the 0.125 inch diameter tube used in this investigation. Column 5 shows the predicted values of bubble diameter from equation (22) where the bubble surrounds the heating tube or wire. Column 6 shows the diameter of a bubble from a flat surface obtained from equation (19). Comparison of experimental results with the predicted values is satisfactory. The maximum error in predicted values never exceeded 22%.

Equation (19) is applicable to flat surfaces only while equation (22) refers to tubes and wires when the bubble completely surrounds the heating tube or wire. Equation (22) predicts that if the heating tube or wire diameter is increased, the departure diameter of the bubble will also increase. This is in agreement with experimental values. Patten [25] obtained a value of maximum bubble diameter of 0.70 inch at 0.935 psia, from a heating wire of 0.018 inch diameter. In this work, the maximum bubble diameter of about 1.8 inches is obtained at a pressure of 0.95 psia from a tube of diameter 0.125 inch.

At some value of heating tube diameter, for a particular pressure, the bubble will not surround the tube completely and equation (22) will not be valid above this heating tube diameter. Assuming that the heating tube surface can be approximated to a flat surface above this heater diameter, equation (19) will then apply. From this assumption, the maximum bubble diameter from a flat surface will be equal to the maximum bubble diameter from a cylindrical surface for a particular value of the cylindrical surface diameter. This

value of tube diameter will correspond to the point where equation (19) becomes valid instead of equation (22). To determine the relationship between the bubble diameter and heating tube diameter when equation (19) replaces equation (22), the two equations are compared under similar conditions of pressure, temperature and heat flux to give

$$D_T = 2\sqrt{D_F \cdot d_o} \qquad (23)$$

From equation (23), the diameter of the heating tube where the bubble diameters from flat and cylindrical heating surfaces are equal is obtained by replacing D_F by D_T

$$\therefore D_T = 4 d_o \qquad (24)$$

From preceding assumption and equation (24), it appears that the bubble does not surround the heating tube completely when the maximum bubble diameter is equal to 4 times the heating tube diameter. At this point, equation (19) may be used to predict maximum bubble diameter instead of equation (22).

From a visual examination of high speed films, the maximum bubble diameter of 0.5 inch at 7.0 psia did not surround the 0.125 inch diameter tube completely confirming the assumption made above.

If the maximum diameter of the bubble from a tube or wire and the diameter of the tube or wire is known, then, from equation (23), it is a simple matter to predict maximum bubble diameter from a flat surface under similar experimental conditions.

Also, if two tubes or wires of different diameters are used for pool boiling under similar conditions, the diameter ratio

of the bubbles is given by,

$$\frac{D_{T1}}{D_{T2}} = \sqrt{\frac{d_1}{d_2}} \qquad (25)$$

where d_1 and d_2 are the outer diameters of heating surfaces and D_{T1} and D_{T2} their corresponding maximum bubble diameters for a given set of experimental conditions.

The maximum bubble diameter values from wires and tubes are modified to correspond to a flat surface using equation (23) and tabulated in column 8 of table 13. Column 8 shows that the derived maximum bubble diameters for a flat surface from experimental values of Patten [25] for a wire of 0.018 inch diameter, and this work for a tube of 0.125 inch diameter agree satisfactorily. Unfortunately, there are no experimental values of bubble diameters available for flat surfaces at low pressures and a direct comparison cannot be made.

These correlations for maximum bubble diameters given by equations (19) and (22) depend upon the experimental values of heat flux and temperature difference between wall and saturation. From table 13, it is noted that the experimental and predicted values of maximum bubble diameter at critical heat flux agree well and are only slightly less than the diameter of bubbles at low heat fluxes. It will, therefore, be reasonable to assume that the maximum bubble diameter is approximately constant in the boiling region.

5.1.3 Second correlation for bubble departure diameter.

A correlation has been found which does not require experimental values of heat flux and temperature difference. Available experimental results are satisfactorily correlated by an

equation of the type (14) modified by a term (p/pcr.). This equation is,

$$D = \lambda_4 \left(\frac{p}{p_{cr.}} \right)^{x_3} \left[\frac{\sigma}{(\rho_L - \rho_V)} \right]^{1/2}$$

and in this form it refers to flat surfaces only although it can obviously be modified by constants in equations (23) and (24) to apply to wires and tubes.

The acceleration due to gravity term is assumed to have no effect on the maximum bubble diameter. This assumption is reasonable since, it was assumed in developing equations (19) and (22) that the maximum bubble diameter only depends upon the energy available in the superheated layer. However, the gravity term will have to be considered in determining the bubble velocity at departure.

From experimental values of maximum bubble diameters obtained in this investigation, suitable values for λ_4 and x_3 are 9.1×10^{-3} and -1 respectively. The resulting equation is,

$$D = 0.0091 \left(\frac{p_{cr.}}{p} \right) \left[\frac{\sigma}{(\rho_L - \rho_V)} \right]^{\frac{1}{2}} \qquad (26)$$

The values of surface tension, σ, were obtained from experimental results of Volyak [37] in the temperature range from 20°C. to 374°C.

Experimental results of Semaria [36, 55] Staniszewski [34] and modified results of Patten [25] and this work to correspond to flat surfaces are plotted in figures 91 and 92. Equations (8), (13), (15) and (26) are also plotted for comparison in figure 91 and equation (26) in figure 92. Equation (26) is also tabulated in column 7 of table 13.

Comparison of equation (26) with experimental results is more satisfactory than existing correlations in the pressure range between 1.0 psia and 2000 psia.

5.2 Prediction of critical heat flux in saturated pool boiling.

5.2.1 Previous Work.

Addoms [38] derived a correlation by dimensional analysis in which the average volumetric vapour disengaging rate per unit area of heating surface is a function of buoyancy term and the liquid thermal diffusivity. The correlation is expressed as,

$$q_{cr.} = \lambda_s \cdot L\rho_v \left[g \cdot \frac{k}{\rho_l c_l} \right]^{\frac{1}{3}} \left[\frac{\rho_l - \rho_v}{\rho_v} \right]^{\frac{1}{2}} \qquad (27)$$

Kutateladze [39] considered the hydrodynamic motion of a non-viscous two phase flow in terms of equations of motion of both phases. By dimensional analysis, the author arrived at the following correlation,

$$q_{cr.} = (0.13 \rightarrow 0.16)\, L\rho_v^{\frac{1}{2}} \left[g g_0 \sigma (\rho_l - \rho_v) \right]^{1/4} \qquad (28)$$

where g_0 = Conversion factor.

and 0.13 and 0.16 are empirical constants.

Borishanskii [40] considered the stability of a liquid jet surrounded co-axially by the vapour phase moving in opposite direction. The effect of viscosity was included and similarity criterion derived from dimensional analysis. The effect of viscosity was found to be small. The expressions derived were,

$$\lambda_c = \frac{q_{cr.}}{L\rho_v^{\frac{1}{2}} \left[g^2 \sigma (\rho_l - \rho_v) \right]^{1/4}} \qquad (29)$$

$$N = \frac{\rho_\ell \cdot \sigma^{3/2}}{g \cdot \mu_\ell^2 \cdot (\rho_\ell - \rho_v)^{\frac{1}{2}}} \qquad (30)$$

and $$\lambda_6 = 0.13 + 4N^{-0.4} \qquad (31)$$

Deissler [41] assumed that all the heat energy in boiling is used to form vapour and that the critical heat flux conditions occurred when successive bubbles leaving the surface touched and coalesced. The velocity of vapour bubbles was determined by equating buoyancy and drag forces on the vapour bubble. Using the Frits relationship for departure diameter of a bubble, the following expression was obtained,

$$q_{cr.} = \lambda_7 \cdot L \rho_v^{\frac{1}{2}} \left[\sigma g (\rho_\ell - \rho_v)\right]^{\frac{1}{4}} \left(\frac{\phi}{C_D}\right)^{\frac{1}{2}} \qquad (32)$$

where CD = Drag coefficient and ϕ = Angle of contact.

It was assumed that the drag coefficient

$$C_D = f_1\left(\frac{\rho_v \cdot V_b \cdot D}{\mu_v}\right) \qquad (33)$$

where μ_v = Viscosity of vapour

V_b = Velocity of bubble.

The value of D in equation (33) was obtained from equation (8). The velocity of the bubble Vb was determined by equating the buoyancy forces on the bubble to viscous drag,

$$V_b = \sqrt{\frac{4}{3C_D}} \cdot \sqrt{\frac{g(\rho_\ell - \rho_v) D}{\rho_v}} \qquad (34)$$

V_b

From equations (32), (33) and (34),

$$\therefore \frac{q_{cr.}}{L \rho_v^{\frac{1}{2}} \left[\sigma g (\rho_\ell - \rho_v)\right]^{1/4}} = f_2\left[\frac{\rho_v^{\frac{1}{2}} \cdot \sigma^{3/4}}{\mu_v \left[g(\rho_\ell - \rho_v)\right]^{1/4}}\right] \qquad (35)$$

Rohsenow and Griffith [43] also assumed that all the heat transferred under critical conditions is used in forming vapour. The product of bubble frequency and bubble diameter was taken as a constant and a buoyancy term was introduced to account for the vapour velocity. The relationship derived is,

$$\frac{q_{cr.}}{L\rho_v} = 143\left[\frac{\rho_l - \rho_v}{\rho_v}\right]^{0.6} \qquad (36)$$

The value of constants 143 and 0.6 for the buoyancy term were obtained from experimental values. It was noted by Ivey [11] that this relation does not contain an acceleration term whereas the magnitude of the acceleration due to gravity does effect the critical heat flux significantly.

Zuber [32, 33, 44] derived the following relationship for critical heat flux in pool boiling,

$$q_{cr.} = \frac{\pi}{24} L\rho_v^{\frac{1}{2}}\left[g g_0 \sigma(\rho_l - \rho_v)\right]^{\frac{1}{4}}\left[\frac{\rho_l}{\rho_l + \rho_v}\right]^{\frac{1}{2}} \qquad (37)$$

The analysis was based on the Taylor instability of a liquid - vapour interface which requires no solid - liquid contact. Various authors have found liquid - solid contact under critical conditions [45, 46]. Stein [47] has shown that Zuber's model is not compatible with the Taylor requirements for instability.

Chang and Snyder [4] considered the equation of motion of a bubble. The model used under critical conditions is shown in figure 93. It was assumed that when one bubble detaches from one site a new bubble initiates at the neighbouring site. Mass acceleration of the bubble was equated to its buoyancy force and the equation integrated to determine the time t in which the bubble will travel a distance of 2D, the assumed distance between successive bubbles.

The analysis was similar to that of Deissler and gave,

$$q_{cr.} = L \rho_v \left(\frac{\pi}{6} D^3\right) \frac{1}{D^2 t} \tag{38}$$

The value of t was obtained from,

$$t = \sqrt{\frac{4 D \rho_v}{g(\rho_l - \rho_v)}} \tag{39}$$

and the value of diameter was obtained from equation (8). Using published data for contact angle, the final expression takes the form,

$$q_{cr.} = (0.17 \longrightarrow 0.23) L \rho_v^{\frac{1}{2}} \left[g g_0 \sigma (\rho_l - \rho_v)\right]^{\frac{1}{4}} \tag{40}$$

Chang and Snyder, loc.cit. also considered capillary waves which were postulated to occur at the interface of the bubble and liquid due to the relative motion of the bubble. For two non-viscid liquids flowing in parallel vertical streams, the interface becomes unstable when their relative velocity is [4],

$$V_r = \left[\frac{g\sigma(\rho_l - \rho_v)}{\rho_v^2}\right]^{1/4} \left[\frac{\rho_l + \rho_v}{\rho_l}\right]^{1/2} \tag{41}$$

Vapour velocity is deduced from the bubble geometry shown in figure 93 as,

$$V_v = \frac{V_r}{1.8} \tag{42}$$

from equations (8), (38) and (39), the relationship is,

$$q_{cr.} = \frac{\pi}{12} L \rho_v \cdot V_v \tag{43}$$

where V_v = Vapour bubblevelocity.

From equations (41), (42) and (43),

$$q_{cr.} = 0.145 L \rho_v^{\frac{1}{2}} \left[g g_0 \sigma (\rho_l - \rho_v)\right]^{\frac{1}{4}} \left[\frac{\rho_l + \rho_v}{\rho_l}\right]^{\frac{1}{2}} \tag{44}$$

Chang [48] later suggested the following correlation for saturated pool boiling, neglecting viscous forces,

$$q_{cr} = 0.13 \sqrt{\rho_l \cdot \rho_v} \cdot L \left[\frac{g\sigma(\rho_l - \rho_v)}{\rho_l^2} \right]^{\frac{1}{4}} \qquad (45)$$

Berenson [49] postulated a model of contraflowing columns of vapour and liquid. The following expression is obtained by minimizing kinetic energy per unit time at a horizontal surface.

$$q_{cr} = \lambda_g L \rho_v^{\frac{1}{2}} \left[g g_0 \sigma (\rho_l - \rho_v) \right]^{\frac{1}{4}} \left[\frac{\rho_l + \rho_v}{\rho_l} \right]^{\frac{1}{2}} \left[1 + \left(\frac{\rho_v}{\rho_l} \right)^{\frac{1}{3}} + \left(\frac{\rho_v}{\rho_l} \right)^{\frac{2}{3}} + \left(\frac{\rho_v}{\rho_l} \right) \right]^{-1} \qquad (46)$$

The analytical model is similar to Chang and Snyder.

It has been shown conclusively in chapter 5.1 that the Fritz equation (8) which does not take into account the thermal energy ~~effects~~, does not fit the experimental data in the sub-atmospheric region,,and at pressures above atmospheric.

In Deissler's correlating equation (35), the Fritz relationship has been used for diameter of a bubble. Therefore, this correlation is of little value. Rohsenow and Griffith's correlation, equation (36), does not contain an acceleration term which Ivey [11] has proved as an essential feature of critical heat flux. Therefore, this equation is open to question.

Zuber's correlation, equation (37), depends upon the Taylor's instability which require no liquid - solid contact. It has been shown in chapter 4 that such contact definitely exists under critical conditions. Hence, the derivation of a correlation based on an unsound model is also of dubious value.

The model used by Chang and Snyder to arrive at equation (40) and (45) and by Berenson to deduce equation (46) are not

compatible with the observations on high speed film taken at critical heat flux. Photographic evidence at critical heat flux indicates a chaotic behaviour of the two phases, therefore, the postulated bubble geometry cannot be valid and the resulting equations are open to question.

The correlations which have no apparent invalid assumptions are those of Kutateladze and Borishanskii, equations (28), (29) and (30), arrived at through dimensional analysis. Assuming the viscosity effects to be negligible, the equations of Kutateladze and Borishanskii are the same. The value of critical heat flux from equation (28) is, therefore, plotted in figures 29 and 94 against pressure. Experimental values of critical heat flux in the sub-atmospheric region, obtained by Patten and Lienhard and Schrock, are modified to correspond to a heater diameter of $\frac{1}{8}$ inch using equation (3), as shown later in this chapter, and plotted in figure 29 along with the experimental values obtained in this investigation. The experimental values of critical heat flux obtained by Kazakova [50] and Morozov [51] are also plotted in figure 94.

From figure 29, it is noted that the correlation (28) does not fit the experimental data. At 1.0 psia, the experimental value of critical heat flux is about 90% higher than predicted by equation (28). It is, therefore, considered necessary to derive a more suitable relationship which may predict the critical heat flux values over the entire pressure range.

5.2.2 Critical heat flux in saturated pool boiling of water.

It has been observed, chapter 4, that the process of heat transfer under critical conditions is apparently chaotic both in time

and in space. However, there are certain outstanding features noticable even under critical conditions which can be generalized. From these features, a model of heat transfer under critical conditions is proposed. An empirical correlation, based on the model, is derived and the value of various constants is obtained from experimental results.

As assumed in chapter 4, the critical heat flux is limited by the finite velocity of the vapour bubble away from the heating surface. Bubbles form on the heating surface when space is provided by departing bubbles. Therefore, the rate of formation of bubbles is equal to the rate at which they can be removed from the heating surface. The velocity of the vapour bubble will depend upon the buoyancy force and drag on the bubble. As assumed in chapter 5.1.2, the bubble latent heat energy accounts for all the energy available in the superheated layer displaced by the bubble. Therefore, it is assumed that, under critical conditions, all the heat transferred from the heating surface is used in the production of vapour.

$$q_{cr.} = \frac{\pi}{6} D^3 \cdot L \rho_v \cdot n \cdot f \qquad (47)$$

where n = Number of bubbles per unit area.

and f = Average frequency of bubbles.

As discussed in chapter 4, under critical conditions, a maximum limit is reached for no. of bubbles forming per site and the total no. of such active sites. Maximum possible no. of bubbles will occur when bubbles touch other bubbles in both planes and coalescence occurs between bubbles from the same site. Therefore,

under ideal conditions,

$$w \propto \frac{1}{D^2} \tag{48}$$

$$\text{and} \quad f \propto \frac{V}{D} \tag{49}$$

where V = Average velocity of vapour away from the heating surface.

Boiling conditions are chaotic and bubbles do not retain spherical shape in later stages of growth. Also, all bubbles are not of the same size and they do not necessarily touch other bubbles on all sides, all the time. A constant factor is introduced to account for this deviation from ideal conditions,

$$n = \frac{\lambda_9}{D^2} \tag{50}$$

$$\text{and} \quad f = \frac{\lambda_{10} \cdot V}{D} \tag{51}$$

From equation (47), (50) and (51),

$$q_{v\alpha} = \frac{\pi}{6} \cdot \lambda_9 \cdot \lambda_{10} \cdot L \rho_v \cdot V \tag{52}$$

As plotted in figures 73, 74, 75, 76 and 77 and discussed in chapter 4, the vapour bubble velocity reaches a constant value before the bubbles leave the heating tube. Therefore, to determine the velocity of the bubble, buoyancy force is equated to drag forces to give,

$$g(\rho_l - \rho_v) \cdot \frac{\pi}{6} D^3 = C_D \cdot \frac{\pi}{4} D^2 \left[\frac{1}{2} \rho_v \cdot V_b^2\right] \tag{53}$$

$$\propto \quad V_b = \left[\frac{4}{3} \frac{D}{C_D} \cdot \frac{g(\rho_l - \rho_v)}{\rho_v}\right]^{\frac{1}{2}} \tag{54}$$

where Vb = Velocity of the bubble at departure.

The use of ρ_v in determining the bubble departure velocity has been suggested by Deissler [41]. The experimental results obtained in this work support ~~him~~ Deissler's view that, under critical conditions, bubbles are mostly surrounded by other vapour bubbles on all sides. Therefore, vapour density is used in determining drag on the vapour bubble.

The bubble velocity as obtained from equation (54) can be used in equation (52) only if the bubbles were perfectly spherical and all bubbles were of the same size. Since no such regularity was observed in size and shape of bubbles under critical conditions, it will be reasonable to assume that actual average velocity of the vapour slug is some function of bubble velocity. Assuming that the drag coefficient is constant over the pressure range, equation (54) may be written

$$V = \lambda_{11}\left[D \cdot g \cdot \frac{(\rho_l-\rho_v)}{\rho_v}\right]^{x_4} \qquad (55)$$

From equations (26), (52) and (55),

$$\frac{q_{cr}}{L\rho_v} = \lambda_{12}\left[\left(\frac{p_{cr}}{p}\right)\left[\frac{\sigma}{(\rho_l-\rho_v)}\right]^{\frac{1}{2}} g\frac{(\rho_l-\rho_v)}{\rho_v}\right]^{x_4} \qquad (56)$$

The empirical values of λ_{12} and x_4 viz. 2.44 and 0.313, are obtained from experimental data of this investigation.

$$\therefore \frac{q_{cr}}{L\rho_v} = 2.44\left[\left(\frac{p_{cr}}{p}\right)\left[\frac{\sigma}{(\rho_l-\rho_v)}\right]^{\frac{1}{2}} g\frac{(\rho_l-\rho_v)}{\rho_v}\right]^{0.313} \qquad (57)$$

Equation (57) is plotted on figures 29, 94 and 95 for comparison with experimental data. The comparison is satisfactory if it can be assumed that some very low critical heat flux values

obtained by Kazakova [50] could be due to premature burnout. This was possible since no stabilizing system was used in determining critical heat fluxes.

5.2.3 Effect of heater diameter on critical heat flux.

From equation (57), critical heat flux is related to the bubble diameter by the relationship, for fixed pressure conditions,

$$q_{cr.} \propto D^{0.313} \tag{58}$$

For cylindrical surfaces when the bubble envelops the heating surface completely, from equation (22),

$$D \propto d_o^{\frac{1}{2}} \tag{59}$$

From equations (58) and (59),

$$q_{cr.} \propto d_o^{0.156} \tag{3}$$

From equation (3), it is clear that critical heat flux will decrease with a decrease in heating wire or tube diameter at pressures where the maximum bubble diameter surrounds the heating surface completely. Assuming this to be true, the experimental values of critical heat flux obtained by Patten [8] and Lienhard and Schrock [21] may be modified to correspond to 0.125 inch diameter tube, used in this work.

These modified values of critical heat flux are plotted in figure 29 for comparison with predicted values from equations (28) and (57). In figures 29, 94 and 95, the predicted values from equation (57) compare favourably with experimental data. Maximum deviation of experimental values from predicted values was less than $\pm$ 30%.

CHAPTER 6

CONCLUSIONS

These studies are confined to nucleate boiling of water in the saturated state from an electrically heated stainless steel tube. Nucleate boiling heat transfer rates up to and including critical heat flux have been determined for saturated pool boiling of deionized water between pressures of 1.0 and 14.7 psia. A stabilizing fluid flowing through the 0.125 inch diameter stainless-steel tube prevented excursion into the film boiling region during these tests. Heat transfer rates are presented for pressures of 1.0, 3.0, 7.0 and 14.7 psia.

High speed films taken at 6000 FPS using a Fastex camera showed that, at critical heat flux in pool boiling, liquid-solid contact existed throughout except for infrequent extremely short intervals. The presence of these extremely short intervals may be due to the small heating surface area considered for these measurements. These short intervals may disappear if a larger heating surface were considered for measurements of this nature. This could account for departure from stable conditions on a non-stabilized heating surface.

Under critical conditions, bubble behaviour is chaotic both in time and in space. No model can correctly account for the actual bubble behaviour during bubble growth and departure under critical conditions.

Maximum bubble diameter under critical conditions is only slightly less than maximum bubble diameter at low heat fluxes, contrary to the observations of Gaertner and Westwater [28] and the prediction of Zuber [23].

Values of bubble growth rate and maximum bubble diameter are

presented for moderate heat fluxes over the same pressure range. The diameter of a bubble at any time during its growth may be related to time by an equation of the type,

$$D = \lambda_2 t^{x_2} \qquad (6)$$

where the values of λ_2 and x_2 vary between various bubbles. The value of x_2 in equation (6) was found to vary among bubbles at the same pressure. The highest value of x_2 at atmospheric pressure was as high as three times the lowest value. One analytical model for bubble growth rate cannot account for such large variations in growth rate under similar experimental conditions.

The temperature gradient in the superheated layer at the time of initiation is approximately linear. The thickness of this layer at initiation of the bubble is very nearly twice the thickness corresponding to pure conduction under similar temperature and heat flux conditions.

Existing correlations for maximum bubble diameter do not satisfactorily predict the maximum bubble size. However, the diameter of the bubble at departure can be predicted fairly well by an energy balance of the vapour and the superheated liquid displaced by the vapour bubble. An average maximum bubble diameter in pool boiling of water may be obtained from the following equation:

$$D = 0.0091 \left(\frac{p_{cr}}{p} \right) \left[\frac{\sigma}{(\rho_L - \rho_V)} \right]^{\frac{1}{2}} \qquad (26)$$

Equation (26) correlates all the available data between pressures of 1.0 and 2000 psia satisfactorily. In the case of cylindrical heating surfaces, the maximum diameter of the bubble is proportional to the square root of the heating element diameter

when the bubble envelopes the heating element completely. This maximum bubble diameter from a cylindrical surface can also be derived by combining equation (26) with equations (23) and (24).

The velocity of the bubble at the time of its departure from the heating surface is constant. This bubble velocity can be obtained byequating buoyancy and drag forces on the vapour bubble.

The hydrodynamic disturbance associated with the bubble growth rate causes disturbance in the superheated layer well away from the origin of disturbance. This disturbance travels at approximately the initial growth velocity of the bubble in all directions. Such an occurrence may well explain sudden change of slope on the heat transfer curve, figure 1, when boiling commences. The bubble at departure produces eddy currents in the liquid resulting in an upward "lift" of the superheated layer. The relative turbulence in the superheated layer after the departure of the bubble is larger than the turbulence during growth, fig. 90. Experiments of this type also confirmed the presence of a thin layer of superheated liquid adjacent to the interface of the growing bubble.

The method of recording temperature transients in the superheated layer using small thermocouples may be used to indicate the existence of bubbles when the heating surface is not visible or high speed camera not available. This method is particularly useful to indicate initiation of the nucleate boiling regime.

Based on the assumption that, under critical conditions, all the superheat energy present in the superheated layer is transferred in the form of latent heat of vapour, a correlation is

developed which predicts the critical heat flux in pool boiling of water. Comparison with all the available data in the pressure range 0.6 psia to critical pressure is satisfactory. Two empirical constants were required to complete this equation which were found experimentally. The resulting equation is;

$$\frac{q_{cr.}}{L\rho_v} = 2.44\left[\left(\frac{b_{cr.}}{P}\right)\left[\frac{\sigma}{(\rho_\ell-\rho_v)}\right]^{\frac{1}{2}} g\left(\frac{\rho_\ell-\rho_v}{\rho_v}\right)\right]^{0.313} \qquad (57)$$

It has also been proposed that for cylindrical heating surfaces, at pressures where the bubble envelops the heating surface completely, the critical heat flux increases with an increase in diameter of the heating element. The proposed relationship is,

$$q_{cr.} \propto d_o^{0.156} \qquad (3)$$

APPENDIX I.

Conditions governing the choice of a stabilizing fluid.

For the stabilizing system to function normally, it was necessary to ensure a heat absorbtion capacity for the system of 7660 B.t.u. per hour, as mentioned in chapter 2.4. Also, boiling in the stabilizing system and deposition of decomposition products of oil had to be avoided for normal functioning. To determine the necessary stabilizing fluid flowrate and pressure requirements in the stabilizing system, the following equations were considered.

The heat transfer equation for the stabilizing fluid is the Dittus - Boelter equation [1],

$$h_{fc} \frac{d_i}{K_{sf}} = 0.023 \; Re^{0.8} \; Pr^{0.4} \qquad (60)$$

Also, $Q = h_{fc} . A_i . \Delta T_{Tf}$ (61)

and $Q = m . C_{sf} . (To - Ti)$ (62)

From equations (60) and (61),

$$Q = 0.023 \frac{k_{sf}}{d_i} . A_i . \Delta T_{Tf} Re^{0.8} Pr^{0.4} \qquad (63)$$

Assuming mean temperature difference to be arithmetic mean, we have

$$\Delta T_{Tf} = T_T - \frac{(Ti + To)}{2} \qquad (64)$$

From equations (63) and (64),

$$Q = 0.023 \; \pi \; k_{sf} . \ell . Re^{0.8} \; Pr^{0.4} \left[T_T - \frac{(Ti + To)}{2} \right] \qquad (65)$$

From equation (62),

$$Q = \frac{\pi}{4} di^2 \; (\rho Vc)_{sf} \cdot (To - Ti) \qquad (66)$$

$$\text{or} \quad \frac{To}{2} = \frac{Ti}{2} + \frac{2Q}{\pi (\rho Vc)_{sf} \, di^2} \qquad (67)$$

From equations (65) and 67 and rearranging,

$$\frac{Q}{0.023} = \pi k_{sf} (T_T - Ti) \, Re^{0.8} \, Pr^{0.4} = \frac{2Q}{di} Re^{-0.2} \, Pr^{-0.6} \qquad (68)$$

From equation (68), the velocity of stabilizing fluid can be calculated if the value of T_T is known. The value of the inner surface temperature of the tube, T_T, was assumed to correspond to point D on figure 1. The value of Ti was taken for the worst case of boiling at 14.7 psia under critical conditions. This value of Ti corresponds to point C on the boiling curve.

Inserting the value of velocity in equation (66), outlet temperature of the stabilizing fluid can be calculated.

Pressure drop across the heating tube.

Frictional pressure drop in the tube is given by,

$$\Delta p_f = \frac{4f \cdot (\rho V^2)_{sf}}{2g} \cdot \frac{l}{di} \qquad (69)$$

From ref. [52], $f = 0.079 \times Re^{-\frac{1}{4}}$ (70)

Pressure drop due to sudden expansion and contraction at exit from and entry to the test section was calculated from the following equations.

$$\Delta p_e = Ke \frac{(\rho V^2)_{sf}}{2g} \qquad (71)$$

$$\Delta p_c = Kc \cdot \frac{(\rho V^2)_{sf}}{2g} \qquad (72)$$

where Ke and Kc are coefficients for sudden expansion and contraction respectively and Δp_e and Δp_c the corresponding pressure drops.

For a diameter ratio of $\frac{0.115}{0.5} = 0.23$,

Kc = 0.44; Ke = 0.898, [52]

For extreme conditions at 14.7 psia,

T_D = 465°F.; Ti = 275°F.; V = 2.07×10^4 ft/hr.

The value of total pressure drop and flowrate for three liquids were as follows:-

Liquid		Pressure drop (psi)	Flowrate (Igph)
Water	Water	0.6	9.5
	Mobiltherm 600	67.0	104
	Shell Voluta 45	94.0	124

It was decided to use water because of low frictional pressure drop, high thermal capacity and freedom from decomposition products.

APPENDIX II

Determination of temperature drop across the tube wall.

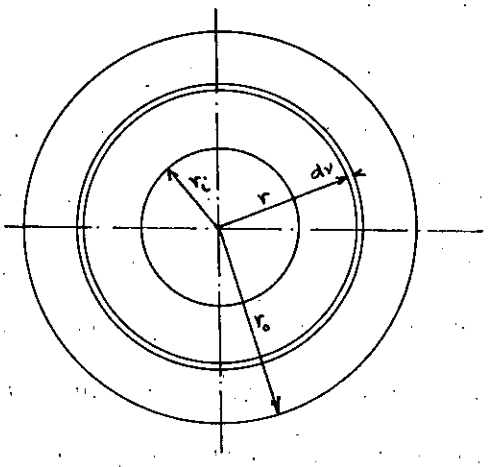

The dimensions of the stainless steel tube used in this investigation were,

Outside diameter = 0.125 inch.

Average thickness = 0.0048 inch $\pm$ 0.0002.

Length. = 6 inches.

The thickness of the tube wall was less than 0.005 inch and the maximum temperature drop across the tube wall never exceeded 10°F. under limiting conditions of critical heat flux at atmospheric pressure. It was, therefore, assumed that the properties of the tube material were constant under these conditions, Leppert and Costello [53], let

H = Constant heat generation rate per unit volume of material.

For steady state conditions, assuming no heat flux at inner surface and radial heat flow only, at any radius

$$H.\pi l \left(r^2 - r_i^2\right) = -2\pi r l k_T \frac{dT}{dr} \qquad (73)$$

$$\text{or} \qquad \frac{H}{2\,k_T}\left(\frac{r^2 - r_i^2}{r}\right) \, dr = - \, dT \qquad (74)$$

Integrating between limits of r_i and r_o; and T_T and Tw,

$$T_T - Tw = \frac{H}{4\,k_T}\left(r_o^2 - r_i^2\right) - \frac{H r_i^2}{2 k_T} \log_e \frac{r_o}{r_i} \qquad (75)$$

Assuming that all the heat generated in the tube wall flows out to the liquid, as was the case in actual experiments,

$$H \cdot v_T = q \cdot A_o \qquad (76)$$

where v_T = Volume of tube material.

$$\text{or} \quad H = q \cdot \frac{2 r_o}{(r_o^2 - r_i^2)} \qquad (77)$$

From equations (75) and (77),

$$(T_T - Tw) = \frac{q r_o}{2 k_T} - \frac{q r_o r_i^2}{k_T (r_o^2 - r_i^2)} \log_e \frac{r_o}{r_i} \qquad (78)$$

For actual values of r_o and r_i,

$$T_T - Tw = 2.03 \times 10^{-4} \cdot \frac{q}{k_T} \qquad (79)$$

where k_T = Thermal conductivity of tube material. Since the temperature drop across the tube wall is small, an arithmetic average value of T_T and Tw is used to fix the thermal conductivity of the material. The values of thermal conductivity of the stainless steel tube at two different temperatures were supplied by the manufacturers of the tube. The value of k_T at 20°C. was 9.192 B.t.u. per hour. ft.^{2} °F., and the temperature coefficient was + 6.51×10^{-3} per degree centigrade rise of temperature.

APPENDIX III

Estimation of heat losses in conductors and tubes.

The location of thermocouples 1.25 inch away from the entrance to and exit from the actual test section introduced an error in heat flux measurements, because of heat losses in conductors and tubes mainly due to conduction and convection.

A simple test was devised to estimate the extent of these losses in conductors and tubes, during experiments in boiling. The following assumptions are made.

1) Since the losses in conductors and tubes are by conduction and convection, the losses depend primarily on the temperature difference between stabilizing fluid and bulk fluid in the test tank.

2) Temperatures measured by the thermocouples are the mean temperatures of the stabilizing fluid flowing past them.

3) The temperature drop in the stabilizing fluid at entry and exit due to losses are equal,

$$\text{i.e. } (T_i - T_2) = (T_3 - T_o)$$

where T_2 and T_3 are the temperatures of the stabilizing fluid at entry to and exit from the test section.

If ΔT_{fb} is the mean temperature difference between stabilizing fluid and bulk in the test tank, then as a first approximation only,

$$\Delta T_{fb} = \frac{(T_i - T_b) - (T_o - T_b)}{\log_e \frac{(T_i - T_b)}{(T_o - T_b)}} \qquad (80)$$

The heat transfer coefficient from the tube outer surface to bulk liquid in the tank was calculated from recommended natural convection equation for horizontal cylinders, McAdam [1]

$$\frac{h_{wa} \cdot d_o}{k_w} = 0.53 \left[\frac{d_o^3 \rho_m^2 g \beta_m \Delta T_{wb}}{\mu_m^2} \left(\frac{c_p \mu}{k} \right)_m \right]^{\frac{1}{4}} \quad (1)$$

Heat transfer coefficients for forced convection from stabilizing fluid to the heater tube inner surface is calculated from the equation,

$$\frac{h_{fc} \cdot d_i}{k_{sf}} = 0.023 \; Re^{0.8} \; Pr^{0.4} \quad (81)$$

Overall heat transfer coefficient between stabilizing fluid and bulk fluid in the test tank is, thus, (based on inner surface),

$$\frac{1}{U} = \frac{1}{h_{wc}} \cdot \frac{d_i}{d_o} + \frac{2l}{k_T} \frac{d_i}{(d_o + d_i)} + \frac{1}{h_{fc}} \quad (82)$$

Total amount of heat transferred in the test section is

$$Qc = U. \quad \Delta T_{fb} \cdot A_i \quad (83)$$

Total heat lost by the stabilizing fluid is given by

$$Q \text{ Total} = (\rho V c)_{sf} \cdot (Ti - To) \quad (84)$$

Heat losses in conductors and tubes is, therefore,

$$Q_L = Q \text{ Total} - Qc \quad (85)$$

If ΔT_i, is the temperature drop in the stabilizing fluid due to losses Q_L only, then

$$\Delta T_i = \frac{Q_L}{(\rho V c)_{sf}} \quad (86)$$

From assumption (3), this loss can be devided equally at inlet and outlet.

$$T_2 = Ti - \Delta T_{fb}/2$$

$$T_3 = To + \Delta T_{fb}/2$$

A first approximation to stabilizing fluid temperatures at actual inlet to and outlet from the test section has, thus, been achieved. It is now necessary to recalculate ΔT_{fb} from equation (80) by replacing Ti and To by T_2 and T_3 respectively. Equations (81) to (86) have also to be recalculated for this new value of ΔT_{fb}.

The value of ΔT_{wb} in equation (1) was assumed a few degrees less than ΔT_{fb}. This assumed value of ΔT_{wb} has to be checked, thus

$$\Delta T_{wb} = \frac{Qc}{A_1 . h_{nc}} \qquad (87)$$

In figure 21, the thermocouple emf equivalent to losses ΔT_l is plotted against the thermocouple emf equivalent to ΔT_{fb}, for a constant stabilizing fluid flowrate of 140 lbs per hour. In actual experiments, a constant flowrate of 140 lbs per hour was maintained. The required emf equivalent of temperature drop in the stabilizing fluid between inlet and outlet was then obtained from figure 21. A sample calculation for water is given here.

Ti = 171.55°F.

To = 166.0°F.

Tb = 92.85°F.

From equation (80), ΔT_{fb} = 75.7°F.

Assumed value of ΔT_{wb} = 68.0°F.

Mean liquid temperature near the heating tube,

$$Tm = \frac{68}{2} + 92.85 = 126.85^{\circ}F.$$

At 127°F.

k_m = 0.3772 B.t.u./hr.°F.ft.

ρ_m = 61.5 lbs/ft^3.

β_m = 2.77 x 10^{-4} °F.$^{-1}$

μ_m = 1.225 lbs/hr.ft.

C_m = 1.0035 B.t.u./lb.°F.

d_o = 1.041 x 10^{-2} ft.

A_o = 1.636 x 10^{-2} ft^2

A = 1.505 x 10^{-2} ft^2

From equation (1), h_{nc} = 316 B.t.u./ft.^{2}hr. °F. ✓

" " (81), h_{fc} = 3640 B.t.u./ft.^{2} hr.°F.

" " (82), U = 310 B.t.u./ft.^{2} hr. °F.

" " (83), Q_c = 353.5 B.t.u./hr.

" " (84), Q Total = 762 B.t.u./hr.

From equation (85), Q_L = 408.5 B.t.u./hr.

" " (86), ΔT_1 = 2.98°F.

T_2 = 170.06°F.

and T_3 = 167.49°F.

Recalculating,

From equation (80), ΔT_{fb} = 75.4°F.

" " (83), Q_c = 353.5°

" " (85), Q_L = 410. B.t.u./hr.

" " (86), ΔT_1 = 3.0°F.

" " (87), ΔT_{ub} = 68.1°F., compared with an assumed value of 68°F., hence satisfactory.

APPENDIX IV.

Sensitivity of the stabilizing fluid system.

Owens [54] defines the sensitivity of the stabilizing system as the ratio of change in stabilizing fluid temperature to the difference in temperature between test section wall and the stabilizing fluid as this temp. difference approaches zero.

$$\text{i.e. Sensitivity} = \lim_{\Delta T_{Tf} \to 0} \frac{\Delta T_{sf}}{\Delta T_{Tf}} \qquad (88)$$

where ΔT_{sf} = temperature change in the stabilizing fluid bulk within the heated length of the test section,

and ΔT_{Tf} = temperature difference between tube inside wall and mean stabilizing fluid bulk.

From a heat balance over the test section,

$$\Delta T_{sf} = \frac{\pi \int_0^l h \cdot \Delta T_{Tf} \cdot di \cdot dl}{m\, C_{sf}} \qquad (89)$$

Assuming that the inner tube diameter and the heat transfer coefficient do not vary along the length, from equation (89),

$$\therefore \Delta T_{sf} = \frac{\pi \cdot h \cdot di \int_0^l \Delta T_{Tf} \cdot dl}{m\, C_{sf}} \qquad (90)$$

$$= \frac{\pi \cdot di \cdot l \cdot h}{m\, C_{sf}} \cdot \overline{\Delta T_{Tf}} \qquad (91)$$

$$\text{where} \quad \overline{\Delta T_{Tf}} = \frac{1}{l} \int_0^l \Delta T_{Tf} \cdot dl \qquad (92)$$

$$\therefore \text{Sensitivity} = \frac{\pi \cdot di \cdot l \cdot h}{m\, C_{sf}} = \frac{4l}{di} \cdot St \qquad (93)$$

where St = Stanton number = $\frac{\pi di^2 \cdot h}{4\, m\, C_{sf}}$

Stanton number for turbulent flow may be obtained from Dittus - Boelter equation (60),

$$St = \frac{0.023}{Re^{0.2} Pr^{2/3}} \quad (94)$$

$$\therefore \text{Sensitivity} = \frac{4\ell}{di} \times \frac{0.023}{Re^{0.2} Pr^{0.67}} \quad (95)$$

Experimental value for water.

Volume flow = 14 Igph = 2.245 ft^3/hour.

di = 9.58×10^{-3} ft.

A_i = 7.21×10^{-5} $ft.^2$

Velocity V = 3.115×10^4 ft/hour.

Re = 2.6×10^4 (for pressure of 14.7 psia)

Pr = 1.754

$\therefore$ Sensitivity = 0.432.

i.e. a temperature difference of 0.432°F. between inlet and outlet temperatures of stabilizing fluid will be observed for every 1°F. difference of temperature between tube inner wall and bulk stabilizing fluid.

Accuracy of stabilising fluid temperature measurement = $\pm$ 0.001 V

$= \pm$ 0.05°F.

$\therefore$ Accuracy of derived average inner wall temperature

$= \pm$ 0.12°F.

APPENDIX V.

Response time of the 0.002 inch diameter thermocouple.

The problem of determining the response time is a complex one. In the arrangement used in this investigation, a thermocouple placed in the superheated layer near the heating tube will have a temperature gradient across its diameter and along its length.

However, Carbon et al [56] have studied the problem carefully and shown by experiments that the heat conducted along the thermocouple wire and heat radiated by the thermocouple junction can be neglected compared with convective heat transfer between the thermocouple and the fluid flowing past it. The authors equation to determine temperature change in the thermocouple with time may be written in the form,

$$(T_4 - Tb) = (T_L - Tb)\left[1 - e^{-\tau/\lambda 13}\right] \qquad (96)$$

$$\text{where} \quad \lambda 13 = \frac{(d\rho c)_{tc}}{4h} \qquad (97)$$

where T_4 = Temperature indicated by the thermocouple τ hours after the change occurs in the liquid by a temperature $(T_L - Tb)$

d = Diameter of the thermocouple wire.

ρ_{tc} = Density of the thermocouple wire.

C_{tc} = Specific thermal capacity of the thermocouple wire.

and h = Coefficient of heat transfer.

The value of a suitable coefficient of heat transfer, for water, may be obtained from, McAdam [1],

$$\frac{hd}{k_f} = 0.42\ (P_r)_f^{0.2} + 0.57\ (Re)_f^{0.5} \cdot (P_r)_f^{0.33} \qquad (98)$$

where k_f = Thermal conductivity of liquid.

The temperature T_f was determined as follows:

$$T_f = \frac{\frac{T_b + T_s}{2} + T_l}{2} \qquad (99)$$

For boiling at 1.0 psia, with an assumed $(T_s - T_b)$ of $40^\circ F$,

$T_s = 142^\circ F.$

$T_b = 102^\circ F.$

$T_4 = 128.9^\circ F.$ for 67.3% of total change in temperature.

$\rho_{tc} = 534$ lbs/ft^3.

$C_{tc} = 0.105$ B.t.u./Lb.$^\circ F.$

$d = 1.67 \times 10^{-4}$ ft.

From equation (99), $T_f = 132^\circ F.$

For liquid velocity past the thermocouple of 10 feet per second, equal to maximum bubble radial velocity,

$V = 10 \times 3600$ FPH

$\rho_l = 62.0$ lbs/ft^3

$\mu = 1.25$ lbs/hr.ft.

$k_f = 0.376$ B.t.u./hr.ft.$^\circ F.$

From equation (98), $h = 3.42 \times 10^4$ B.t.u./ft.^{2} hr.$^\circ F.$

From equation (97), $\lambda_{13} = 6.9 \times 10^{-8}$ hour.

From equation (96), $\tau = 7.65 \times 10^{-8}$ hour.

$= 0.276$ millisecond.

APPENDIX VI.

Use of LASER in boiling experiments.

Advantage was taken of a demonstration by a technical representative of Hughes Aircraft Company to experiment on the use of a LASER as an energy source for providing nucleation at a point.

LASER model 200 with power supply model 250 was used to provide a coherent source of light. The specification of the ruby crystal was

Composition : 0.04% Cr_2O_3 in Al_2O_3

Size : 0.375 inch diameter x 1.5 inches long.

Diameter of beam at

point of focus : 0.375 inch.

optical axis 90^0 with respect to rod axis.

Details of the LASER source were as follows:

Focal length of the lens = 0.75 inch.

Peak power = 10 KW.

Power input duration = 1 millisecond

Power input to LASER = 700 Joules.

Power output from LASER = 1.4 Joules approximately.

Input Voltage = 13.50 volts.

Wavelength of light source = 6943^0 A.

A small glass tank with inside dimensions 2 inches x $\frac{1}{2}$ inch x $2\frac{1}{4}$ inch high was used as the boiling tank. A silicone rubber gasket provided a seal between the perspex top and the sides of the tank. A stainless steel rod $\frac{1}{16}$ inch diameter was sharpened to a needle point and blackened at the needle point by oxidation. The rod was fixed to the perspex top with its needle point located

0.75 inch above the bottom of the tank. The tank was filled with hot water and connected to a vacuum pump through a vacuum break valve.

The LASER was located 2 cms away from the stainless steel needle. Pressure in the tank was reduced until the bulk of the liquid started boiling. When steady state was reached, a pulse of one millisecond duration with maximum energy input of 10 KW over an area of 0.11 square inch was passed. In one millisecond duration, two or three bubbles formed at the tip of the stainless steel needle.

The advantages of a point source with controlled instant of bubble formation are numerous. The first one is saving in time, effort and expense associated with high speed photography if a bubble fails to develop in the short recording period. Secondly, the thermocouple bridge can be located at any desired distance away from the source of bubbles. This would solve the problem of relying on the chance formation of a bubble in the vicinity of the thermocouple. The disadvantages of a point source have already been pointed out at the beginning of chapter 2.

The LASER source of energy provide just the means of creating bubbles at a desired position. However, the power input from the available LASER source is neither constant with time nor over the area. The problem of measurement of heat flux and temperature difference Twb would remain with such an arrangement. The additional problem of determining the absorption coefficient for a metal boiling surface is introduced if a LASER source is used.

TABLE 1.

Heat transfer rate measurements.

Approximate pressure 1.0 psia

Series 1

Pressure	Temperature difference		Heat Flux
p (psia)	$T_w - T_s$ (^oF)	$T_s - T_b$ (^oF)	q/A (B.t.u./Ft.^{2}hr.)
1.02	26.2	2.6	6.65×10^3
1.01	31.0	2.0	9.60×10^3
1.01	38.5	1.9	2.60×10^4
1.00	46.8	1.40	3.01×10^4
1.02	49.5	2.8	9.20×10^4
1.00	54.6	2.4	16.82×10^4
1.00	59.6	2.3	18.90×10^4
1.02	65.5	3.6	22.40×10^4
1.01	71.8	2.5	24.20×10^4
1.01	76.6	2.2	25.25×10^4
1.00	81.2	1.9	24.90×10^4
1.00	86.3	2.5	25.0×10^4
1.00	81.8	2.2	28.4×10^4
1.01	83.5	2.1	25.0×10^4
1.02	81.8	2.5	25.4×10^4

TABLE 2.

Heat transfer rate measurements.

Approximate pressure = 1.0 psia.

Series 2

Pressure	Temperature difference		Heat Flux
p (psia)	$T_w - T_s$ (^oF)	$T_s - T_b$ (^oF)	q/A (B.t.u./Ft^2.hr.)
1.02	87.9	2.0	26.4×10^4
1.05	78.0	1.8	25.9×10^4
1.03	73.4	2.2	24.5×10^4
1.02	70.4	2.4	23.5×10^4
1.05	68.0	1.9	22.9×10^4
1.01	64.1	2.1	20.0×10^4
1.04	63.8	1.6	20.9×10^4
1.02	58.1	2.1	19.5×10^4
1.03	58.5	1.0	16.2×10^4
1.05	50.0	1.9	11.4×10^4
1.04	42.2	1.8	4.5×10^4
1.04	35.5	0.0	9.4×10^3

TABLE 3.

Heat transfer rate measurements.

Approximate pressure = 1.0 psia.

Series 3

Pressure	Temperature difference		Heat Flux
p (psia)	$T_w - T_s$ ($^\circ F$)	$T_s - T_b$ ($^\circ F$)	q (B.t.u./Ft^2.hr.)
1.06	36.7	0.9	1.41×10^4
1.07	42.3	1.7	3.82×10^4
1.05	46.4	0.9	12.90×10^4
1.06	51.8	1.0	15.70×10^4
1.05	56.2	2.0	18.55×10^4
1.07	60.7	3.0	21.0×10^4
1.03	66.7	1.6	22.85×10^4
1.03	69.5	2.5	24.4×10^4
1.02	74.0	1.6	25.8×10^4
1.02	79.0	1.3	25.9×10^4
1.03	82.6	1.0	25.5×10^4
1.03	84.8	-0.3	26.2×10^4

TABLE 4.

Heat transfer rate measurements.

Approximate pressure = 3.0 psia.

Series 1

Pressure	Temperature difference		Heat flux
p (psia)	$T_w - T_s$ (^oF)	$T_s - T_b$ (^oF)	q (B.t.u./Ft^2.hr.)
3.0	13.75	-0.1	2.0×10^3
2.96	18.3	-0.1	5.3×10^3
2.96	20.5	-0.45	9.2×10^3
2.94	26.7	0.2	1.09×10^4
2.98	31.4	0.95	1.58×10^4
2.97	35.8	0.65	2.31×10^4
2.98	39.2	0.8	5.5×10^4
2.97	42.8	0.9	1.07×10^5
2.95	46.7	1.05	1.47×10^5
2.94	51.2	0.8	1.50×10^5
2.98	53.0	1.5	2.10×10^5
2.96	57.2	1.1	2.32×10^5
2.94	62.3	0.7	2.68×10^5
2.94	67.4	1.25	2.78×10^5
2.93	71.5	1.15	2.91×10^5
2.97	76.8	1.45	3.02×10^5
2.96	80.8	1.6	2.95×10^5
2.91	85.9	1.15	2.89×10^5

TABLE 5.

Heat transfer rate measurements.

Approximate pressure = 3.0 psia.

Series 2

Pressure	Temperature difference		Heat flux
p (psia)	$T_w - T_s$ (^oF)	$T_s - T_b$ (^oF)	q (B.t.u./Ft^2.hr.)
2.88	78.8	0.8	2.93×10^5
2.95	69.2	0.5	2.92×10^5
2.98	61.8	1.3	2.72×10^5
2.98	55.4	1.0	2.09×10^5
2.96	46.0	0.75	1.46×10^5
2.99	40.85	0.25	7.61×10^4
2.98	35.6	0.0	3.19×10^4
2.94	29.4	0.2	1.54×10^4
2.93	24.8	0.7	1.02×10^4
3.01	20.9	1.1	8.66×10^3
3.01	18.4	0.0	5.3×10^3

TABLE 6.

Heat transfer rate measurements.

Approximate pressure = 3.0 psia.

Series 3

Pressure	Temperature difference		Heat flux
p (psia)	$T_w - T_s$ (^oF)	$T_s - T_b$ (^oF)	q (B.t.u./Ft^2.hr.)
3.00	26.6	1.3	1.74×10^4
3.00	32.9	1.5	2.85×10^4
3.02	38.2	2.1	5.55×10^4
3.00	43.3	1.2	11.65×10^4
3.00	48.8	1.3	17.3×10^4
2.98	54.8	1.2	20.9×10^4
2.98	60.0	1.6	24.65×10^4
2.97	66.9	1.2	27.1×10^4
2.97	71.2	1.4	28.0×10^4
3.0	75.0	2.0	30.0×10^4
2.98	79.2	2.3	30.6×10^4
2.98	83.2	1.3	30.6×10^4
2.98	82.1	1.2	30.8×10^4

TABLE 7

Heat transfer rate measurements.

Approximate pressure = 7.0 psia.

Series 1

Pressure	Temperature difference		Heat flux
p (psia)	Tw-Ts (^{o}F)	Ts-Tb (^{o}F)	q (B.t.u./Ft^2.hr.)
7.20	17.7	0.45	4.0×10^3
7.16	22.3	0.8	8.56×10^3
7.14	27.35	0.75	1.67×10^4
7.07	32.55	0.4	2.13×10^4
7.04	37.35	0.45	3.42×10^4
7.04	41.2	0.7	6.6×10^4
7.02	44.4	0.6	1.64×10^5
7.01	48.1	0.5	2.17×10^5
6.97	52.2	0.2	2.56×10^5
7.01	58.1	0.85	3.02×10^5
7.01	61.8	0.65	3.18×10^5
6.98	70.8	0.5	3.43×10^5
6.98	73.5	-0.2	3.22×10^5

TABLE 8

Heat transfer rate measurements.

Approximate pressure = 7.0 psia.

Series 2

Pressure	Temperature difference		Heat flux
p (psia)	$T_w - T_s$ (^oF)	$T_s - T_b$ (^oF)	q (B.t.u./Ft^2/hr.)
6.97	69.3	0.4	3.24×10^5
6.94	66.2	0.6	3.23×10^5
6.97	60.4	0.7	3.09×10^5
6.94	55.4	1.2	2.86×10^5
7.04	48.0	0.4	2.27×10^5
7.07	44.2	0.3	1.70×10^5
7.05	40.4	0.2	9.9×10^4
7.04	35.5	0.2	3.93×10^4
6.98	29.5	0.8	2.3×10^4
6.92	24.5	1.1	8.42×10^3
6.98	20.0	0.5	6.54×10^3
6.93	15.2	1.1	3.96×10^3

TABLE 9

Heat transfer rate measurements.

Approximate pressure = 7.0 psia.

Series 3

Pressure	Temperature difference		Heat flux
p (psia)	Tw-Ts (^{o}F)	Ts-Tb (^{o}F)	q (B.t.u./Ft^2.hr.)
6.99	21.8	1.75	7.5×10^3
6.98	27.0	1.7	1.31×10^4
6.93	37.9	1.9	3.4×10^4
6.95	44.0	1.9	9.74×10^4
7.01	48.8	0.35	2.41×10^5
6.99	55.7	-0.25	2.88×10^5
6.99	62.6	-0.45	3.04×10^5
6.97	68.0	-0.45	3.13×10^5
6.96	72.8	-0.75	3.10×10^5
7.03	72.5	-0.60	3.22×10^5
7.02	75.3	-0.90	3.21×10^5
7.00	69.1	-1.10	3.17×10^5
6.99	73.8	0.05	3.12×10^5
7.00	69.7	3.1	3.25×10^5

TABLE 10.

Heat transfer rate measurements.

Approximate pressure = 14.4 psia

Series 1

Pressure	Temperature difference		Heat flux
p (psia)	Tw-Ts (^{o}F)	Ts-Tb (^{o}F)	q (B.t.u./Ft^2.hr.)
14.3	5.75	1.05	3.93×10^3
14.3	7.4	0.25	6.23×10^3
14.3	10.75	0.05	9.25×10^3
14.3	15.3	-0.25	1.22×10^4
14.3	19.05	-0.45	1.85×10^4
14.3	24.6	-.0.45	2.27×10^4
14.3	29.3	-0.45	7.0×10^4
14.3	32.6	-0.35	2.0×10^5
14.3	33.55	-0.25	3.0×10^5
14.3	42.0	-0.25	3.95×10^5
14.3	45.4	0.05	4.4×10^5
14.47	48.0	-0.05	4.9×10^5
14.46	51.25	0.0	5.2×10^5
14.46	55.4	-0.1	5.3×10^5
14.45	60.6	-0.1	5.3×10^5
14.44	63.3	-0.2	5.0×10^5
14.43	65.9	-0.3	49.6×10^4
14.48	67.2	-0.2	49.5×10^4
14.47	66.0	-0.25	49.6×10^4
14.46	68.8	-0.4	48.9×10^4
14.44	70.9	-0.6	48.8×10^4

TABLE 11

Heat transfer rate measurements.

Approximate pressure = 14.45 psia

Series 2

Pressure	Temperature difference		Heat flux
p (psia)	Tw-Ts (^{o}F)	Ts-Tb (^{o}F)	q (B.t.u./Ft^2.hr.)
14.44	64.6	-0.5	5.01×10^5
14.46	55.7	-0.8	5.18×10^5
14.46	47.4	-0.9	4.77×10^5
14.46	40.1	-0.7	3.59×10^5
14.45	35.7	-0.3	2.66×10^5
14.45	30.1	-0.3	1.60×10^5
14.45	24.7	-0.6	3.96×10^4
14.64	16.9	-0.2	1.44×10^4
14.64	7.4	-0.2	6.27×10^3

TABLE 12

Heat transfer rate measurements.

Approximate pressure = 14.6 psia

Series 3

Pressure	Temperature difference		Heat flux
p	Tw-Ts	Ts-Tb	q
(psia)	(^{o}F)	(^{o}F)	(B.t.u./Ft^2.hr.)
14.61	23.65	-0.35	2.22×10^4
14.61	30.5	-0.45	7.74×10^4
14.62	33.5	-0.15	2.09×10^5
14.62	38.3	-0.15	2.84×10^5
14.62	43.3	-0.1	3.97×10^5
14.59	47.3	-0.55	4.90×10^5
14.58	52.8	-0.7	5.24×10^5
14.58	57.2	-0.5	5.26×10^5
14.60	61.6	-0.9	5.4×10^5
14.58	63.3	-0.1	5.3×10^5

TABLE 13.

Maximum diameter of bubbles in saturated pool boiling.

essure aia	Heat flux B.t.u/Ft.^{2}hr.	Temperature Difference Tw-Ts °F.	Mean Diameter of Bubble D (Experimental). IN.	Diameter of bubble from tube. EQN.(22) IN.	Diameter of bubble from flat surface EQN.(19) IN.	Diameter of bubble from flat surface EQN.(26) IN.	Experimental value of diameters for tubes modified to correspond to a flat surface. IN.	Maximum bubble diameter EQN.(8) IN.	Reference for experimental values of diameter
581	1.47×10^5	65.8	0.87	0.66	-	5.3 -	10.5 -	0.122	Patten [2]
935	1.47×10^5	60.5	0.46	0.44	-	3.45	3.34	0.120	"
28	1.74×10^5	60.0	0.25	0.26	-	0.91	0.94	0.115	"
0	5.6×10^4	44.0	1.6 ± 0.2	1.51	4.5	3.4	4.8	0.118	This wo
0	2.6×10^5	84.0	1.3 ± 0.1	1.30	3.3	3.4	3.4	0.118	"
0	6.68×10^4	39.0	$1.05 \pm .05$	0.78	1.0	1.06	1.9 ?	0.115	"
0	3.1×10^5	80.0	0.9 ± 0.2	0.76	1.01	1.06	1.9	0.115	"
0	3.5×10^4	29.0	0.45	-	0.55	0.41	-	0.113	"
0	6.1×10^4	30.5	0.50	-	0.363	0.41	-	0.113	"
0	3.3×10^5	70.0	0.35 ± 0.1	-	0.354	0.41	-	0.113	"
7	4.8×10^4	24.0	$0.1 \rightarrow 0.19$	-	0.142	0.19	-	0.11	"
7	5.2×10^5	60.0	-	-	0.096	0.19	-	0.11	"

Patten's Eqn. $D_{max}^2 = 3N_J y d_o$.

TABLE 14

$$D = \lambda_2 . t^{x_2} \quad (6)$$

Pressure (psia)	λ_2 (Average)	x_2 (Max.)	x_2 (Min.)	x_2 (Average)
1.0	2.24	1.15	0.64	0.75
3.0	0.51	0.742	0.308	0.47
7.0	0.30	0.525	0.358	0.44
14.7	0.041	0.536	0.176	0.325

TABLE 15

Bubble growth velocity and pressure pulse velocity in nucleate boiling

Pressure	Bubble Reference No.	Position of initiation	Radial Bubble growth rate at initiation	Velocity of disturbance	Distance of the thermocouple from tube upper surface.
(psia)		(IN.)	(Ft/sec)	(Ft/sec)	(IN.)
1.02	07B1	1.02	6.6	8.5	0.019
1.01	12B2	1.09	8.1	5.9	0.014
1.01	12B3	1.17	9.6	7.9	0.014
1.01	12B6	0.615	5.8	5.7	0.014
0.98	16B4	0.835	4.6	6.1	0.006
0.98	16B6	1.16	5.5	6.0	0.006
1.06	25B3	1.71	6.95	2.8	0.046
1.06	25B5	1.25	3.8	1.5	0.046
1.06	26B2	0.855	4.5	5.1	0.046
3.08	17B1	0.65	7.0	3.80	0.006
3.08	17B4	0.65	9.6	6.3	0.006
3.08	17B5	0.65	3.7	5.4	0.006
3.08	17B6	0.65	8.0	5.4	0.006
3.08	17B7	0.835	7.25	7.2	0.006
3.08	17B8	0.65	11.6	7.2	0.006

REFERENCES

1) McAdams, W.H., "Heat Transmission", 3rd ed., McGraw - Hill, New York, 1954.
2) Gunther, F.C., and Kreith, F., "Photographic Study of Bubble Formation in Heat Transfer to Subcooled Water", Heat Transfer and Fluid Mechanics Institute, 1949, p. 113-19.
3) Forster, K.E., and Greif, R., "Heat Transfer to a Boiling Liquid - Mechanism and Correlation," Trans. A.S.M.E., Vol. 81C, February 1959, p. 43 - 53.
4) Chang, Y.P., and Snyder, N.W., Heat Transfer in Saturated Boiling", Chemical Engineering Progress, Symposium Series No. 30, 1960, p. 25 - 38.
5) Rohsenow, W.M., "A Method of Correlating Heat Transfer Data for Surface Boiling of Liquids", Trans. A.S.M.E., vol. 74, 1952, p. 969 - 76.
6) Levy, S., "Generalised Correlation of Boiling Heat Transfer", Trans. A.S.M.E., vol. 81C, February 1959, p. 37.
7) Bernath, L., "A Theory of Local Boiling Burnout and its Application to Existing Data", Chemical Engineering Progress, Symposium Series No. 30, 1960, p. 95 - 116.
8) Patten, T.D., "Studies in Nucleate Boiling", Report No. R49, McGill University, August 1958.
9) Berenson, P.J., "Experiments on Pool Boiling Heat Transfer", Int. Jour. Heat and Mass Transfer (IJHMT), vol. 5, October 1962, p. 985 - 1,000.
10) Bernard, J.S., "Observation of Transition Boiling Heat Transfer Phenomenon", Contract W-31-109-Eng-38., ORSANL - 6175, June 1960.
11) Ivey, H.J., "Acceleration and Critical Heat Flux in Pool Boiling Heat Transfer", Proceedings. Inst. Mech. Engrs., vol. 177, No.1, 1963.
12) Poletarkin, P.G., Petrov, V.I., and others", " A New Method for the Investigation of Heat Transfer in the Boiling of Liquids", Dokl. Akad. Nauk., S.S.S.R, vol. 90, No. 5, 1953, p. 775 - 76. A.E.R.E. Translation 11/3/5/966; 1957.
13) Nukiyama, S.," Experiments on the Determination of Maximum and Minimum Values of the Heat Transferred Between a Metal Surface and Boiling Water", Jour. Society Mech. Engrs., JAPAN, vol. 37, 1934, p. 367 - 74. A.E.R.E. Translation 854.
14) Braunlich, R.H., S.M. Thesis in Chemical Engineering, M.I.T. 1941. [from ref. (1)]
15) Cryder, D.S., and Finalborgo, A.C., "Heat Transmission from Metal Surfaces to Boiling Liquids; Effect of Liquid Temperature on the Liquid Film Coefficient", Trans. A.I.Ch.E., vol. 33, 1937, p. 346 - 61.
16) Van Stralen, S.T.D., "Heat Transfer to Boiling Binary Mixtures", British Chemical Engineering, vol. 4, No. 1, Jan. 1959, p. 8.
17) Nishikawa, K., and Urakawa, K., "An Experiment of Nucleate Boiling Under Reduced Pressure", Memo. Faculty Engineering, Kyushu Univ., vol. 19, No. 3, March 1960, p.139 - 147.
18) Bonilla, C.F., and Perry, C.H., "Heat Transfer to Boiling Binary Mixtures", Trans. A.I.Ch.E., vol.37, 1941, p. 685 - 705.

19) Cichelli, M.T., and Bonilla, C.F., "Heat Transfer to Liquids Boiling Under Pressure", Trans. A.I.Ch.E., vol. 41, 1945, p.755 - 87; and Trans. A.I.Ch.E., vol. 42, 1946, p. 411 - 12.

20) Kurihara, H.M., and Myers, J.E., "The Effect of Superheat and Surface Roughness on Boiling Coefficients", Trans. A.I.Ch.E., Vol. 6, No. 1, March 1960, p.83.

21) Lienhard, J.H., and Schrock, V.E., "The Effect of Pressure, Geomertry and the Equation of State upon the Peak and Minimum Boiling Heat Flux", A.S.M.E. - A.I.Ch.E. Joint Heat Transfer Conference, paper No. 62-HT-3.

22) Wilson, E.B., "An Introduction to Scientific Research", 1st ed., McGraw - Hill, New York, 1952.

23) Suber, N., "Nucleate Boiling - The Region of Isolated Bubbles and the Similarity with Natural Convection", I.J.H.M.T., vol. 6, No. 1, Jan. 1963.

24) Stock, B.J., "Observation on Transition Boiling Heat Transfer Phenomenon", Contract. W-31-109-eng-38, O.T.S., June 1960, 78 p.

25) Patten, T.D., Private Communication.

26) Jakob, M., "Heat Transfer", 1st ed., John Wiley and Sons, New York, 1950.

27) Zmola, P.C., "Investigation of Mechanism of Boiling in Liquids", Ph.D. Thesis, Purdue Univ., W. Lafayette, Indiana, June 1950.

28) Gaertner, R.F., and Westwater, J.W., "Population of Active Sites in Nucleate Boiling Heat Transfer", Chemical Engineering Progress, Symposium Series No. 30, 1960.

29) Fritz, W., "Calculation of Maximum Volume of Vapour Bubble", Physik. Zeit., vol. 36, 1935, p. 379.

30) Griffith, P., "Bubble Growth Rate in Boiling", Trans. A.S.M.E., vol. 80, No.3, April 1958, p. 721 - 27.

31) Bankoff, S.G., and Mikesell, R.D., "Growth of a Bubble in a Liquid of Initially Non-uniform Temperature Field", A.S.M.E., Annual meeting, 58-A-105, Dec. 1958.

32) Zuber, N., "On the Stability of Boiling Heat Transfer", Trans. A.S.M.E., vol. 80, 1958, p.711.

33) Zuber, N., and Tribus, M., "Further Remarks on the Stability of Boiling Heat Transfer", Report No. 58-5, project No.34, A.E.C.U - 3621, U.S.A.E.C., Dept. of Eng., Univ. of Calif., California.

34) Staniszewski, B.E., "Nucleate Boiling Bubble Growth and Departure", ONR, NONR - 1841 (39). D.S.R. Proj. No.7 - 7673, August 1959.

35) Chang, Y.P., "An Analysis of Critical Conditions and Burnout in Boiling Heat Transfer" - section I & II", Contract AT-(11-1)-785, July 1961, Univ. of Notre Dame, Indiana.

36) Semeria, R.L., " An Experimental Study of Characteristics of Vapour Bubbles", Symp. on two phase flow, paper No. 7, Inst. of Mech. Engrs., 7.2.1962, p.26.

37) Volyak, A.D., "Surface Tension of Water Measured Between 20°C. and 354°C.", Dokl. Akad. Nauk., S.S.S.R, vol. 74, No.2, 1950, p.307 - 10.

38) Addoms, J.N., "Heat Transfer at High Rate to Water Boiling Outside Cylinders", D.Sc. Thesis, Chem. Eng., M.I.T., 1948.

39) Kutateladze, S.S., "The Hydrodynamic Model of the Heat Exchange Crisis in Boiling Liquids with Free Convection", Academy of Science, USSR, TOM xx Bb III, 11. 1950.

40) Borishanskii, V.M., "An Equation Generalizing Experimental Data on the Cession of Bubble Boiling in a Large Volume of Liquid", Zhurn. Tekh. Fiz., vol. 25, 1956, p.252. Soviet-Physics - Tech. Physics, vol.1, No. 2, p.438.

41) Deissler, R.G., "Prediction of Critical Heat Fluxes for Saturated or Slightly Subcooled Forced and Natural Convection Boiling", Heat Transfer Symp., Columbis Univ., 1954, (from ref. [43]).

42) Cole, R., "A Photographic Study of Pool Boiling in the Region of Critical Heat Flux", Jour. A.I.Ch.E., Vol. 6, No. 4, Dec. 1960, p.533.

43) Rohsenow, W., and Griffith, P., "Correlation of Maximum Heat Flux Data for Boiling of Saturated Liquids", Chem. Eng. Progress Symp., vol. 52, No. 18, 1956, p.47.

44) Zuber, N., Tribus, M., and Westwater, J.W., "The Hydrodynamic Crisis in Pool Boiling of Saturated and Subcooled Liquids", Int. Development in Heat and Mass Transfer, pt. II. A.S.M.E. 1961, p.230 - 6.

45) Borishanskii, V.M., "Heat Transfer to a Liquid Freely Flowing over a Surface Heated to a Temperature Above the Boiling Point", Problems of heat transfer during change of state, AEC-tr-3405, 1953, p.109.

46) Berenson, P.J., "Transition Boiling Heat Transfer", 4th National heat transfer conference, A.I.Ch.E. - A.S.M.E., 1960, preprint 18.

47) Stein, R.P., Task IX, Tech. Note., IXTN-3-38, 8.10.1958, Dept. of Mech. Eng., Columbia University, p. 1-33.

48) Chang, Y.P., "Some Possible Critical Conditions in Nucleate Boiling", A.S.M.E., vol. 85, No.2, May 1963. p. 89.

49) Berenson, P.J, "Transition Boiling Heat Transfer from a Horizontal Surface", MIT, Division of Sponsored research, March, 1960, proj. No.7 - 8077, 117 p., from ref. [11]

50) Kazakova, E.A., "The Influence of Pressure on the First Crisis in Boiling Water from a Horizontal Surface", Problems of heat transfer with change of phase, GEI. Moscow, 1953.

51) Morozov, V.G., "New Experimental Data on Critical Heat Loads at Boiling of Liquids on a Submerged Heating Surface". IJHMT, vol. 5, July 1962, p.661-6.

52) Glasstone, S., "Principles of Nuclear Reactor Engineering", MacMillan & Co. Ltd., 1956.

53) Leppert, Costello, C.P., and Hoglund, B.M., "Boiling Heat Transfer to Water Containing a Volatile Additive", Trans. A.S.M.E., vol.80, 1958, p.1395.

54) Owen, W.L., "An Analytical and Experimental Study of Pool Boiling with particular Reference to Additives", Ph.D. Thesis, Univ. of Aberdeen, 1961.

55) Semeria, R., "Echanges Thermiques. - Caractéristiques des Bulles de Vapeur sur une paroi Chauffante dans l'eau en ébullition à haute pression", C.R. Acad. Sc., t. 256, p.1227 - 30. Séance du 4 février 1963, Groupe 5.

56) Carbon, M.W., Kutsch, H.J., and Hawkins, G.A., "The Response of Thermocouples to Rapid Gas Temperature Changes," Trans. A.S.M.E., vol. 72, 1950, p.655.

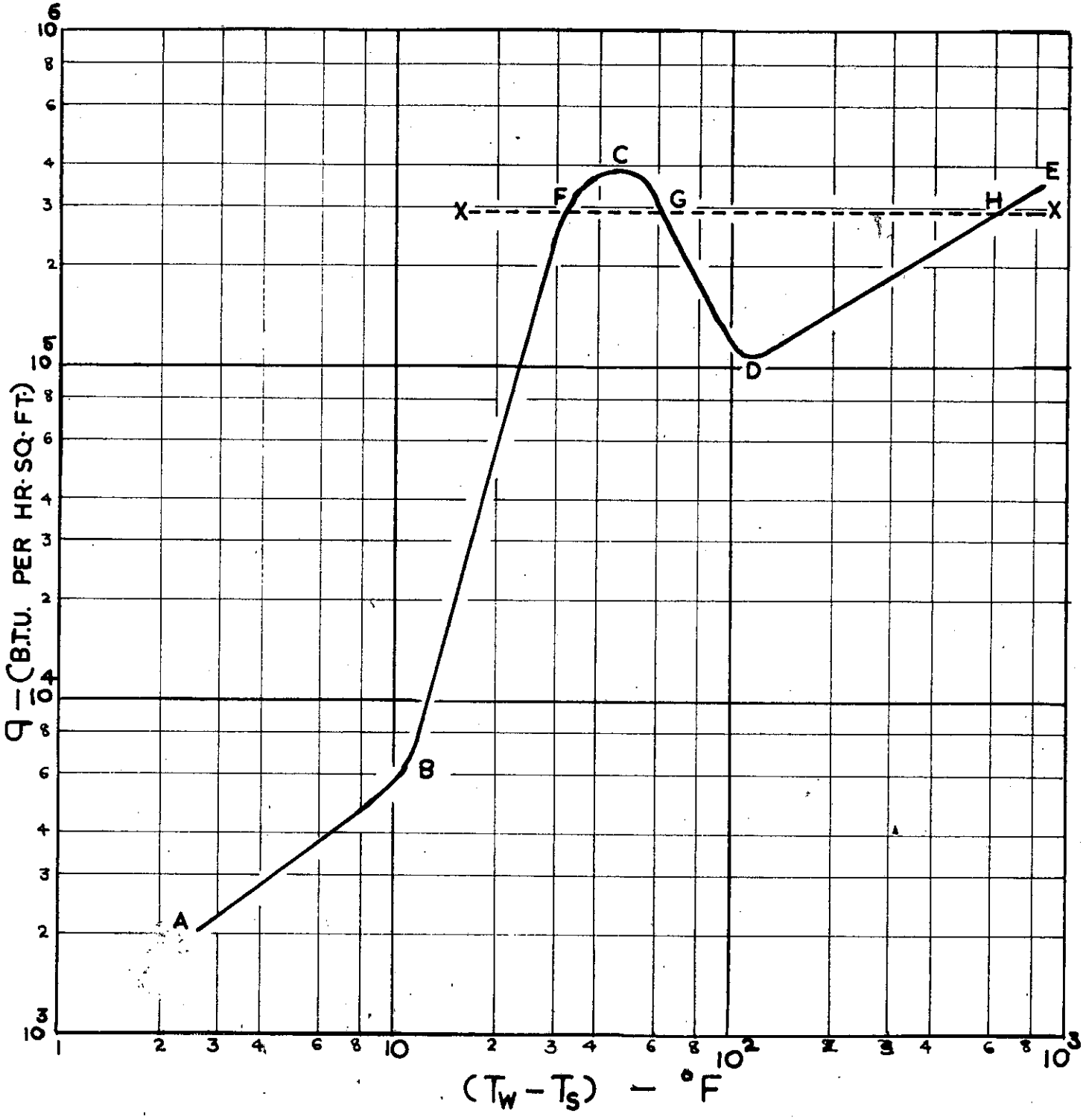

FIG·1.

A TYPICAL CURVE OF HEAT TRANSFER Vs SURFACE TEMPERATURE IN BOILING.

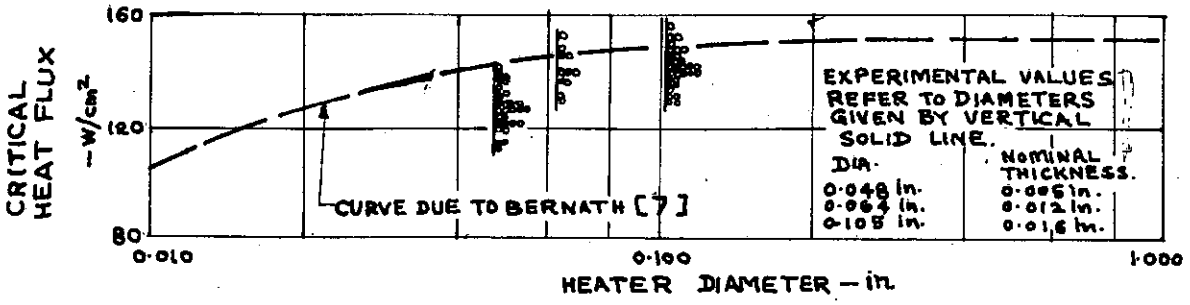

EFFECT OF HEATER DIA. ON CRITICAL HEAT FLUX.
FIG·2 (REPRODUCED FROM REF. [11].)

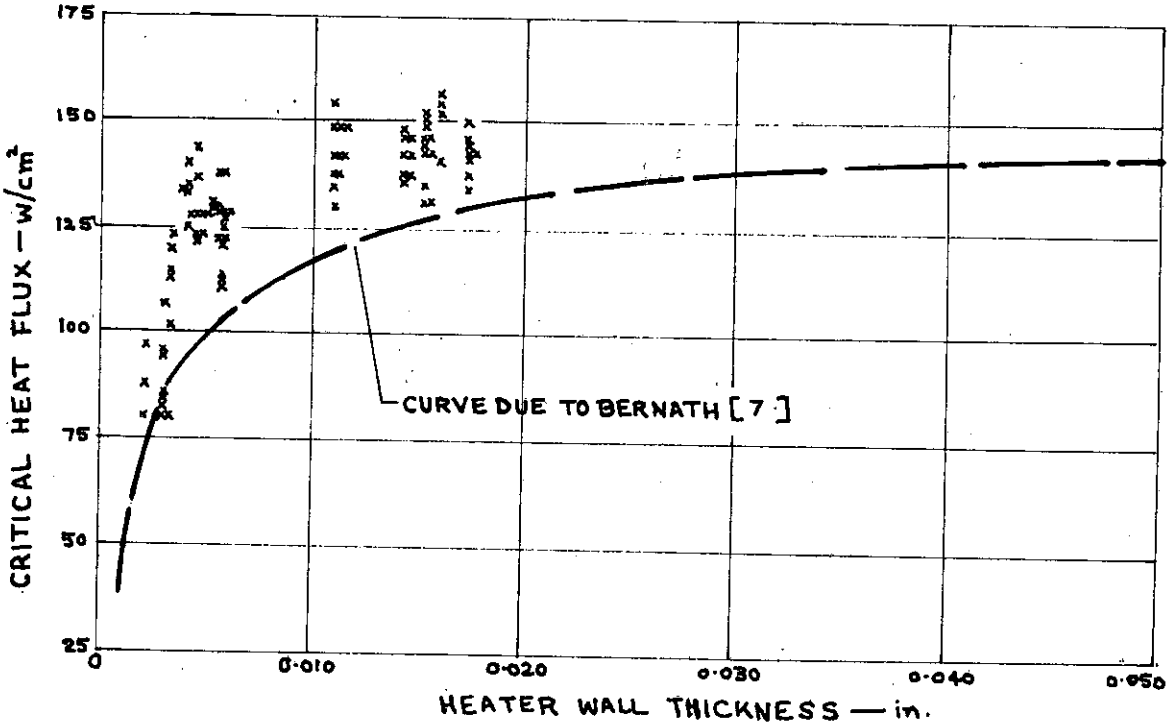

EFFECT OF HEATER WALL THICKNESS ON CRITICAL HEAT FLUX.
FIG·3 (REPRODUCED FROM REF. [11].)

DETAILS OF ASSEMBLY OF HEATING TUBE, CONDUCTOR, THERMOCOUPLE SUPPORTS FOR MEASURING STABILIZING FLUID TEMPERATURE AND 'O' RING SEAL AT TANK WALL.

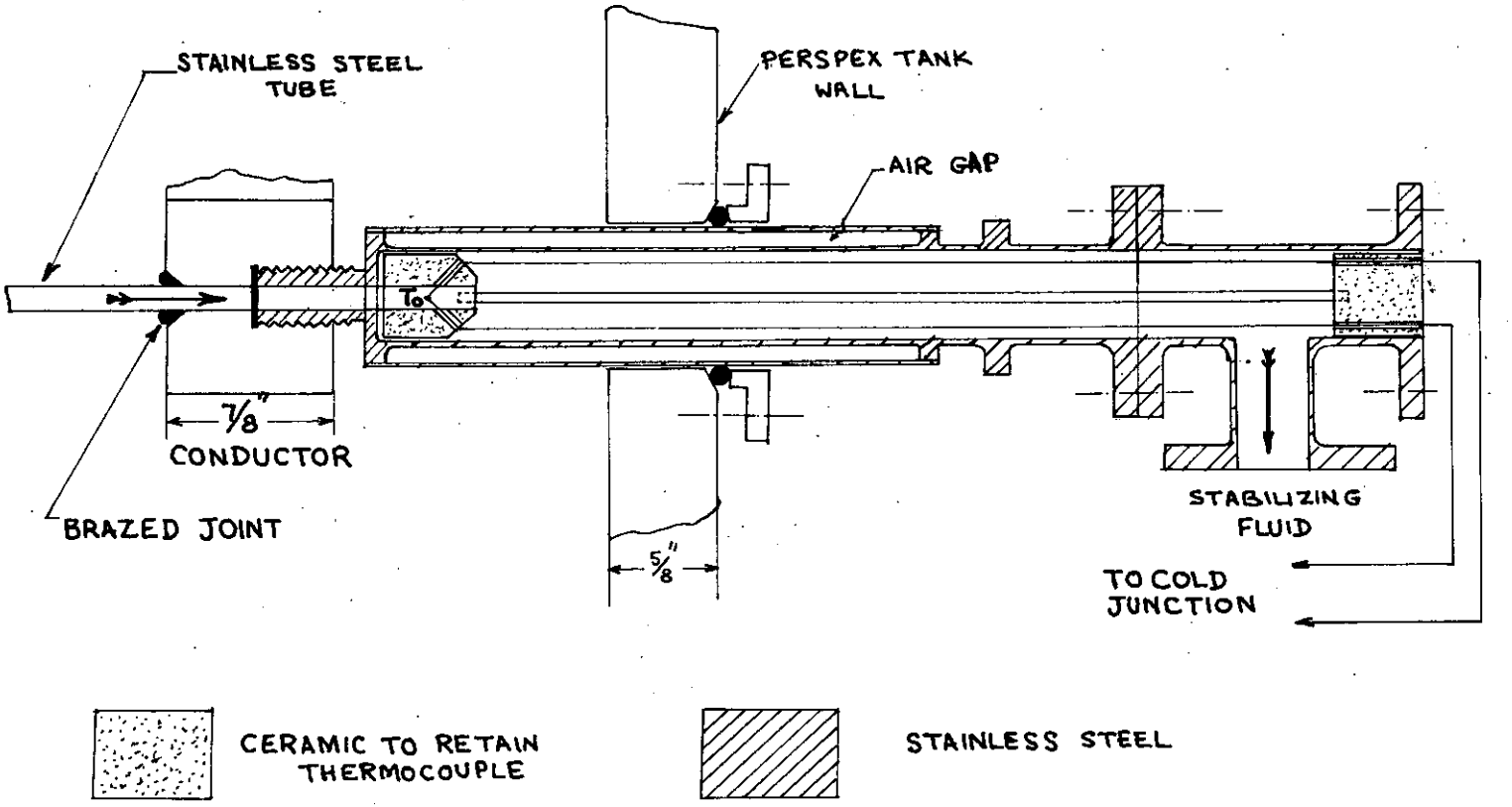

SECTION

FIG·4

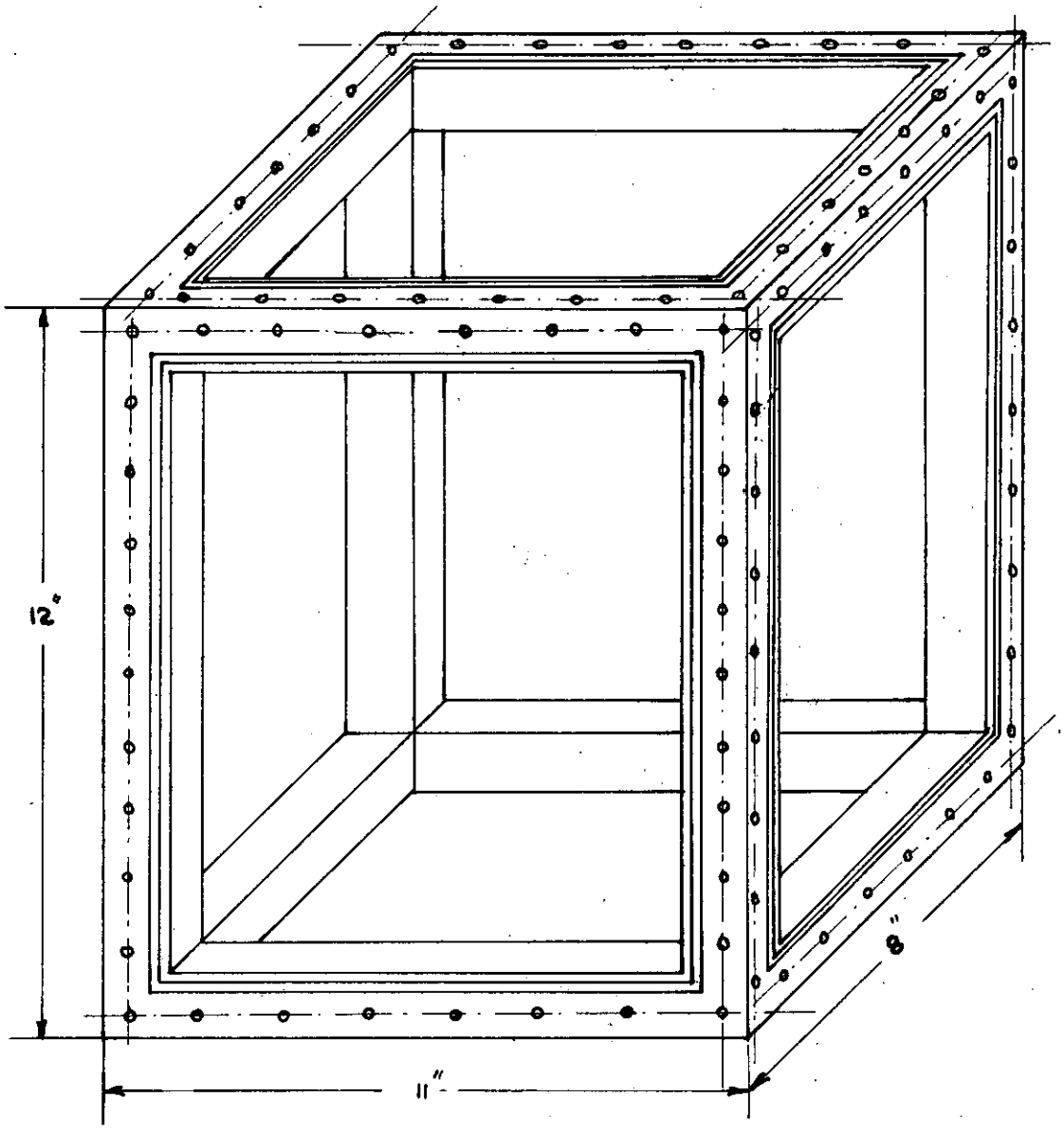

TANK FRAME, TANK NO·2

FIG·5

VACUUM CIRCUIT

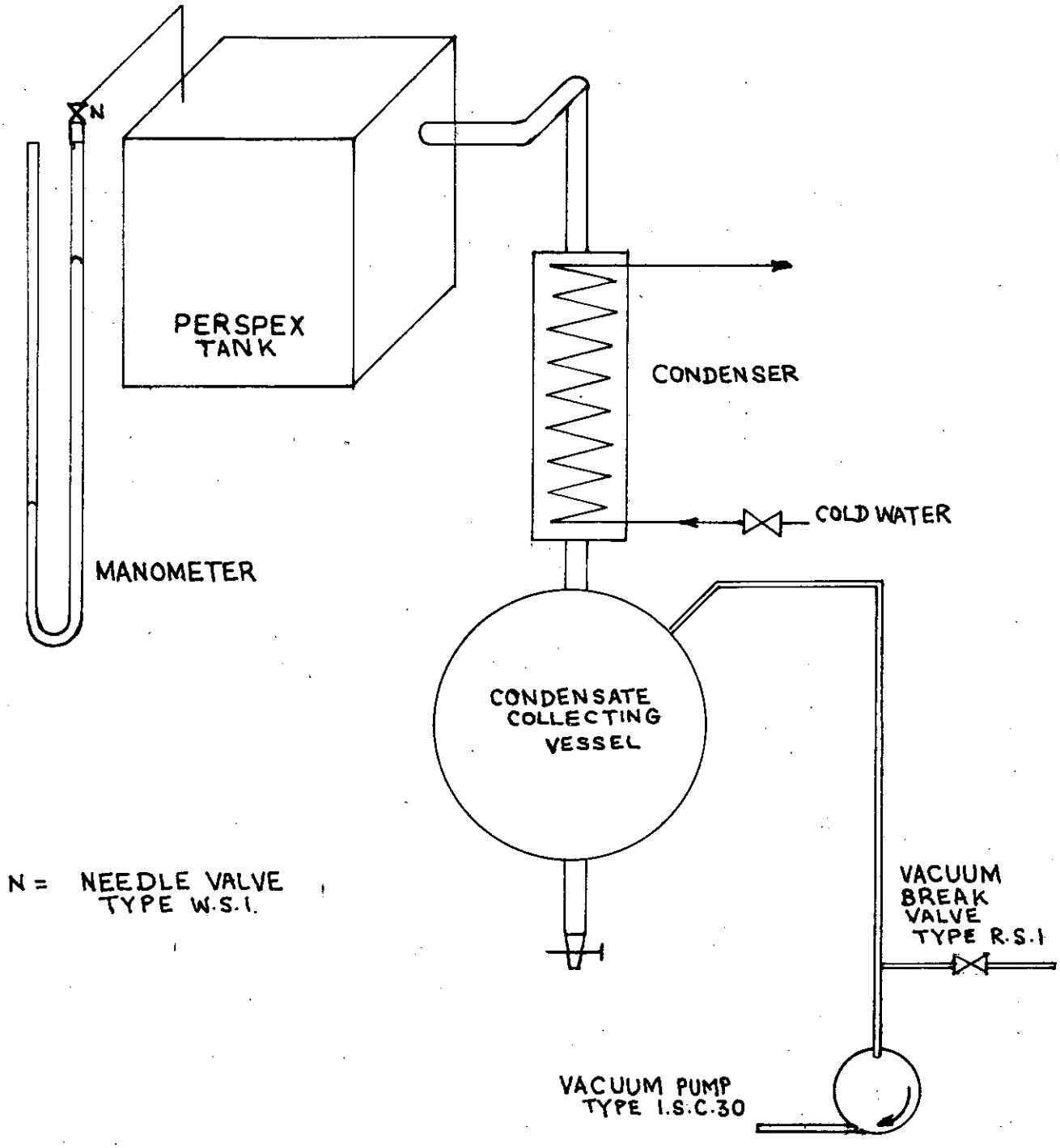

FIG·6

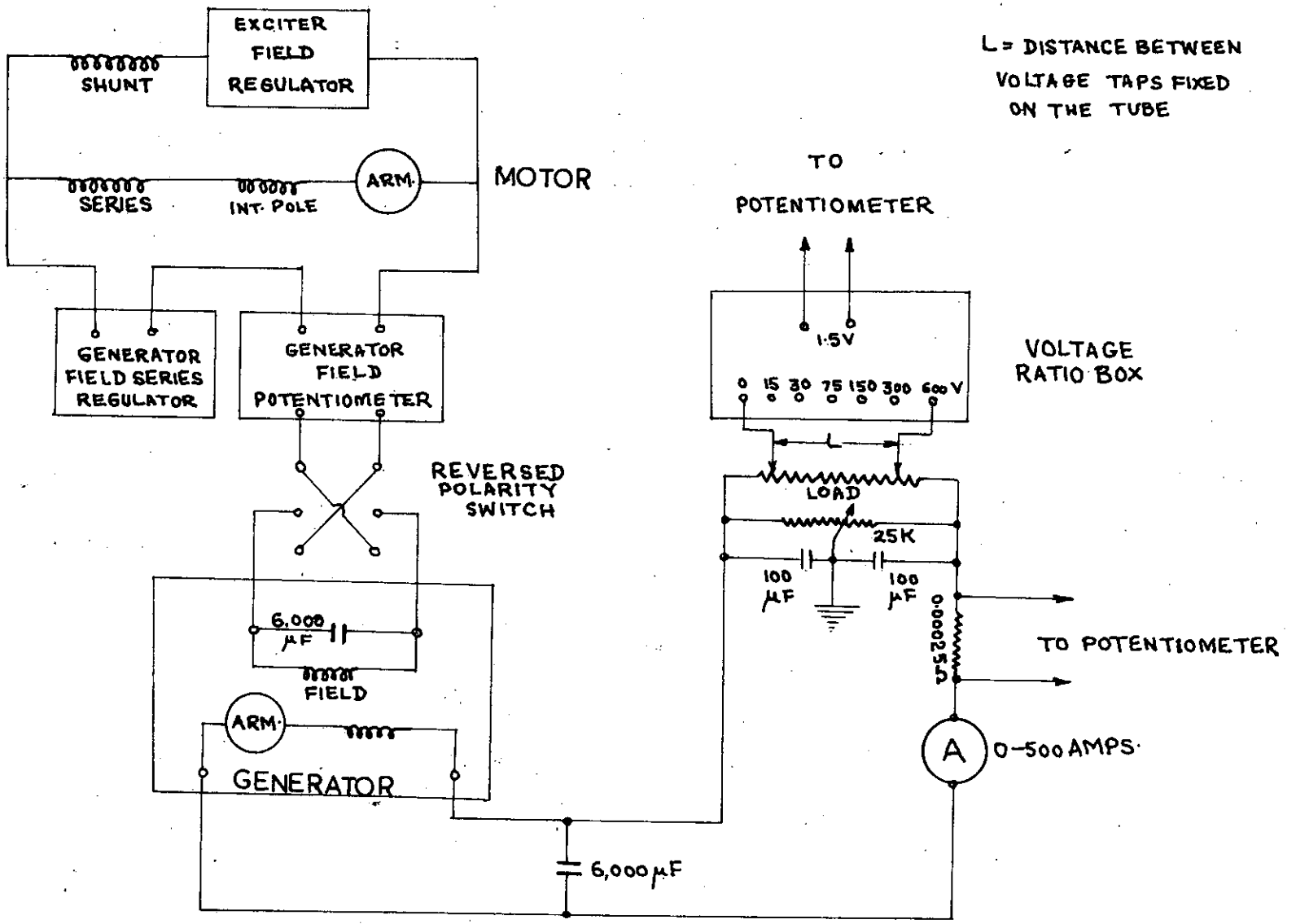

POWER CIRCUIT FIG·7

STABILIZING CIRCUIT

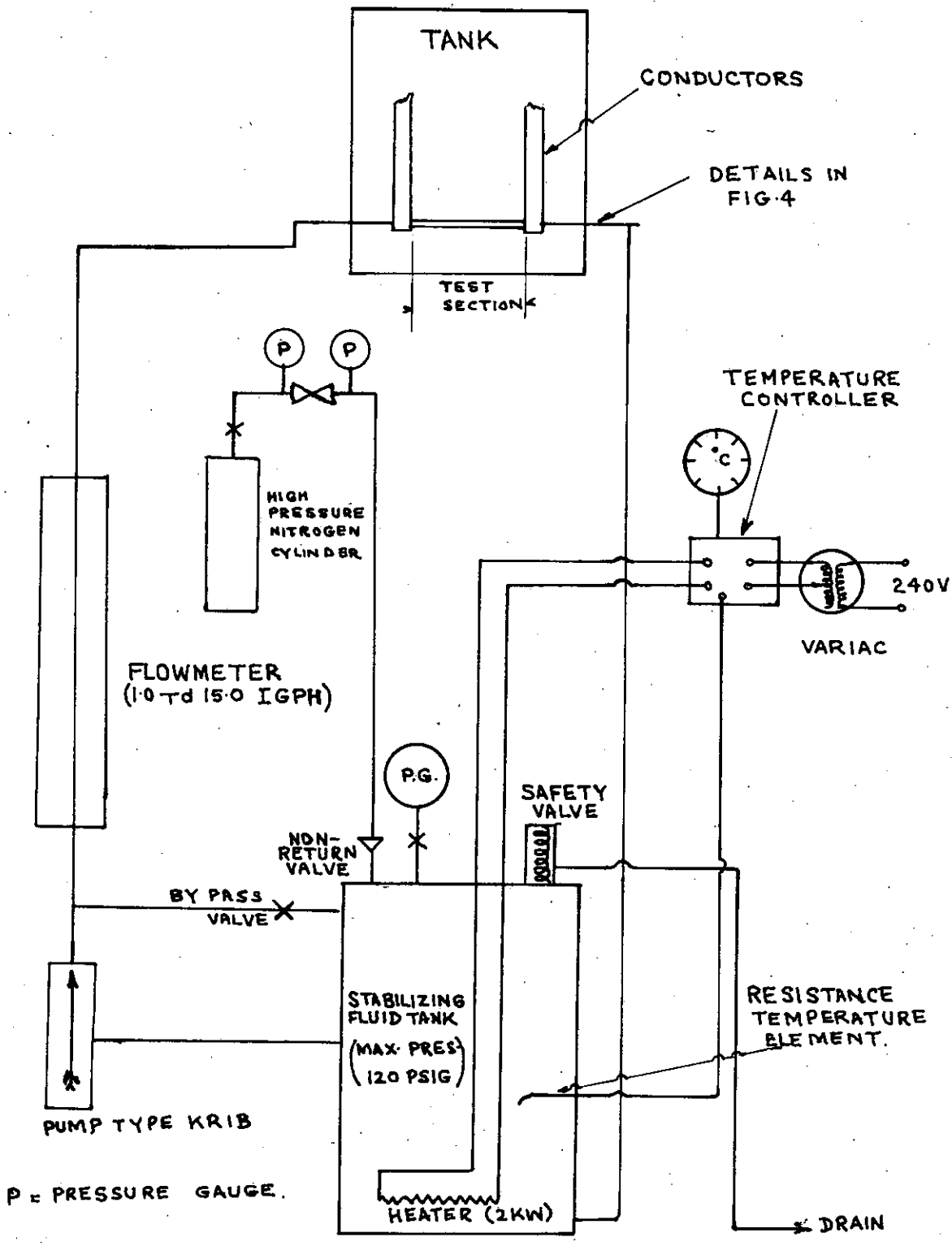

FIG·8

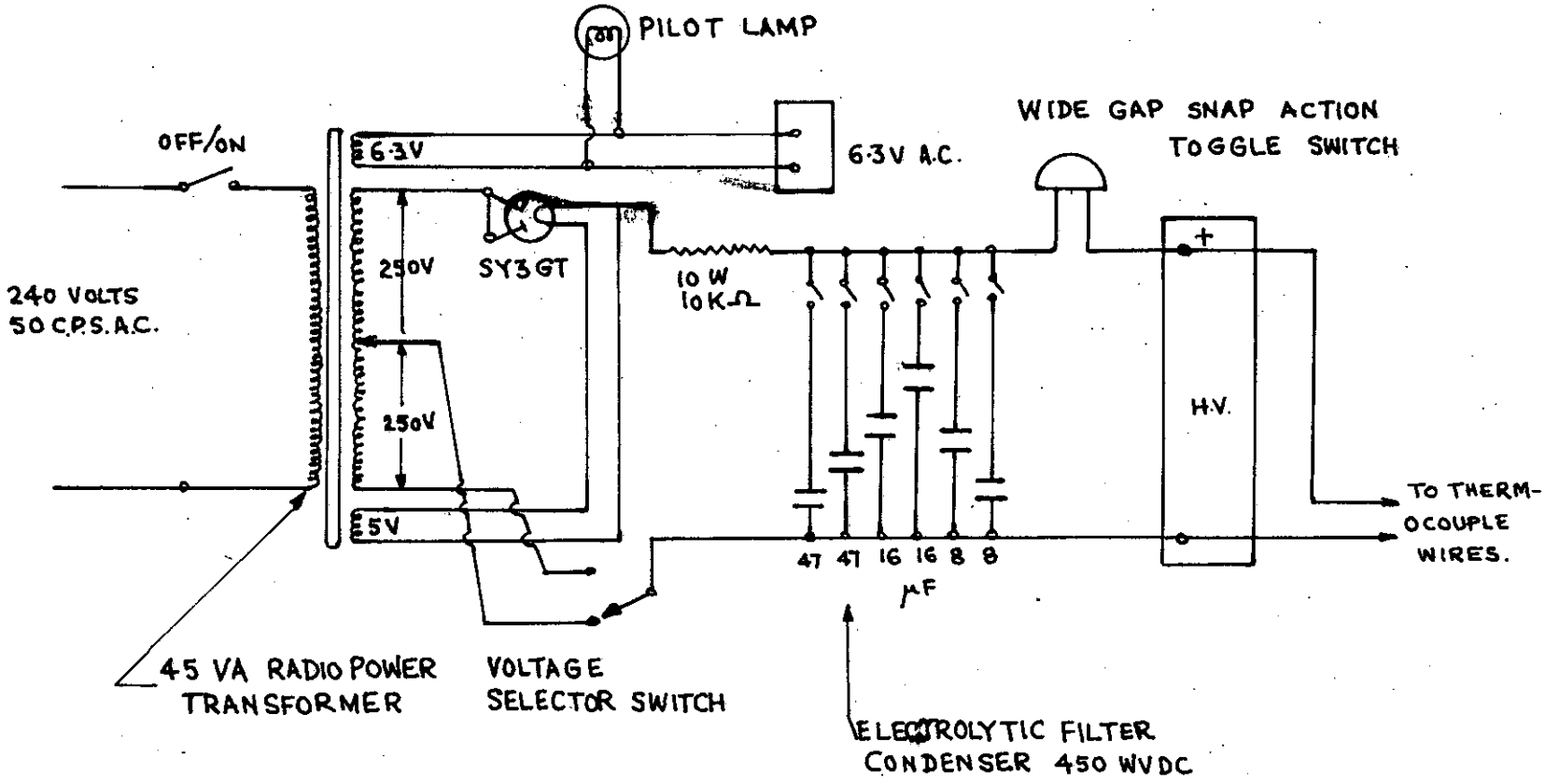

SMALL ARC WELDER FOR THERMOCOUPLE WIRES

FIG·9

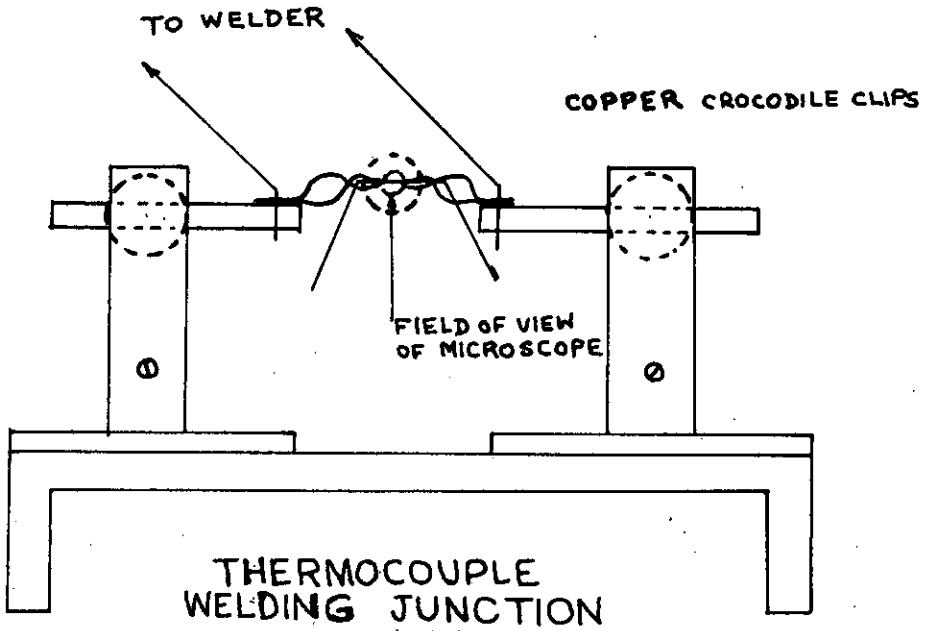

THERMOCOUPLE
WELDING JUNCTION

FIG·10

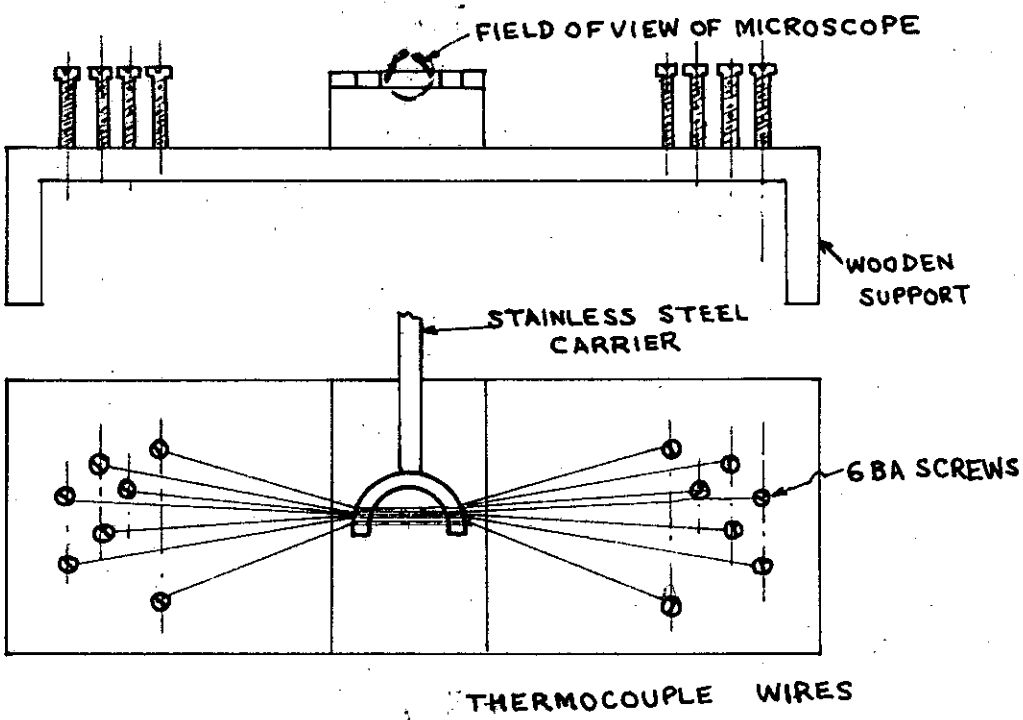

THERMOCOUPLE BRIDGE JUNCTION

FIG·12

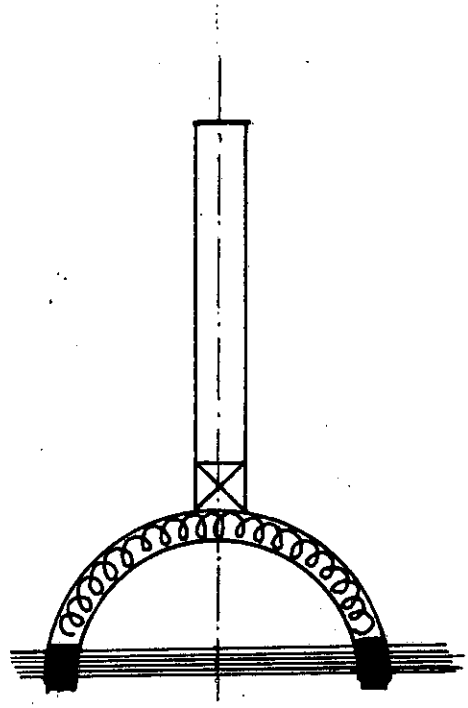

THERMOCOUPLE CARRIER TYPE 1.

FIG 11a

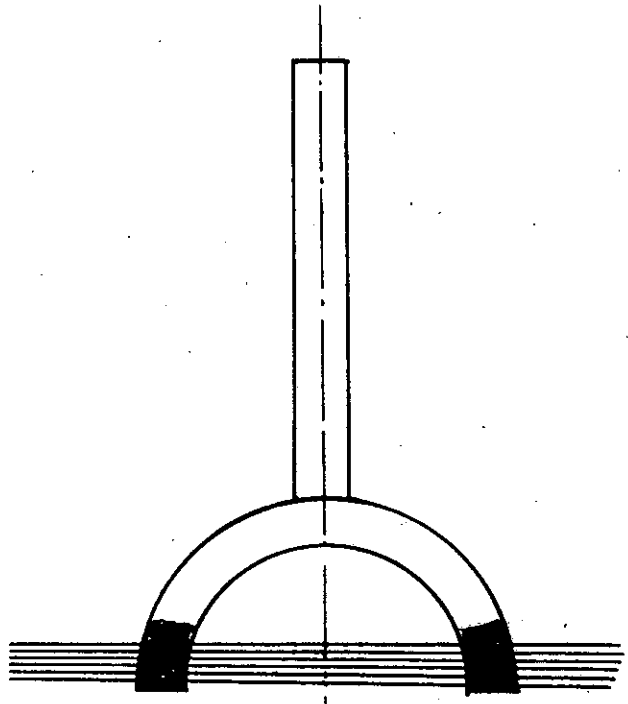

THERMOCOUPLE CARRIER TYPE 2.

FIG 11b

MAGNIFIED PHOTOGRAPH OF THE THERMOCOUPLE JUNCTIONS AS IN FIG. 11a.

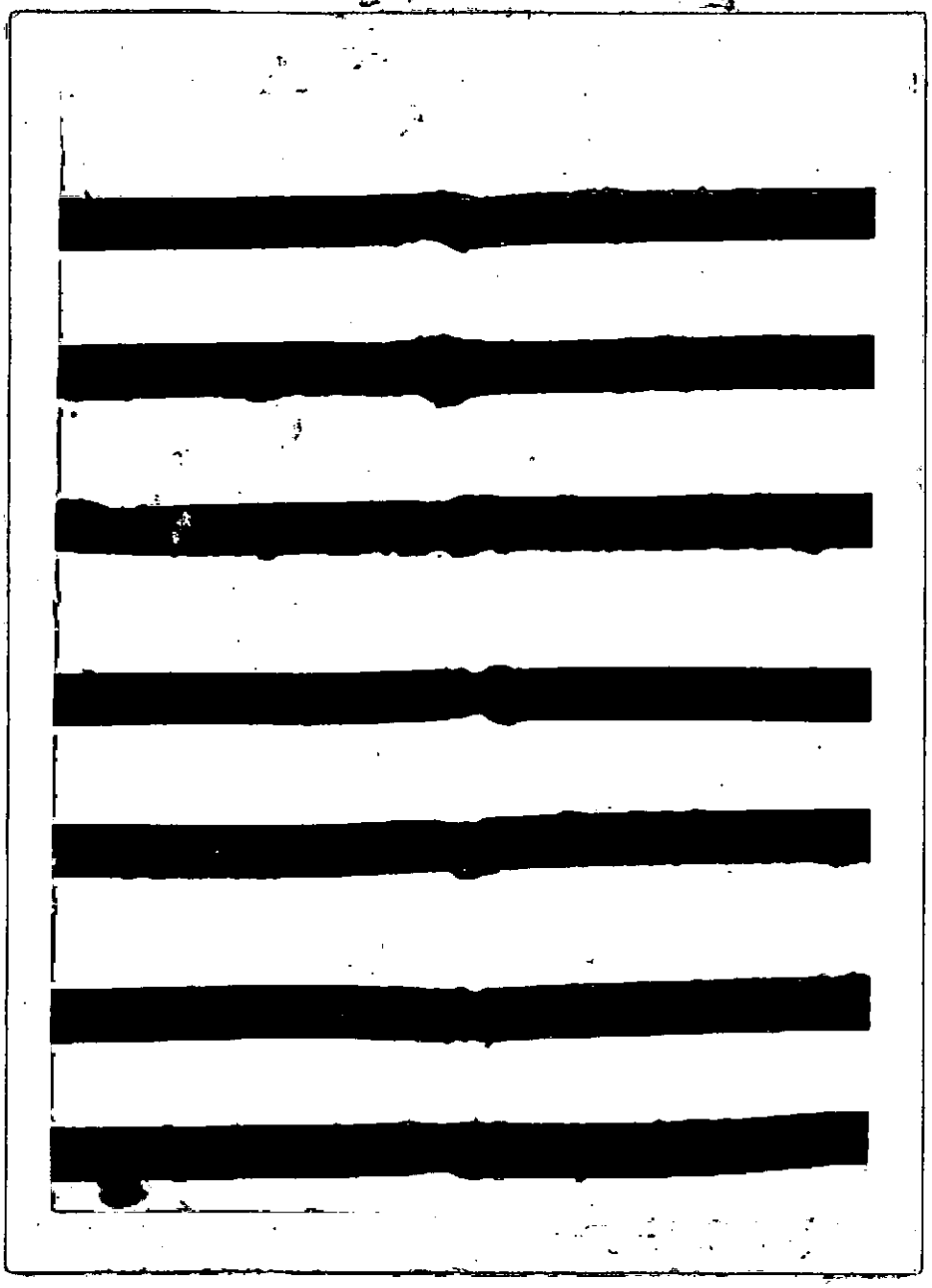

FIG. 13

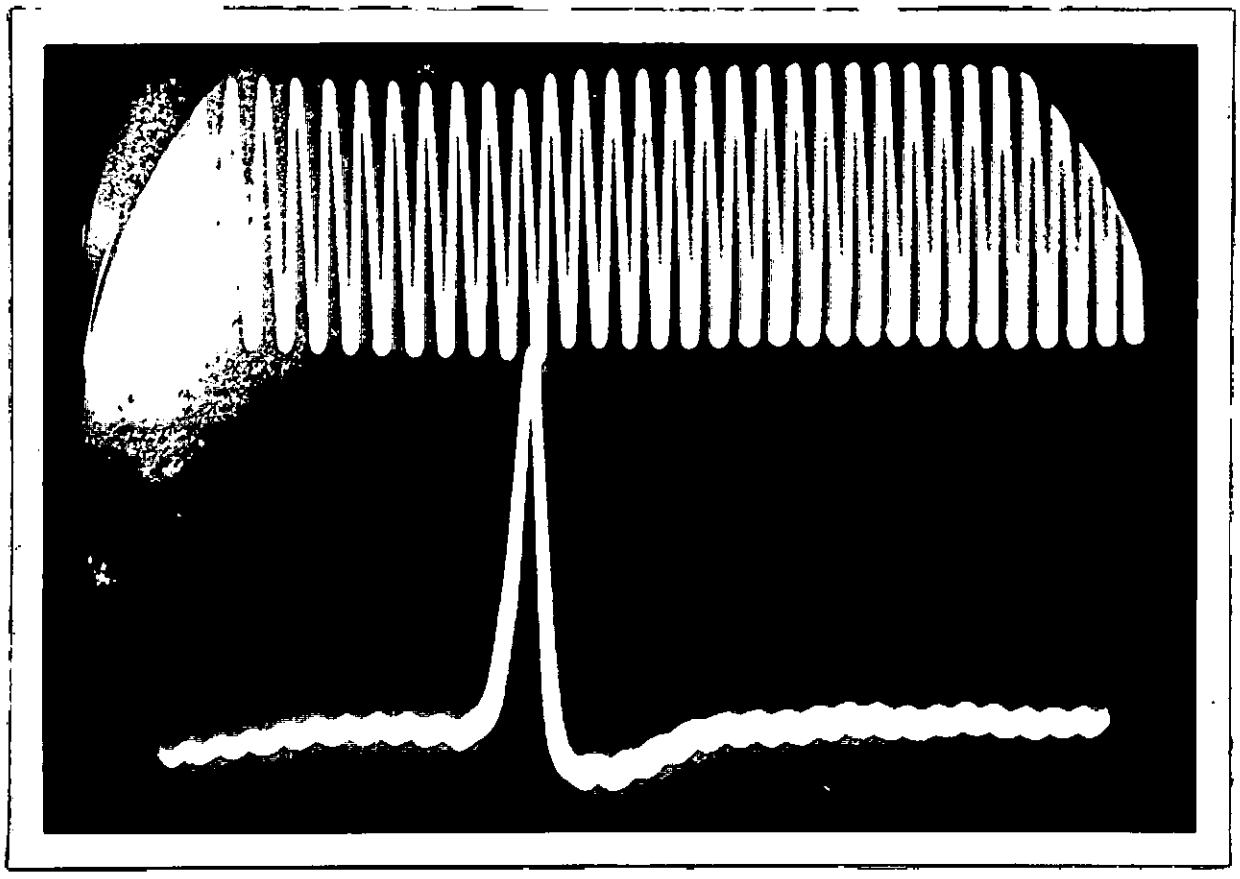

FIG·14
TEMPERATURE TRANSIENT IN THE SUPERHEATED LAYER.

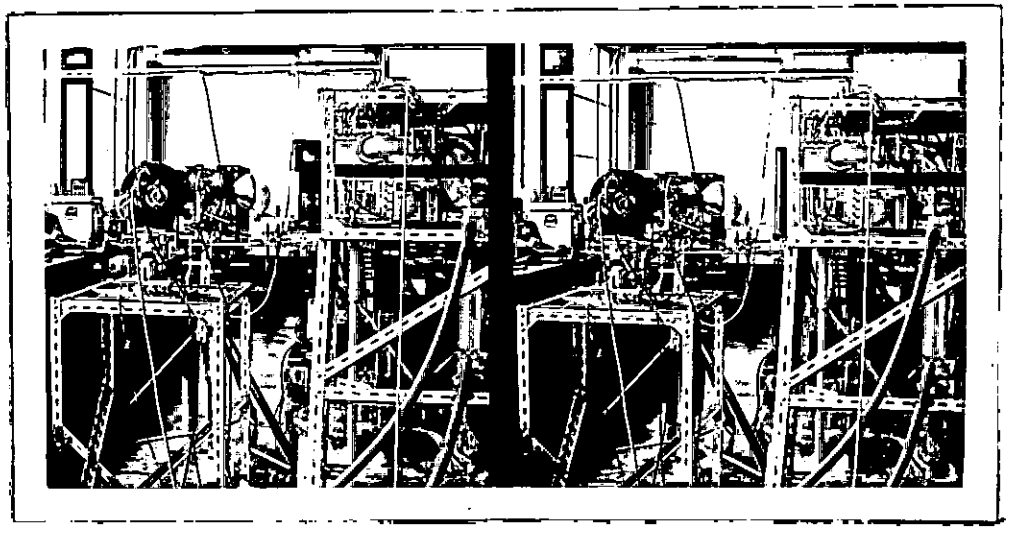

FIG·15
STEREOSCOPIC VIEW OF THE EXPERIMENTAL ARRANGEMENT

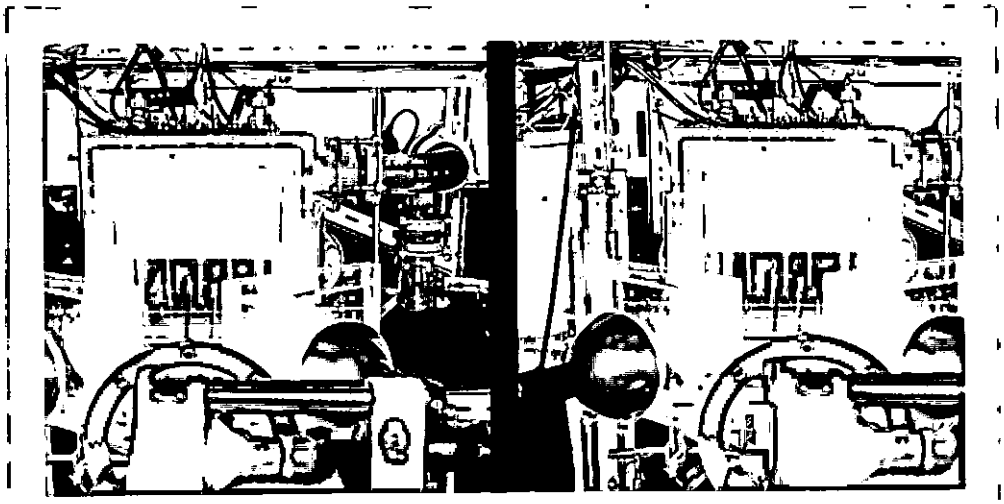

FIG. 16

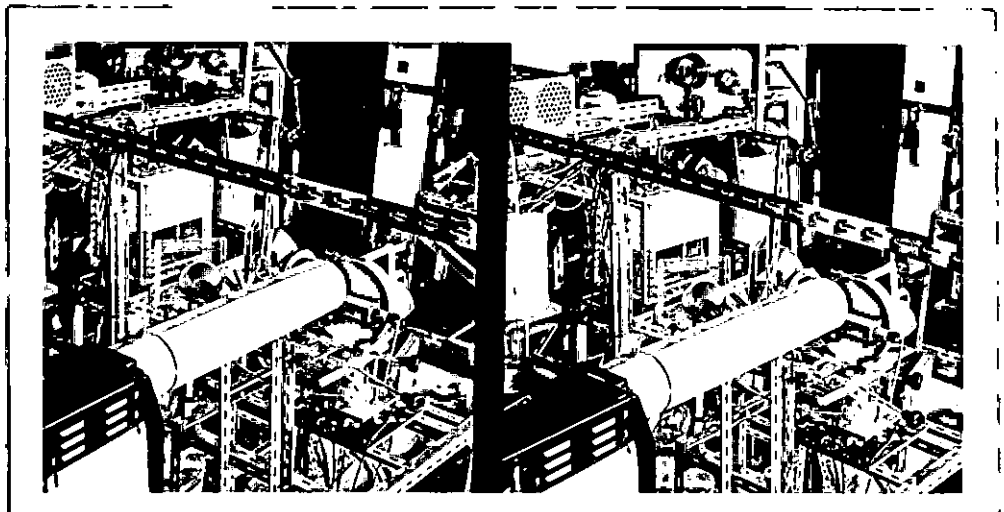

FIG. 17

FIG. 18

STEREOSCOPIC VIEWS OF THE EXPERIMENTAL ARRANGEMENT

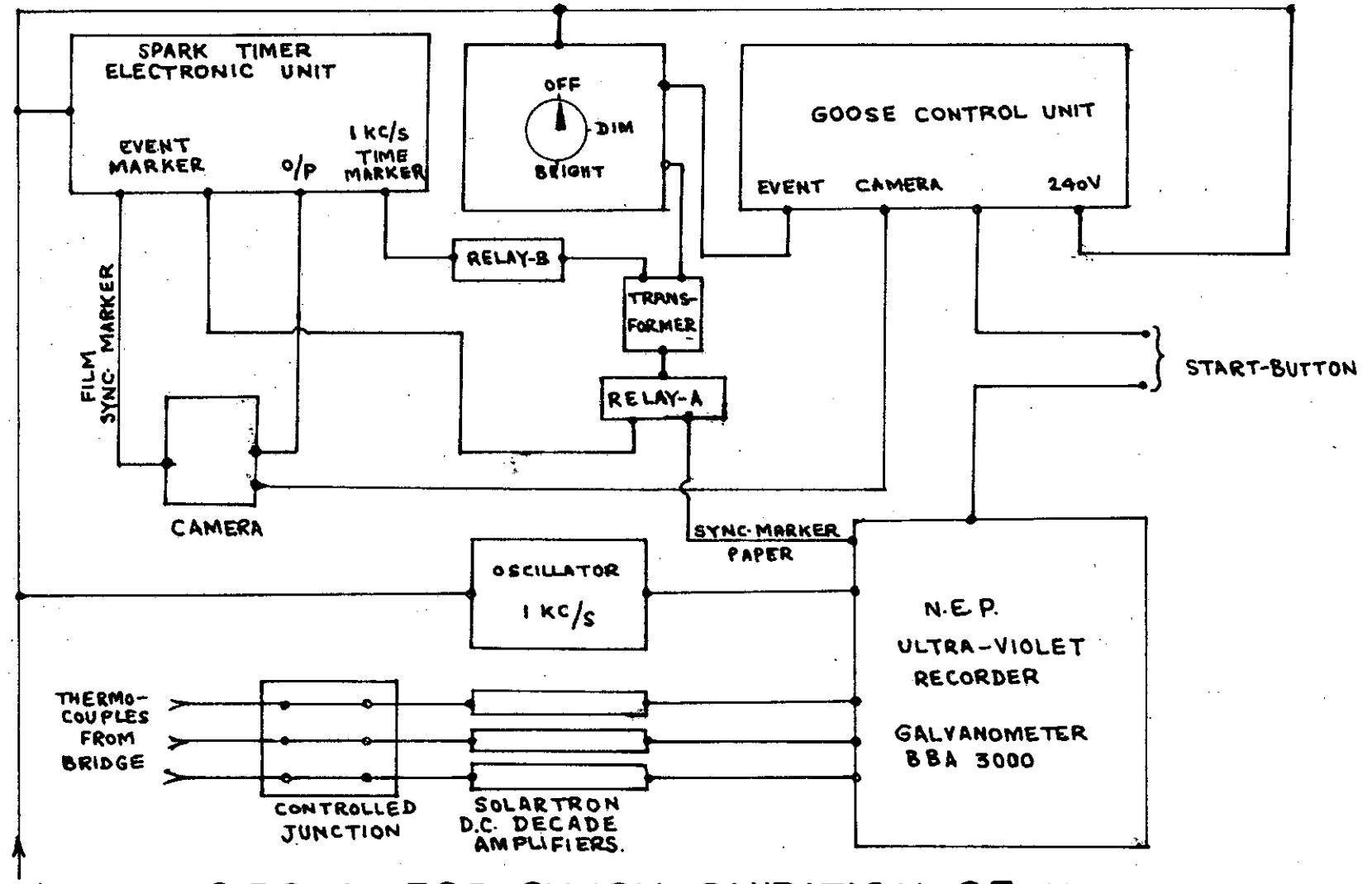

CIRCUIT FOR SYNCHRONIZATION OF U.V.-RECORDER AND HIGH SPEED CAMERA

FIG·19

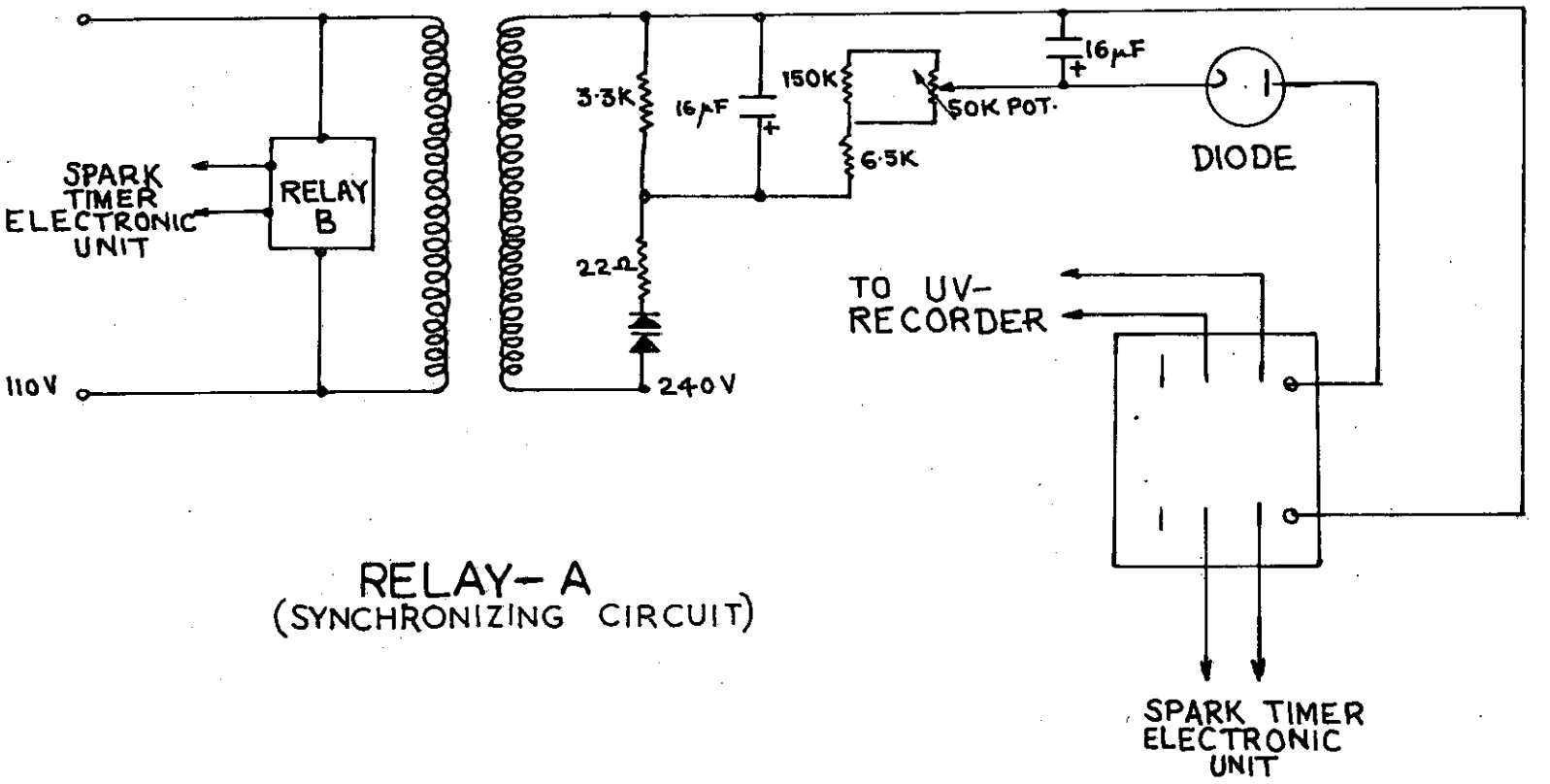

RELAY– A
(SYNCHRONIZING CIRCUIT)

FIG·20

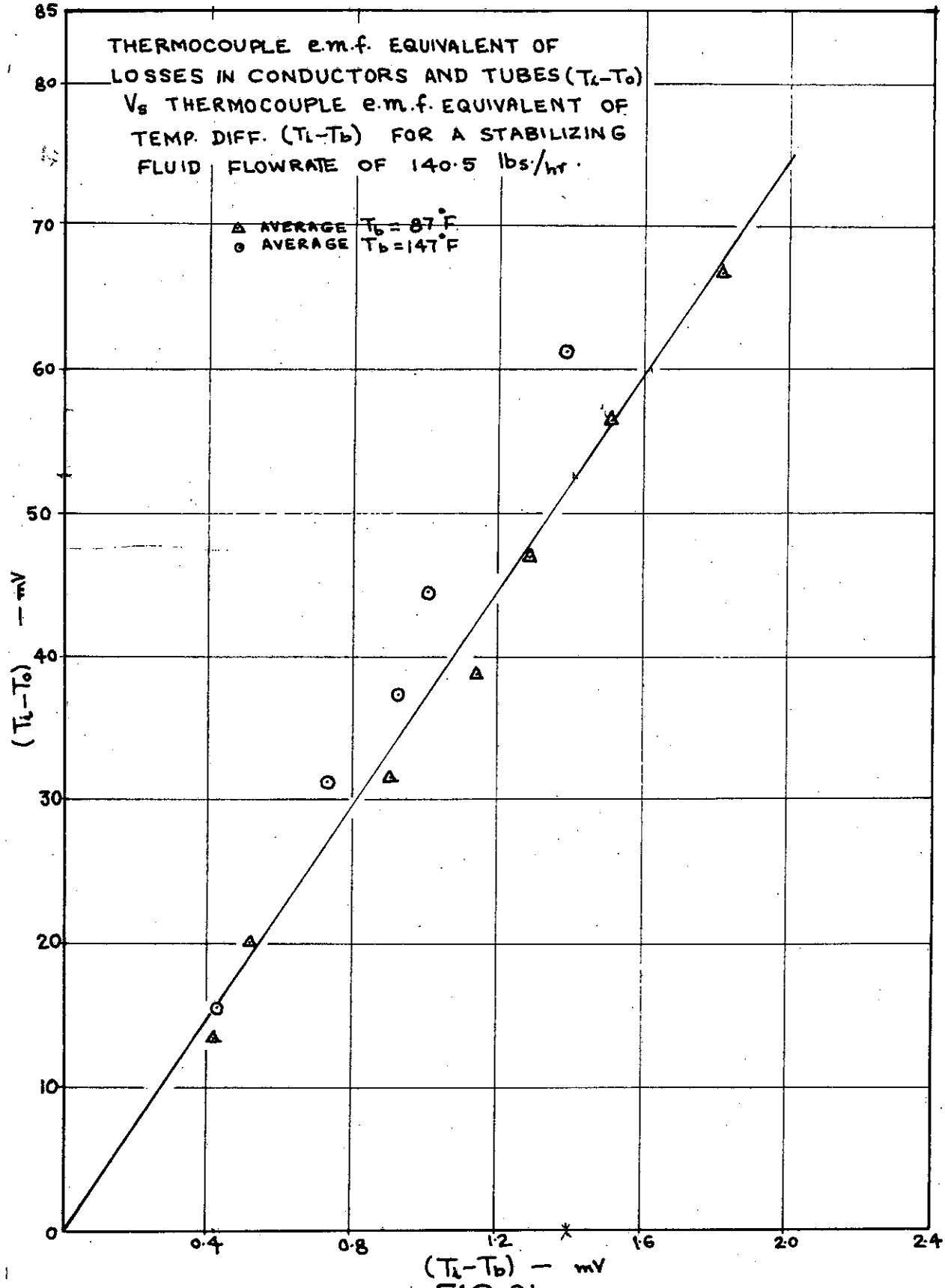
THERMOCOUPLE e.m.f. EQUIVALENT OF LOSSES IN CONDUCTORS AND TUBES ($T_L - T_o$) Vs THERMOCOUPLE e.m.f. EQUIVALENT OF TEMP. DIFF. ($T_L - T_b$) FOR A STABILIZING FLUID FLOWRATE OF 140·5 lbs./hr.
△ AVERAGE T_b = 87°F
⊙ AVERAGE T_b = 147°F
$(T_L - T_o)$ — mV
$(T_L - T_b)$ — mV
0
10
20
30
40
50
60
70
80
85
0·4
0·8
1·2
1·6
2·0
2·4

FIG·21

MICROMETER ARRANGEMENT FOR ADJUSTING S.S. CARRIER.

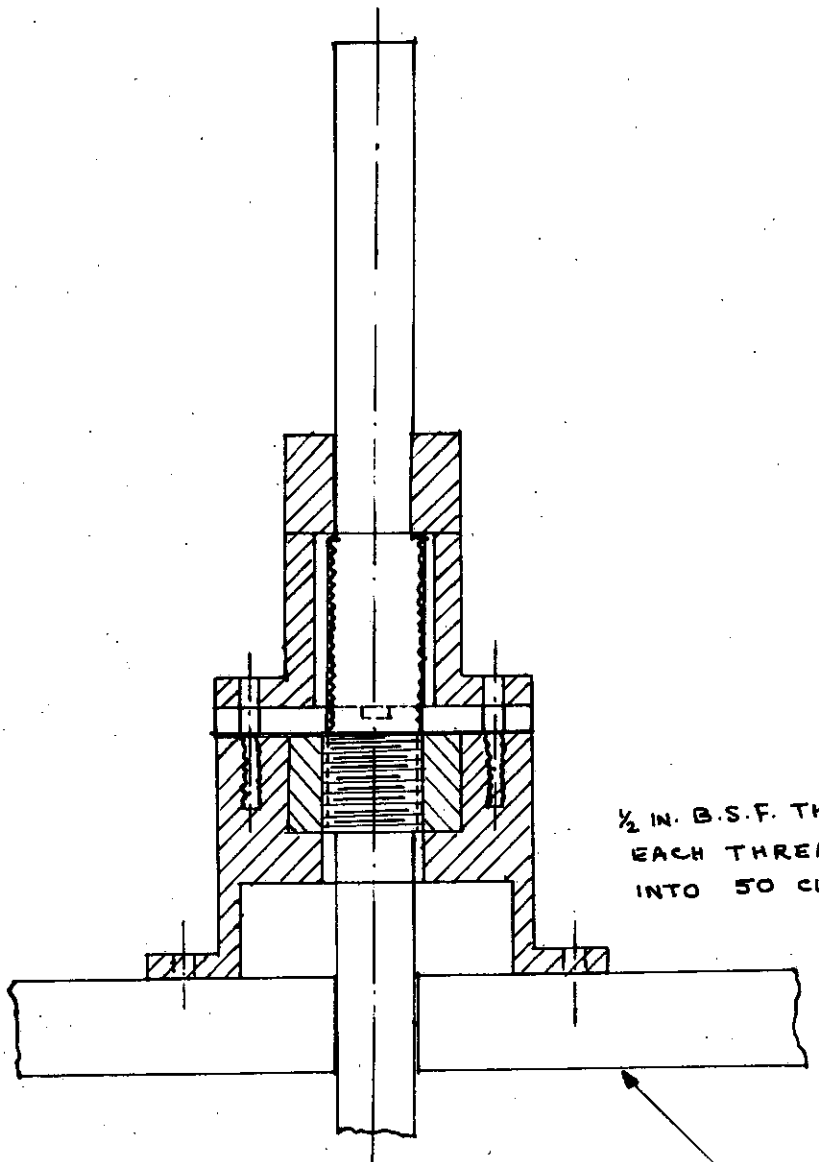

FIG·22

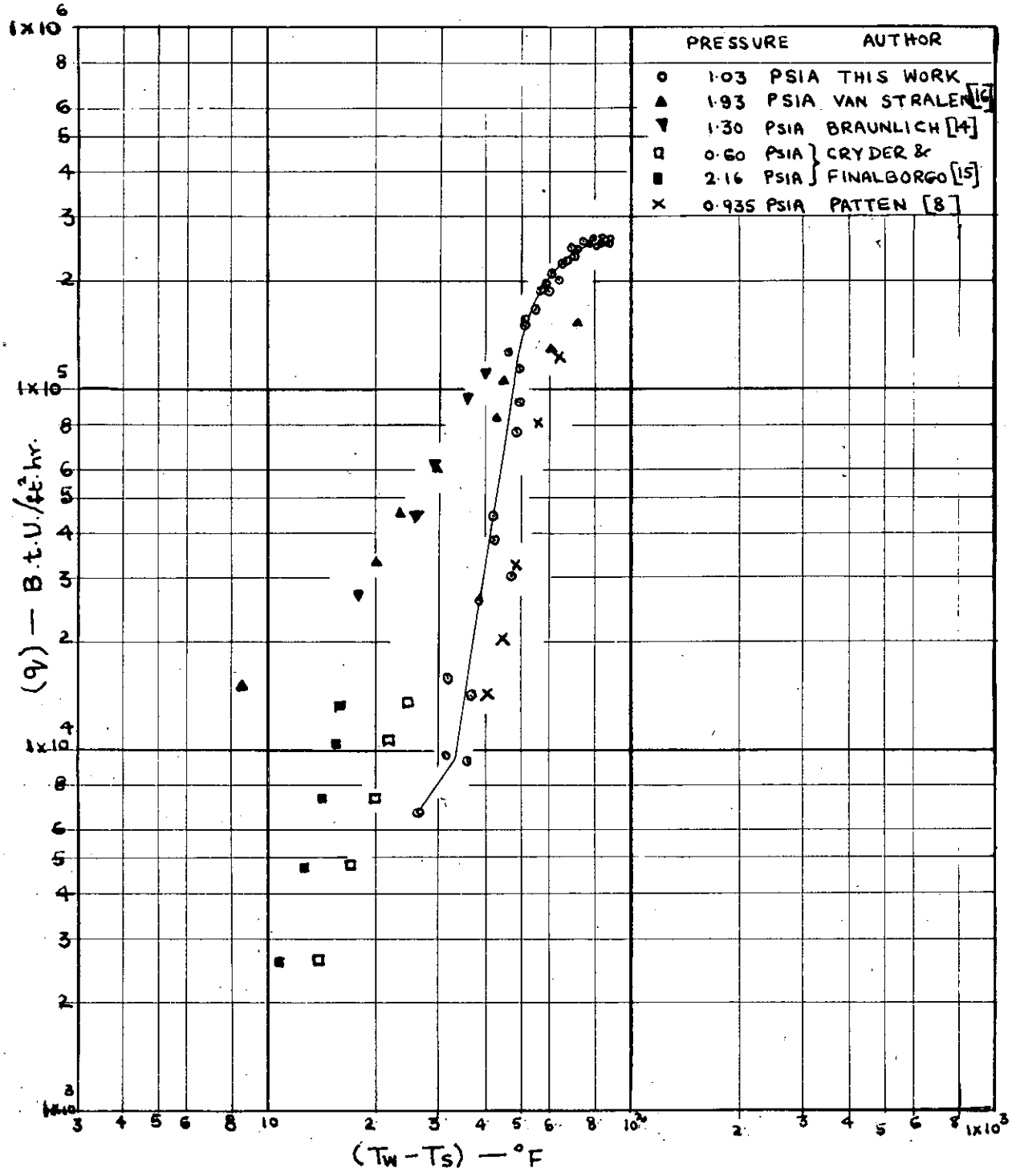

HEAT FLUX V TEMP. DIFFERENCE FOR POOL BOILING OF WATER UNDER SATURATED CONDITIONS.

FIG·23

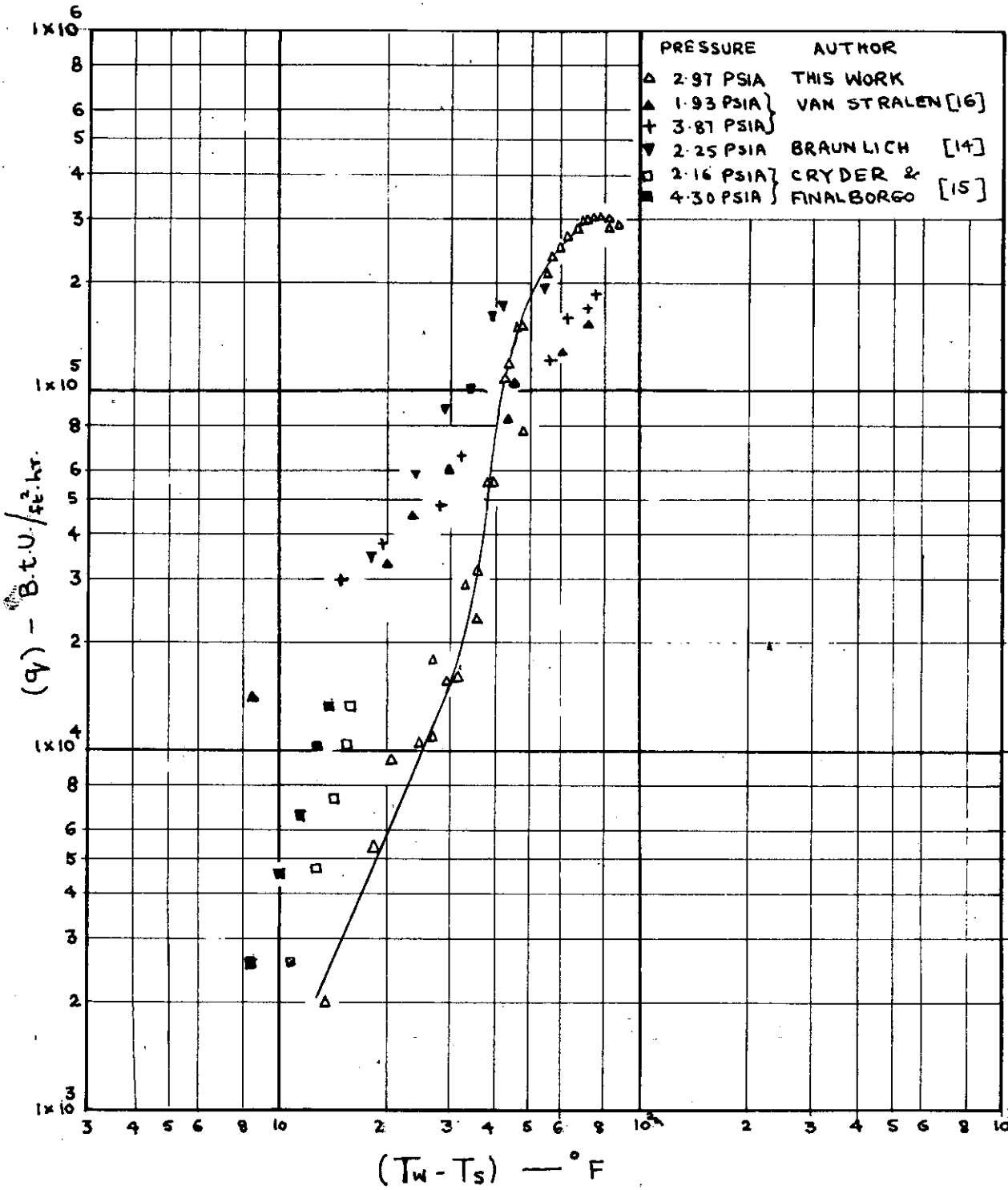

HEAT FLUX V TEMP. DIFFERENCE FOR POOL BOILING OF WATER UNDER SATURATED CONDITIONS.

FIG·24

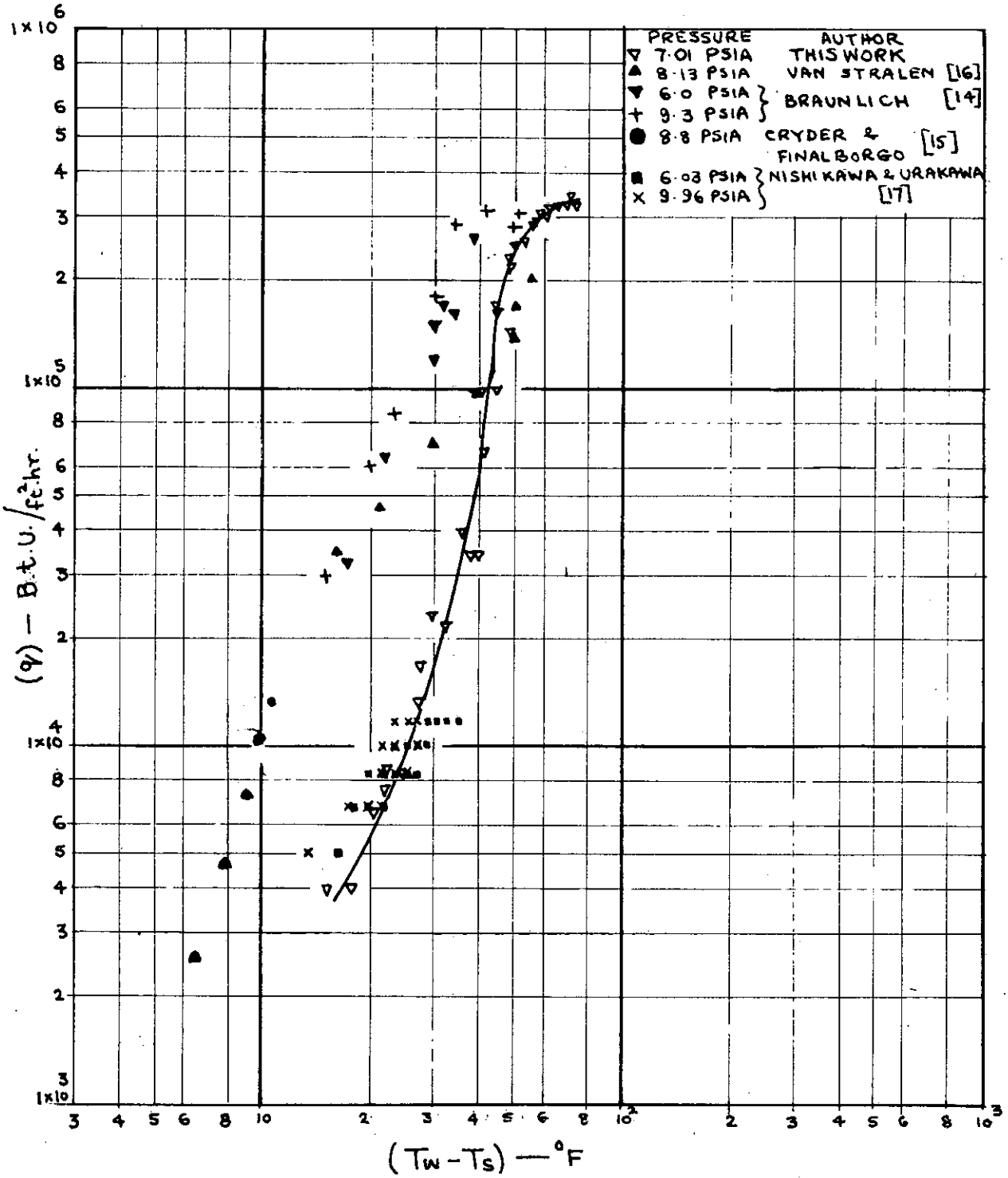

HEAT FLUX V TEMP. DIFFERENCE FOR POOL BOILING OF WATER UNDER SATURATED CONDITIONS.

FIG. 25

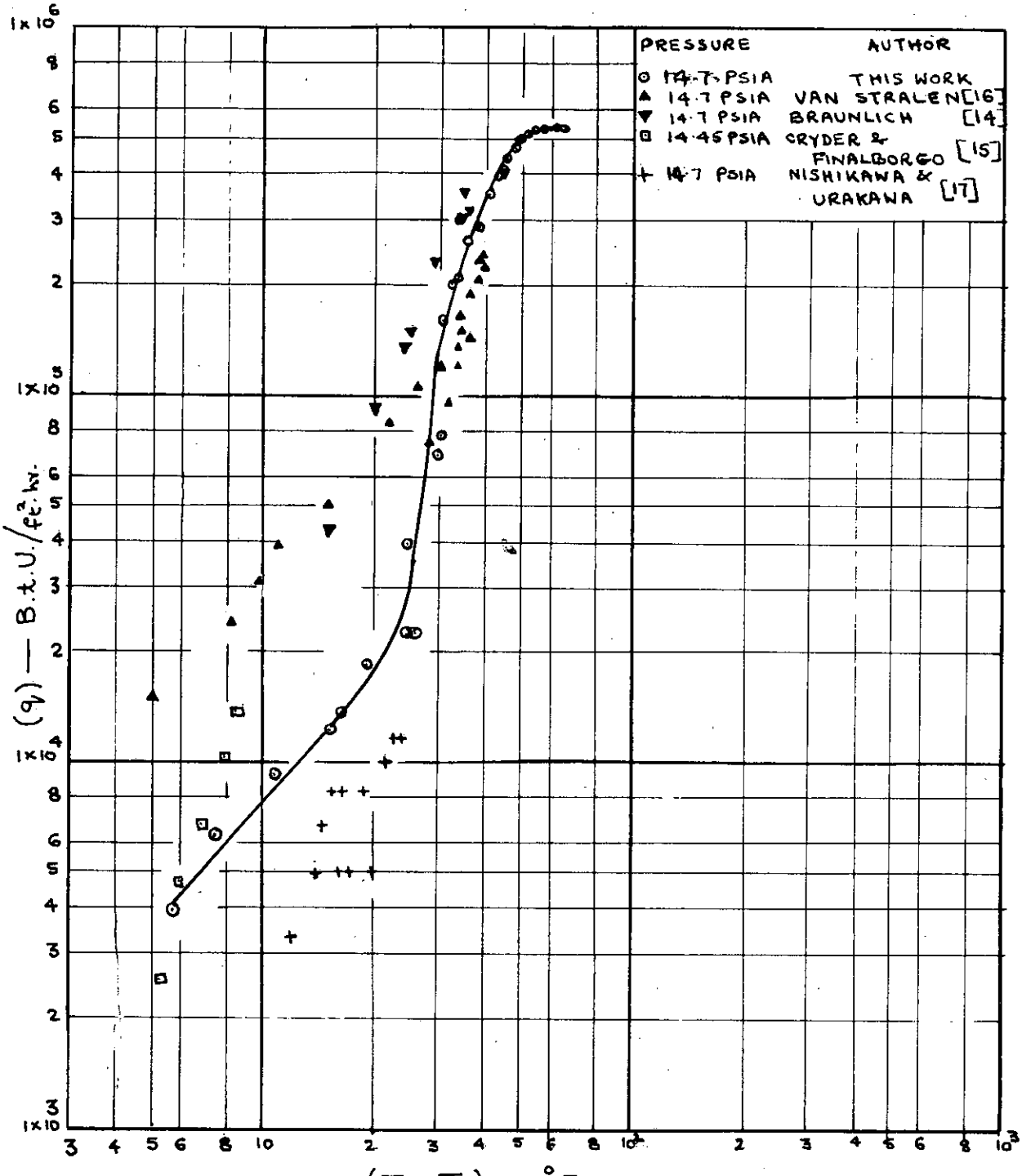

HEAT FLUX V TEMP. DIFFERENCE FOR POOL BOILING OF WATER UNDER SATURATED CONDITIONS.

FIG. 26

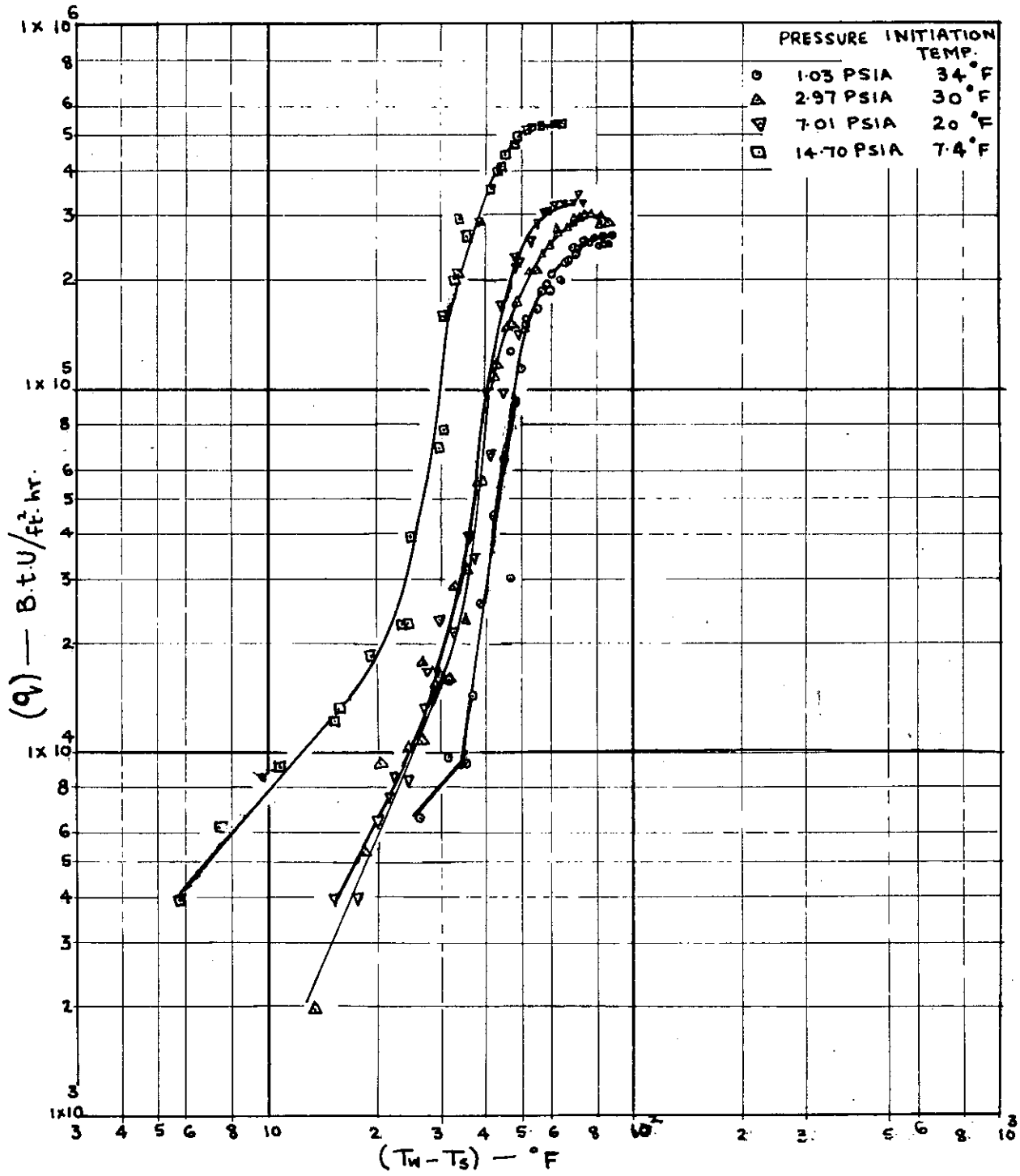

HEATFLUX Vs TEMP. DIFFERENCE FOR POOL BOILING OF WATER UNDER SATURATED CONDITIONS.

FIG·27

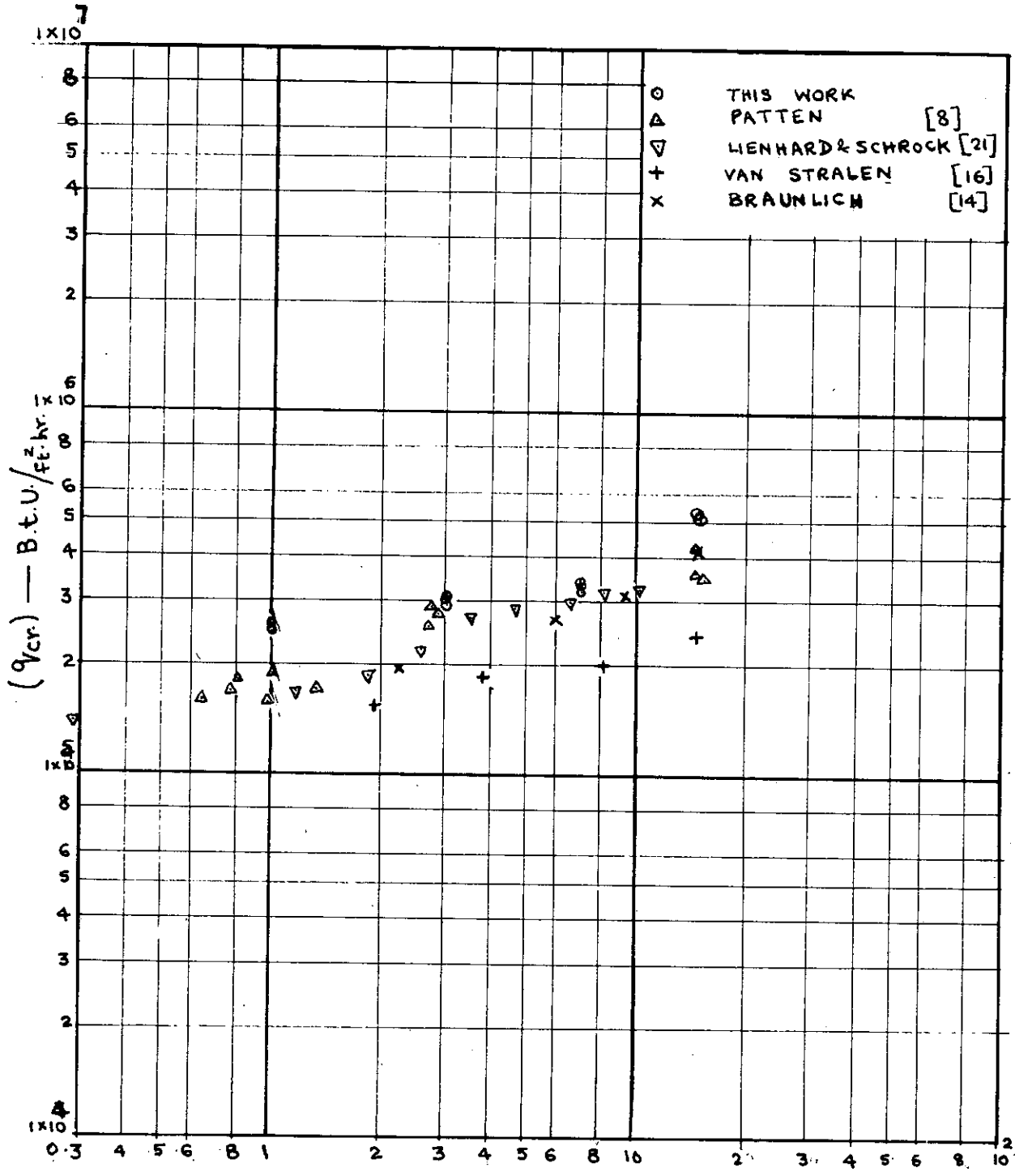

CRITICAL HEAT FLUX V PRESSURE FOR POOL BOILING OF WATER UNDER SATURATED CONDITIONS.

FIG·28

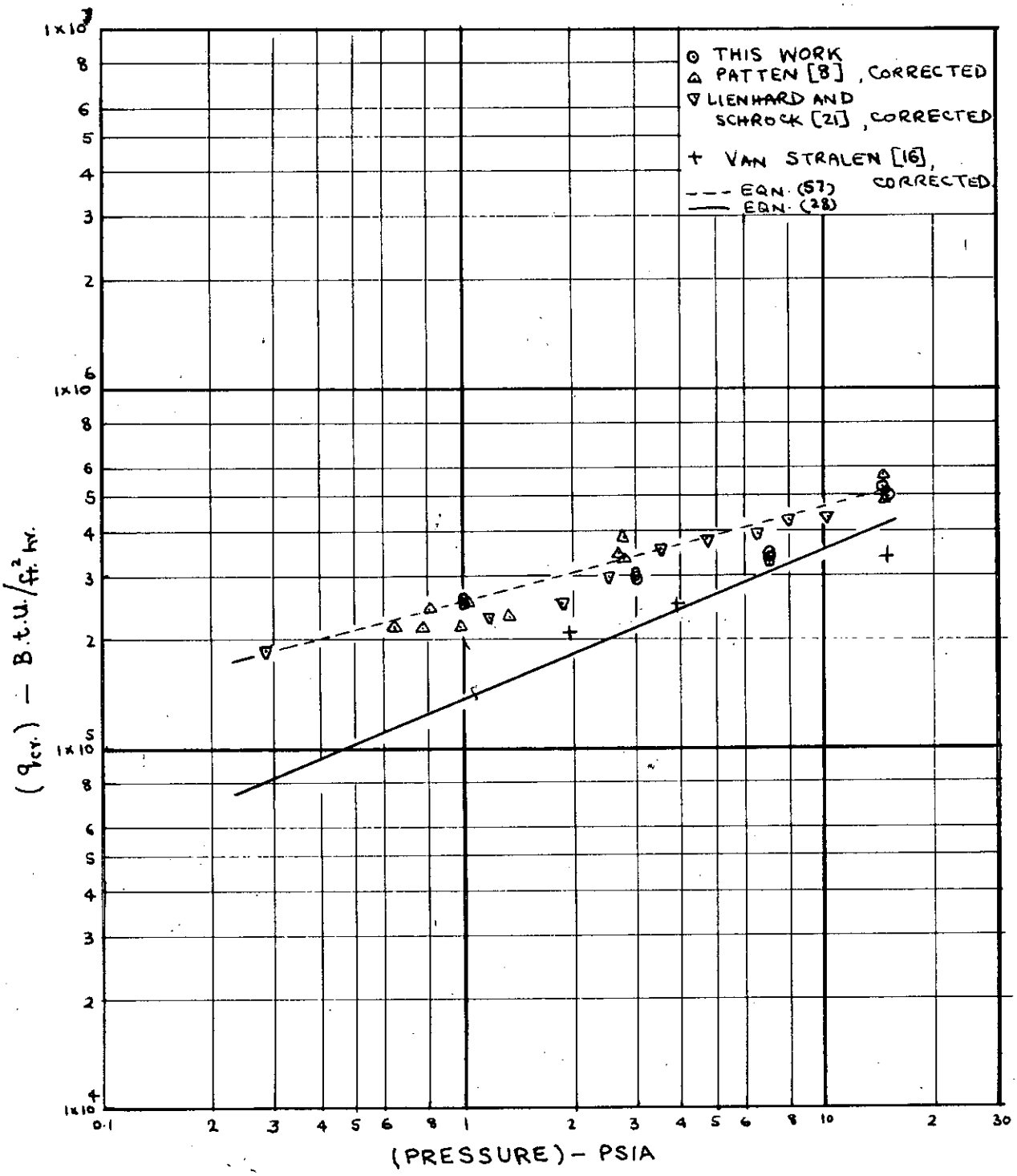

CRITICAL HEAT FLUX V PRESSURE FOR POOL BOILING OF WATER UNDER SATURATION CONDITIONS.

FIG·29

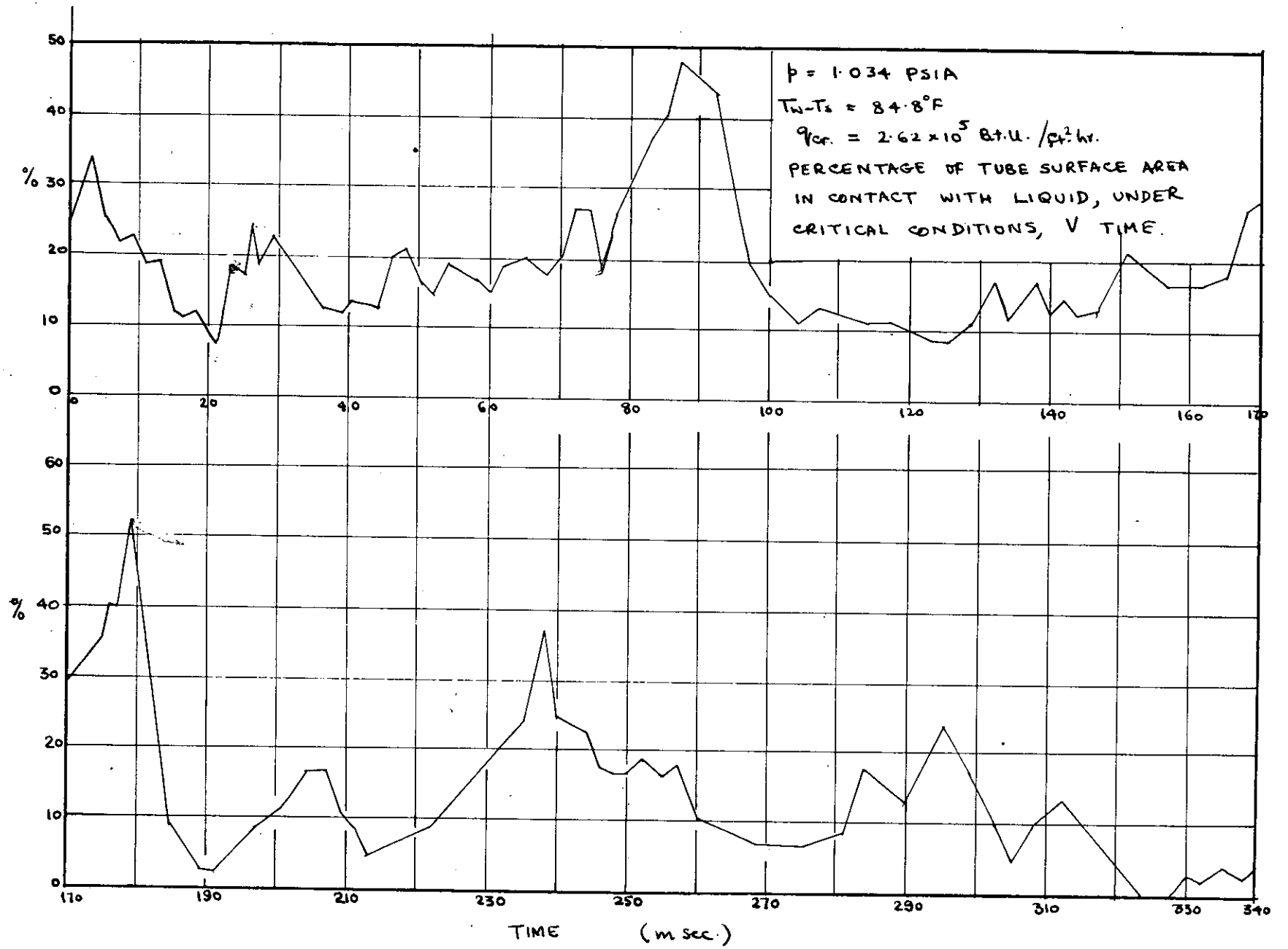
p = 1·034 PSIA
$T_w - T_s$ = 84·8°F
$q_{cr.}$ = 2·62 × 10^5 B.t.u./ft.² hr.
PERCENTAGE OF TUBE SURFACE AREA IN CONTACT WITH LIQUID, UNDER CRITICAL CONDITIONS, V TIME.
%
0
10
20
30
40
50
60
0
20
40
60
80
100
120
140
160
170
190
210
230
250
270
290
310
330
340
TIME (m sec.)

FIG. 30

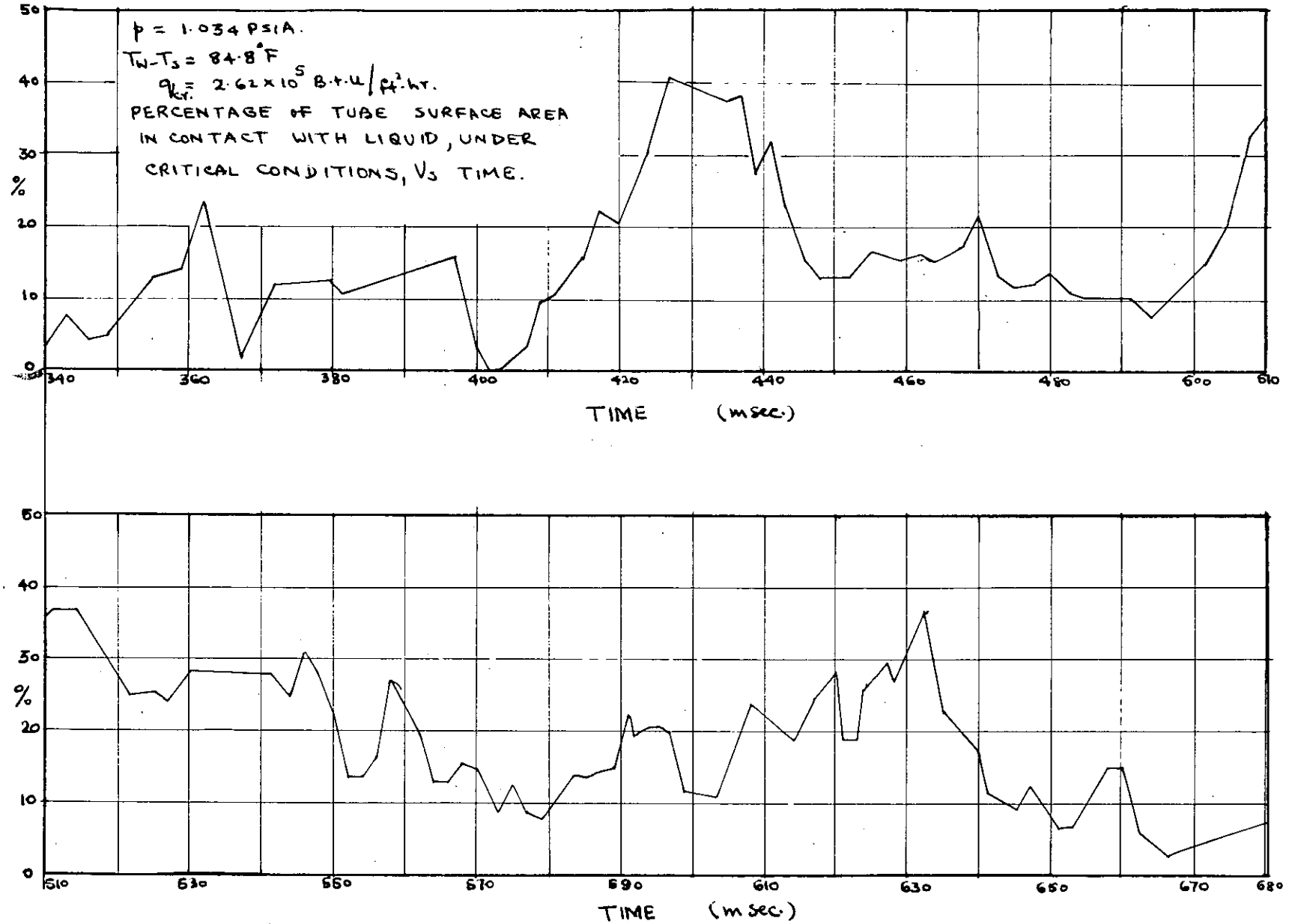
p = 1.034 PSIA.
$T_W - T_s$ = 84.8°F
$q_{kr.}$ = 2.62 x 10^5 B.t.u/ft².hr.
PERCENTAGE OF TUBE SURFACE AREA IN CONTACT WITH LIQUID, UNDER CRITICAL CONDITIONS, V_s TIME.
%
TIME (msec.)
%
TIME (msec.)

FIG. 30 (-CONT'D-)

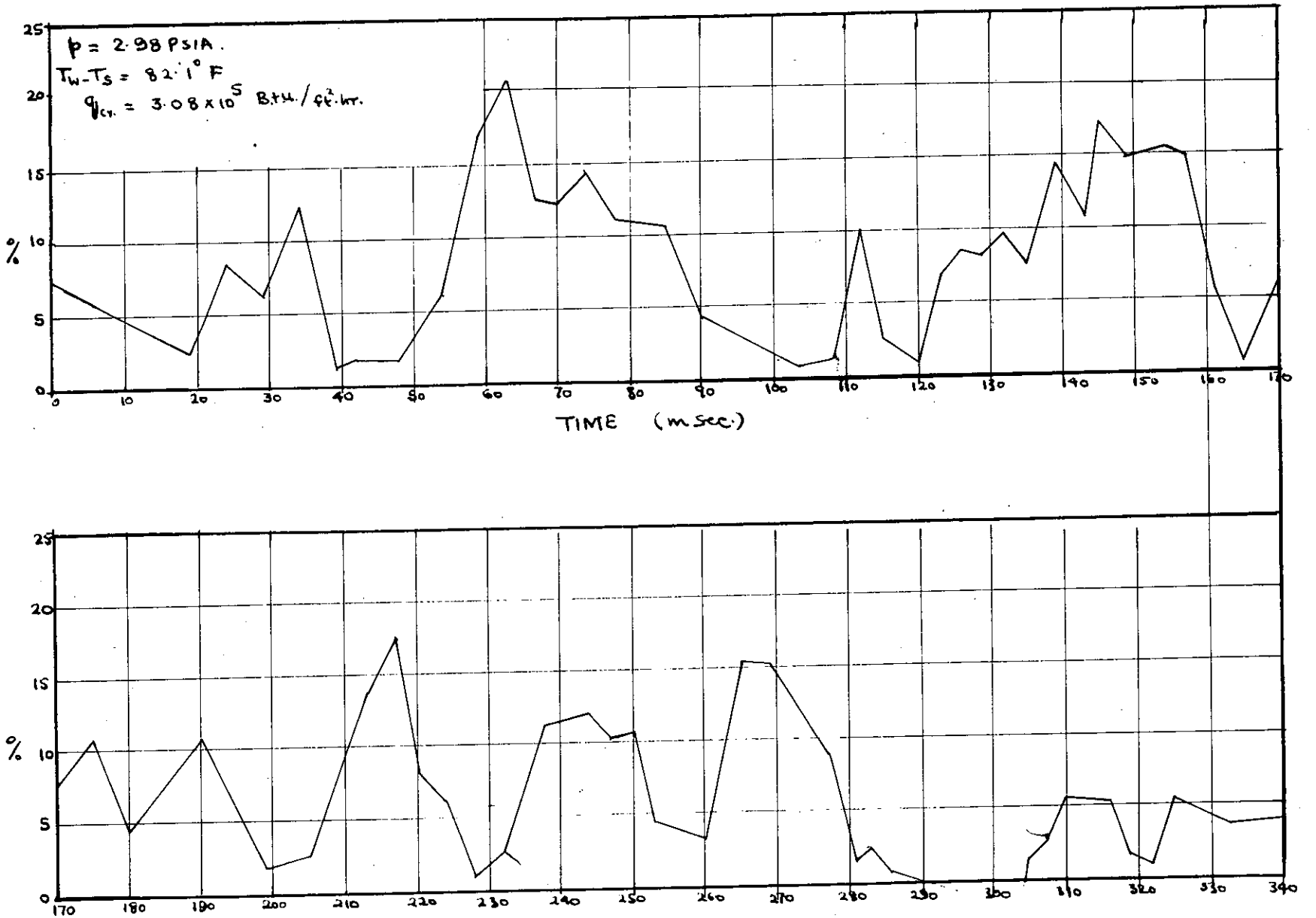

PERCENTAGE OF SURFACE AREA OF THE TUBE IN CONTACT WITH LIQUID UNDER CRITICAL CONDITIONS V TIME.

FIG. 31

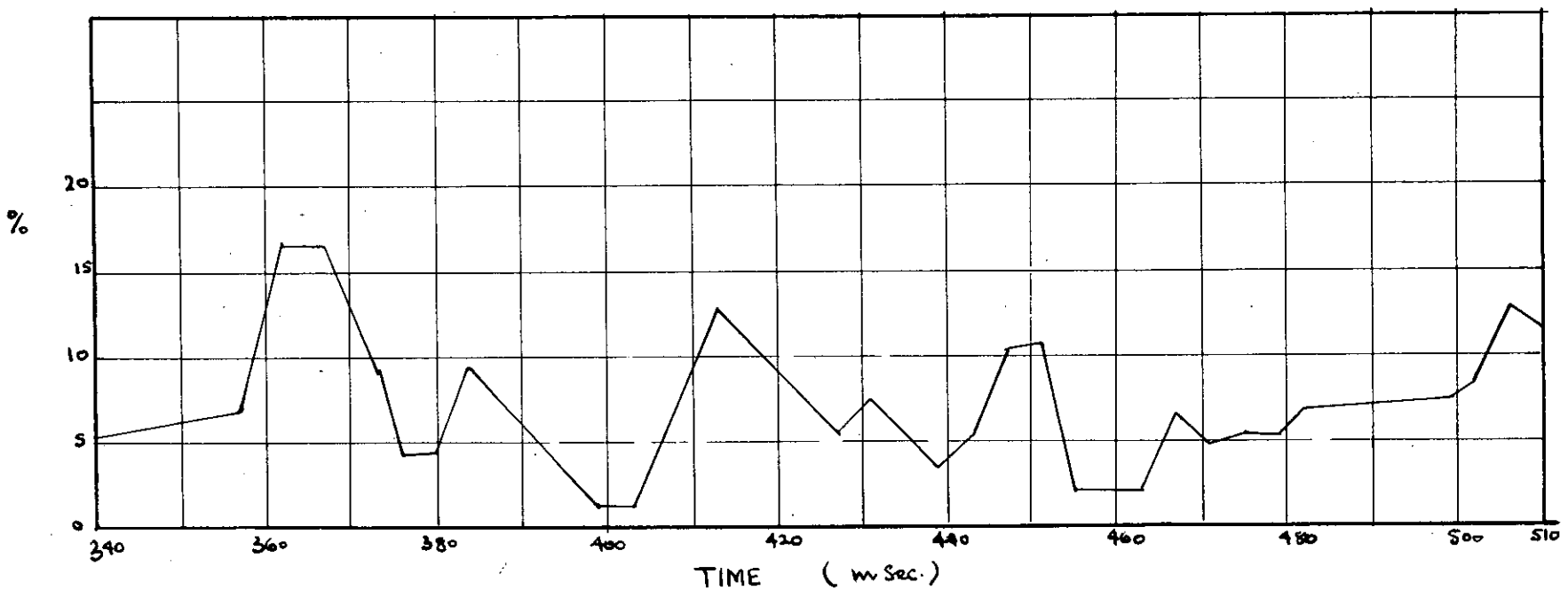

FIG. 31 (CONT'D).

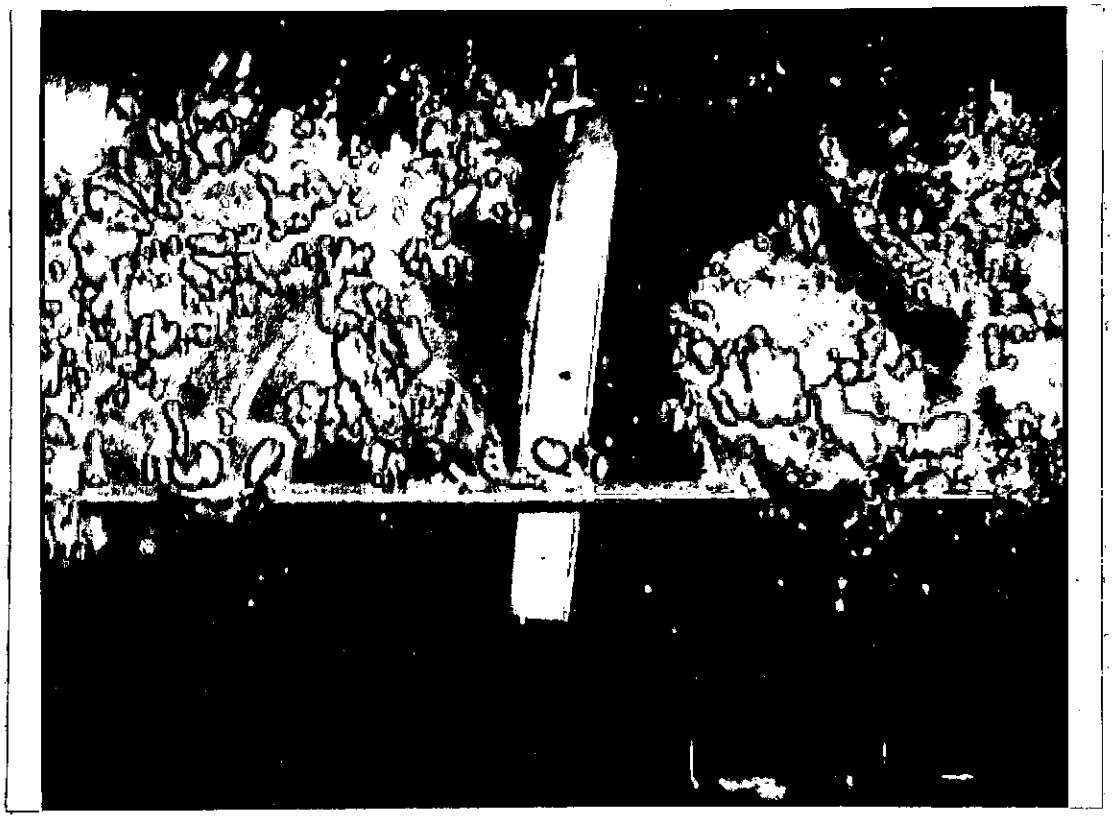

FIG. 32 PRESSURE 1·0 PSIA.

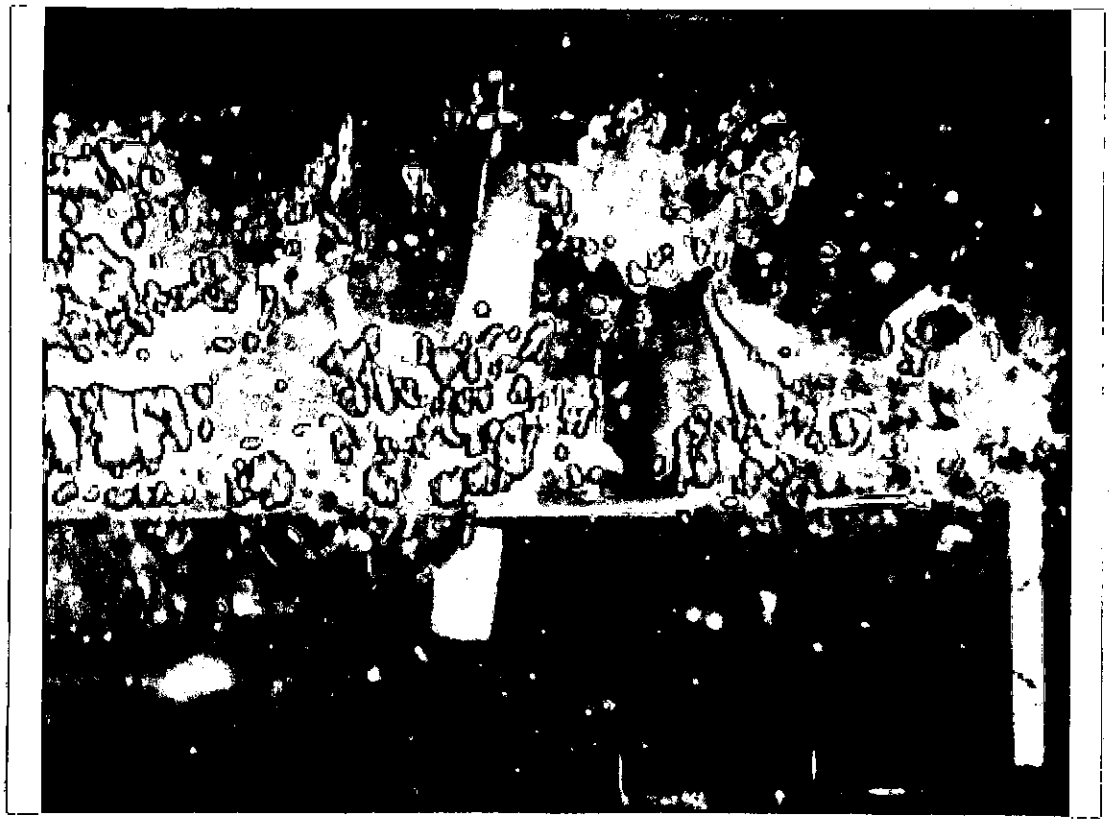

FIG. 33 PRESSURE 3·0 PSIA

NUCLEATE BOILING AT MAXIMUM HEAT FLUX.

FIG. 34 PRESSURE 7.0 PSIA

FIG. 35 PRESSURE 14.7 PSIA

NUCLEATE BOILING AT MAXIMUM HEAT FLUX.

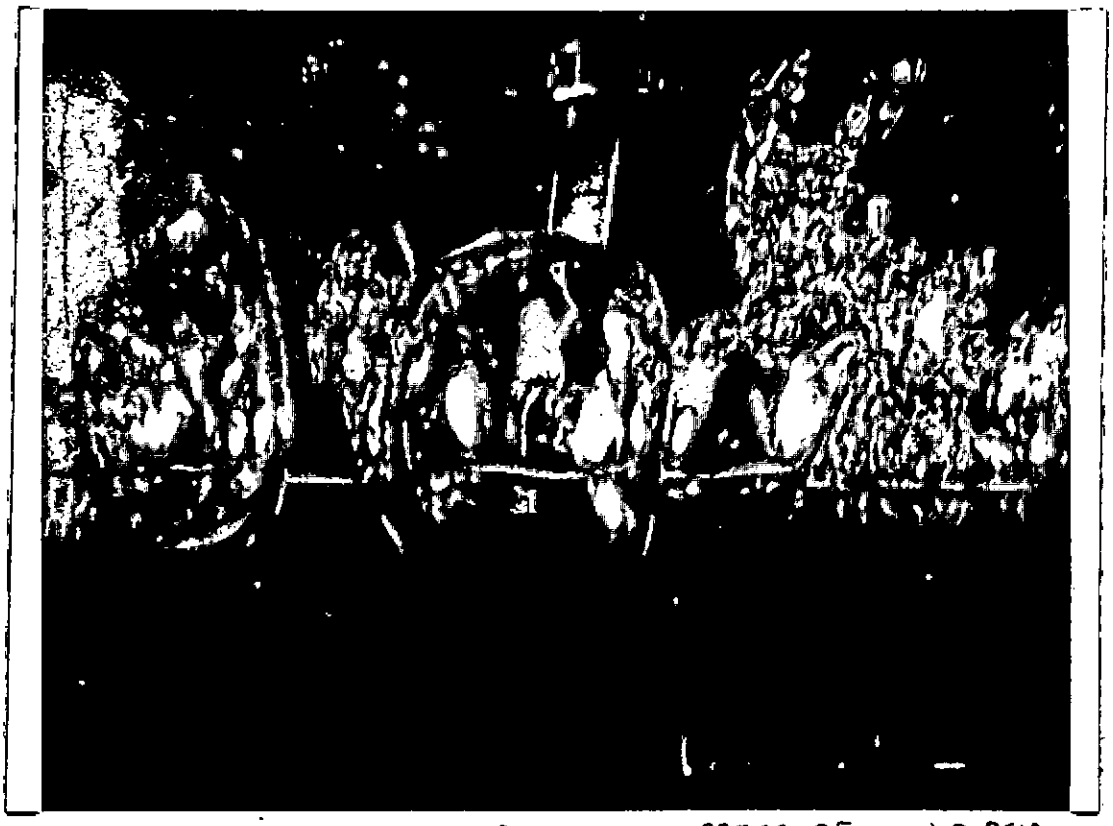

FIG. 36 PRESSURE 1.0 PSIA

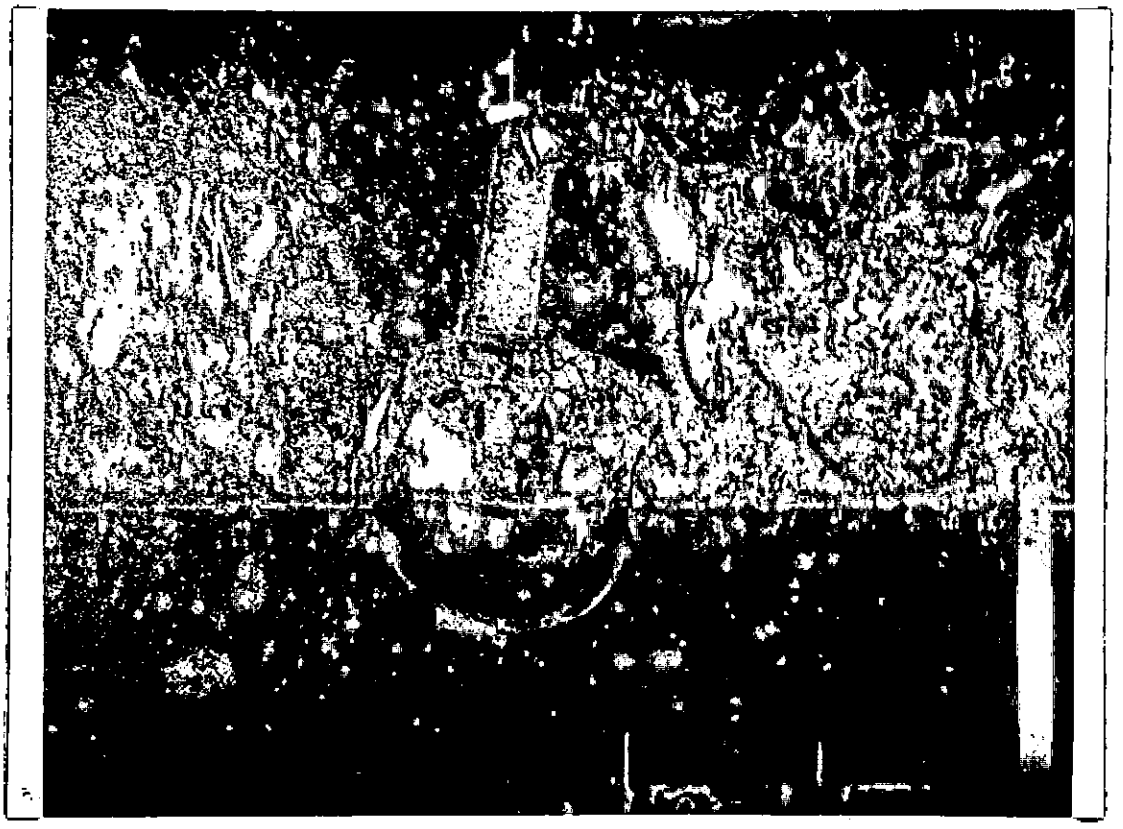

FIG. 37 PRESSURE 3.0 PSIA

NUCLEATE BOILING AT MAXIMUM HEAT FLUX.

FIG. 38 PRESSURE 7.0 PSIA

FIG. 39 PRESSURE 14.7 PSIA

NUCLEATE BOILING AT [redacted] MAXIMUM HEAT FLUX.

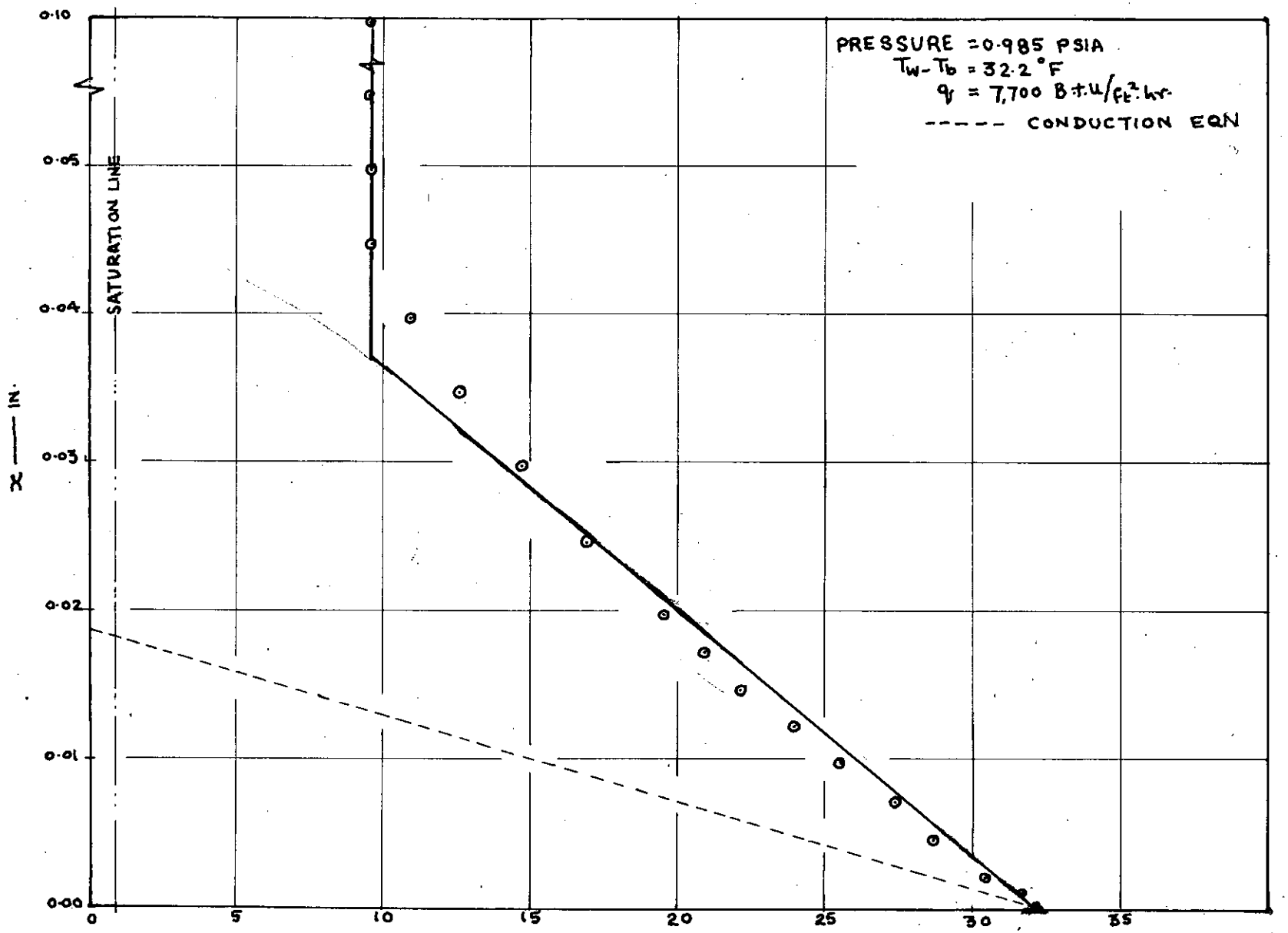

TEMP. GRADIENT IN THE SUPERHEATED LAYER

FIG. 40

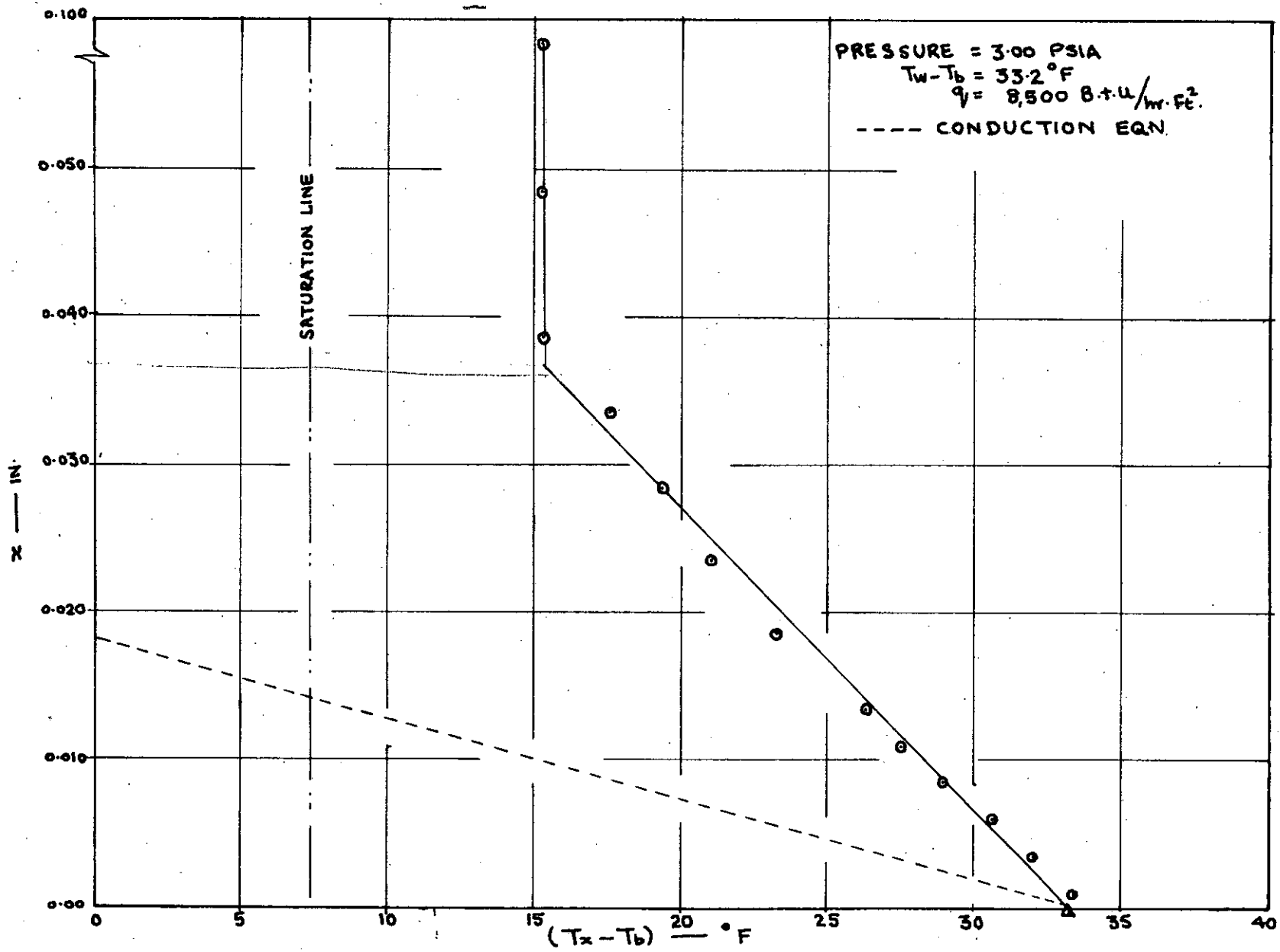

TEMPERATURE GRADIENT IN THE SUPERHEATED LAYER.

FIG·41

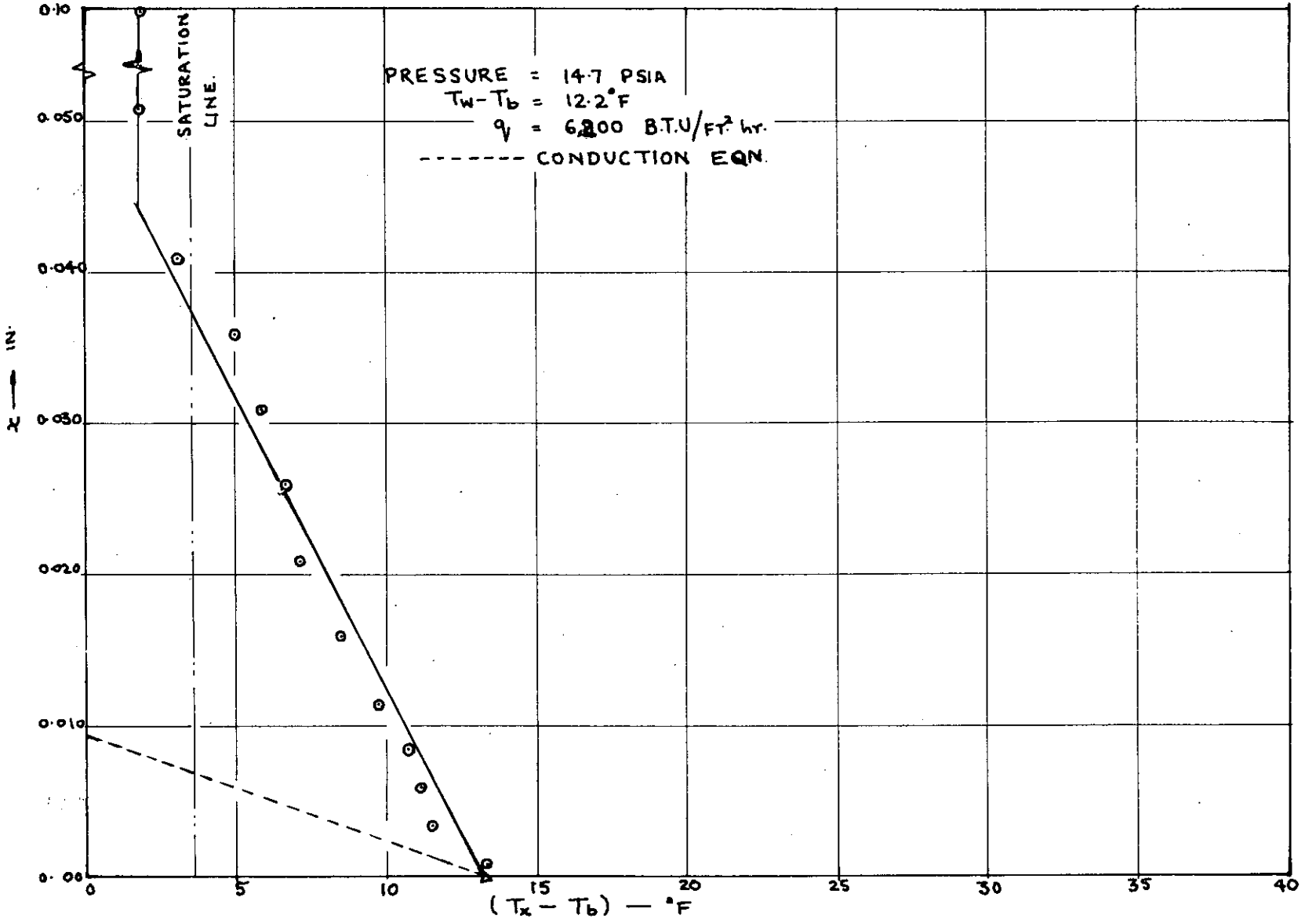

TEMPERATURE GRADIENT IN THE SUPERHEATED LAYER.

FIG·42

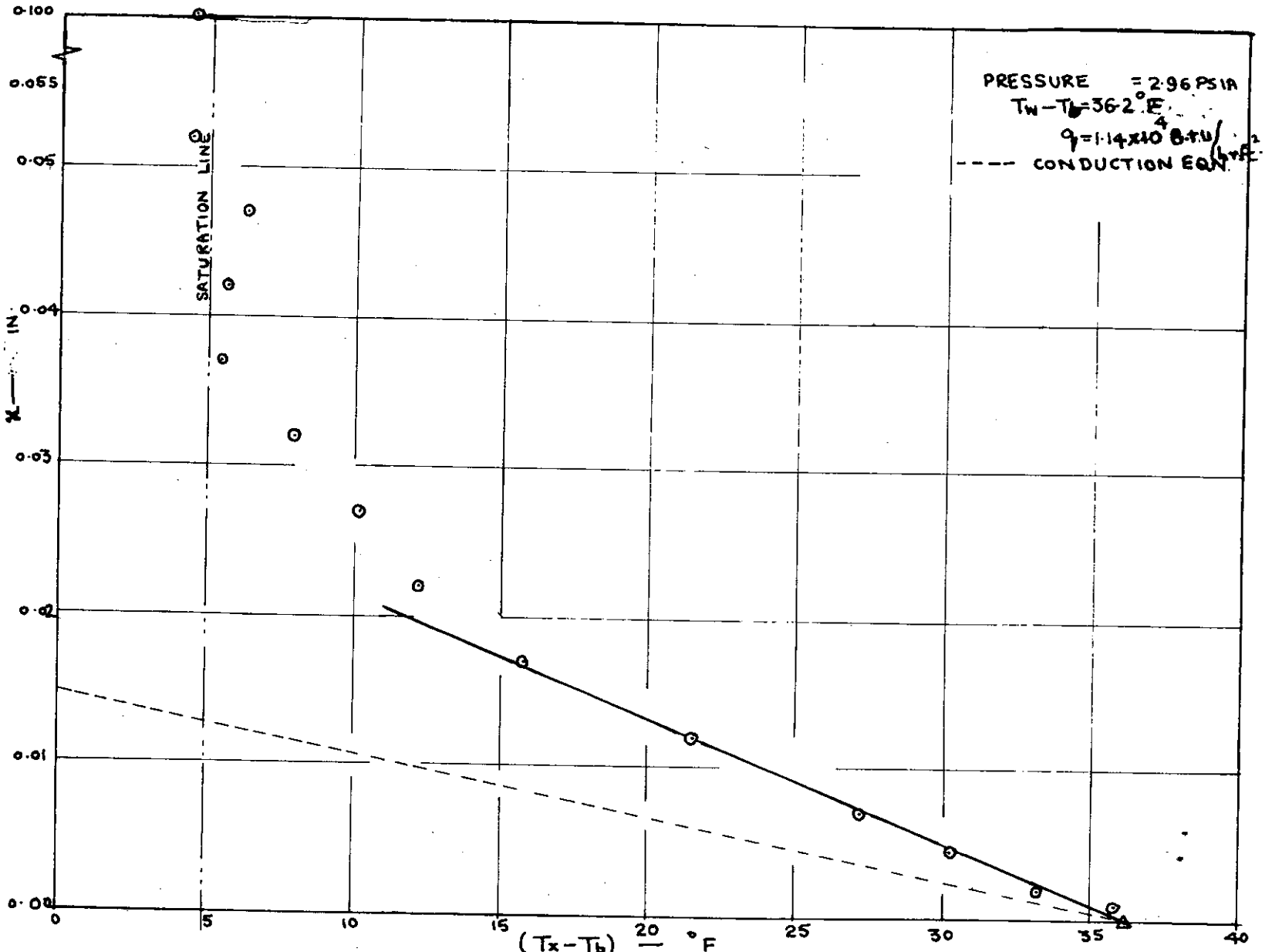

TEMPERATURE GRADIENT IN THE SUPERHEATED LAYER.

FIG. 43

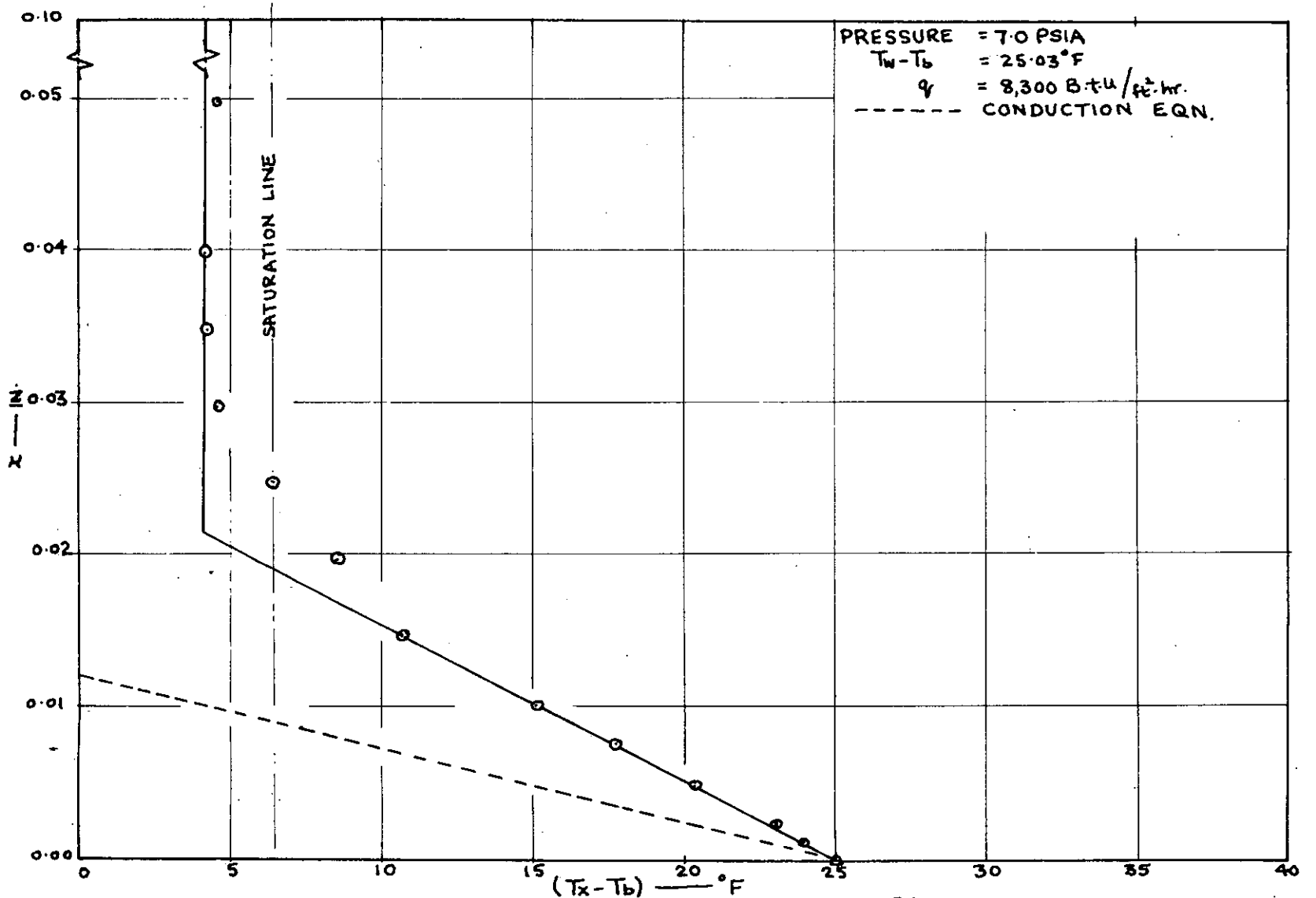

TEMP. GRADIENT IN THE SUPERHEATED LAYER.

FIG·44

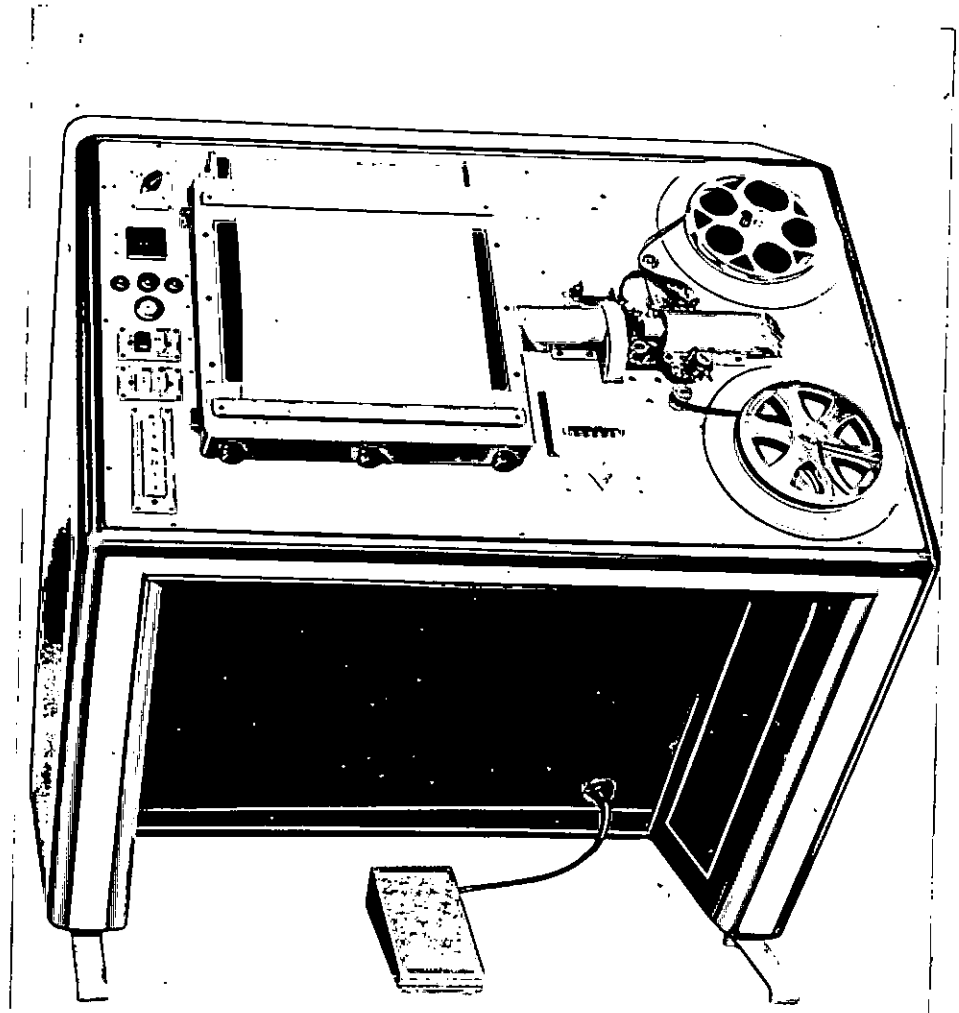

FIG. 45

LYTEX IV – 16 ANALYSING PROJECTOR

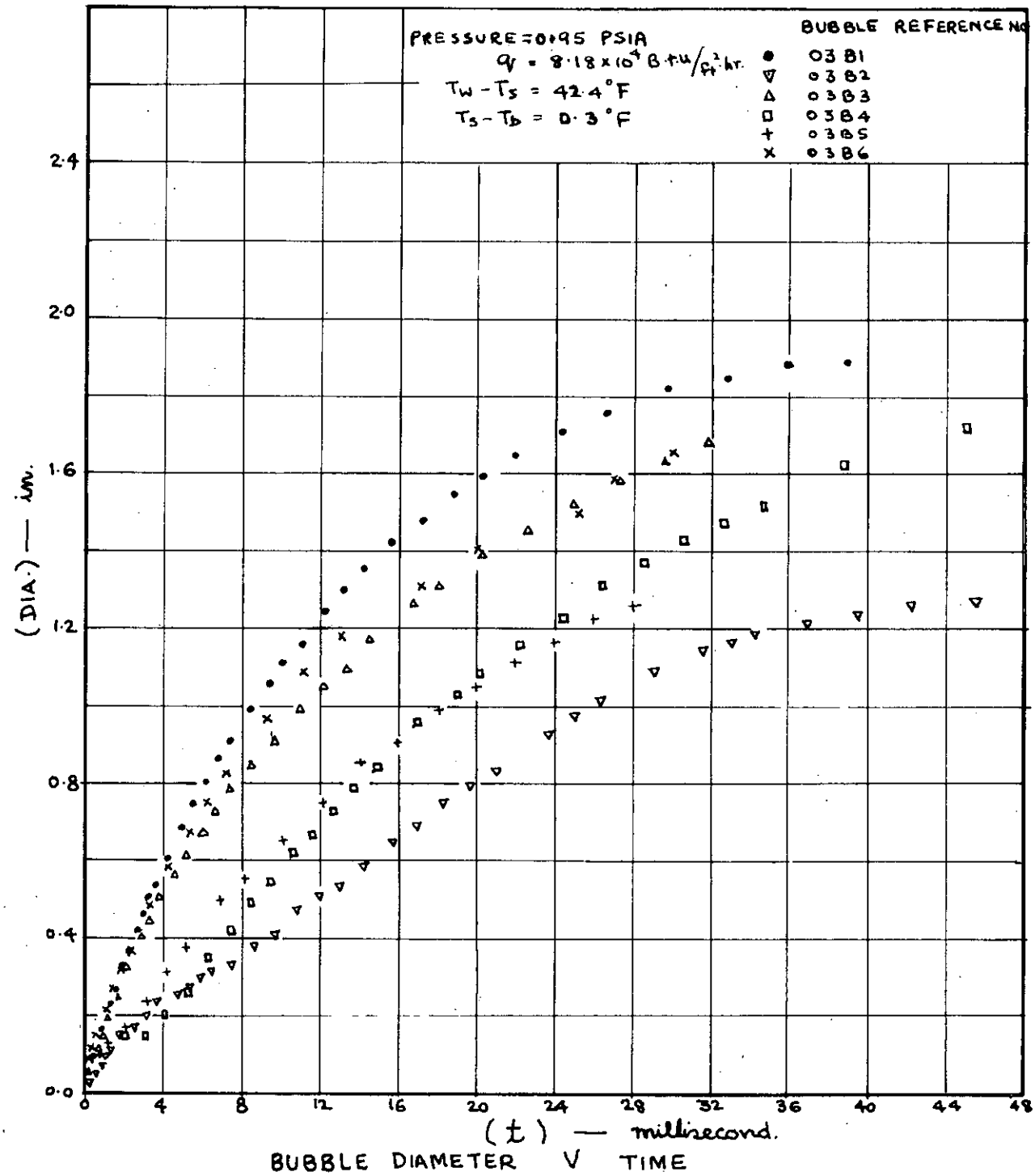

BUBBLE DIAMETER V TIME

FIG·46

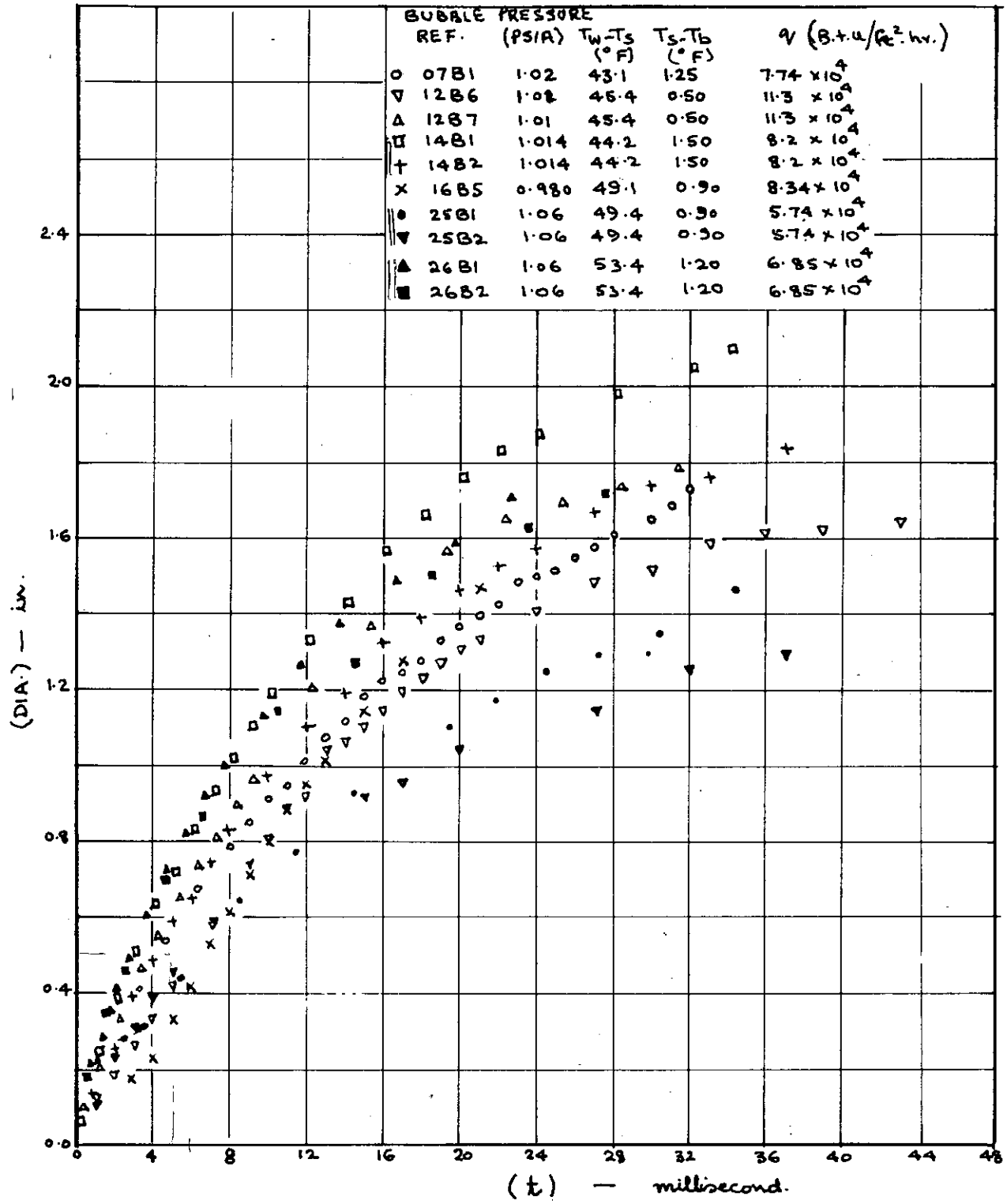

BUBBLE DIAMETER V TIME

FIG·47

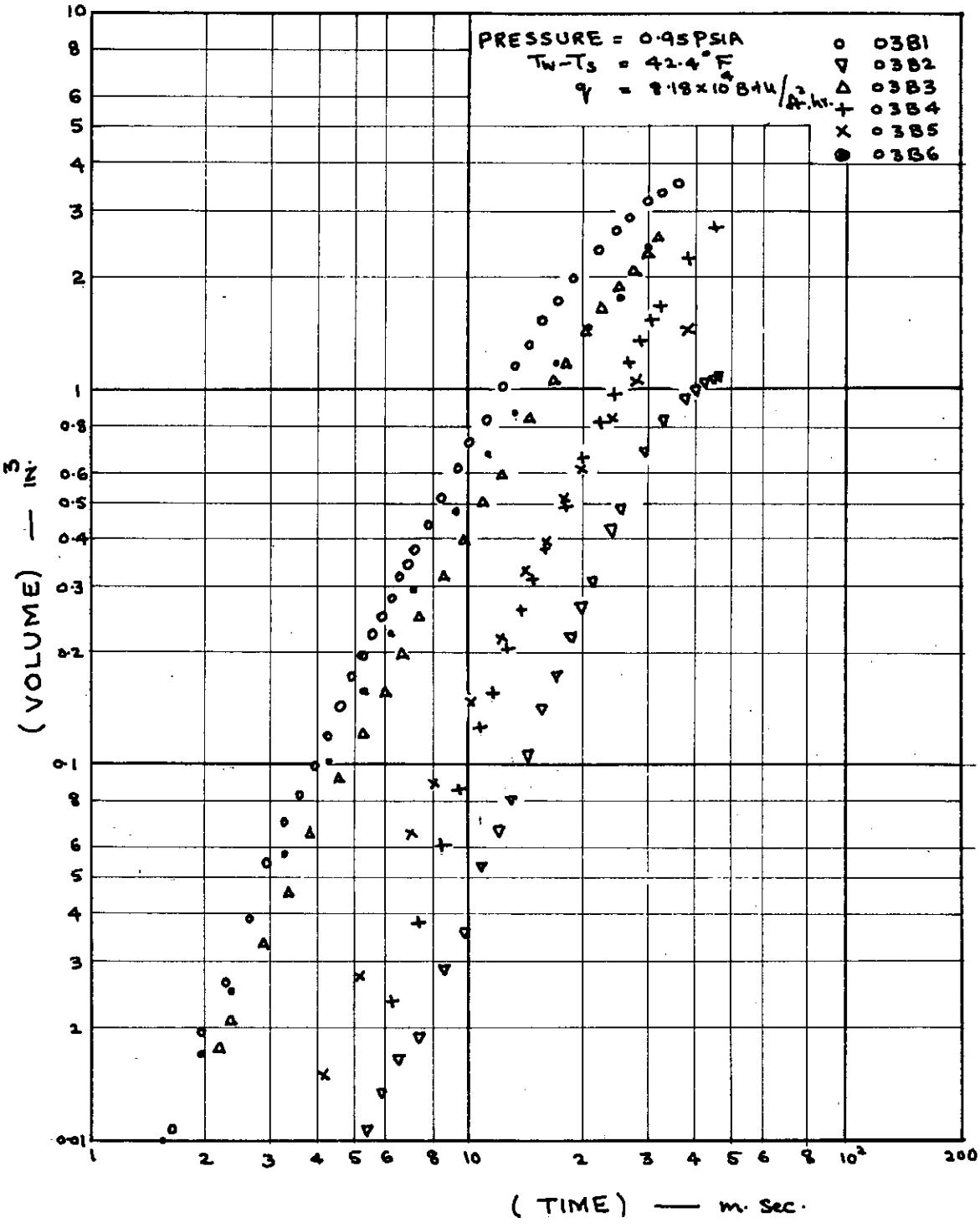

BUBBLE VOLUME V TIME

FIG. 48

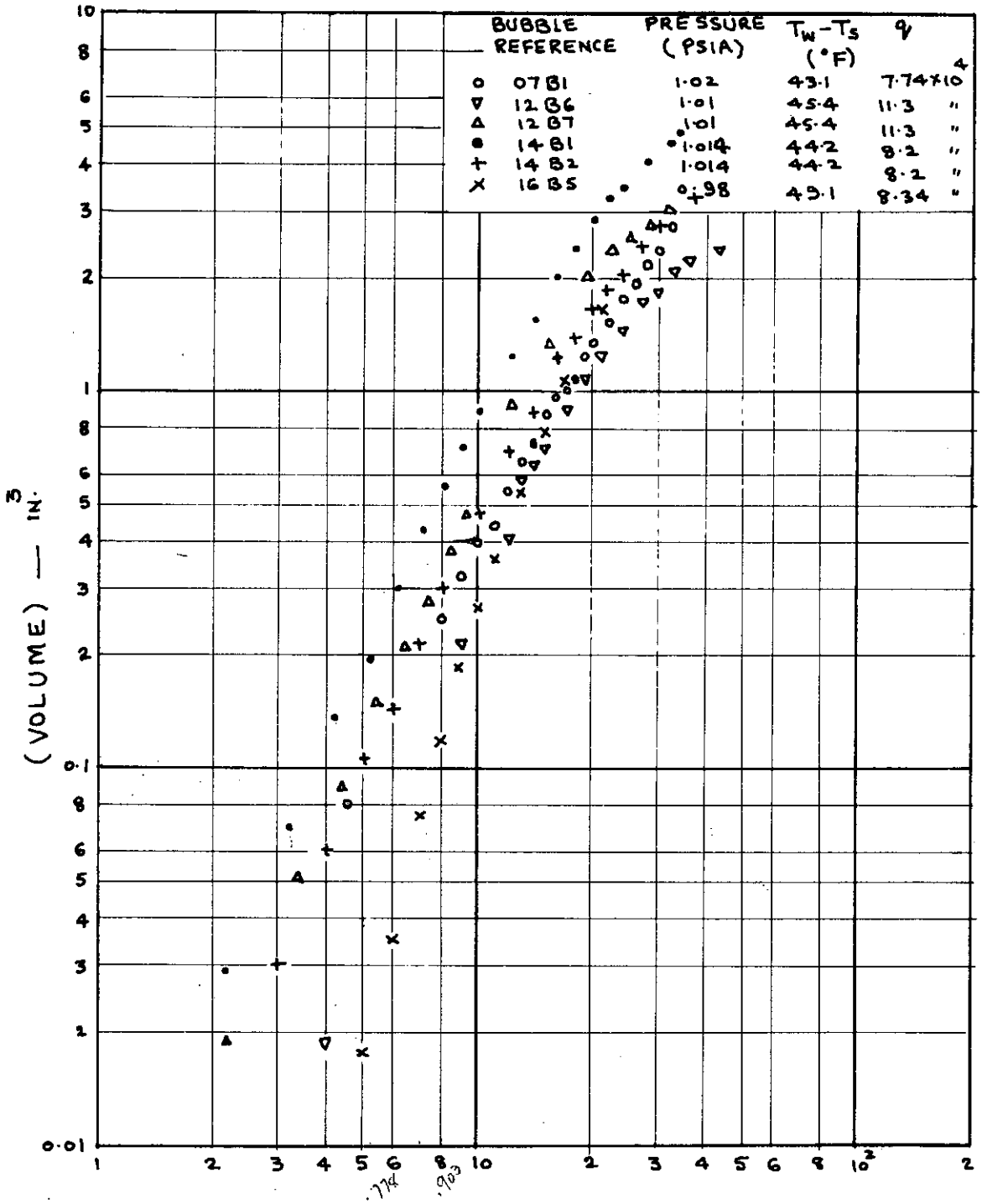

BUBBLE VOLUME V TIME.

FIG·49

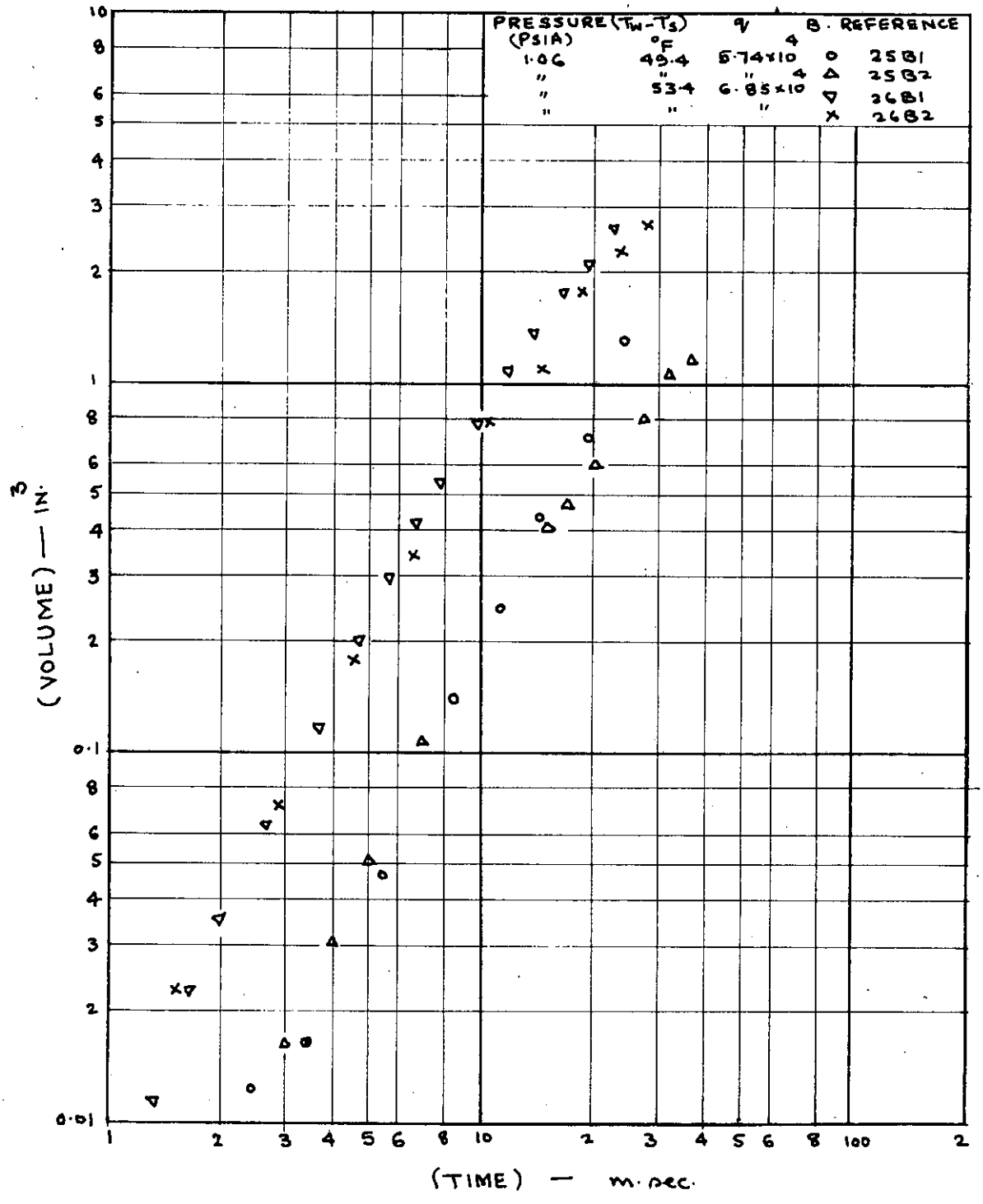

BUBBLE VOLUME V TIME

FIG·50

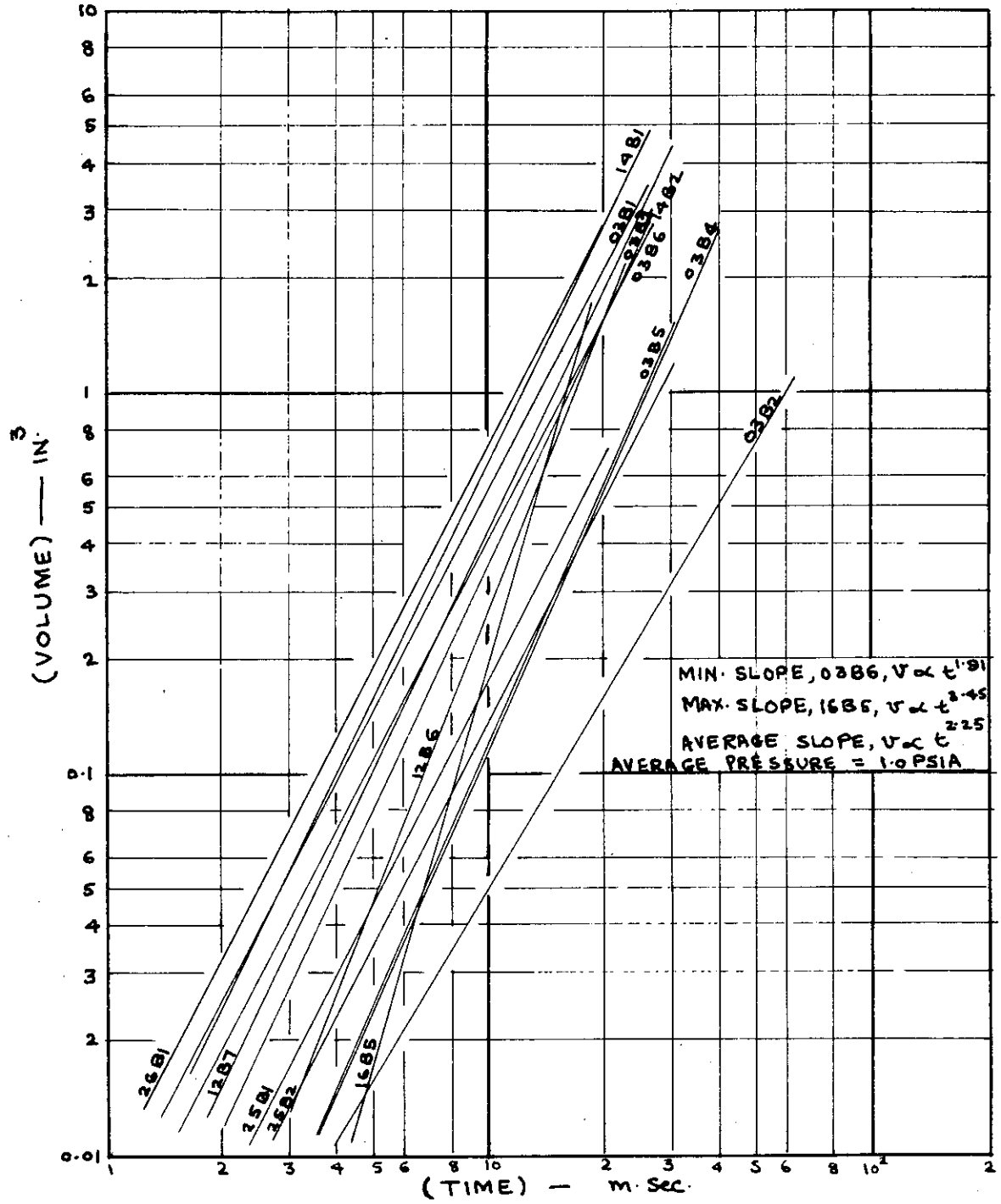

BUBBLE VOLUME V TIME (REGRESSION LINES).

FIG·51

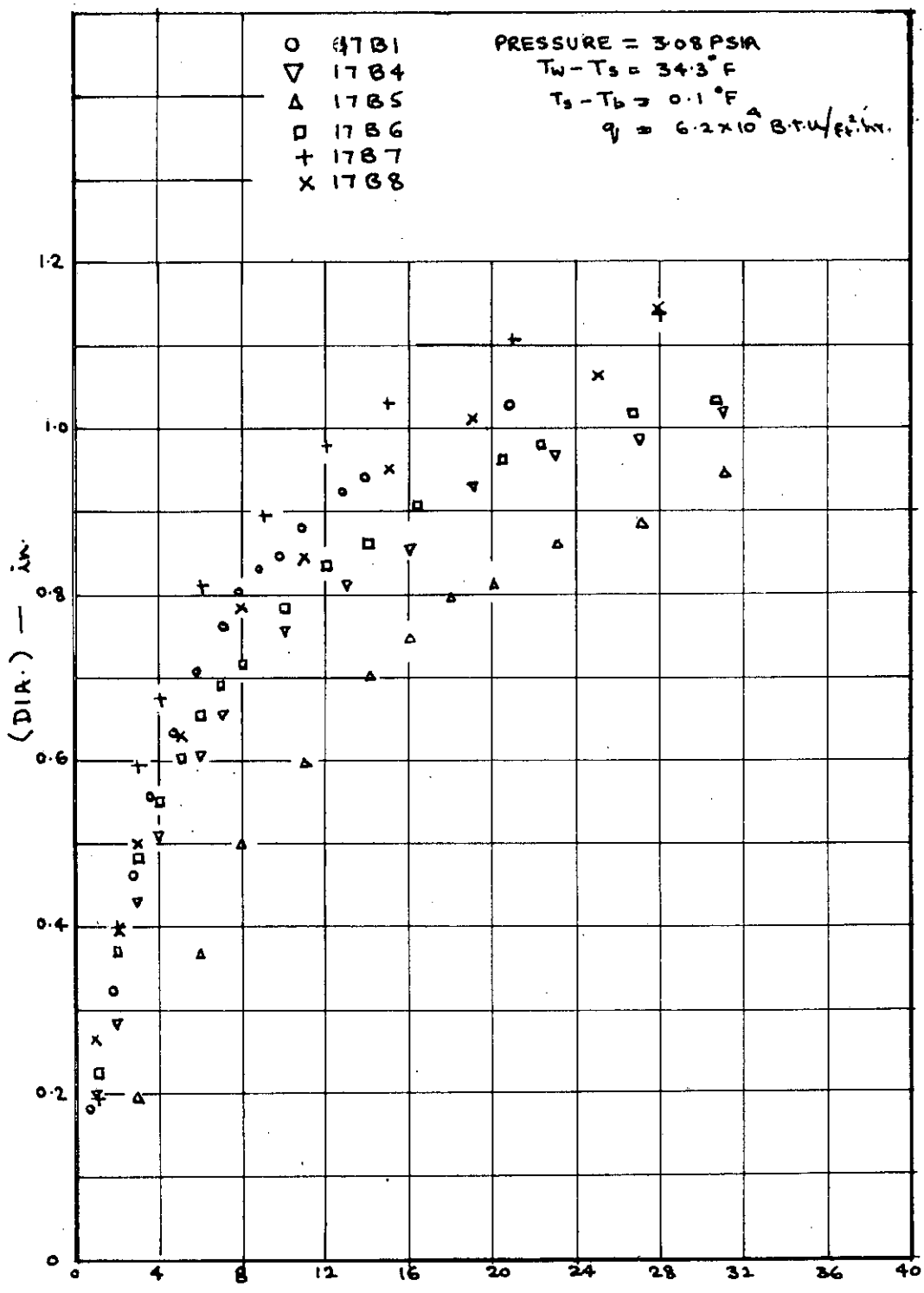

BUBBLE DIAMETER V TIME

FIG·52

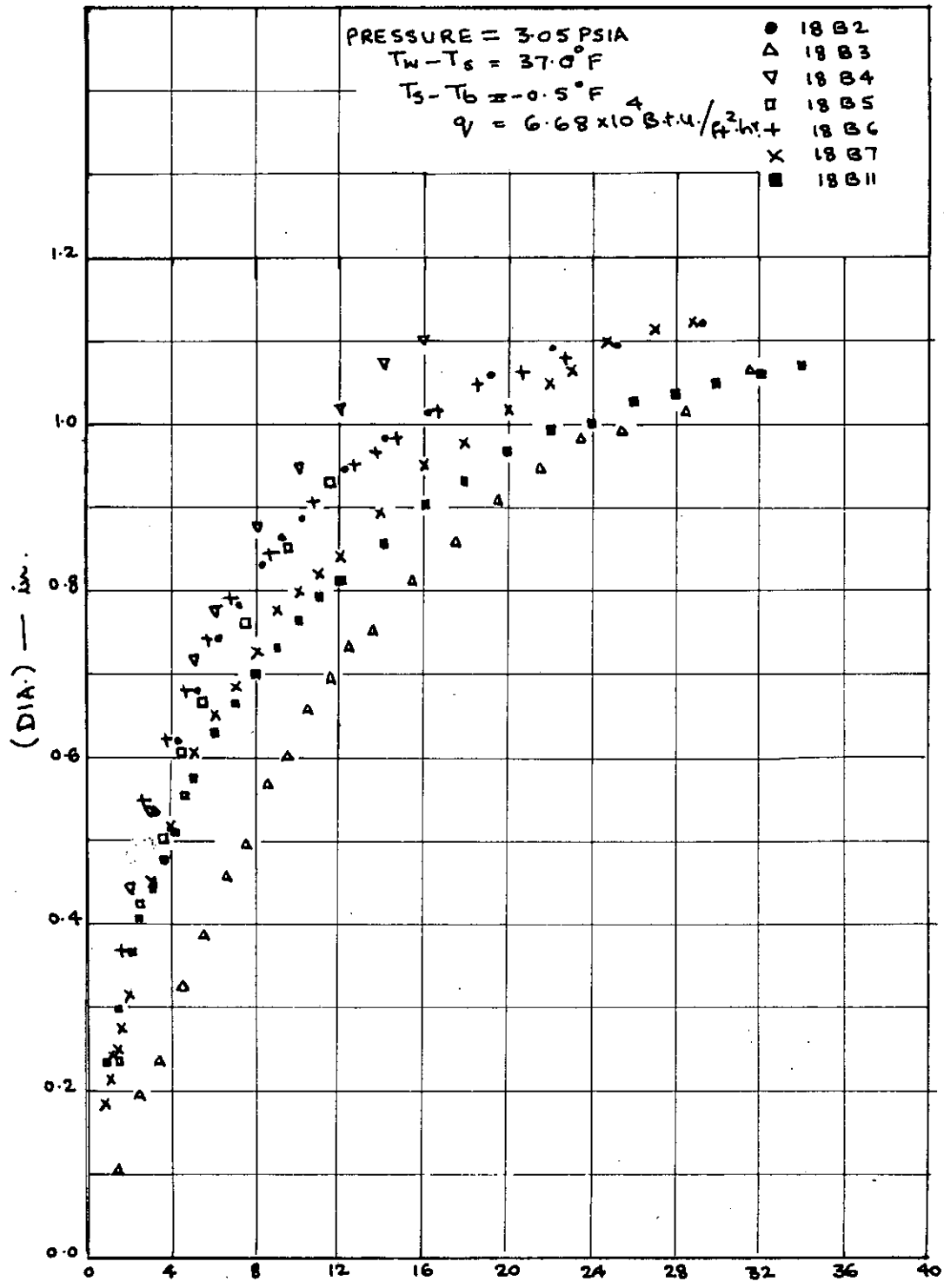

BUBBLE DIAMETER V TIME

FIG·53

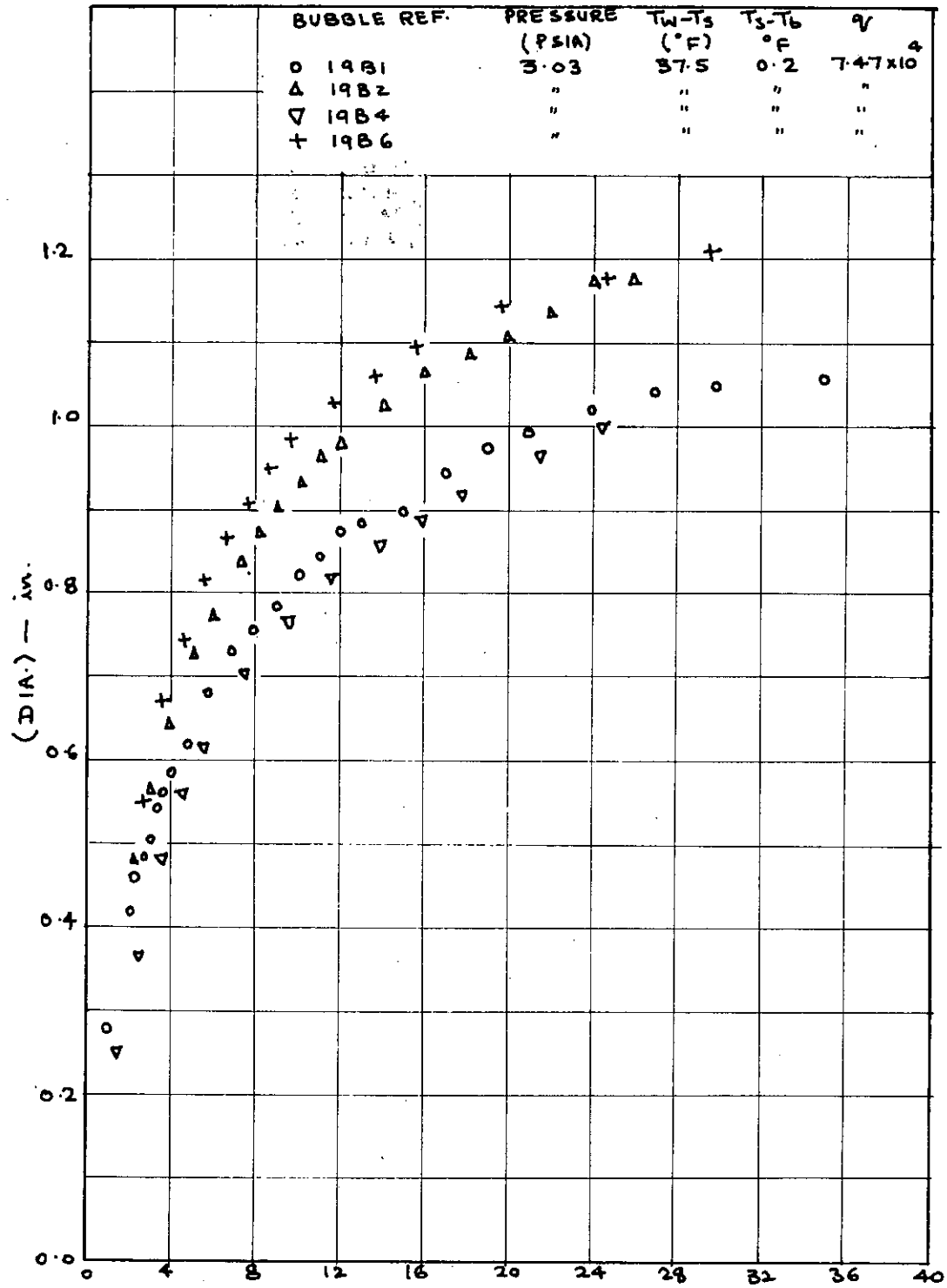

BUBBLE DIAMETER V TIME

FIG·54

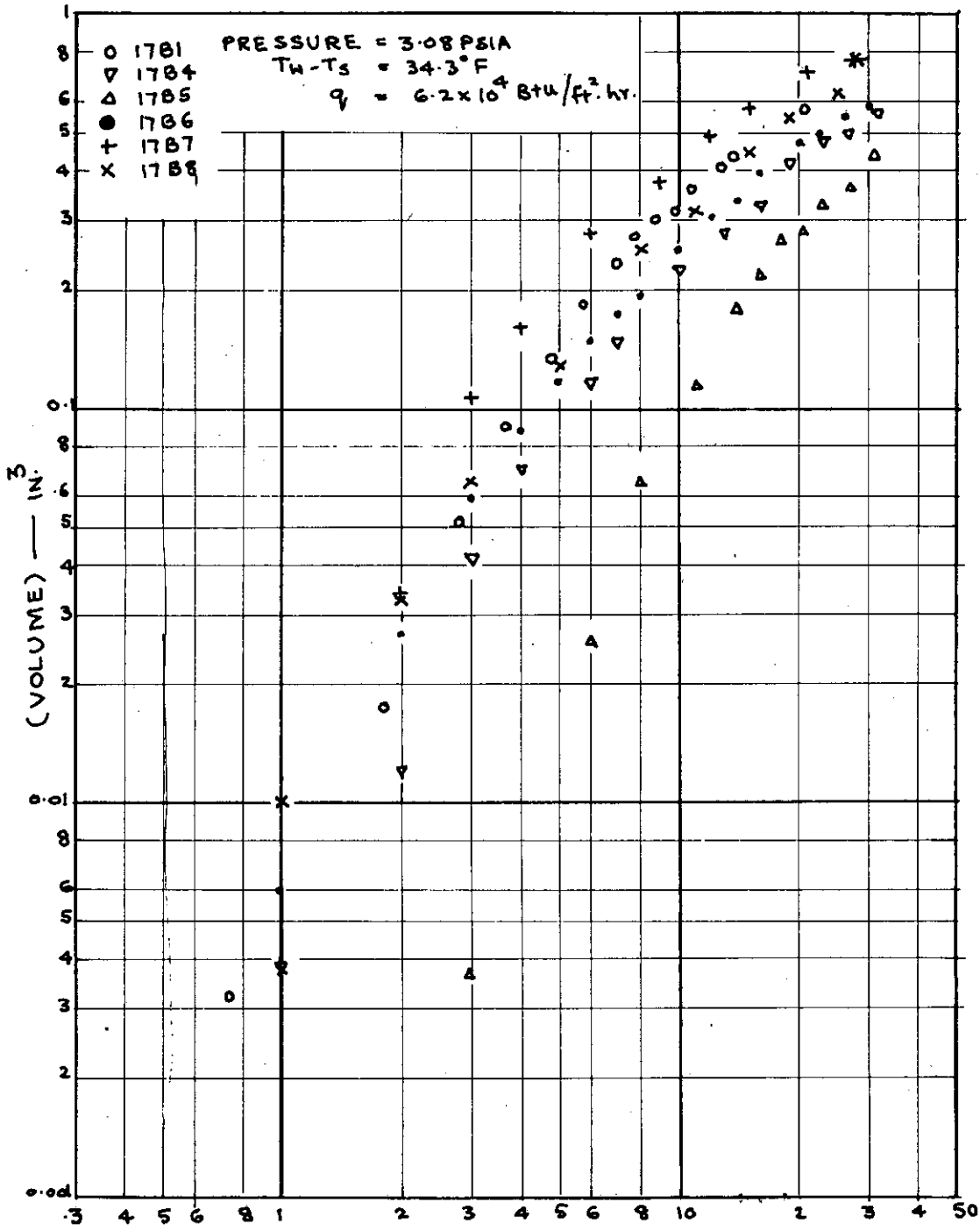

BUBBLE VOLUME V TIME

FIG·55

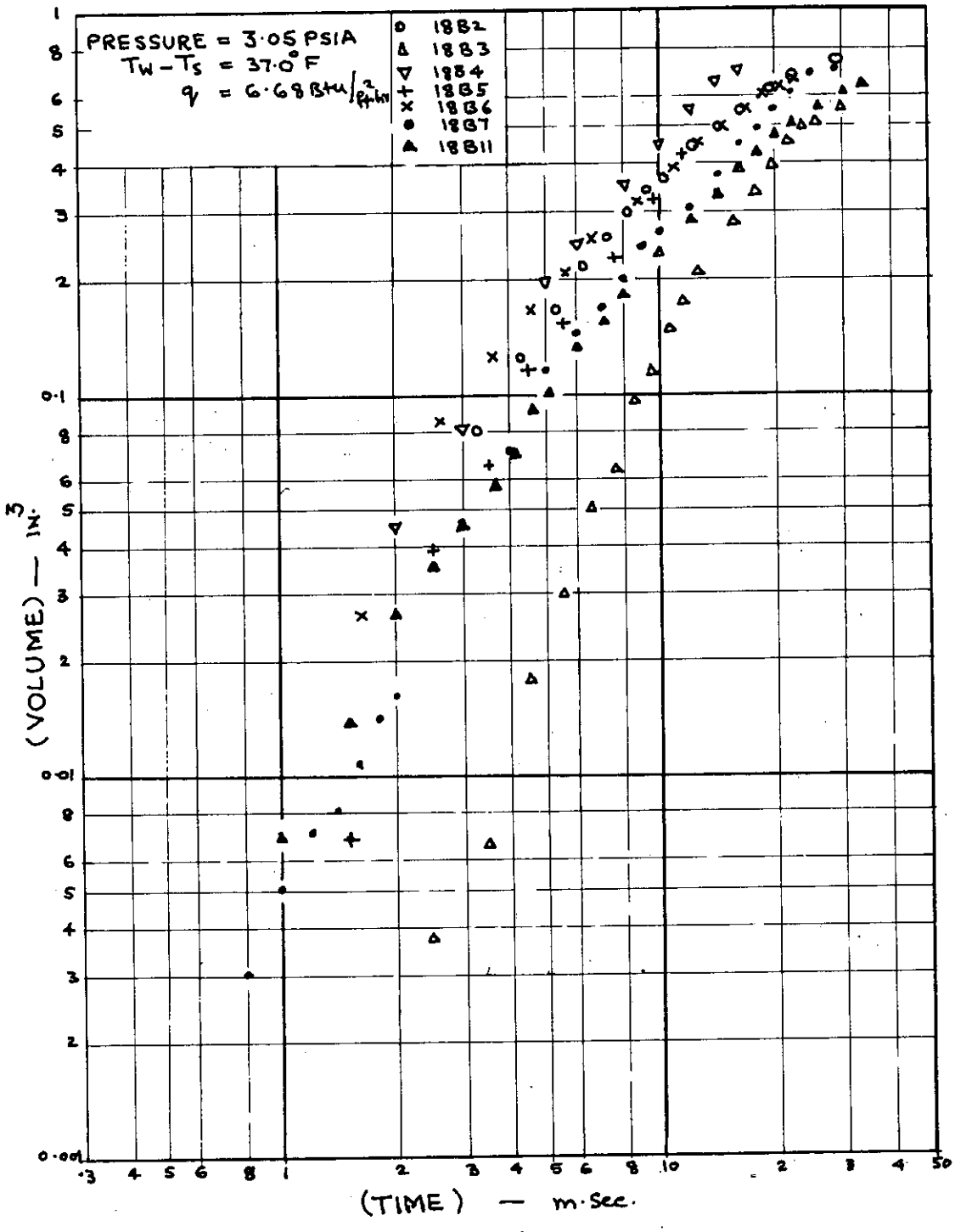

BUBBLE VOLUME V TIME

FIG·56

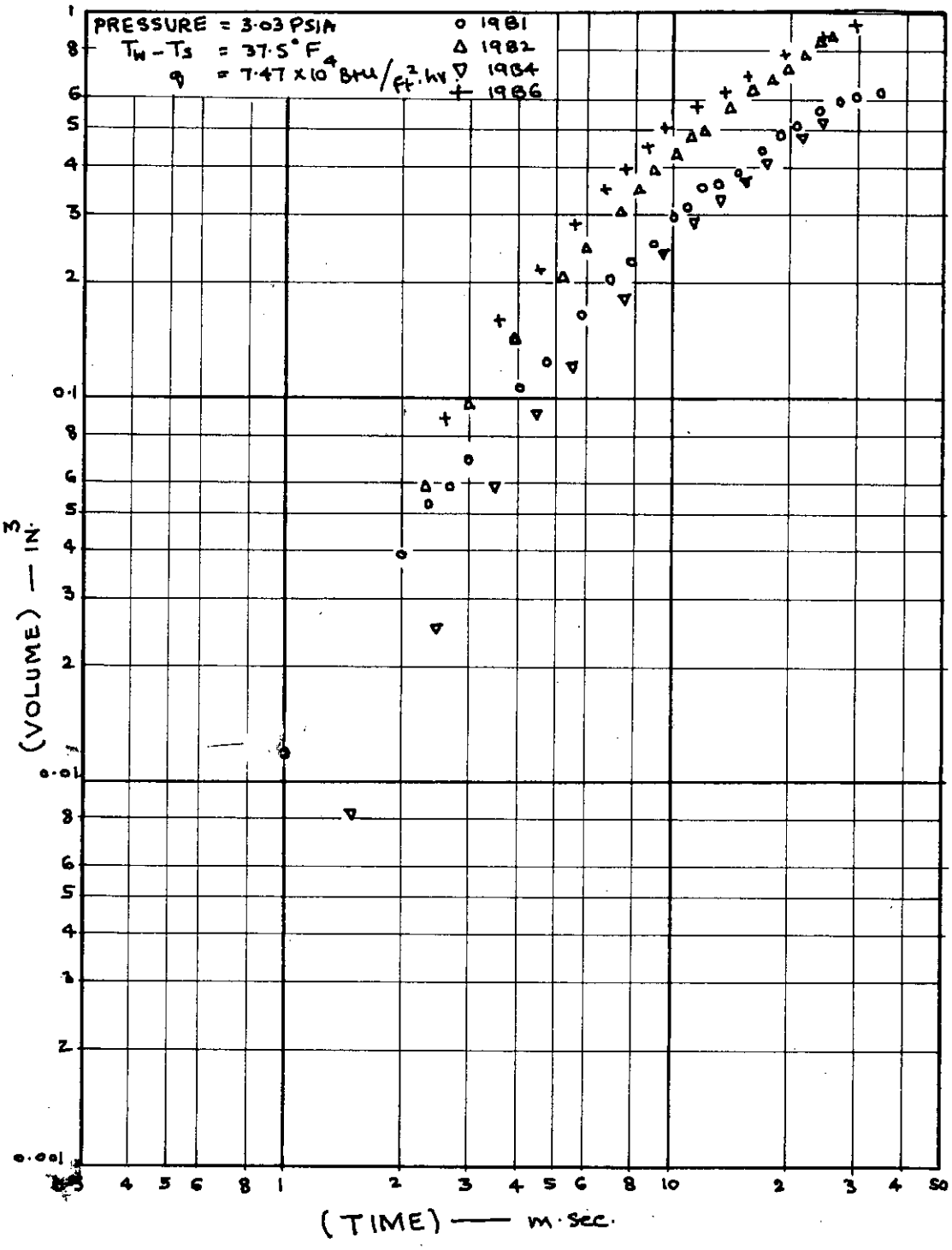

BUBBLE VOLUME V TIME

FIG·57

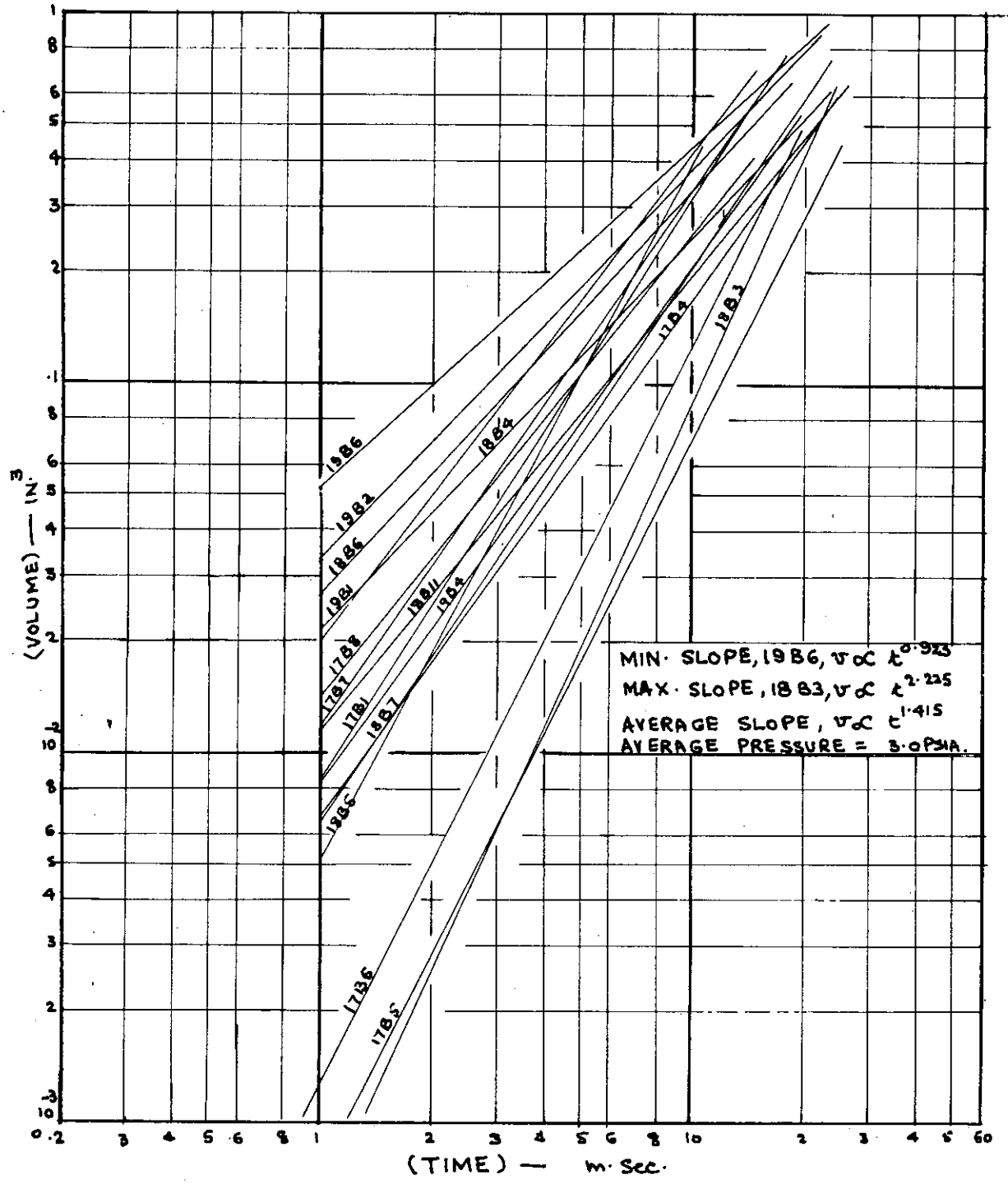

BUBBLE VOLUME V TIME
(REGRESSION LINES)

FIG·58

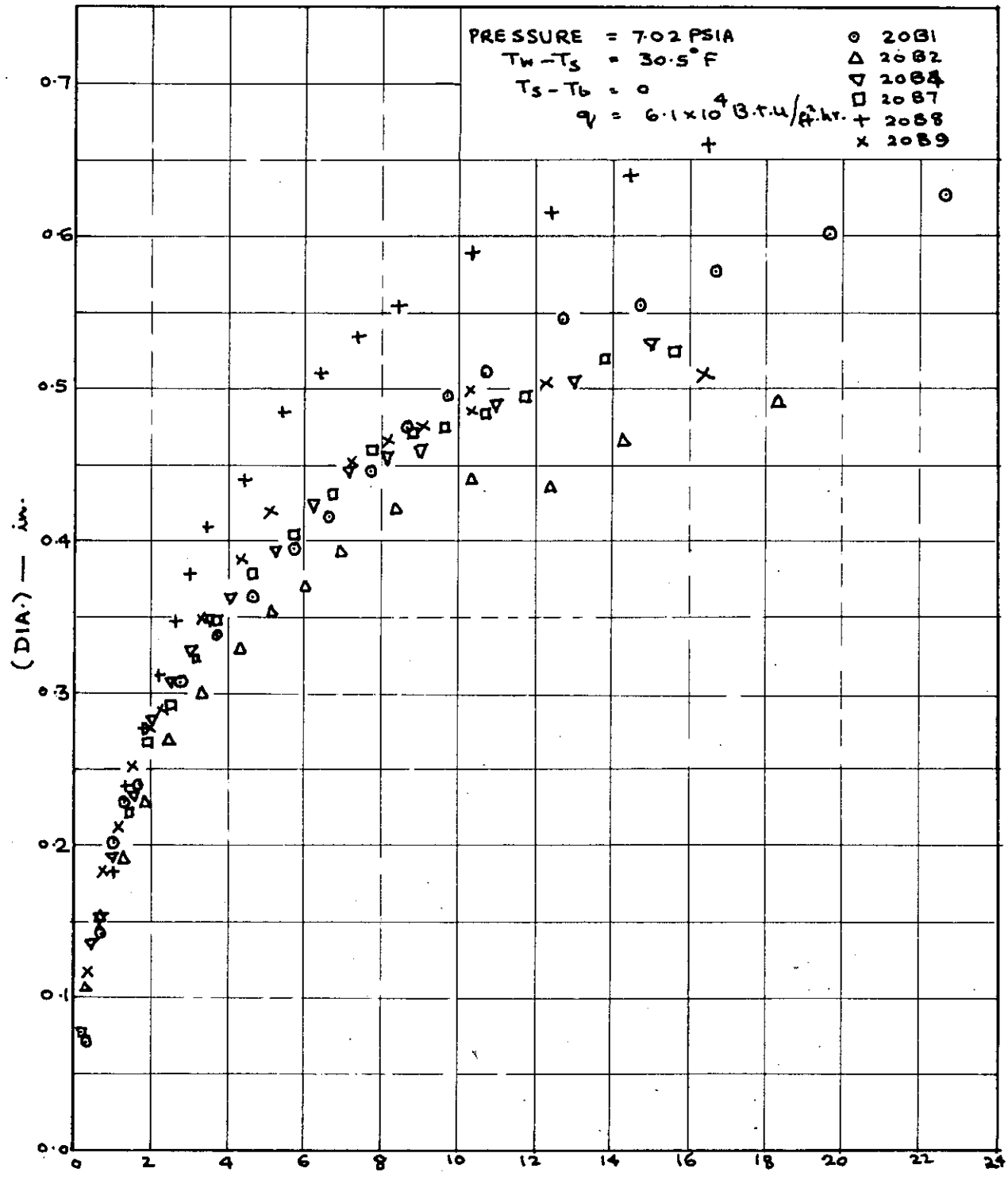

BUBBLE DIAMETER V TIME

FIG·59

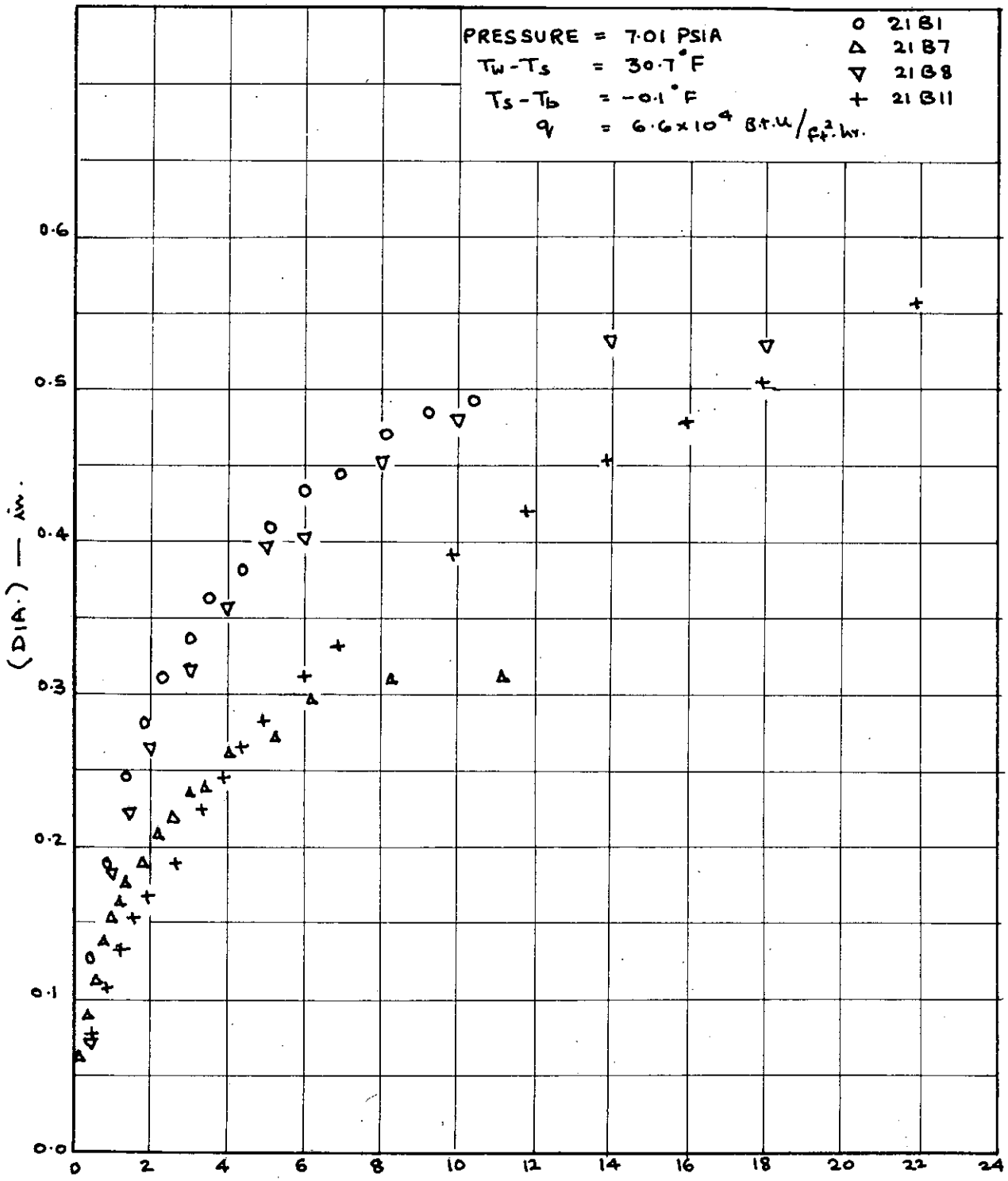

BUBBLE DIAMETER V TIME

FIG·60

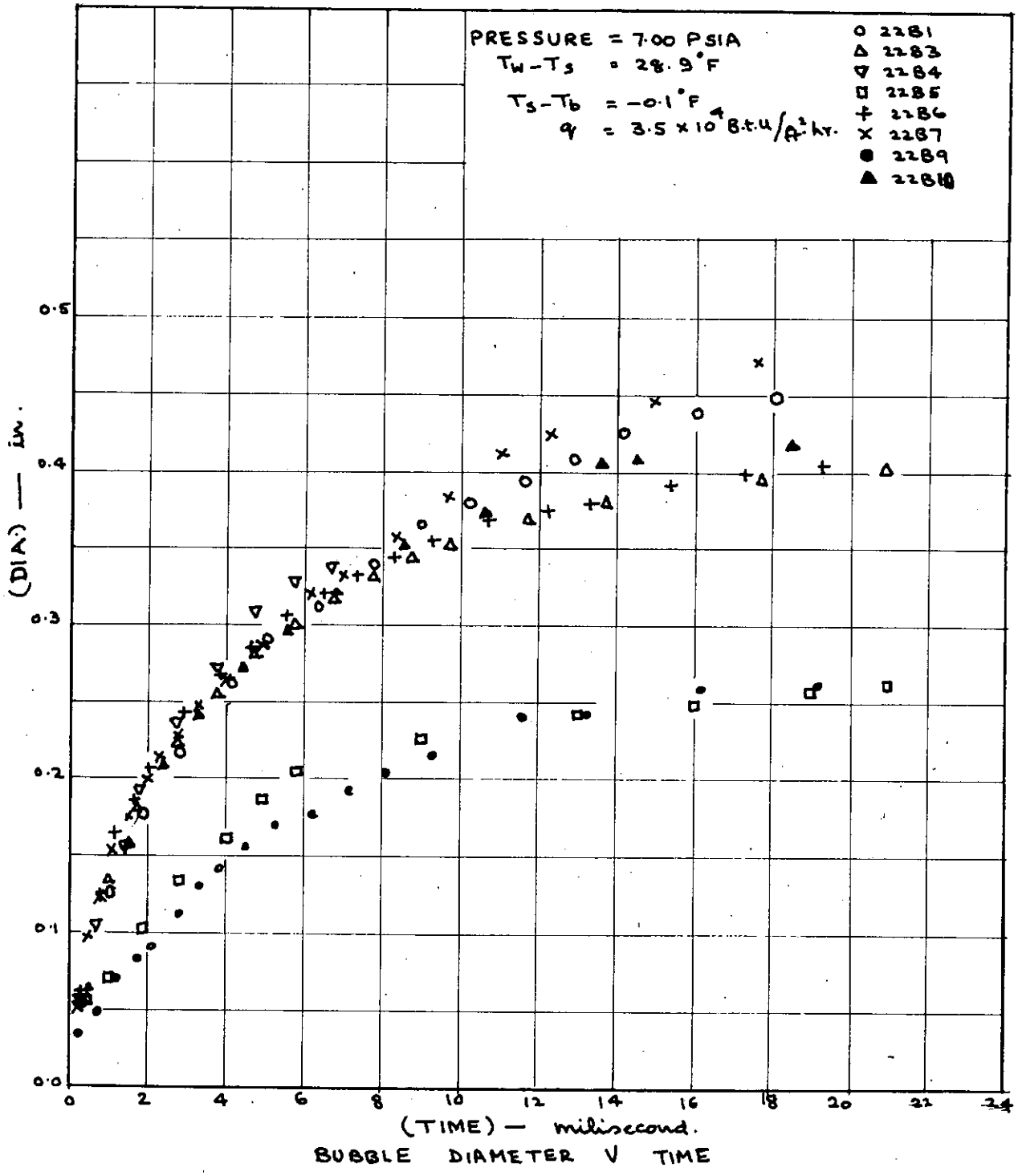

BUBBLE DIAMETER V TIME

FIG·61

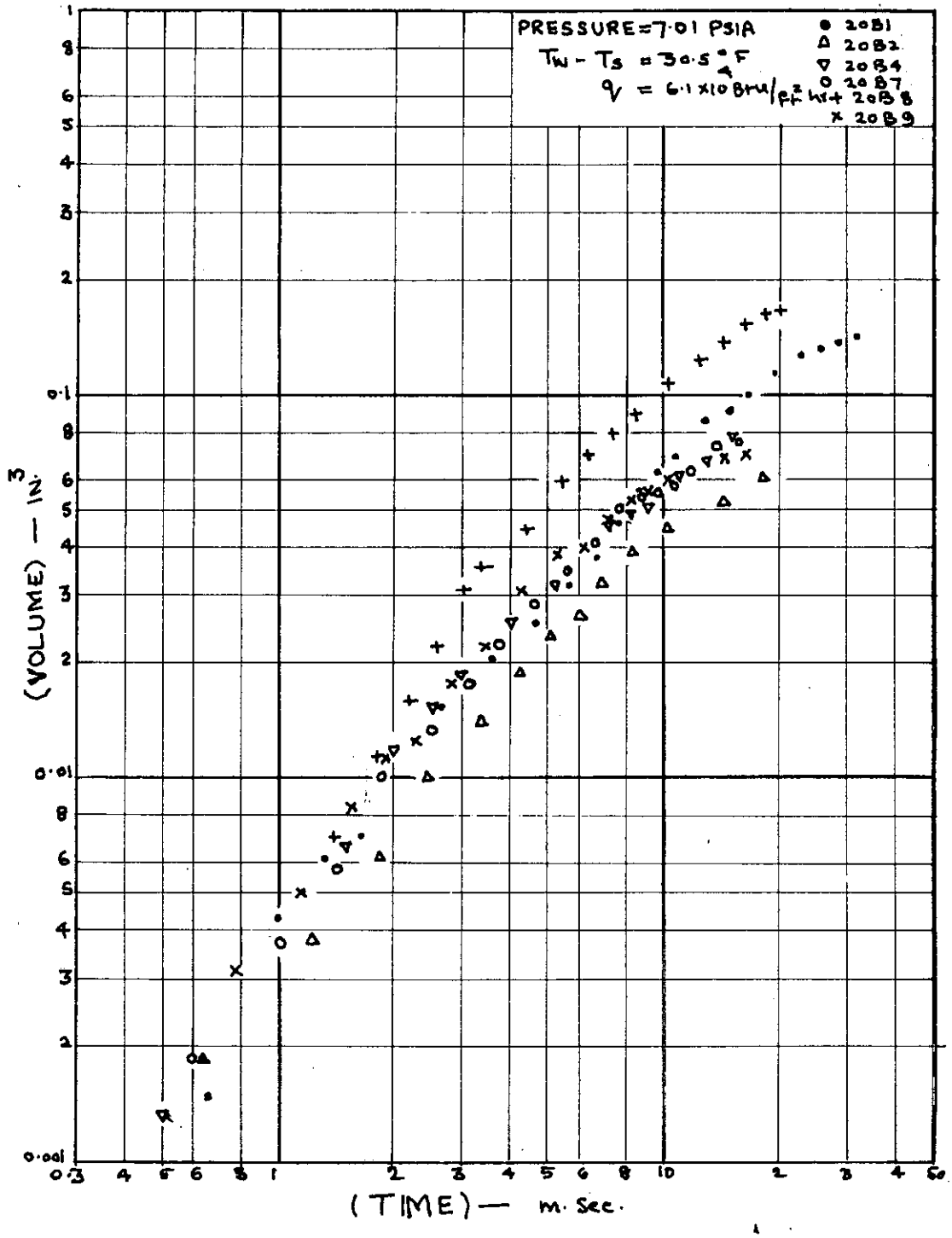

BUBBLE VOLUME V TIME

FIG·62

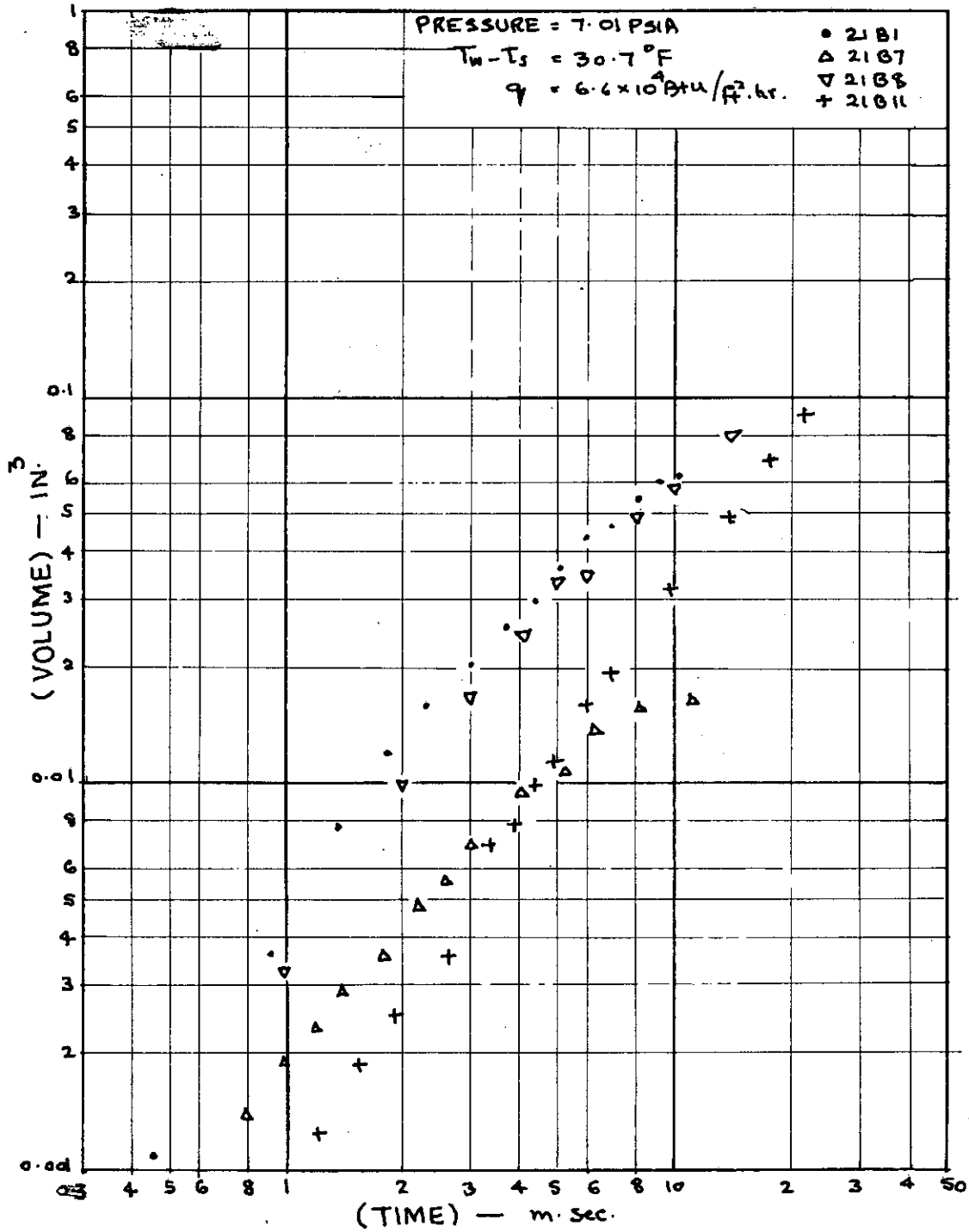

BUBBLE VOLUME V TIME

FIG·63

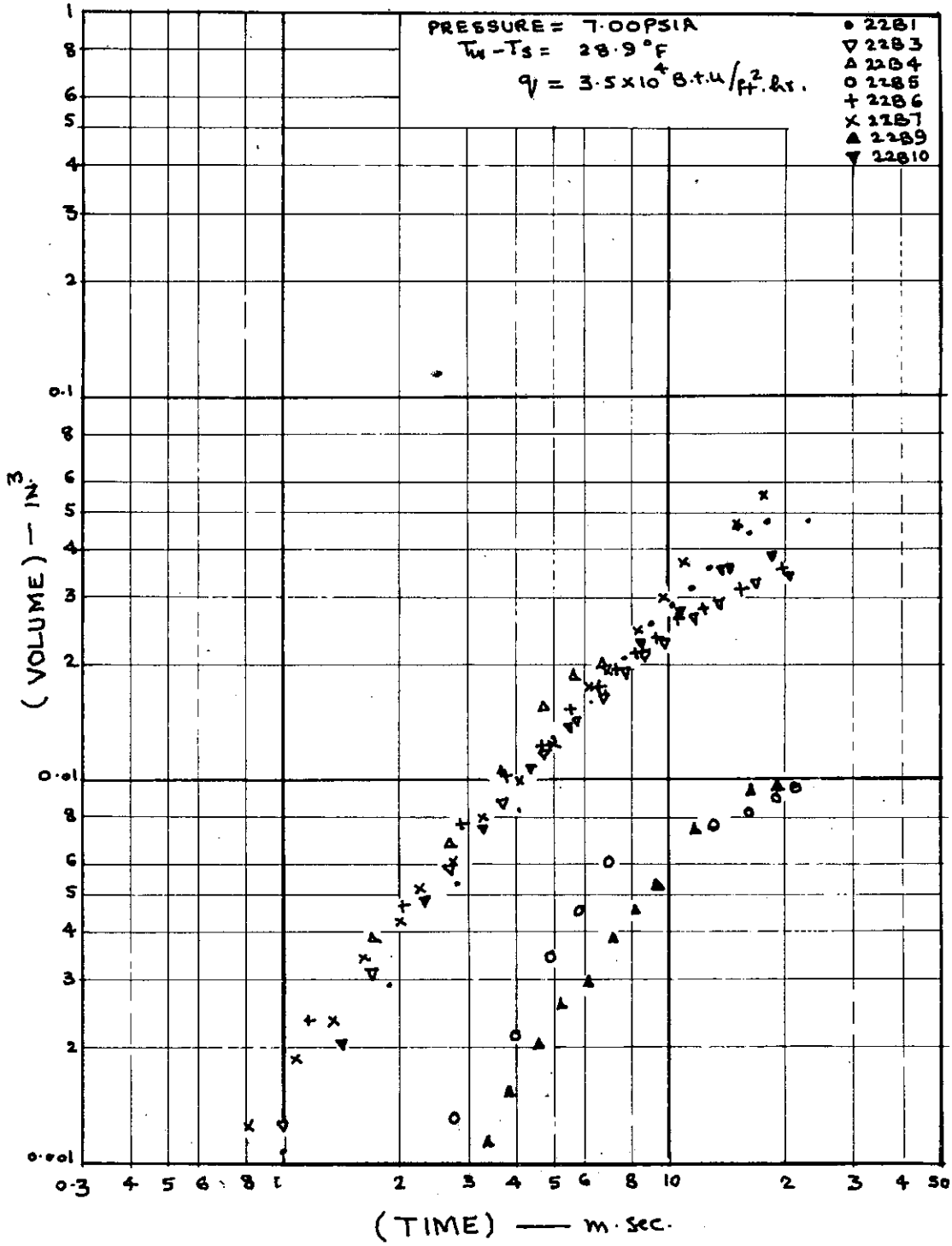

BUBBLE VOLUME V TIME

FIG·64

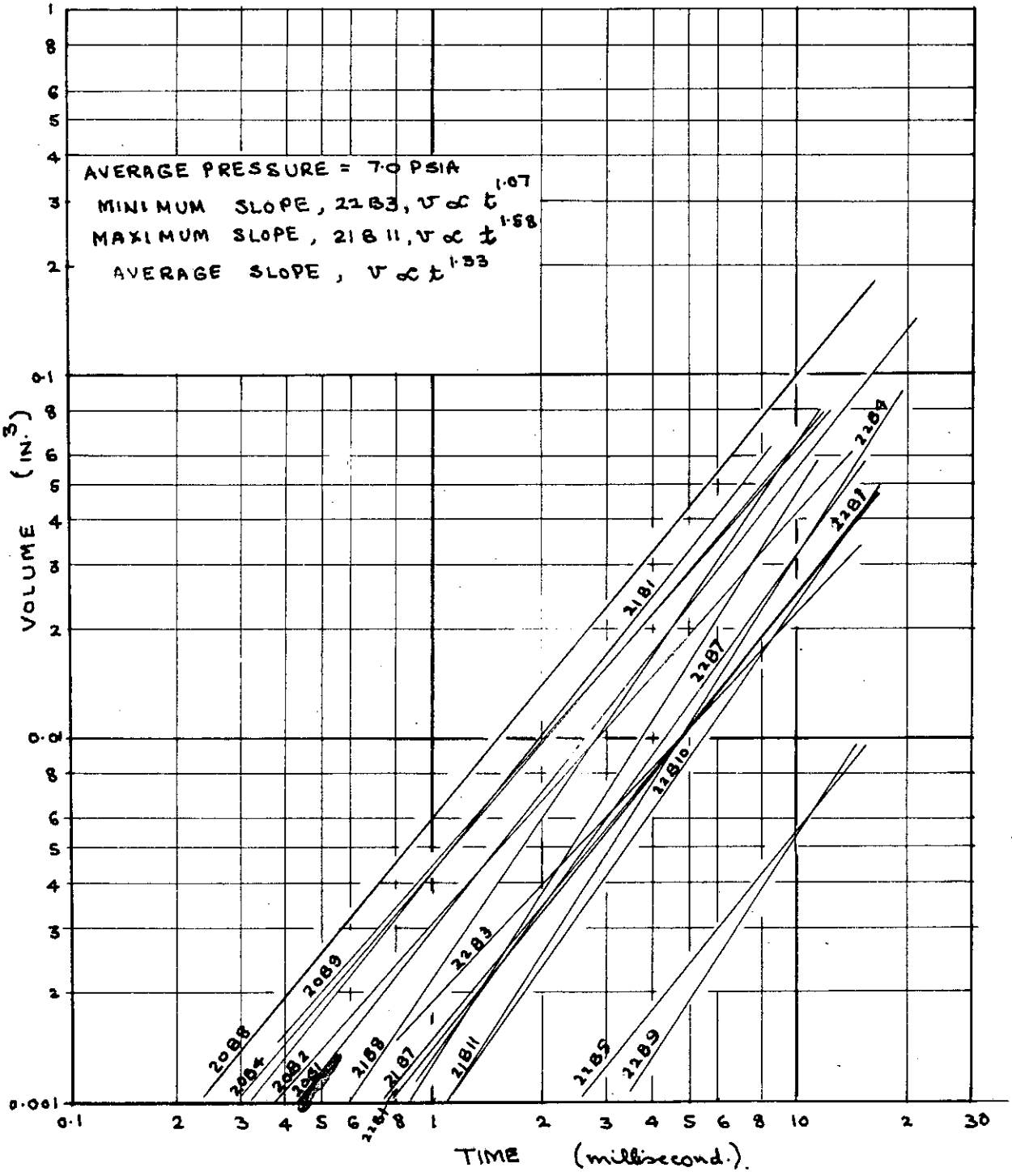

BUBBLE VOLUME V TIME
(REGRESSION LINES).

FIG. 65

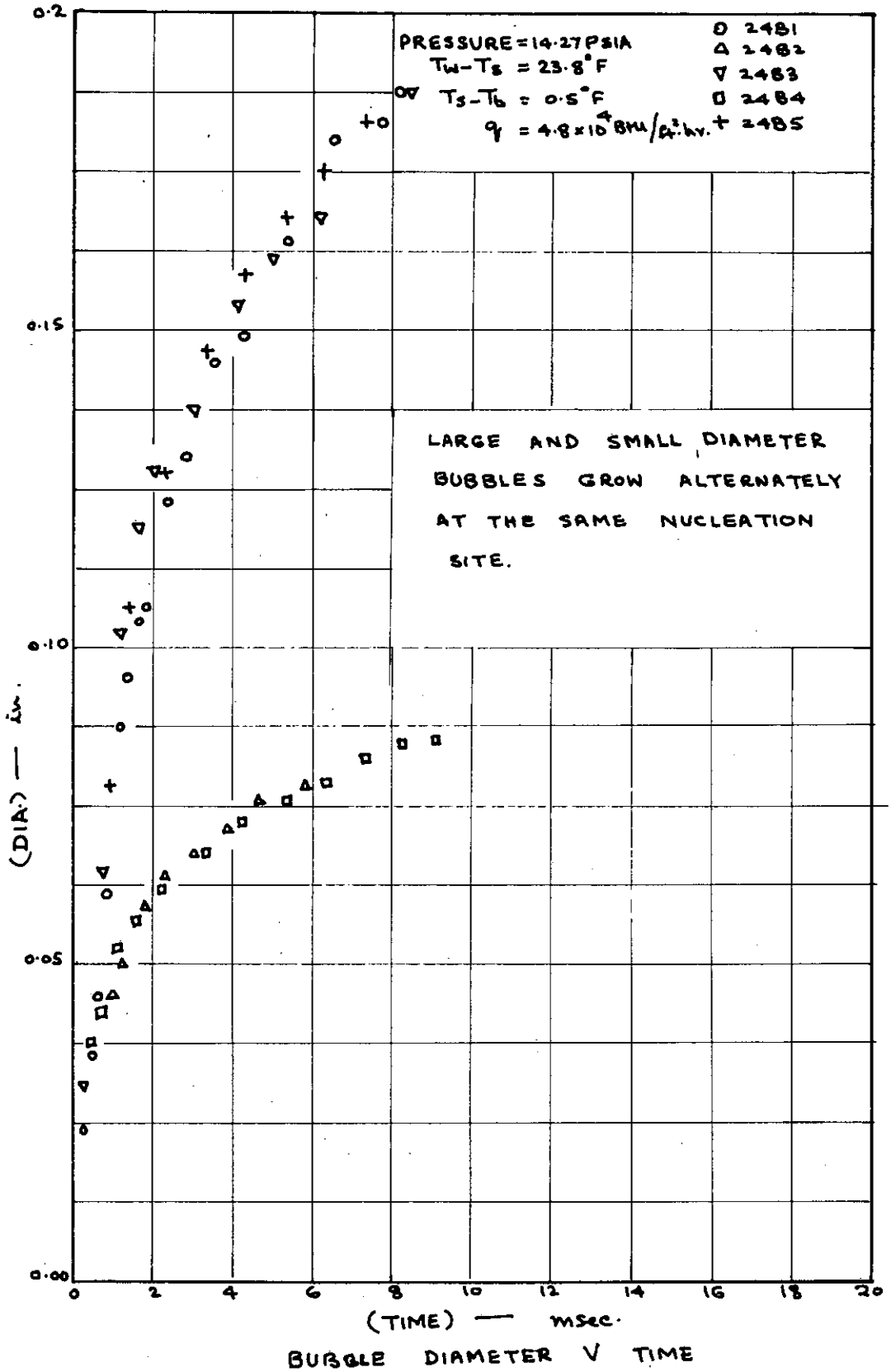

BUBBLE DIAMETER V TIME

FIG·66

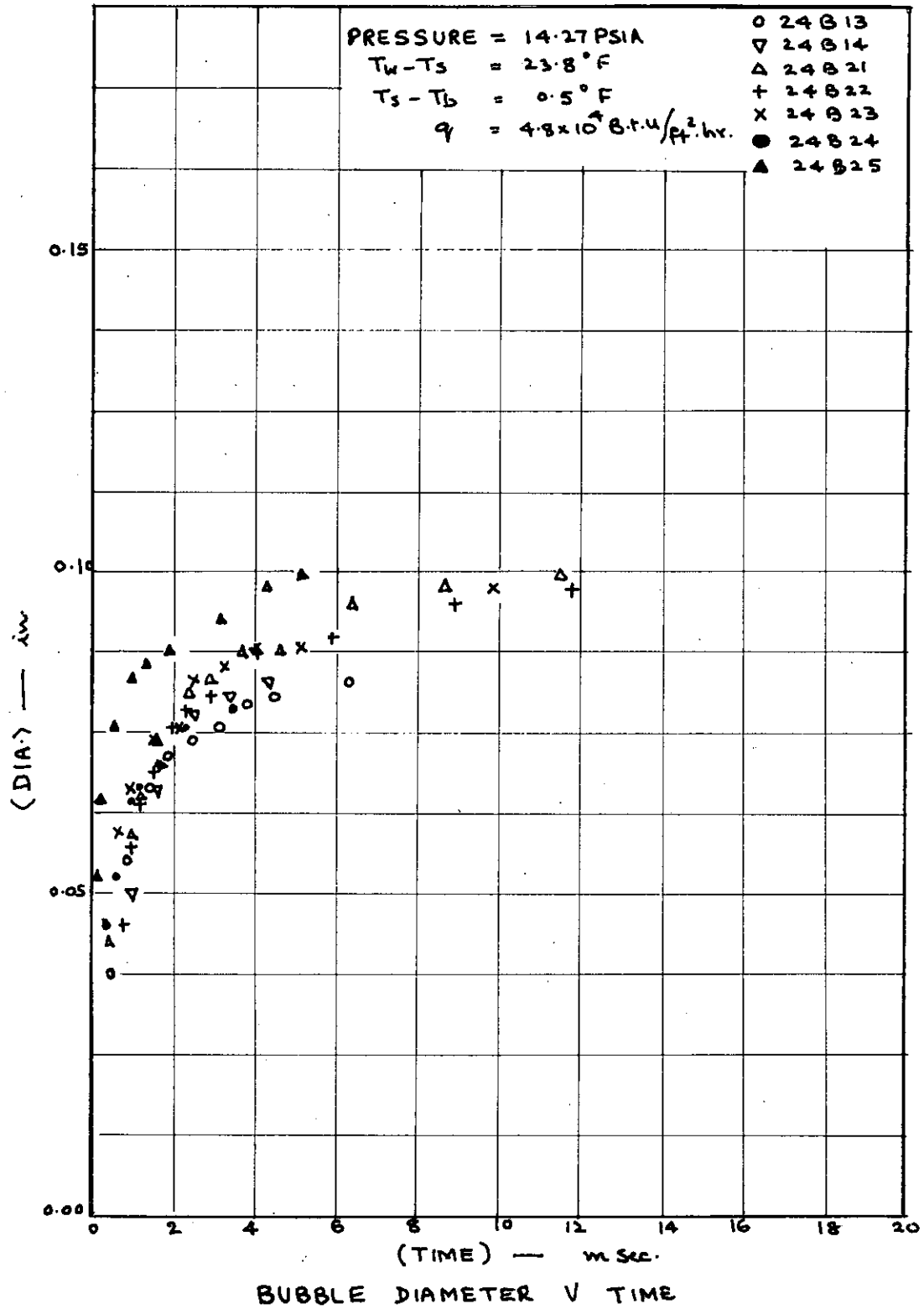

BUBBLE DIAMETER V TIME

FIG·67

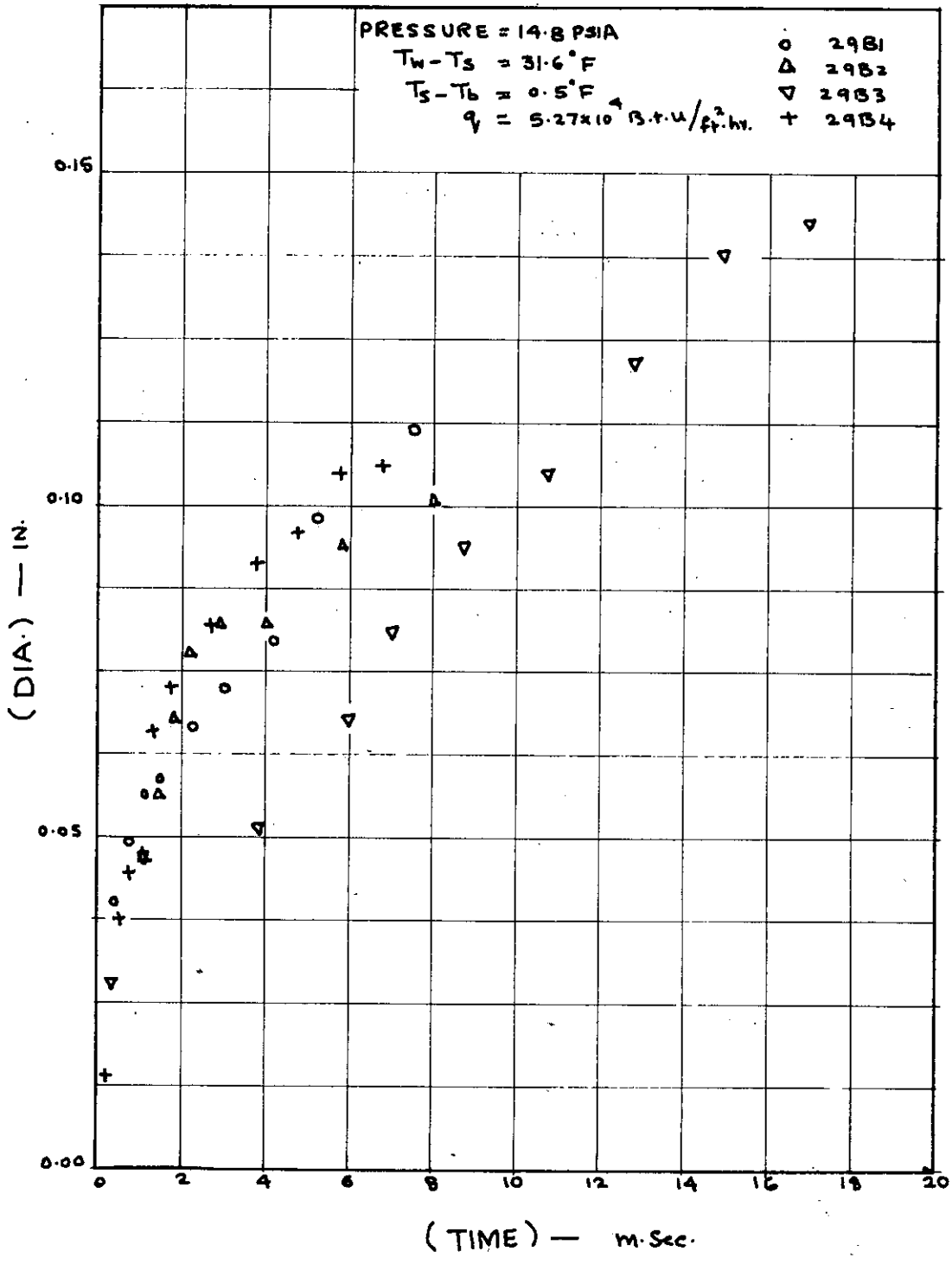

BUBBLE DIAMETER V. TIME

FIG·68

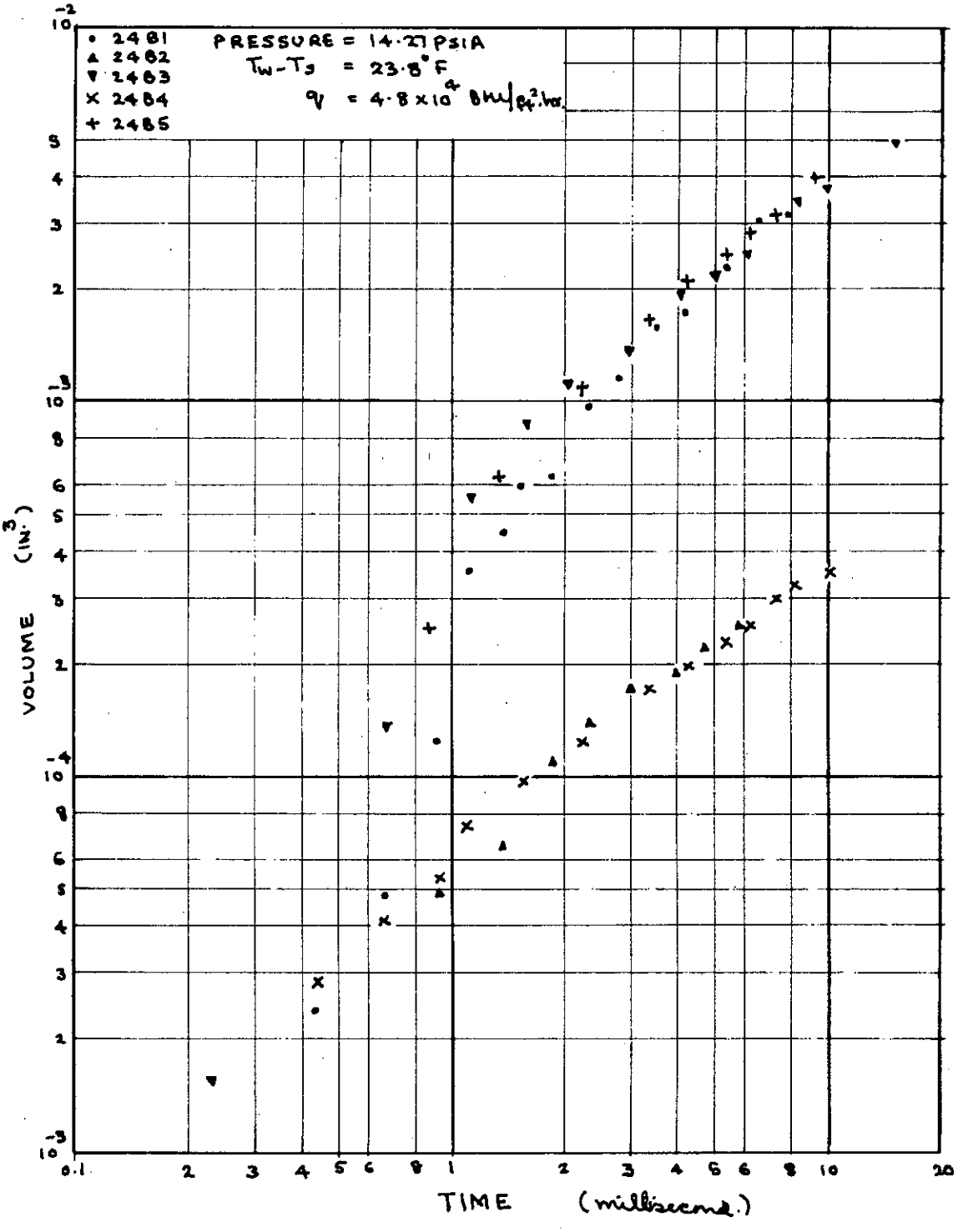

BUBBLE VOLUME V TIME

FIG·69

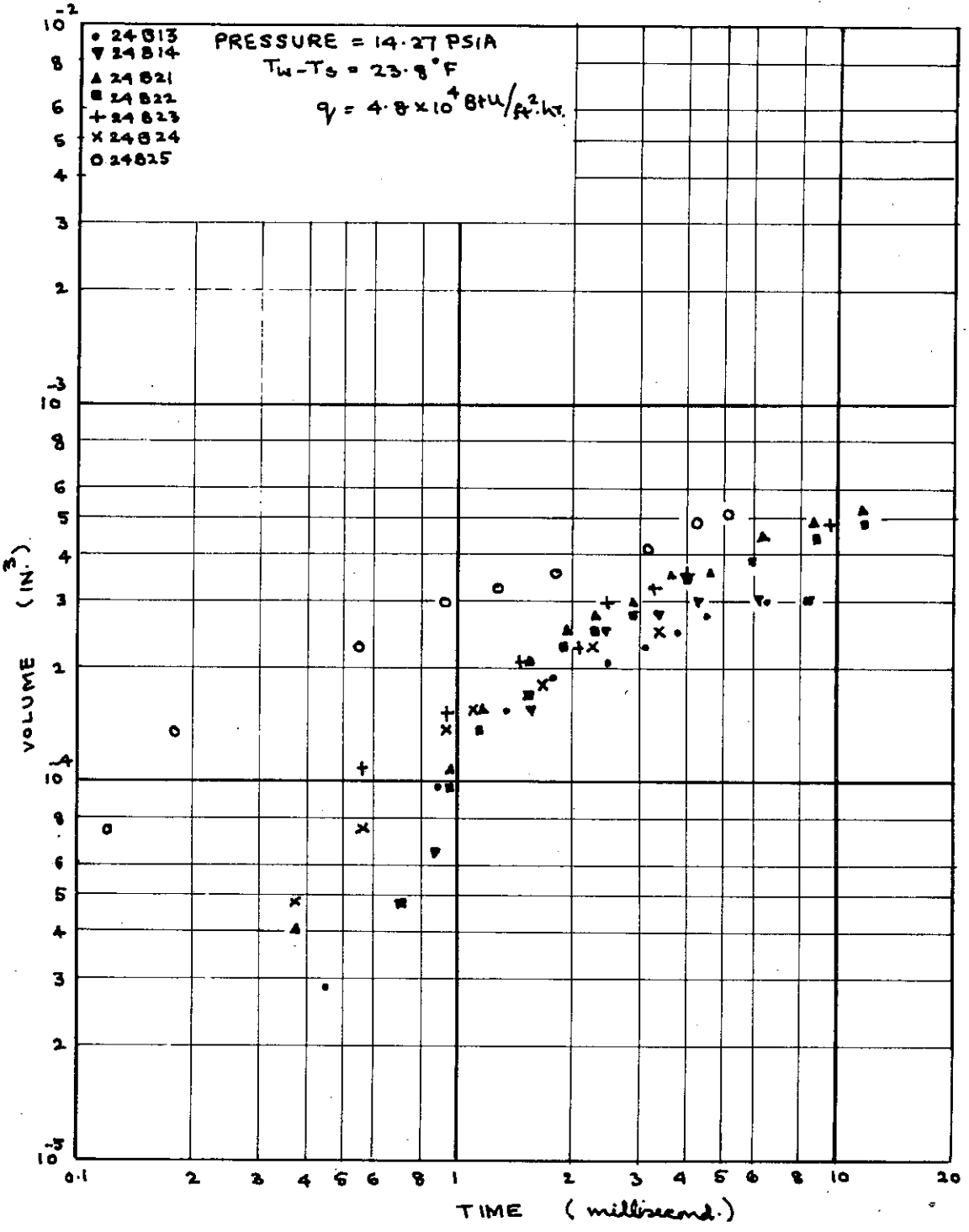

BUBBLE VOLUME V TIME

FIG·70

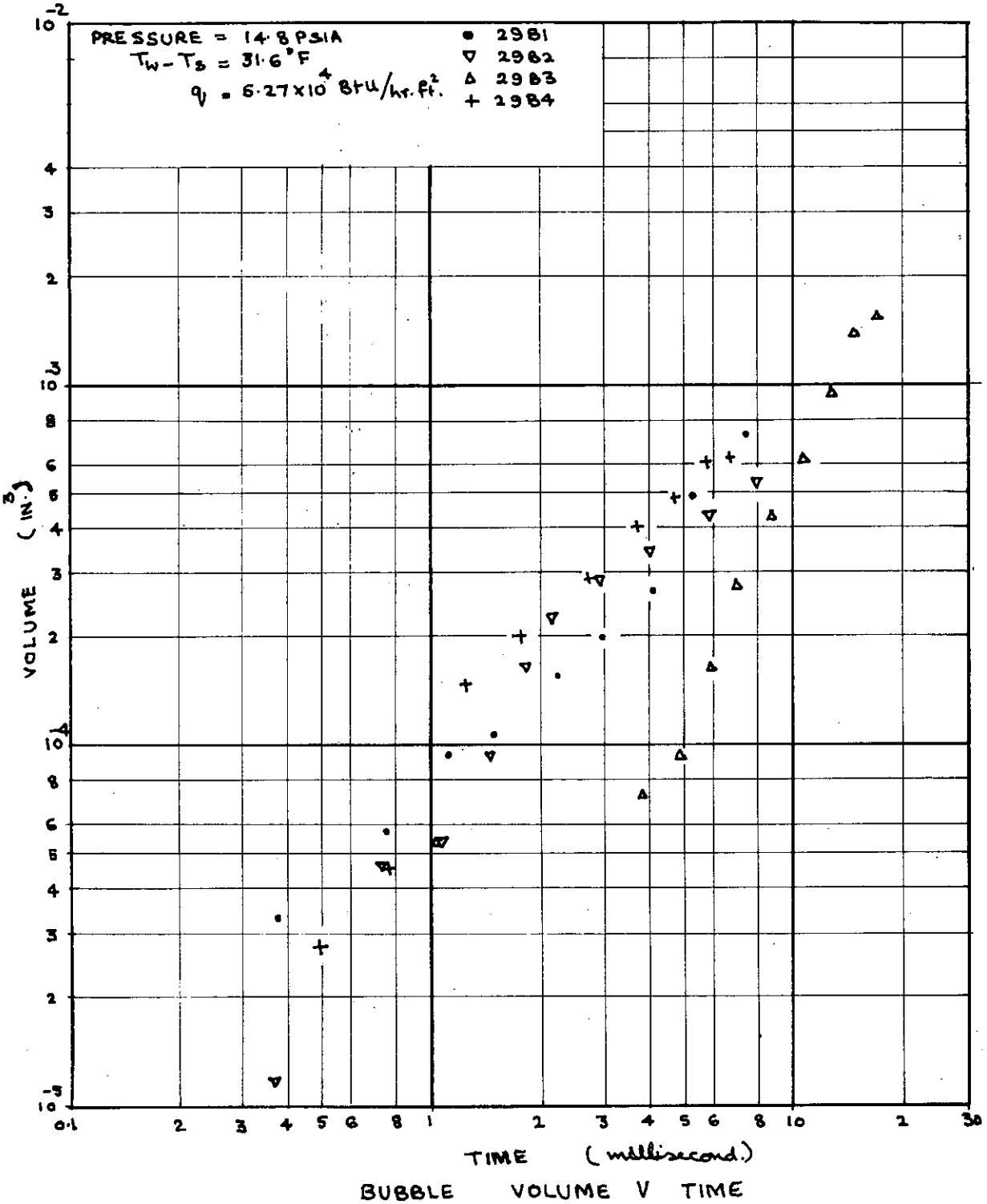

BUBBLE VOLUME V TIME

FIG·71

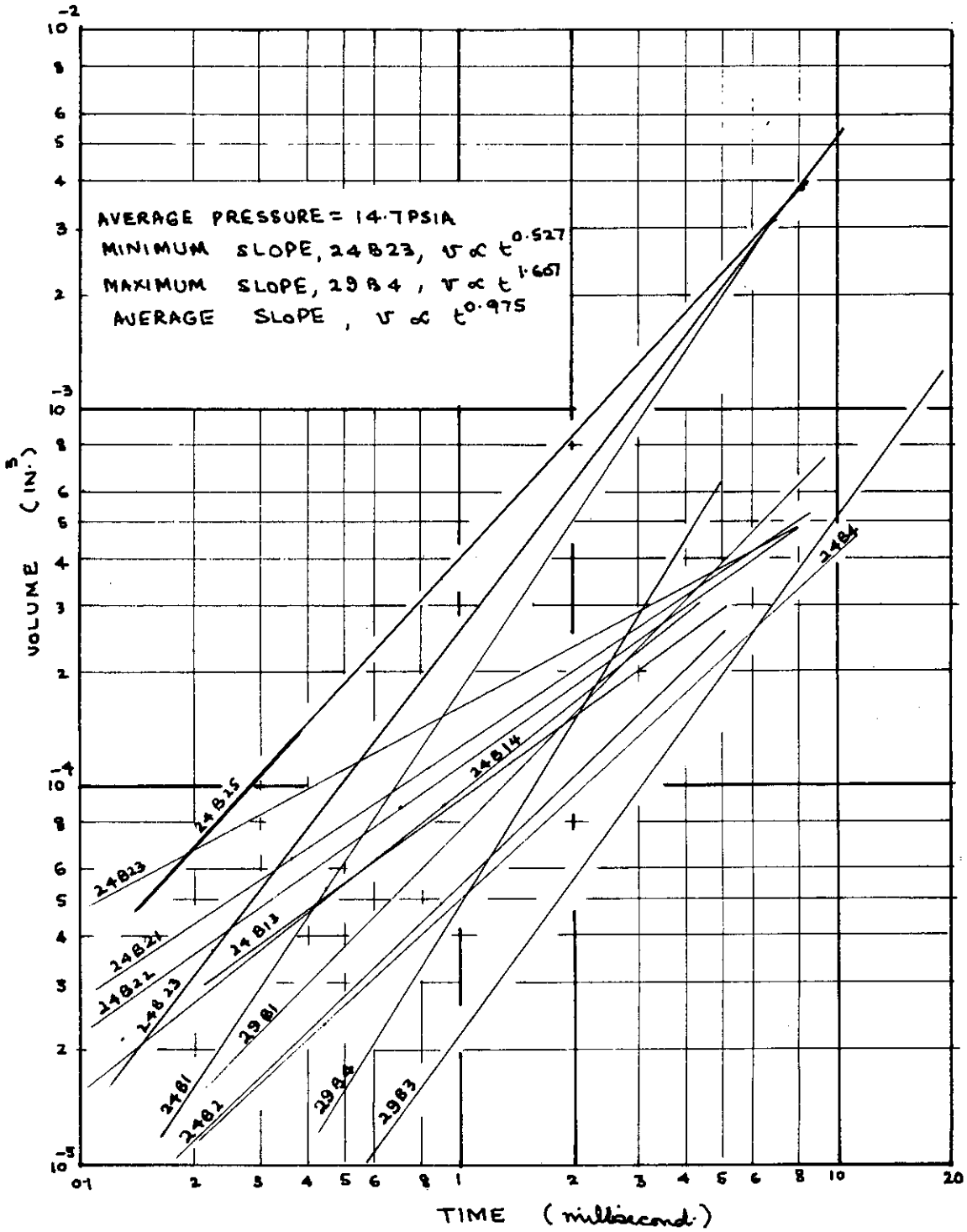

BUBBLE VOLUME V TIME
(REGRESSION LINES)

FIG·72

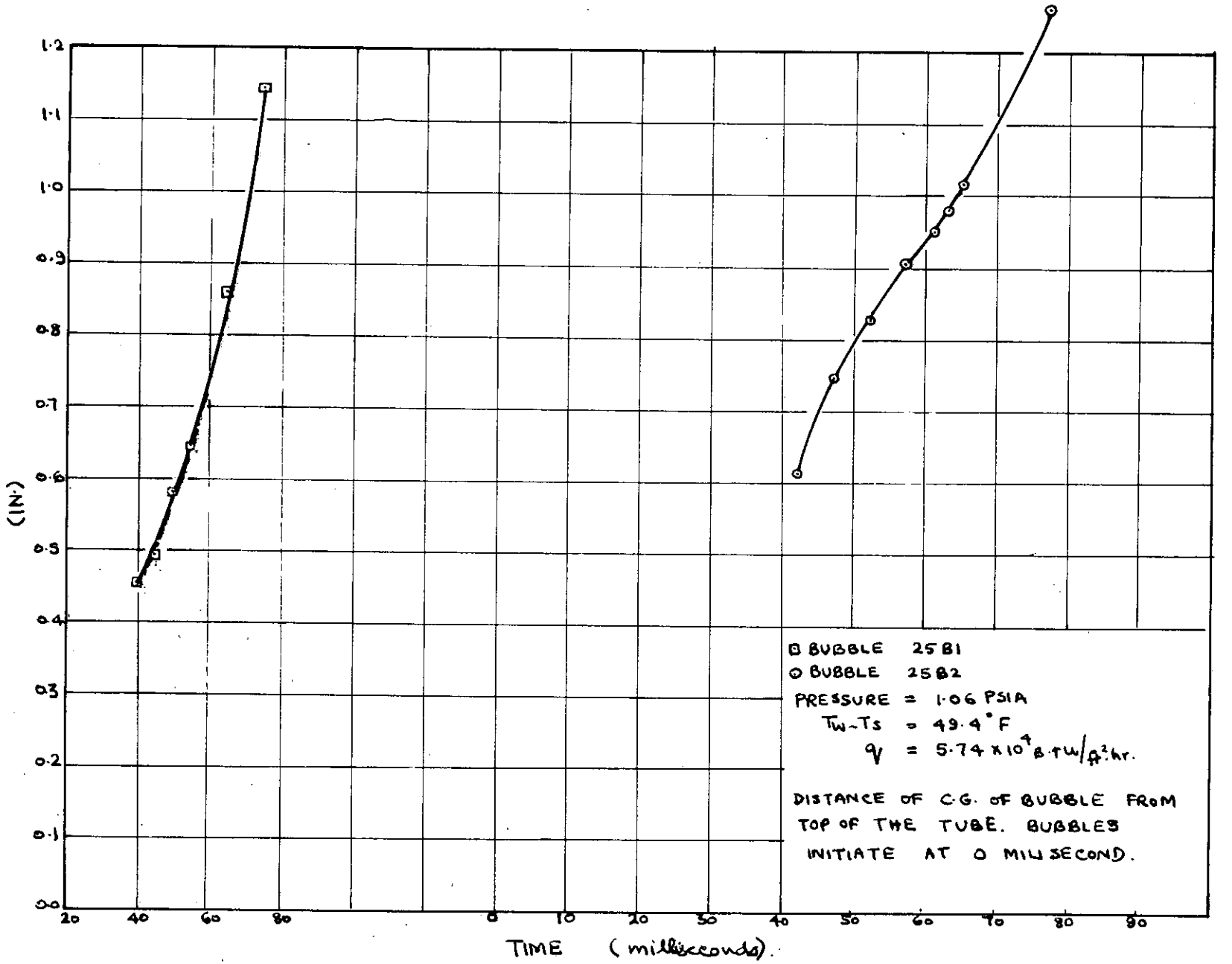
1·2
1·1
1·0
0·9
0·8
0·7
0·6
0·5
0·4
0·3
0·2
0·1
0·0
(IN·)
20
40
60
80
0
10
20
30
40
50
60
70
80
90
TIME (milliseconds).
⊡ BUBBLE 25 B1
⊙ BUBBLE 25 B2
PRESSURE = 1·06 PSIA
$T_W - T_S$ = 49·4 °F
q_V = 5·74 × 10⁴ B·TU/ft²·hr.
DISTANCE OF C·G· OF BUBBLE FROM TOP OF THE TUBE. BUBBLES INITIATE AT 0 MILLISECOND.

FIG·73

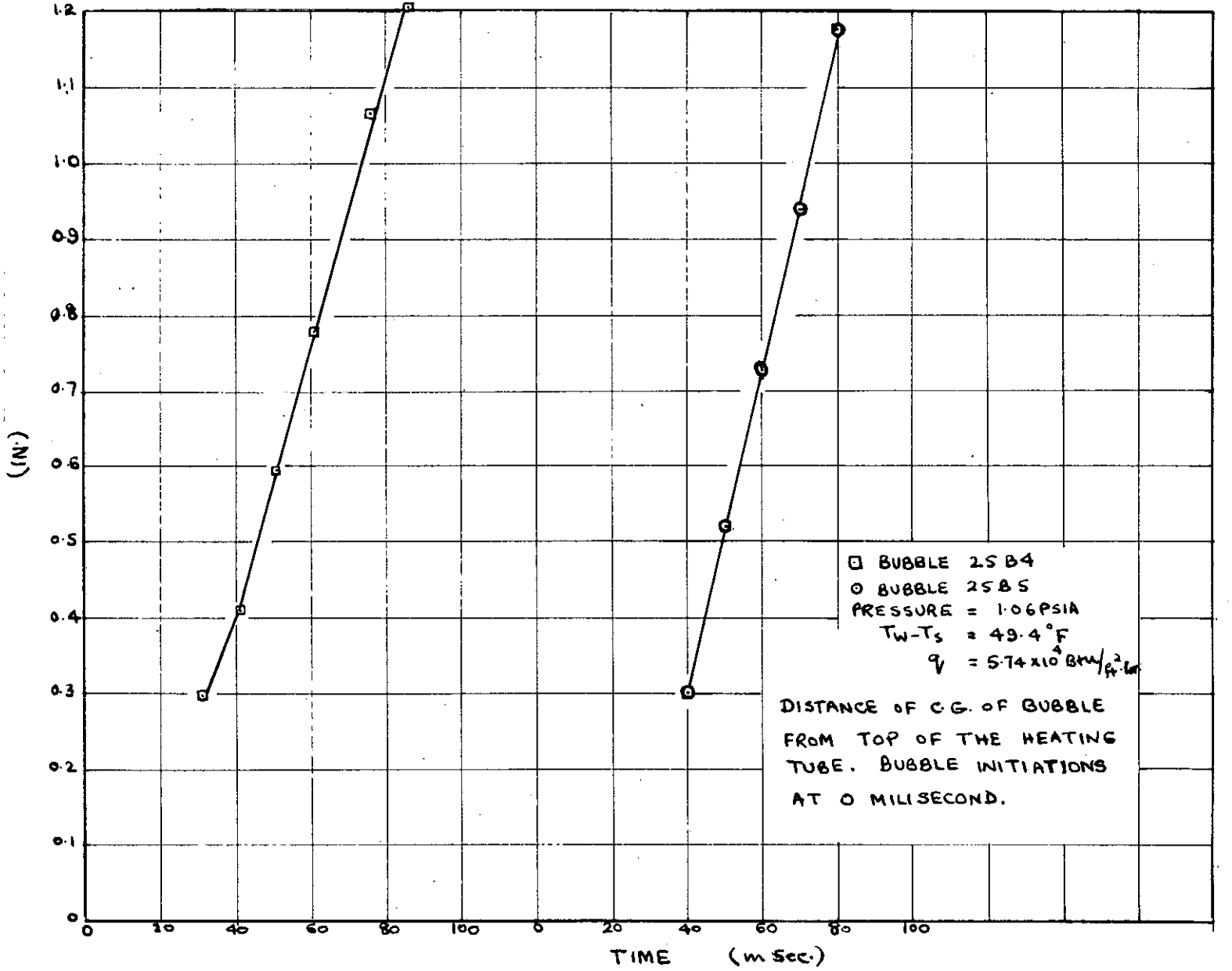
1·2
1·1
1·0
0·9
0·8
0·7
0·6
0·5
0·4
0·3
0·2
0·1
0
(N)
0
20
40
60
80
100
0
20
40
60
80
100
TIME (m Sec.)
□ BUBBLE 2S B4
○ BUBBLE 2S B5
PRESSURE = 1·06 PSIA
$T_W - T_S$ = 49·4 °F
q_V = 5·74 x 10⁴ Btu/ft²·hr
DISTANCE OF C.G. OF BUBBLE FROM TOP OF THE HEATING TUBE. BUBBLE INITIATIONS AT 0 MILISECOND.

FIG. 74

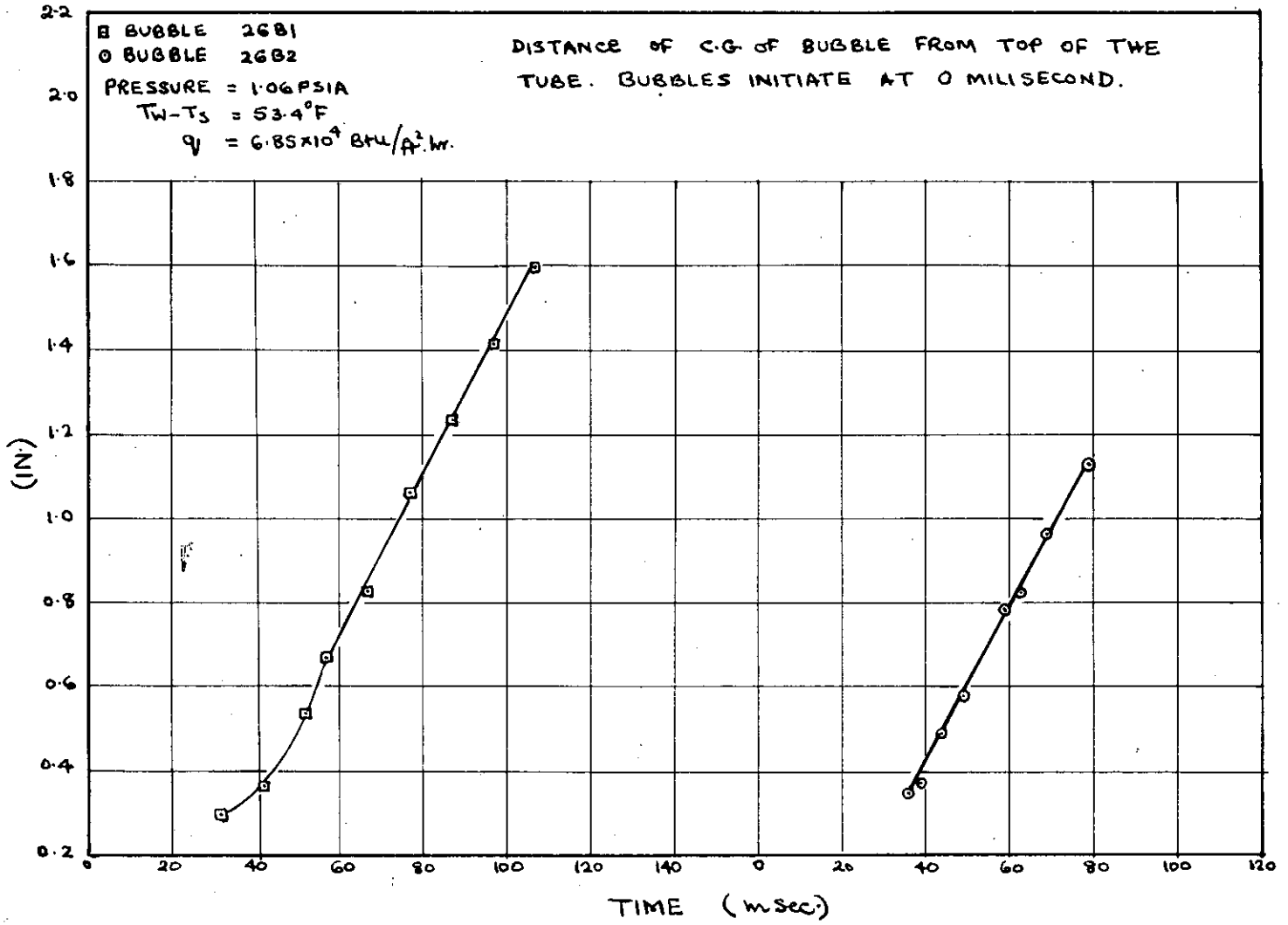
■ BUBBLE 26B1
○ BUBBLE 26B2
PRESSURE = 1.06 PSIA
$T_W - T_S$ = 53.4°F
q_J = 6.85 × 10⁴ BTU/ft².hr.
DISTANCE OF C.G. OF BUBBLE FROM TOP OF THE TUBE. BUBBLES INITIATE AT 0 MILLISECOND.
(IN)
2.2
2.0
1.8
1.6
1.4
1.2
1.0
0.8
0.6
0.4
0.2
0
20
40
60
80
100
120
140
0
20
40
60
80
100
120
TIME (m sec.)

FIG·75

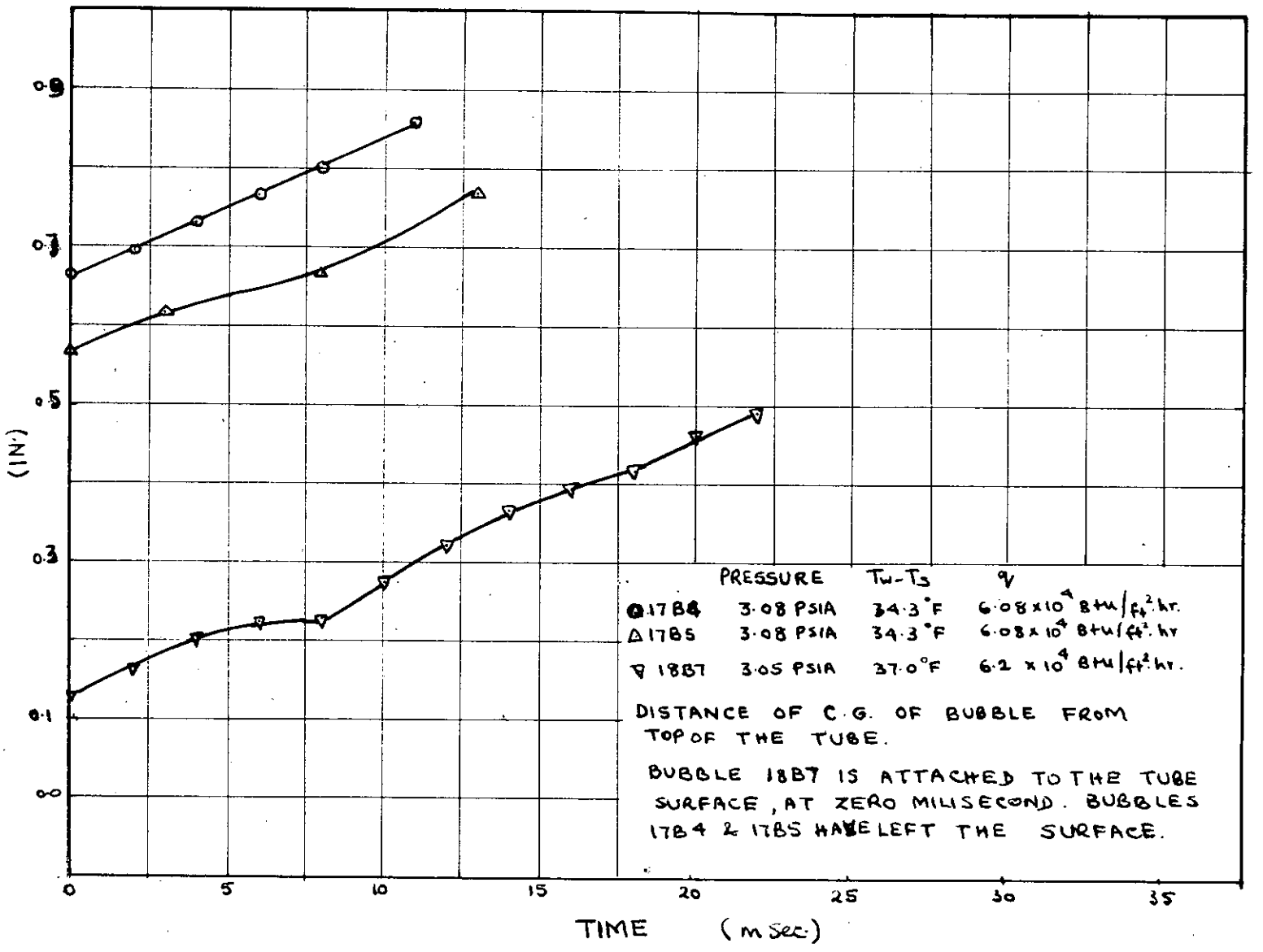
0.9
0.7
0.5
0.3
0.1
0.0
(IN.)
0
5
10
15
20
25
30
35
TIME (m Sec.)
PRESSURE Tw-Ts q
● 1784 3.08 PSIA 34.3°F 6.08x10⁴ Btu/ft².hr.
△ 1785 3.08 PSIA 34.3°F 6.08x10⁴ Btu/ft².hr
▽ 1887 3.05 PSIA 37.0°F 6.2 x10⁴ Btu/ft².hr.
DISTANCE OF C.G. OF BUBBLE FROM TOP OF THE TUBE.
BUBBLE 1887 IS ATTACHED TO THE TUBE SURFACE, AT ZERO MILISECOND. BUBBLES 1784 & 1785 HAVE LEFT THE SURFACE.

FIG. 76

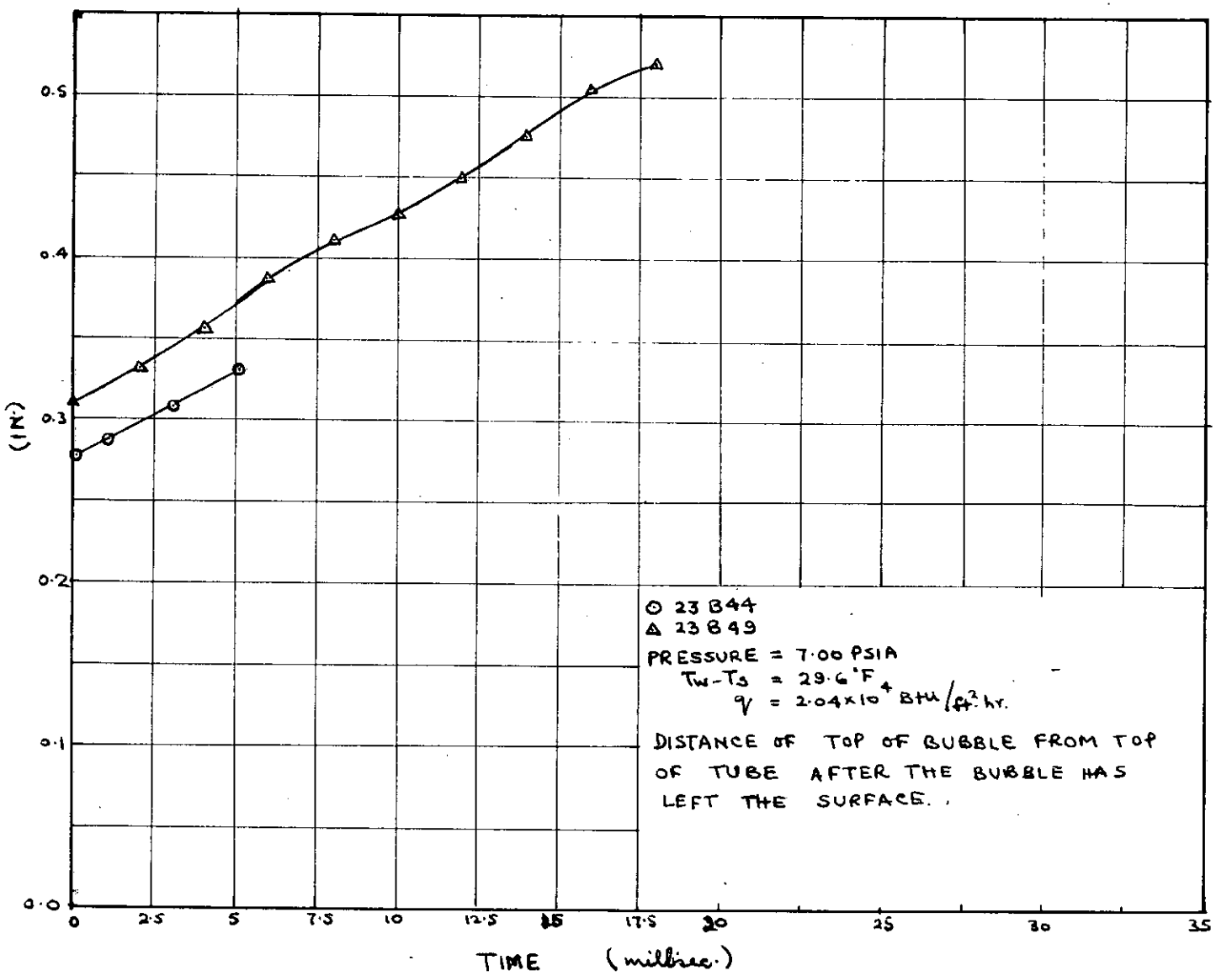
0.5
0.4
0.3
0.2
0.1
0.0
(N)
0
2.5
5
7.5
10
12.5
15
17.5
20
25
30
35
TIME (millisec.)
⊙ 23 B44
△ 23 B49
PRESSURE = 7.00 PSIA
Tw-Ts = 29.6 °F
q = 2.04×10⁴ BTU/ft² hr.
DISTANCE OF TOP OF BUBBLE FROM TOP OF TUBE AFTER THE BUBBLE HAS LEFT THE SURFACE.

FIG·77

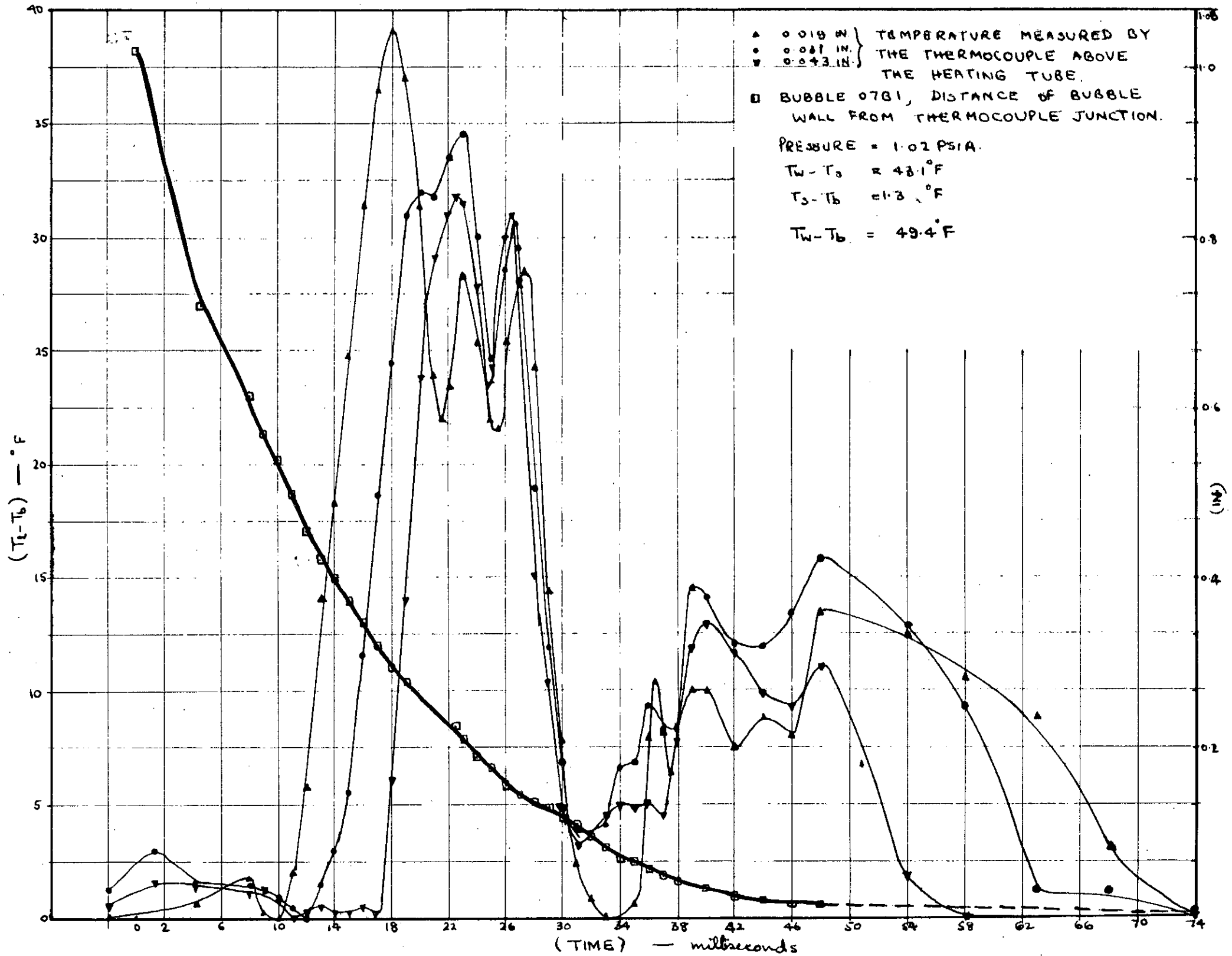

TEMPERATURE TRANSIENTS NEAR THE HEATING TUBE DUE TO BUBBLE GROWTH IN NUCLEATE BOILING.

FIG 78

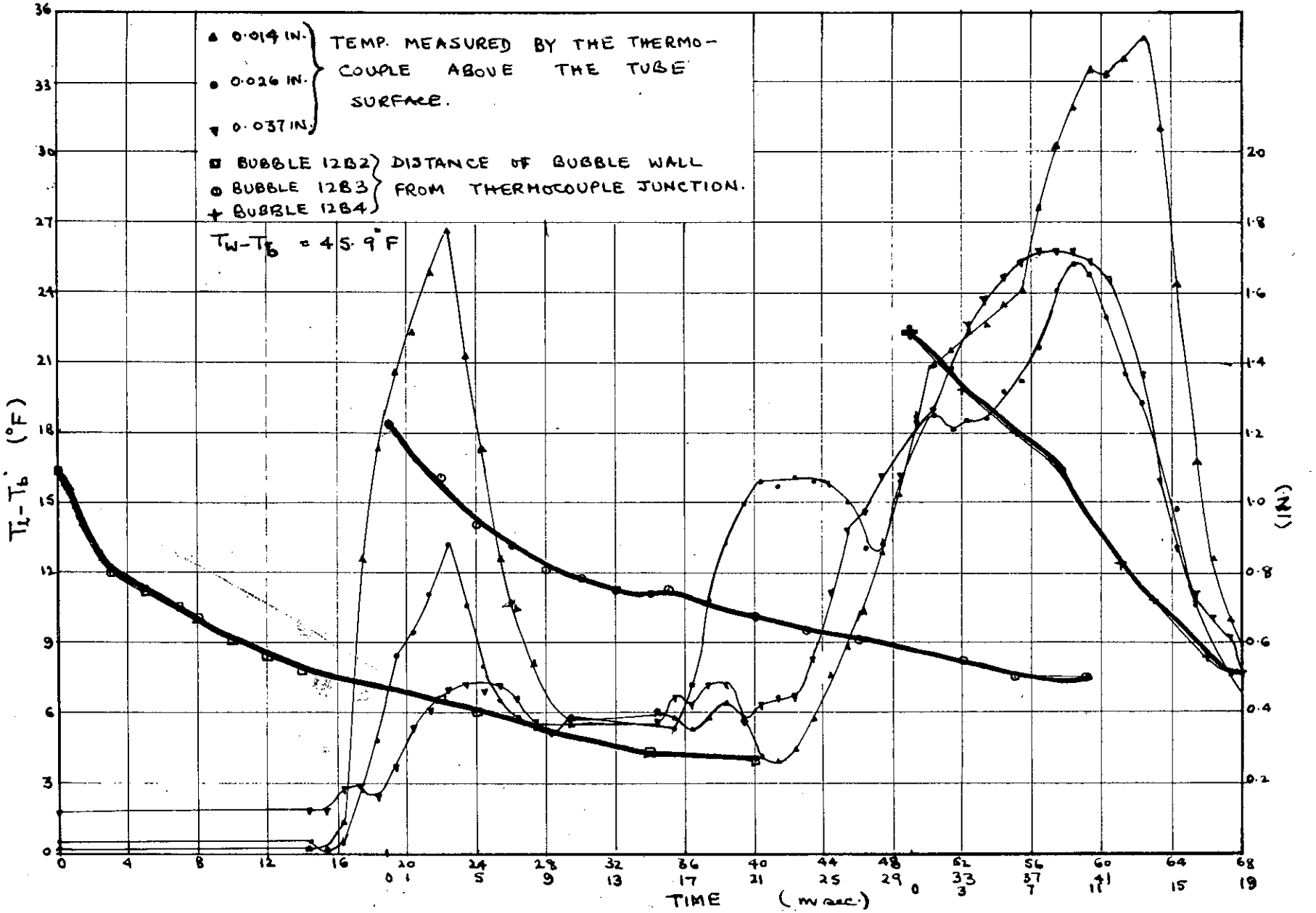

TEMPERATURE TRANSIENTS NEAR THE HEATING TUBE DUE TO BUBBLE GROWTH IN NUCLEATE BOILING.

FIG·79

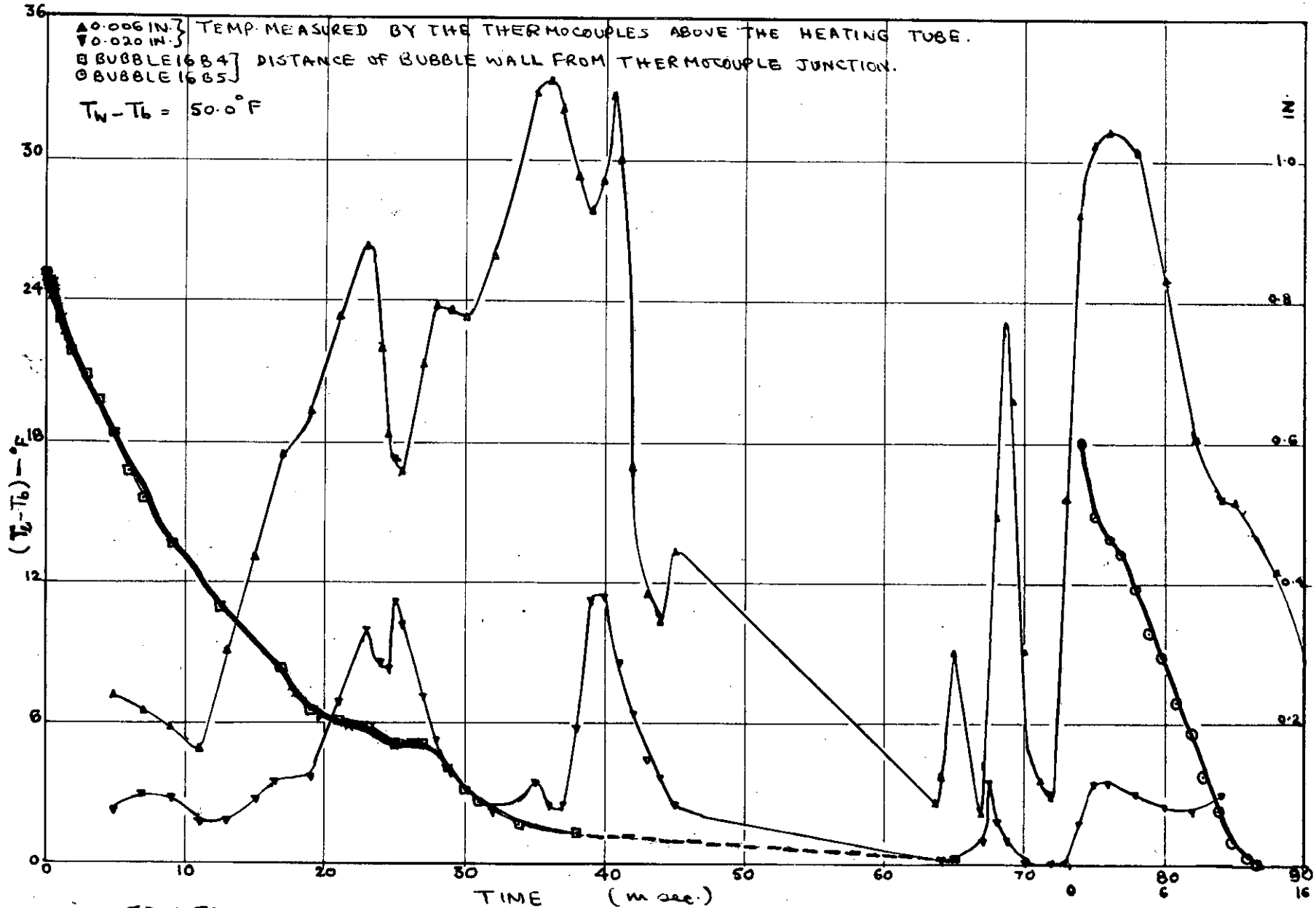

TEMP TRANSIENTS NEAR THE TUBE DUE TO BUBBLE GROWTH IN NUCLEATE BOILING.

FIG·80

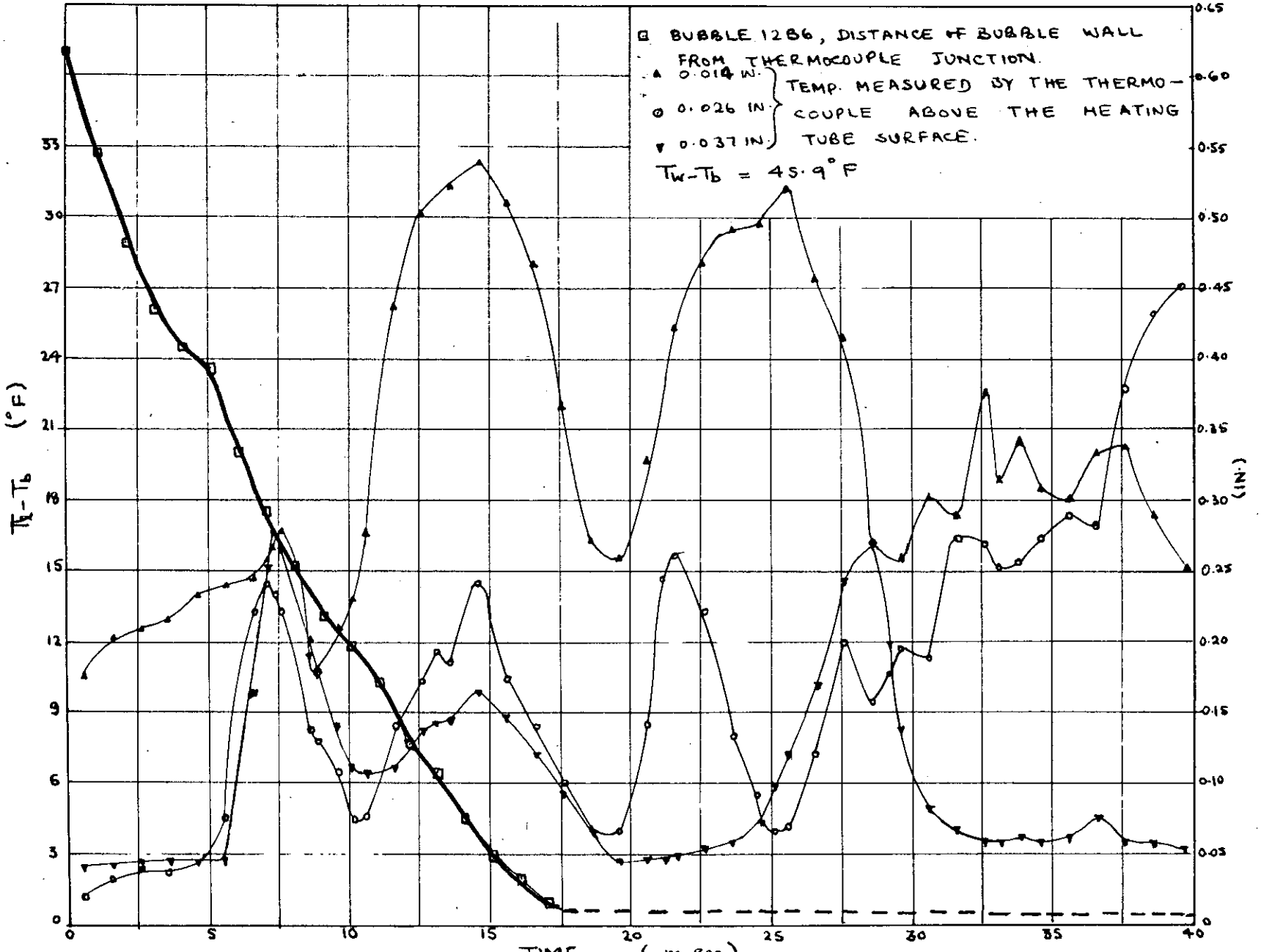

TEMP. TRANSIENTS NEAR THE HEATING TUBE DUE TO BUBBLE GROWTH IN NUCLEATE BOILING.

FIG·81

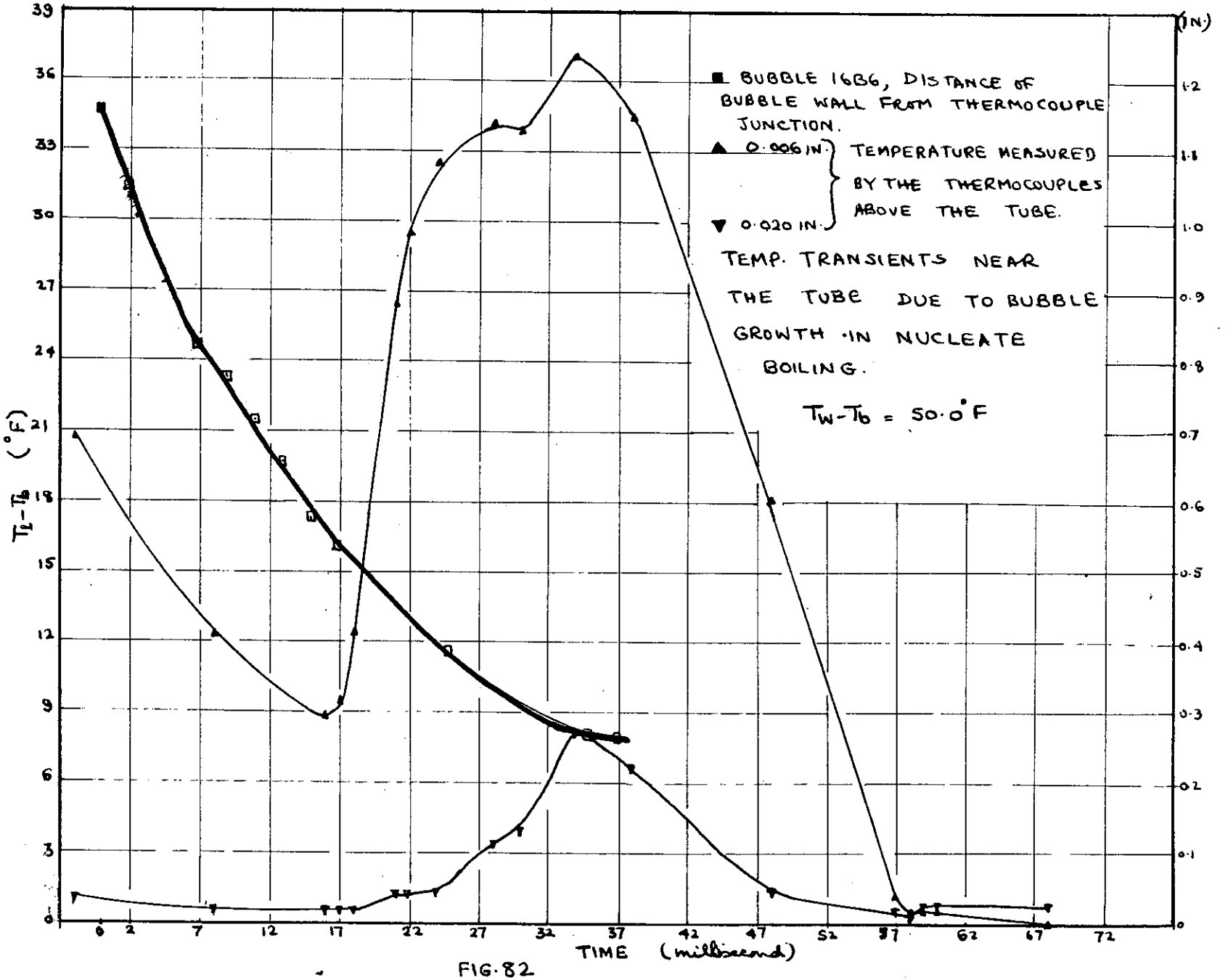
■ BUBBLE 1686, DISTANCE OF BUBBLE WALL FROM THERMOCOUPLE JUNCTION.
▲ 0·006 IN.
▼ 0·020 IN.
TEMPERATURE MEASURED BY THE THERMOCOUPLES ABOVE THE TUBE.
TEMP. TRANSIENTS NEAR THE TUBE DUE TO BUBBLE GROWTH IN NUCLEATE BOILING.
$T_W - T_b$ = 50·0°F
$T_L - T_b$ (°F)
TIME (millisecond)
(IN.)

FIG·82

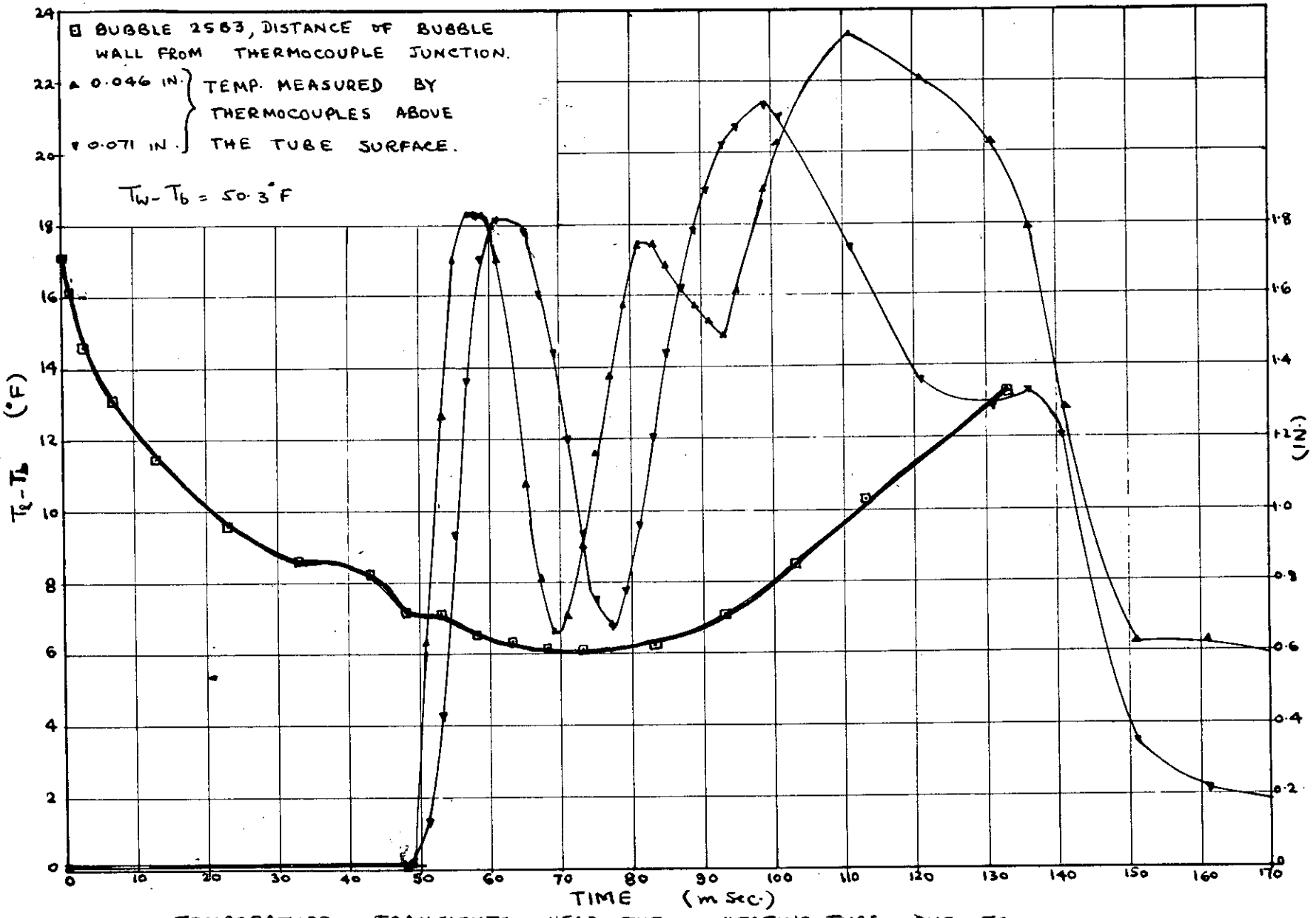

TEMPERATURE TRANSIENTS NEAR THE HEATING TUBE DUE TO BUBBLE GROWTH IN NUCLEATE BOILING.

FIG. 83

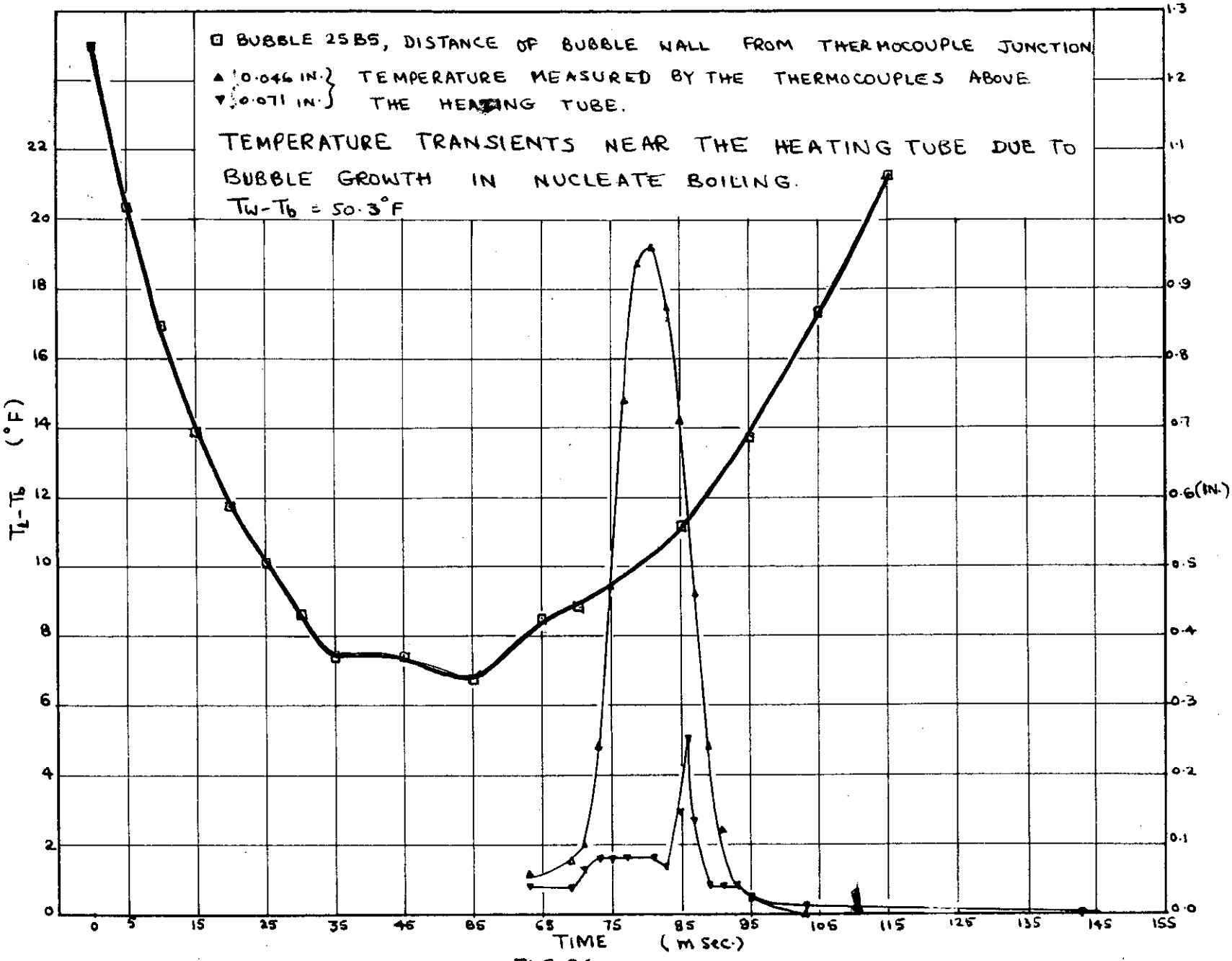
BUBBLE 25B5, DISTANCE OF BUBBLE WALL FROM THERMOCOUPLE JUNCTION
▲ 0·046 IN. } TEMPERATURE MEASURED BY THE THERMOCOUPLES ABOVE
▼ 0·071 IN. } THE HEATING TUBE.
TEMPERATURE TRANSIENTS NEAR THE HEATING TUBE DUE TO BUBBLE GROWTH IN NUCLEATE BOILING.
$T_W - T_b$ = 50·3°F
$T_L - T_b$ (°F)
TIME (m sec.)
(IN.)
0 5 15 25 35 46 65 75 85 95 105 115 125 135 145 155
0 2 4 6 8 10 12 14 16 18 20 22
0·0 0·1 0·2 0·3 0·4 0·5 0·6 0·7 0·8 0·9 1·0 1·1 1·2 1·3

FIG·84

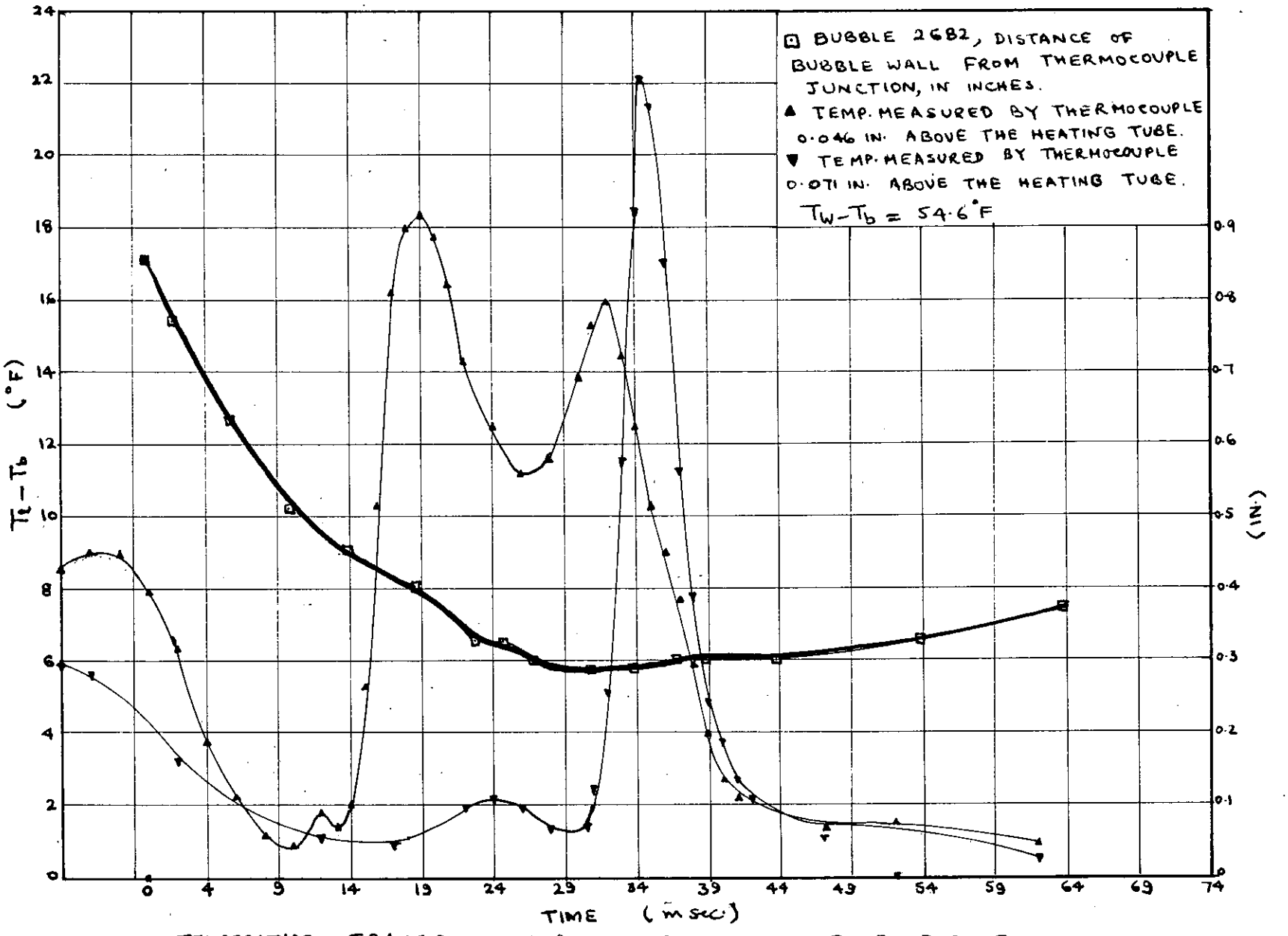

TEMPERATURE TRANSIENTS NEAR THE HEATING TUBE DUE TO BUBBLE GROWTH IN NUCLEATE BOILING.

FIG·85

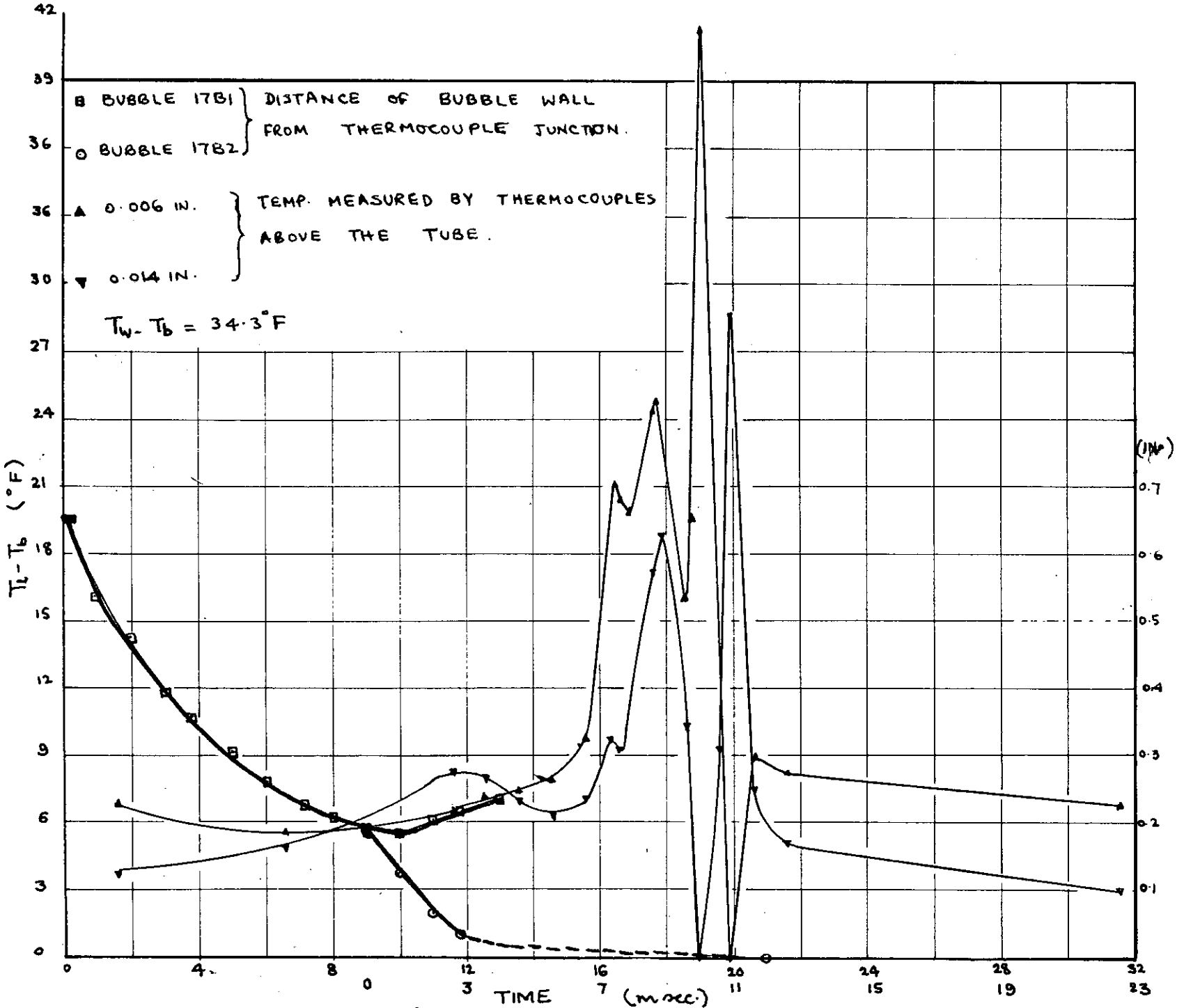

TEMP. TRANSIENTS NEAR THE TUBE DUE TO BUBBLE GROWTH IN NUCLEATE BOILING.

FIG. 86

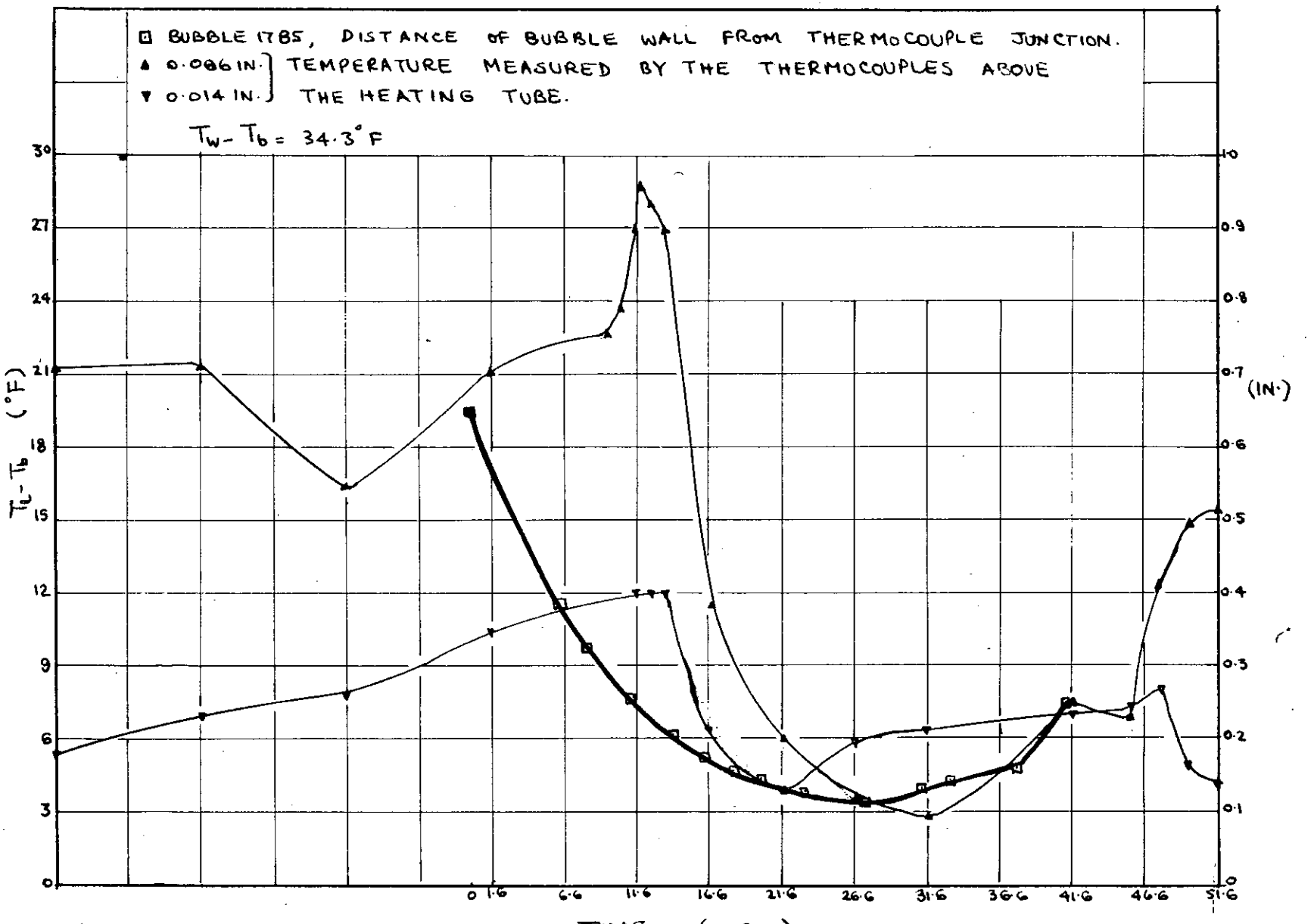

TEMP. TRANSIENTS NEAR THE HEATING TUBE DUE TO BUBBLE GROWTH IN NUCLEATE BOILING.

FIG 87

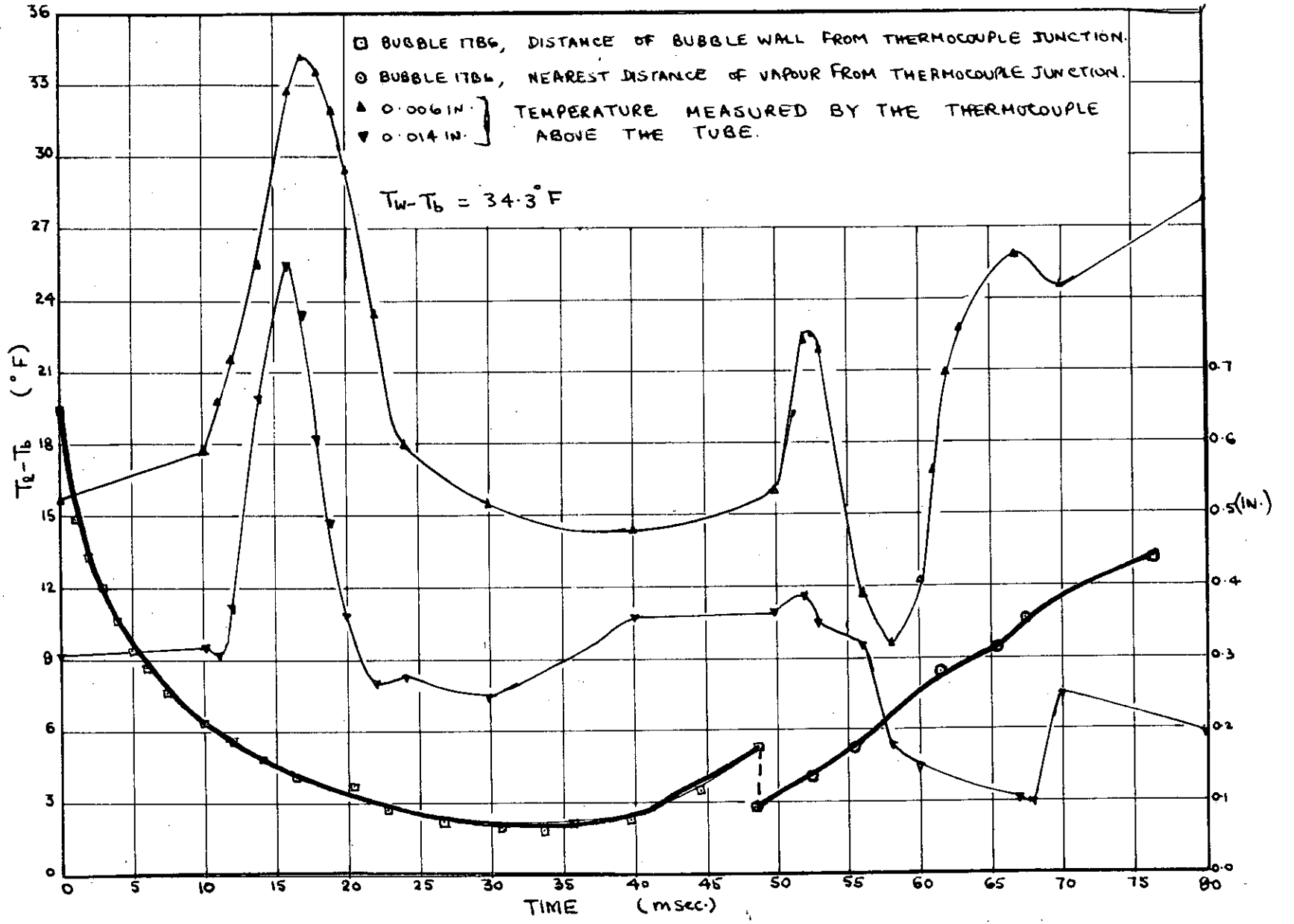

TEMPERATURE TRANSIENTS NEAR THE HEATING TUBE DUE TO BUBBLE GROWTH IN NUCLEATE BOILING.

FIG·88

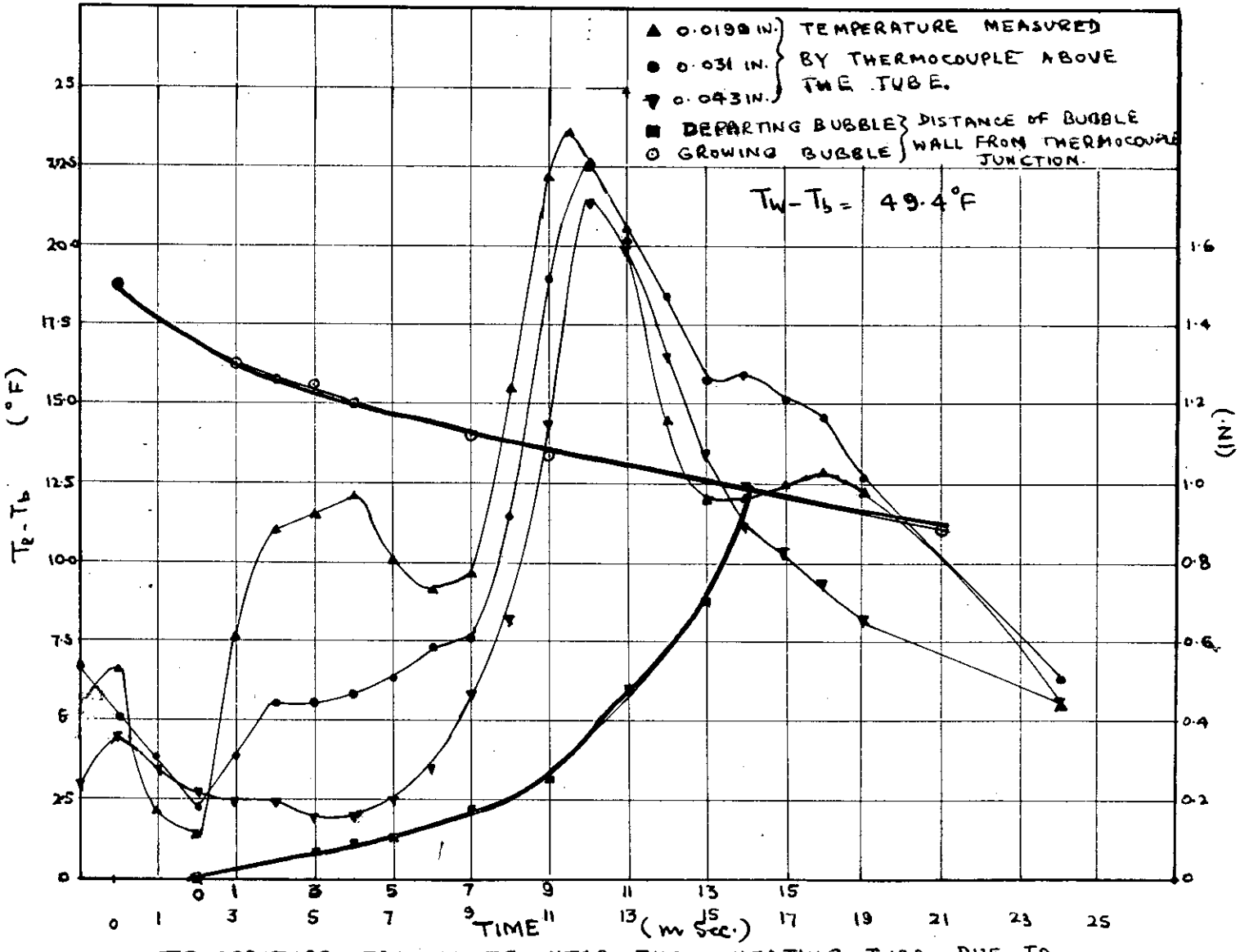

TEMPERATURE TRANSIENTS NEAR THE HEATING TUBE DUE TO BUBBLE GROWTH IN NUCLEATE BOILING.

FIG·89

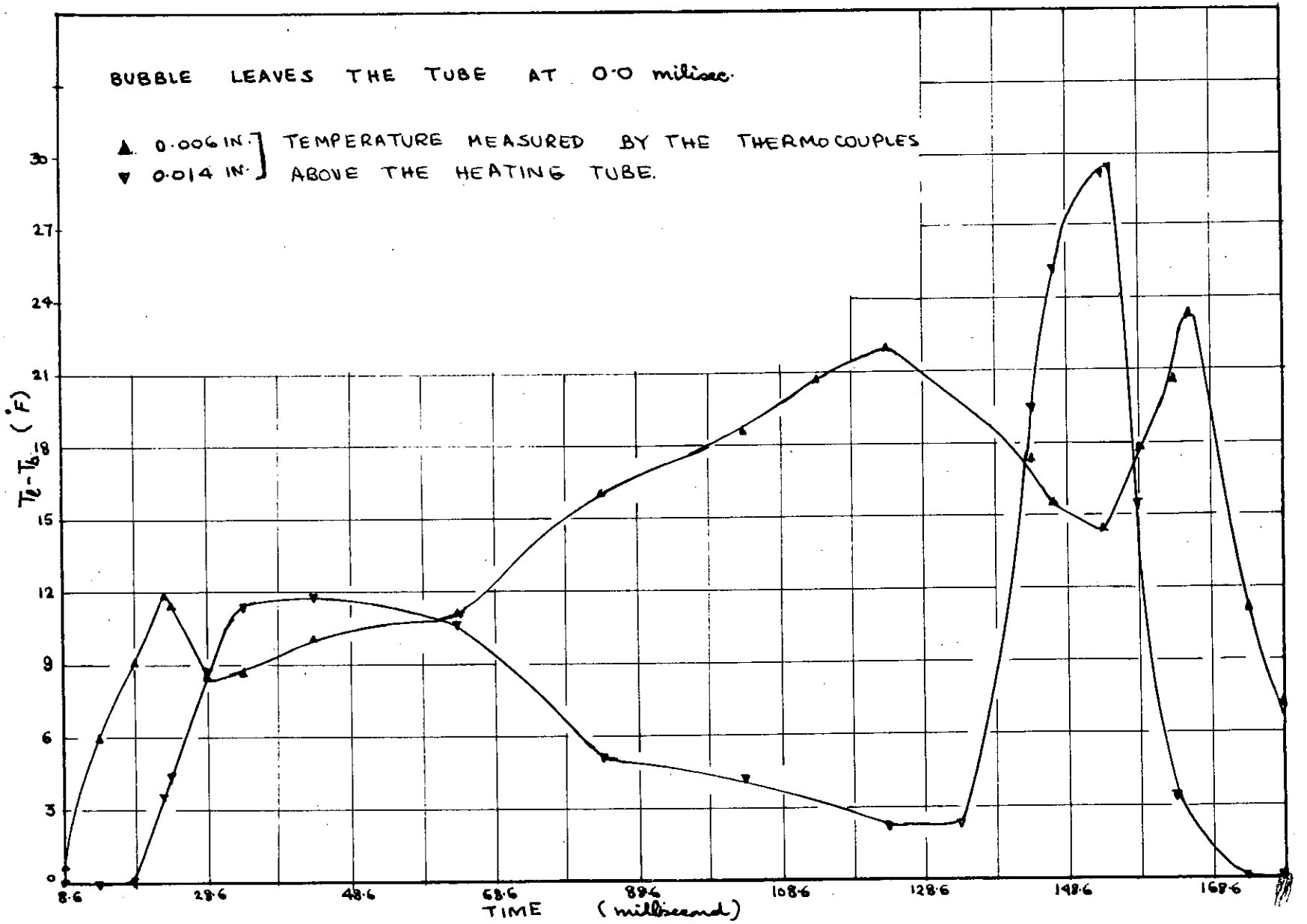

TEMP TRANSIENTS NEAR THE HEATING TUBE DUE TO BUBBLE GROWTH IN NUCLEATE BOILING.

FIG. 90

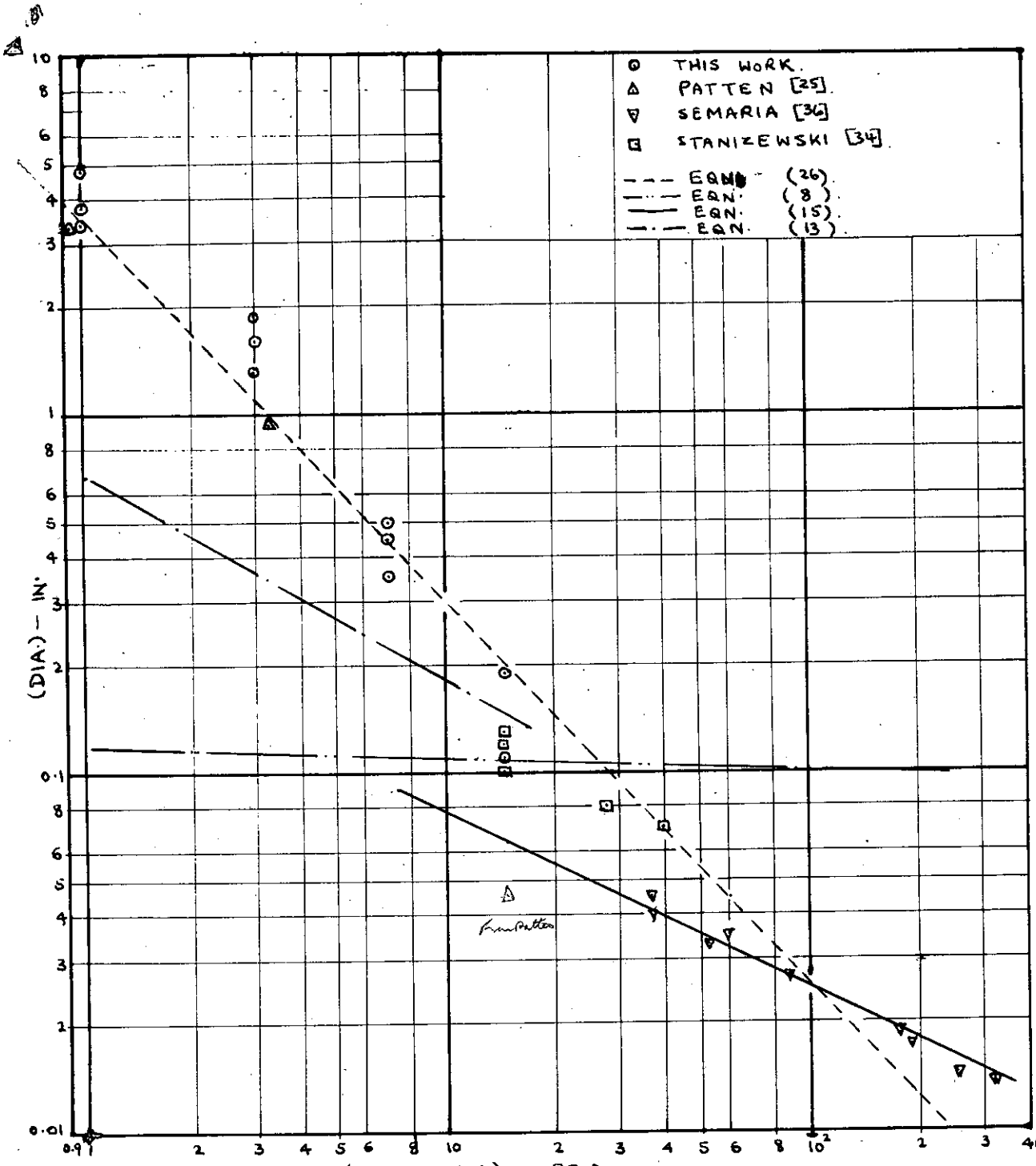

MAXIMUM BUBBLE DIAMETER V PRESSURE IN SATURATED POOL BOILING OF WATER.

FIG. 91

MAXIMUM BUBBLE DIAMETER V_S PRESSURE IN SATURATED POOL BOILING OF WATER.

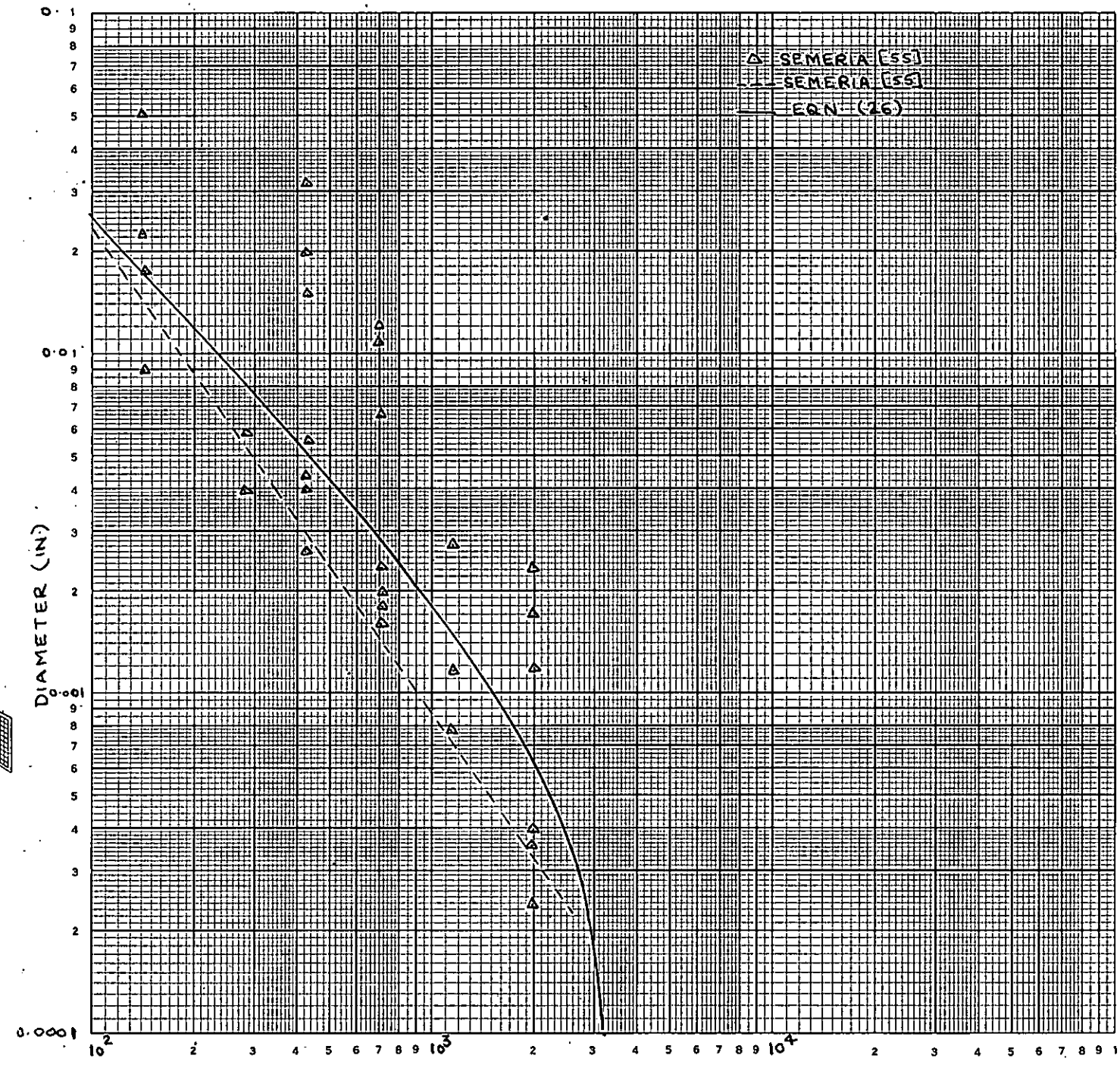

PRESSURE (PSIA)

FIG. 92

PROPOSED MODEL FOR CRITICAL HEAT FLUX OF CHANG AND SNYDER [4].

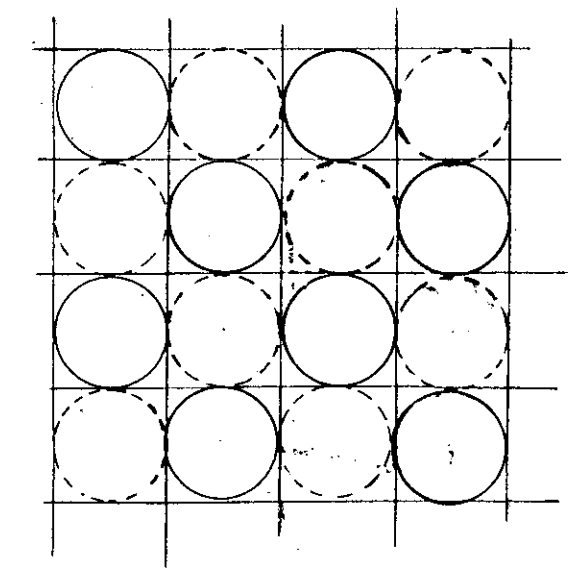

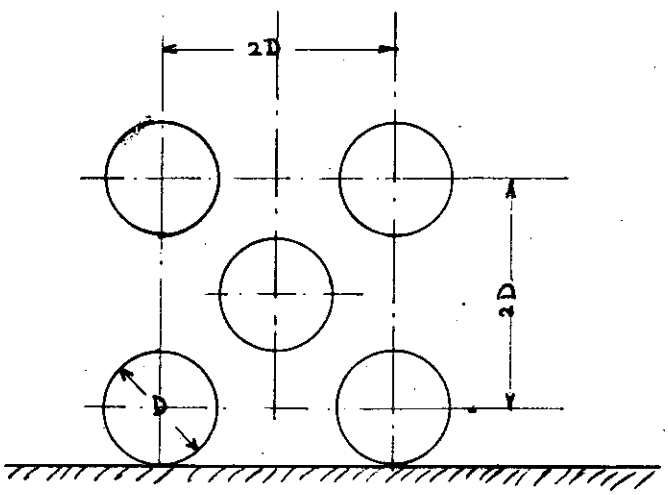

FIG. 93

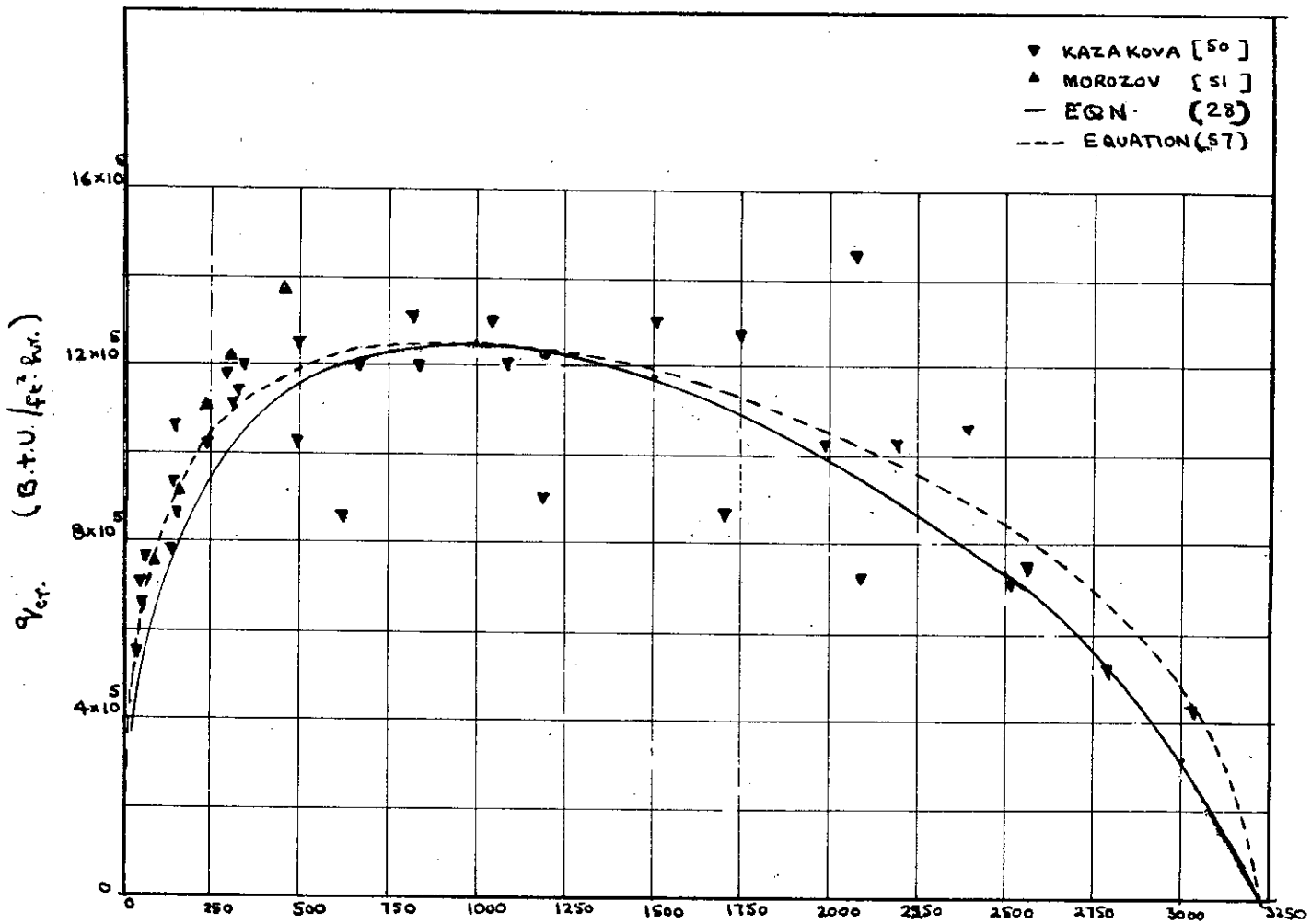

CRITICAL HEAT FLUX V PRESSURE, FOR SATURATED POOL BOILING OF WATER.

FIG 94

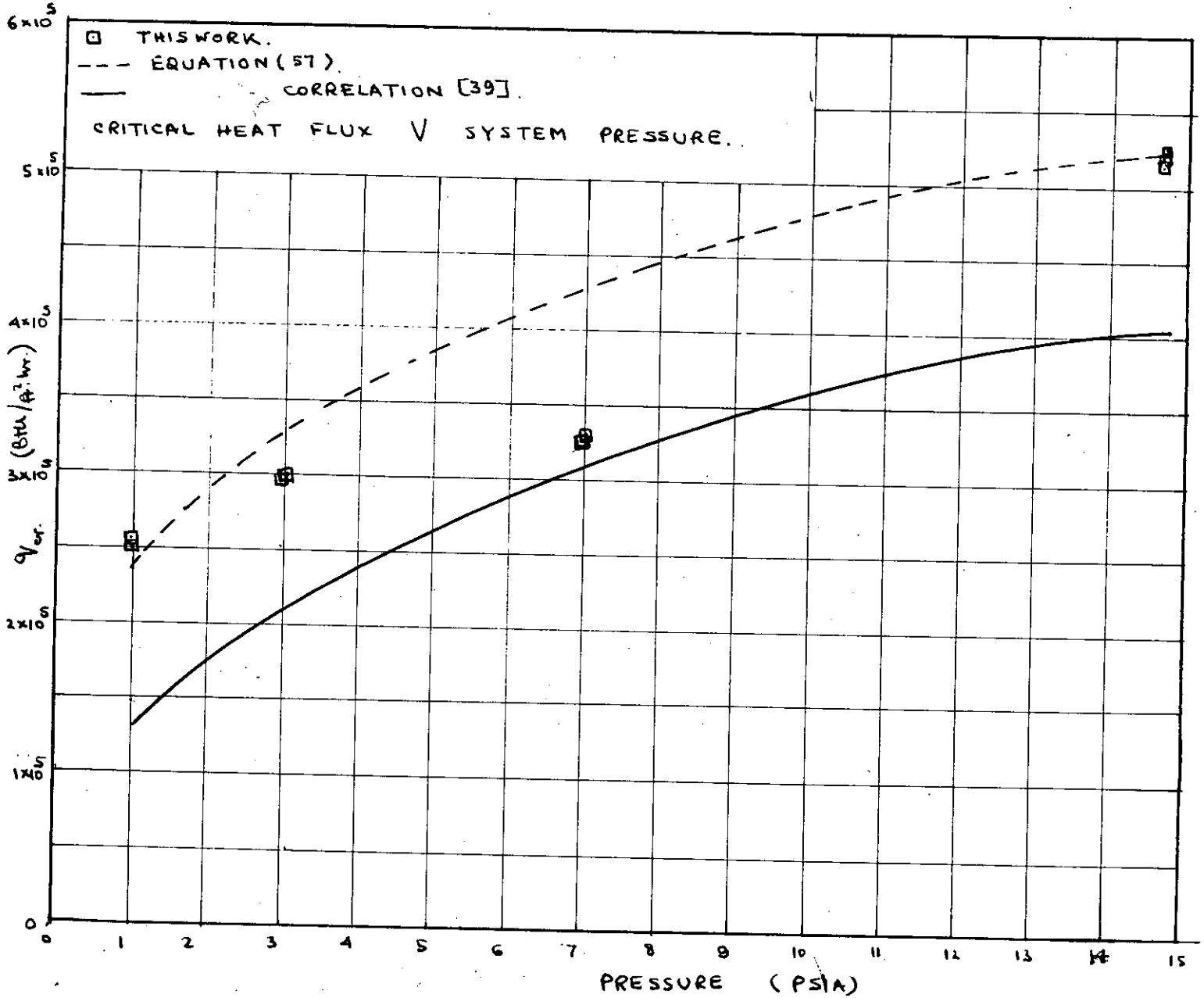
THIS WORK.
EQUATION (57).
CORRELATION [39].
CRITICAL HEAT FLUX V SYSTEM PRESSURE.
q_{cr} (BTU/ft².hr.)
6x10⁵
5x10⁵
4x10⁵
3x10⁵
2x10⁵
1x10⁵
0
0 1 2 3 4 5 6 7 8 9 10 11 12 13 14 15
PRESSURE (PSIA)

FIG. 95